SOLAR WATER DESALINATION USING MULTI-EFFECT WATER STILLS WITH REDUCED INTERNAL PRESSURE

NABIL ELSHARIF

PhD

2018

SOLAR WATER DESALINATION USING MULTI-EFFECT WATER STILLS WITH REDUCED INTERNAL PRESSURE

NABIL ELSHARIF

A thesis submitted in partial fulfilment
of the requirements of the
University of Northumbria at Newcastle for the
degree of Doctor of Philosophy

Research undertaken in the
School of Engineering and Environment

June 2018

Abstract

The application of solar energy is one prospective solution to meet the sharp increase in global energy demand and alleviate the environmental issues, caused by the use of fossil fuels. Solar thermal energy has been actively utilized to operate small-scale desalination systems and solar water stills, which are one of the most promising technologies in the field of seawater desalination.

A desalination system, consisting of multi-effect solar water still coupled to evacuated tube solar collectors and a novel modification of small fluid piston energy converter has been studied at Northumbria University. The task in this research was to experimentally test the possibility of the operation of system with capability to self-reduce the internal pressure inside the still in order to increase its productivity. It was demonstrated that the system was able to achieve vacuum conditions and maintain this level of pressure without using an external vacuum pump.

In the theoretical investigation a thermodynamic mathematical model of the proposed system has been developed and used to solve the governing equations in a Matlab/Simulink environment. The output data was obtained in terms of variation of the pressure and temperatures inside the system as well as its distillate productivity. In the experimental investigation, the above described distillation system was developed at Northumbria University based on a laboratory prototype of a dynamic solar multi-effect water still and fluid piston energy converter designed and built previously by Prof K.

Mahkamov. Series of experimental tests and numerical simulations were performed for the climatic conditions of Benghazi city in Libya.

After validation of the mathematical model against previously published theoretical results and the experimental data obtained in this study, further investigations of the influence of decreasing internal pressure on the performance of the system was conducted. Overall, investigations confirm that this novel system demonstrates considerable improvement in the distillate productivity when compared to conventional solar stills.

List of Contents

List of Figures

List of Tables

Acknowledgment

First, I must express my greatest gratitude and thanks to Almighty Allah for his providential care of me and for giving me the courage, determination and guidance in conducting this research work.

Special and foremost, I would like to express my heartily thanks and gratitude to my supervisor, Professor Khamid Mahkamov for his professional supervision, leadership, continued support and invaluable help during this PhD study.

I would like to thank and gratitude to my beloved father for his continuous support, encouragement and prayer during the course of my academic journey. Furthermore, I would like to thank my brother, my sisters and my brothers and sisters in law for their support and assistance over the years of my study.

My sincere prayer addressed to Almighty Allah for the souls of my mother, and my parents in law who have passed away but they are still alive in my heart and their words of encouragement still resonate in my mind.

My special thanks and gratefulness must go to my beloved wife for her generous love, support, care and patience since the beginning of my study. Also, thanks to my children Ahmed, Ayah, Muaath, and Zein.

I would like also to take this opportunity to gratitude the Ministry of Education and the Culture Affairs Department of the Libyan Embassy in London for providing the managerial and financial support during my PhD study.

Moreover, I would like to thank Dr Gamal Hashem, Dr Khaled Hossin and Dr Saleh Etaig for their support, advice and help during the period of this research.

Many thanks also should go to the colleagues, academic and technical staff at Northumbria University for their support, cheerfulness and encouragement.

Declaration

I declare that the work contained in this thesis has not been submitted for any other award and that it is all my own work. I also confirm that this work fully acknowledges opinions, ideas and contributions from the work of others.

Name: NABIL ELSHARIF

Signature:

Date: June 2018

Nomenclature

A_s	area, m^2
A_{ws}	Surface area of the still walls, m^2
A_{SC}	the absorber area of the solar collector, m^2
C_p	specific heat capacity at constant pressure J/kg.K
D	diffusion coefficient from water vapour to dry air inside each stage (m^2/sec).
g	acceleration of gravity, m/s^2
G_T	total solar radiation, W/m^2
G_{sc}	Solar constant =1367 W/m^2
hfg	latent heat of vaporization, J/kg
K	thermal conductivity (W/m.K)
L	the gap between the stage (m)
$\dot{m}$	mass flow rate, kg/sec
M	waterbed mass, kg
M_a	molar mass of air
M_v	molar mass of water vapour
Nu	Nusselt number,
P	pressure, pa
P_o	internal pressure of the system, (Pa)
Q_H	heat input, W
Ra	Rayleigh number, $Ra = Gr.Pr$
T	temperature, K
T_a	the ambient temperature, K

U_t total convection heat transfer coefficient, $W/m^2 K$

Greek symbols

β Thermal expansion coefficient (K^{-1})

η_{SC} Solar collector efficiency

μ Viscosity, (kg/m.s)

ρ Density, (kg/m^3)

ν Kinematic viscosity (m2/s)

α thermal diffusivity (m^2/sec)

θ incidence angle of the beam solar radiation

θ_z solar zenith angle

Subscripts

a air

c condensation surface

i stage number

m mixture

s saline waterbed

v vapour

Chapter 1 Introduction

1.1 Background

The availability of freshwater has become a matter of critical concern and one the most important global issues because of rapid depletion of existing freshwater resources. It is believed that world population growth and the dramatic increase in agricultural and industrial activities all over the world have led to the depletion and contamination of available water resources [1]. According to United Nations studies, many developing countries in the Middle East and North Africa (MENA), as shown in Figure 1.1, are confronted with the problem of the persistent over-use of fresh water due to growing populations and intensification of agricultural and industrial activities, causing the rapid depletion and contamination of available potable water resources [2].

Although less than one-third of the earth's surface is land and more than two-thirds is the hydrosphere, only about 2.6% of the earth's water is potable while more than 97% of it is undrinkable. Seawater generally has salinity levels between 35,000 and 45,000 ppm and the acceptable limit of the total dissolved salt in drinkable water, according to World Health Organisation (WHO), must not exceed 500 ppm in general and for some particular cases 1000 ppm [3]. Therefore, seawater cannot be directly used for human, industrial and agricultural use but currently many countries rely on seawater desalination as an unlimited source of potable water [4]. Garcia-Rodriguez (2002) [5] states that the daily capacity of

drinkable water produced from seawater desalination across the world is approximately 23 x 10^6 cubic metres.

However, producing potable water by means of conventional seawater desalination processes consumes huge amounts of fossil fuels. It is estimated that the production of 13 million cubic metres of potable water per day requires the burning of 130 million tons of oil per year. Furthermore, the International Energy Outlook predicted in 2011 that the world's energy consumption was expected to increase from 533 Exa-Joules (EJ) in 2008 to 812 EJ in 2035 [6] .

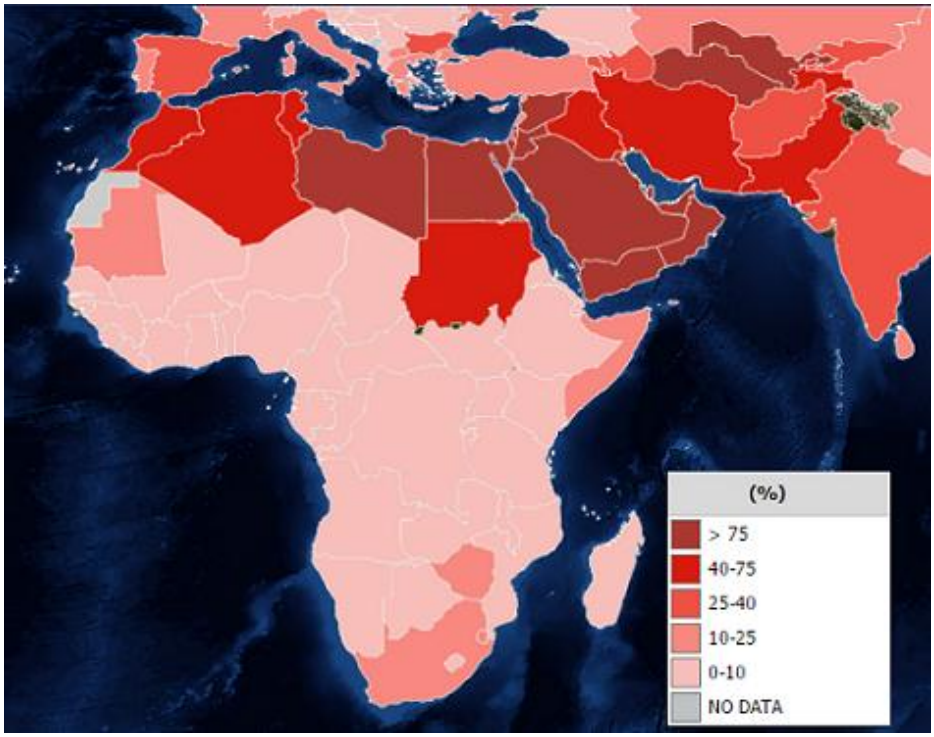

Figure 1.1 Percentage of depletion of freshwater resources [2].

Figure 1.2 demonstrates global energy consumption according to a report issued by the Renewable Energy Policy Network for the 21st Century in 2016 [7]. It can be seen that

fossil fuels are the dominant energy resource used to satisfy the global demand, representing around 78.3%. All renewable energy sources represent about 19.2% of the total, while the remaining demand of 2.5% is obtained by utilizing nuclear energy.

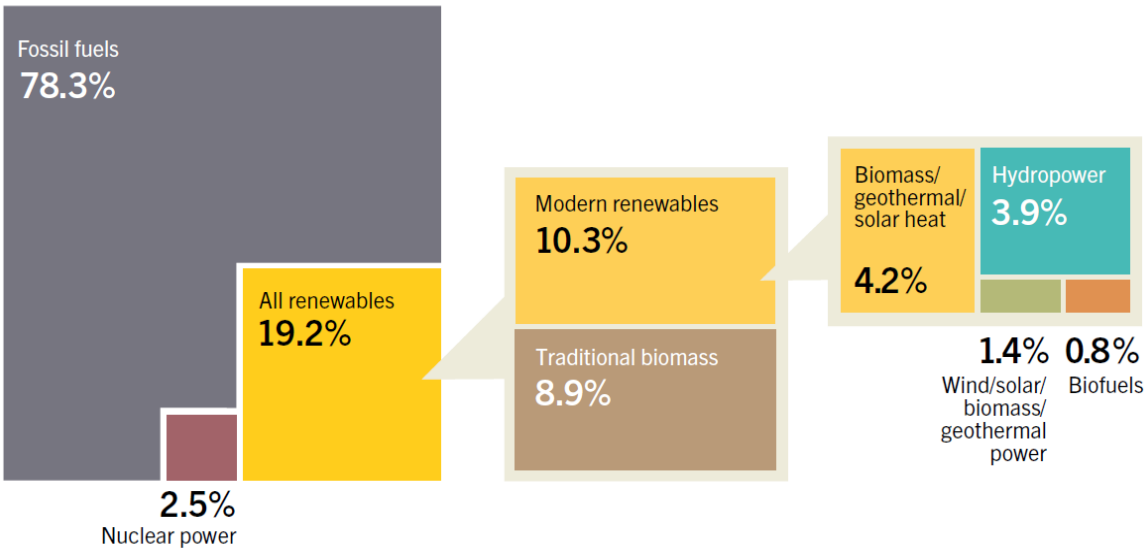

Figure 1.2 Estimated renewable energy share of global energy consumption [7].

For all the aforementioned reasons, numerous studies have been conducted concerning the utilization of alternative energy sources such as renewable energy to power various desalination systems. One of these renewable energy resources is solar energy. Solar energy is a sustainable, non-depleting and environmentally friendly energy source and can be used directly as the thermal energy without any conversion process or it can be converted into electrical power first, using PV technology. Therefore, solar energy is considered to be one of the most important clean sources of renewable energy which could be utilized in various engineering applications.

Seitz and Hite (2012) [8] pointed out that the total amount of solar energy received by the planet throughout one year is approximately ten times that available from all reserves of fossil fuels and uranium on the earth. The annual amount of energy reaching the Earth from the sun is estimated to be about 82 x 10^{15} Watts which is more than 5200 times global energy consumption in 2006 [9].

Figure 1.3 demonstrates the annual solar irradiation in the MENA region. It is obvious that many countries in the region receive considerable amount of solar radiation. Therefore, taking into consideration levels of energy consumption and the environmental impact of burning carbon-rich fuels, it is clear that the coupling of solar energy to seawater desalination to produce potable water is a promising option.

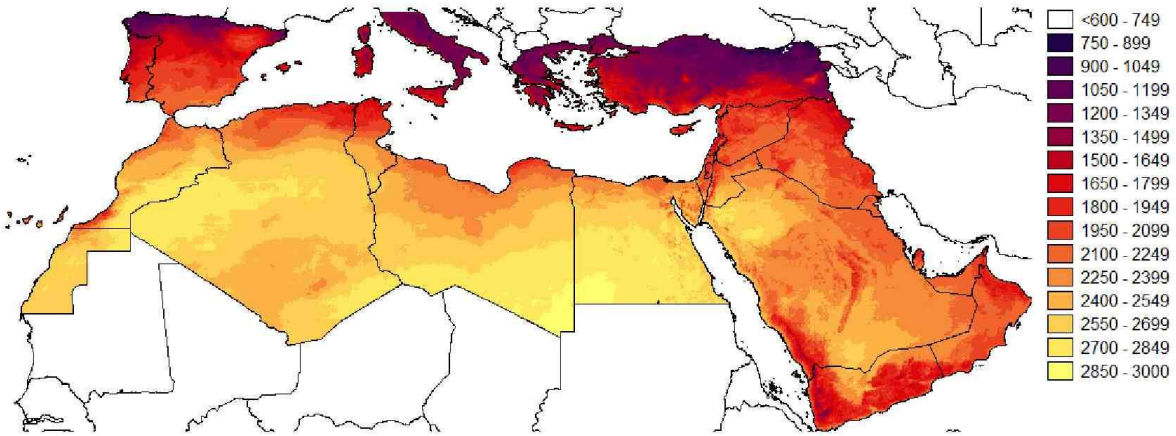

Figure 1.3 Annual direct normal solar irradiation in MENA in kW h/m^2 [10]

1.2 Problem Statement

In recent decades, extensive research has been carried out on solar desalination systems in order to enhance their performance and to improve their cost-effectiveness. Solar basin-type solar stills are considered to be a promising renewable technology that can be used to produce potable water using solar thermal energy. The major benefits of these systems are their simple construction, low maintenance requirements and high flexibility and safety in operation. Nevertheless, the intermittent availability of solar radiation affects the performance of these systems and, because such systems are often characterized by relatively low production capacity, it is a challenging task to improve the performance of solar water stills in terms of productivity and efficiency.

This research makes a contribution to the growing field of scientific studies of renewable energy applications, and specifically to using solar energy in seawater desalination systems. The original method to enhance the performance of a small-scale solar desalination system is presented in this study. The research introduces theoretical and experimental investigations of a dynamic solar water desalination using multi-effect water stills with reduced internal pressure. This system was initially developed by Prof K. Mahkamov. A dynamic water desalination laboratory prototype was built at Northumbria University. It consists of a water still with four stages coupled to evacuated tube solar collectors and a fluid piston energy converter. This energy converter was tested to find out its capacity to achieve vacuum conditions inside the desalination system so it could operate under low pressure, which is below the atmospheric level. When internal pressure is reduced, the corresponding saturation temperature of the seawater also is reduced in the

system. This drop in pressure and saturation temperature intensifies the evaporation process and leads to an increase in the productivity of the system.

In this project, a theoretical and experimental investigations were carried out on the performance of multi-effect water stills. In the theoretical study, a dynamic mathematical model was developed in MATLAB/Simulink environment which consists of a system of ordinary differential equations, to simulate the operation of the proposed system. Experimental tests have been conducted on the developed set-up in the University's Energy Laboratory. During the experiments, operational parameters were monitored and recorded and the experimental results obtained were utilized to examine the accuracy of the mathematical model, which in turn, was used to propose further improvements in the system.

1.3 Aims and Objectives

The aim of this work is to investigate experimentally and theoretically the operation of a solar water desalination system consisting of a multi-effect water still, evacuated tube solar collectors with heat pipes, and a fluid piston energy converter. In order to achieve vacuum conditions inside the system without using an external vacuum pump, the fluid piston converter coupled to evacuated solar collectors, is used to evacuate air from the system and consequently reduce its internal pressure for the intensification of saline water evaporation.

The system was comprehensively studied under different operating conditions in order to investigate the effect of reducing internal pressure on the performance. The main objectives of this study can be summarised as follows:

a) To develop a dynamic mathematical model of the operation of a multi-effect water desalination system to be used for theoretical analysis and to propose design improvements.

b) To build a laboratory prototype of the proposed desalination system to conduct experiments in order to determine the performance of the system in Libyan climatic conditions.

c) To use the developed mathematical model to carry out investigations on the performance of the system and propose further modifications in the design to improve its performance.

1.4 Contribution to Knowledge

This project proposes original design for solar desalination based on application of multi-effect still, coupled to fluid piston thermal energy converter, with both being run with thermal energy output in a solar collector. Investigations of the performance of such the novel small-scale desalination system were performed. The operation of the proposed system under self-provided vacuum conditions was investigated. An accurate dynamic numerical simulation model was developed, for evaluation of the overall performance of the desalination system over a broad range of operating conditions. This model, which was experimentally calibrated, can be used to evaluate the system performance throughout any day over the different seasons and at any geographical location.

1.5 Research Outcomes

The findings of this study have been partially presented in the following conference papers:

1. N. Elsharif and K. Mahkamov. Multi-effect solar water still with evaporation pressure self-reduction capability. *Proceedings of the 6th International Conference on Clean and Green Energy (ICCGE)*, Frankfurt, Germany, 2017.
   This paper was selected as the most excellent oral presentation in the conference, see Appendix A.

2. Above paper is published in *Journal of Clean Energy Technologies*, Vol. 6, No. 2, March 2018.

3. N. Elsharif, K. Mahkamov, K. Hossin and G. Hashem. Enhancing the performance of a multi-effect solar water still using evaporation pressure self-reduction technique. *Proceedings of the International Research Conference on Sustainable Energy, Engineering, Materials and Environment (IRCSEEME)*, Newcastle, United Kingdom.

4. The developed mathematical model of the evacuated multi-stage solar stills can be used to conduct further investigations for application of this technology at different geographical location and seasons in Libya.

5. The developed experimental setup will be introduced at a number of educational institutes in Libya in order to spread the knowledge of such the system and also to find a government subsidy to assist the commercialisation of the system and make it available to all arid areas.

1.6 Thesis Outlines

This research has been conducted in several stages and, accordingly, the structure of the thesis reflects the logical sequence of the execution of the research. In addition to this introductory chapter, the thesis contains the following:

- **Chapter 2 Solar Desalination Systems.** In this Chapter, a comprehensive literature review of previously published research on solar desalination systems is presented. Special attention was paid to the operating principles of various solar systems, their designs and system configurations and associated advantages and drawbacks, as well as to recent achievements in solar water desalination technologies. In the final part of this chapter, the main conclusions made from the literature review and a description of the knowledge contributions of this research are presented.
- **Chapter 3 Mathematical Modelling of the Dynamic Multi-Effect Solar Water Still.** This Chapter is devoted to developing a thermodynamic mathematical model of the dynamic multi-effect solar water still. This includes the design and the operating principles of the proposed system. The mathematical model is developed by applying mass and energy balance for all stages of the system and deriving the governing equations. Subsequently, the governing equations of the system are solved using a Simulink/Matlab environment, and finally the numerical results from the mathematical model are presented and discussed.
- **Chapter 4 Experimental Investigation of the Dynamic Multi-Effect Solar Water Still.** The experimental set-up of the laboratory prototype of an evacuated multi-stage solar desalination system is presented. Moreover, all the components

of the solar still and instrumentation with sensors and data acquisition system, used to conduct the experiments and to collect data, are described. Finally, the experimental procedures and the experimental results obtained are presented and discussed.

- **Chapter 5 Validation of Mathematical Model with Experimental Results.** The dynamic mathematical model of the evacuated multi-stage solar desalination system was validated against the experimental results obtained. Furthermore, this chapter presents an analysis of the agreement between the numerical and experimental results in terms of the temperature and distillate productivity of each stage of the system.
- **Chapter 6 Influence of Internal Pressure Level on the Performance of the Multi-Effect Solar Water Still.** This Chapter presents further investigation of the effect of the pressure level inside the stages on the performance of the desalination system. The performance of the proposed desalination system at different pressure levels is investigated and discussed.
- **Chapter 7 Conclusions and Recommendations for Future Work.** This Chapter presents the significant findings of the study and the conclusions from the theoretical and experimental work. Finally, recommendations for future investigations are described.

Chapter 2 Solar Desalination Systems

In this chapter types of solar energy driven water desalination systems and their principal of operation, advantages and drawbacks are described. An extensive review was performed on recently conducted research on solar water desalination technologies. Finally, the contribution of this project and its main research activities are discussed.

2.1 Introduction

Interest in renewable energy resources such as solar energy has grown due to significant negative environmental impact of using fossil fuels. Among the broad range of application of solar energy, its utilization to drive brackish water desalination systems is very important for numerous countries. These solar-assisted systems, called solar water desalination systems, can be classified into two types, based on the driving power. In the first, the desalination system is operated autonomously by converting solar energy into the required thermal energy to drive the phase-change process without the aid of external energy sources. Solar energy can be transformed into thermal energy by means of various solar energy collectors: flat plate, stationary compound parabolic, evacuated tube and concentrating collectors [1].

In the second type of solar desalination systems, solar energy is used to support conventional desalination systems. This may involve conversion to thermal energy, such as in non-membrane-based solar desalination systems, including multi-stage flash (MSF) desalination, multi-effect distillation (MED), vapour compression (VC) desalination and freeze desalination. Alternatively, PV technology can be used to produce the electrical

power needed to operate membrane-based solar desalination systems, such as in solar powered reverse osmosis desalination, solar-powered electro-dialysis (ED) and solar-powered membrane distillation (MD) [11].

2.2 Solar Desalination Technologies

Production of potable water by means of conventional seawater desalination processes requires a large amounts of fossil fuel, negatively affecting the environment. Therefore, taking into consideration the energy consumption involved and the long-term negative environmental impact of burning hydrocarbon fuels, the application of solar energy for seawater desalination to produce potable water is a very attractive alternative.

Based on the mechanisms of harnessing solar energy, solar desalination processes can be categorized into two sorts namely, direct and indirect processes. In the former, solar radiation is absorbed and utilized to produce distillate in the same unit. Meanwhile in the latter, the desalination processes occur through two separate subsystems: the first is the solar energy collection system used to transform solar energy into thermal energy, and the second is the desalination system [12] .

2.3 Direct Desalination Systems

Various designs and configurations of direct solar desalination techniques have been developed, which include solar stills, humidification-dehumidification processes and solar chimneys.

2.3.1 Solar Stills

A single basin-type solar still is a simple solar technology that can be utilized to produce potable water from impure, brackish water. Desalination processes in solar stills mimic the natural hydrological cycle of evaporation and condensation. The principles of the solar desalination processes in nature and in a single solar still are demonstrated in Figures 2.1 and 2.2 respectively.

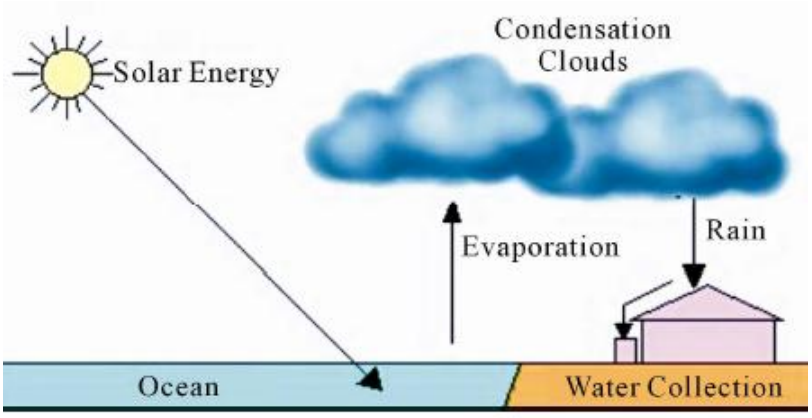

Figure 2.1 Principle of desalination process in nature [13]

Saline water in the basin of the still is heated up by the incident solar radiation, which passes through the glass cover of the still, and evaporates. The distilled water vapour condenses on the underside surface of the glass and all impurities such as salts, contaminants and solid materials remain in the basin. Eventually, the condensed distillate trickles into the trough and is collected in a freshwater container [14]. Solar stills can be categorized based on basin water temperature into two basic groups: low temperature passive solar stills and high temperature active solar stills.

2.3.1.1 *Low Temperature Passive Solar Stills*

Low temperature passive solar stills are solar distillers that only use the rays of the sun for operation and do not deploy any external heat sources to heat up the water in the basin. In this review, particular attention is paid to the most common designs of passive solar stills: basin-type, wick, and diffusion solar stills and also some special designs of solar stills.

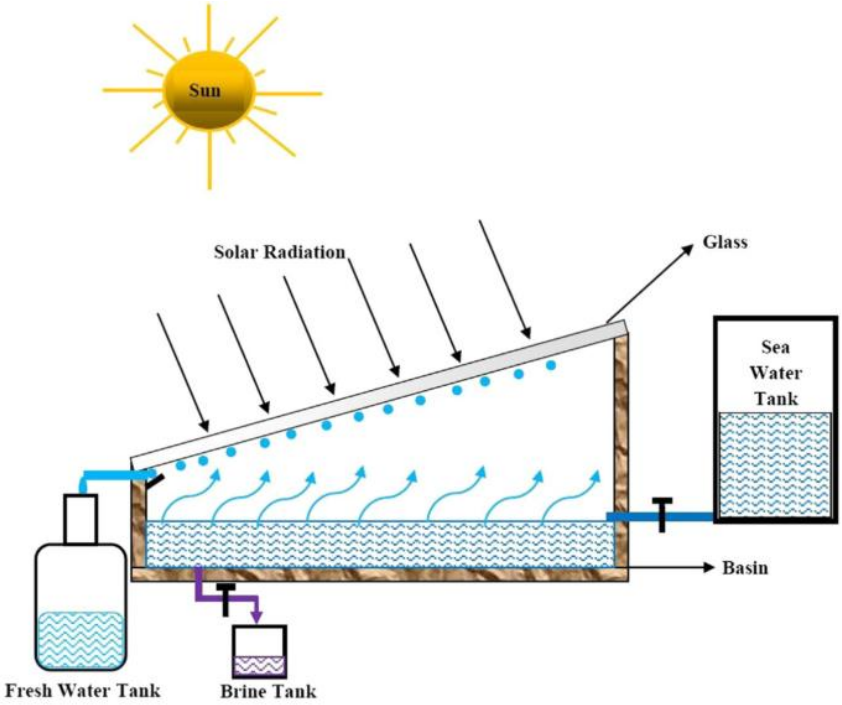

Figure 2.2 Description of solar desalination process [11].

Basin-type Solar Stills

The single basin solar still is simple to construct and operate. In general, this type of still comprises a thermally insulated, air-tightened enclosure which contains a black painted basin and a sloping transparent glass cover. A schematic diagram of a conventional single-basin solar still is presented in Figure 2.3.

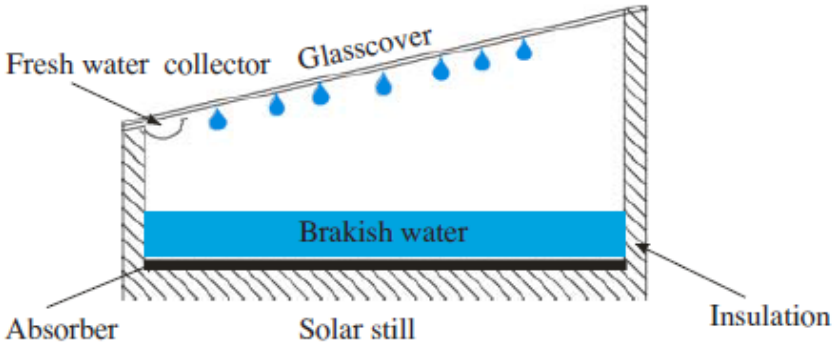

Figure 2.3 Schematic diagram of a single basin solar still [15]

The performance of the solar still is generally evaluated by its productivity which is the amount of freshwater produced by the system per area of solar collectors used. The productivity of ordinary basin-type solar stills is relatively low. In this context, many extensive experimental and analytical investigations have been conducted on single basin stills in order to improve their efficiency and productivity. These efforts have focused on the primary factors affecting their performance: the design of the still, enhancing the condensation and evaporation processes, or increasing the temperature difference between the saline water and condensing surface basin.

Tiwari and Tiwari [16] presented a theoretical and experimental investigation into the performance of a single slope still. The investigation was conducted throughout one year for various depths of water in the basin. The results showed that a solar still with shallower water generally provided higher productivity over the year, and its daily yield in summer was around 67% greater than in winter. Tiwari et al. in [17] carried out an experimental study on a single basin still with a single slope and double condensing chamber. They stated that, due to a high difference in vapour pressure between the two chambers, there

was a considerable enhancement in thermal performance, with an increase in the daily distillate yield between 35% and 77% compared to the conventional solar still.

Moreover, El-Sebaii [18] developed a mathematical model for a triple-basin solar still to investigate the effect of the mass of water in each basin with various wind speeds on still performance. It was found that these parameters have a considerable influence on the total daily yield. Al-Karaghuli and Alnaser [19, 20] conducted a theoretical and experimental investigation of the performance of single basin and double basin solar stills. They reported that the daily average production of the double basin still was about 40% greater than that of the single basin still. Furthermore, a numerical study of the influence of still cover inclination and solar radiation on the performance of a stepped solar still was reported by El-Samadony et al. [21]. It was found that the inclination angle of the glass cover together with solar radiation have a strong influence on the productivity of the stepped solar still.

Further attempts were made to investigate the performance of the single basin solar still. Thus, Khare et al. [22] developed a 3-dimensional CFD model of a single slope still. They conducted a parametric study to improve the productivity by using various basin materials and water depth. Similar investigations were carried out by Panchal and Patel [23]. Feilizadeh et al. [24] investigated theoretically and experimentally the distillate productivity enhancement of a single slope basin-type water still by varying the still's dimensions. They stated that the production rate decreases with the increase of the height of the still's wall and can be increased by extending the still’s length. The optimal length to width ratio was found to be 2.5.

In addition, Altarawneh et al. [25] studied numerically and experimentally the performance of a single basin water stills with various glass cover shapes namely, single slope, double slope and pyramidal cover. It was reported that the solar still with pyramidal cover demonstrated less productivity compared to the other. Khechekhouche et al. [26] conducted experimental investigations of the seasonal changes on the productivity of a basin type solar still in Algeria. It was observed that the weather conditions were significantly influential on the still's productivity and the daily productivity in summer and winter were found to be 1127 and 119 ml, respectively.

Enhancing the Condensation and Evaporation Processes

It has been found that the rate of condensation and evaporation and consequently the productivity of a solar still could be enhanced by increasing the glass-water temperature difference. Abu-Hijleh and Mousa [27] studied the influence of cooling the glass cover with water film on the performance of a single solar still. The results showed that the efficiency of the still was enhanced by up to 20%. Haddad et al. [28] presented a mathematical model of a basin-type still, augmented by a radiative cooling system which was used as a condenser in order to improve the condensation process. They stated that the proposed modification led to significant enhancements in still's efficiency. A comparative experimental study of the performance of an asymmetric single basin still, fitted with mirrors on its internal walls, and of a symmetric single basin solar still was conducted by Al-Hayek and Badran [29]. The results showed that the productivity of the asymmetric still was 20% greater than that of the symmetric still, whereas of the former efficiency was increased by 11%. Moreover, Fath and Hosny [30] conducted a theoretical study of the thermal performance of an unsymmetrical double slope basin still where one of its glass

covers was equipped with fins and permanently positioned in the shaded area, to be used as an additional condenser. They concluded that the productivity of the proposed still was greater by about 55% than the reference case.

Many attempts have been made to enhance the evaporation and condensation processes in basin-type solar stills. Hidouri et al. [31] presented a theoretical and experimental investigation results, using a heat pump to increase the evaporation and condensation rates and to enhance the performance of a basin-type solar still. The heat pump condenser was submerged in basin water and the evaporator was located close to the tilted glass cover. It was observed that utilizing the heat pump increased the daily yield of the still by 10 litre/m^2 while the average efficiency was increased by 60%. A theoretical and experimental investigation of a single basin still with a pyramid-shaped glass cover was conducted by Mahian and Kianifar [32]. A schematic diagram of their pyramid-shaped solar still is presented in Figure 2.4. They studied the effect of forced convection caused by a low-cost fan inside the still. The results obtained illustrated that the daily production of freshwater increased by about 56%.

Taamneh and Taamneh [33] also studied experimentally the performance of a pyramid basin solar still enhanced by a fan operated using a PV panel. They claimed that the influence of forced convection by the fan improved the still's productivity by 25% compared to a typical solar still.

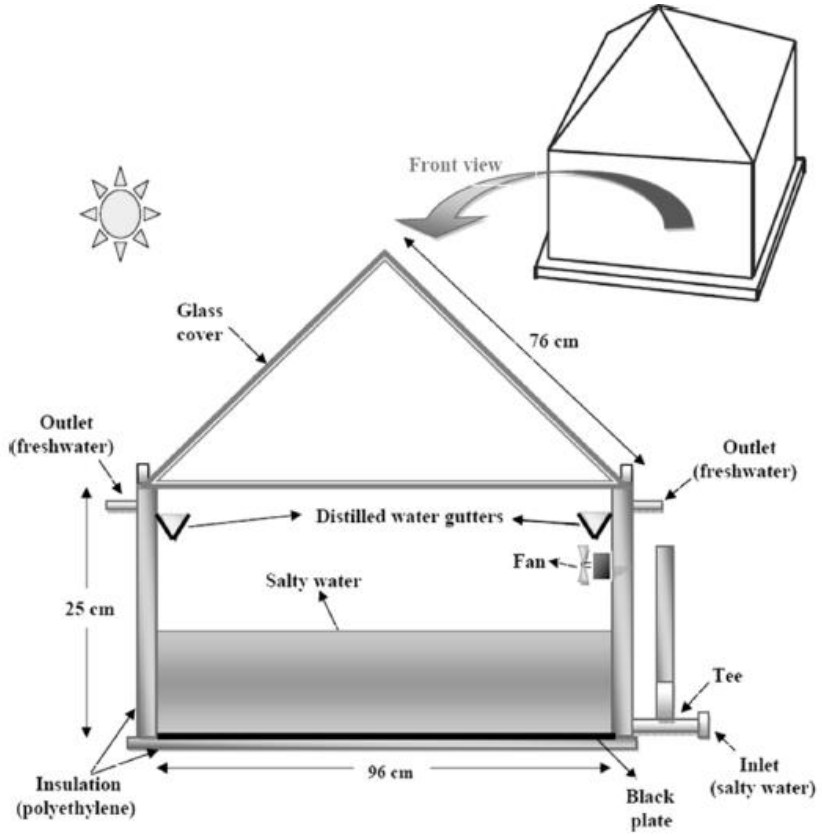

Figure 2.4 Schematic diagram of a pyramid-shaped solar still [32]

Also, a number of attempts were made to improve the performance of the conventional stills by enhancing the evaporation process. Hassan and Abo-Elfadl [34] carried out experimental investigations on the effect of using different types of condensers. Four condensers were used: glass, aluminium plate, aluminium heat sink with fins and covered aluminium plate, see Figure 2.5. The authors stated that the type of condenser used had a great influence on the performance of solar stills.

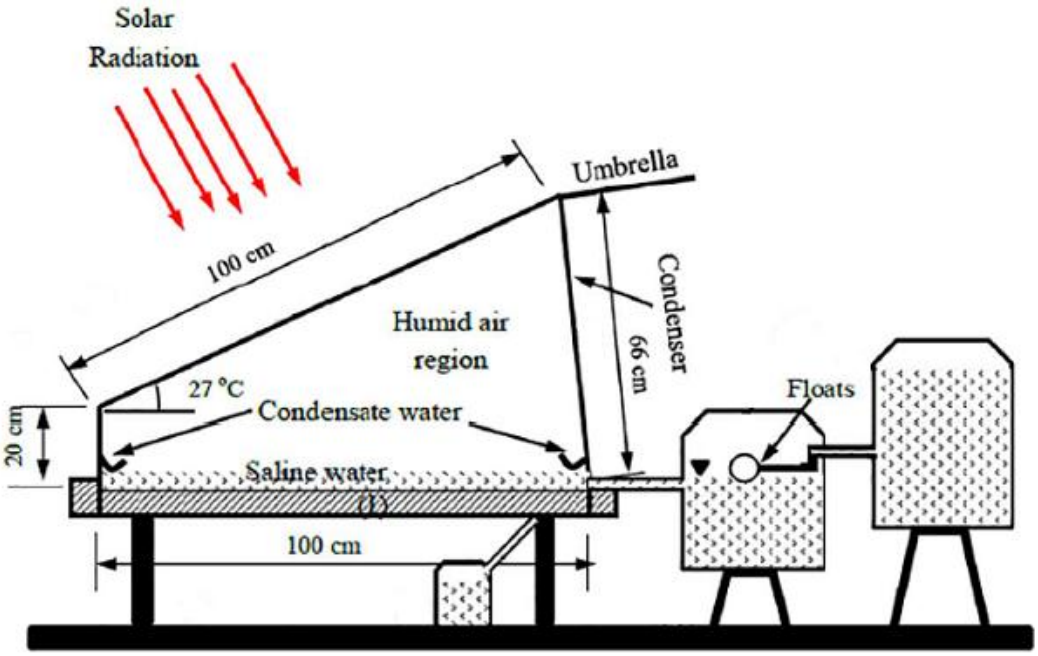

Figure 2.5 Single slope solar still with condenser [34].

Kumar et al. [35] presented a hybrid (PV/T) active solar still in which the saline water is pre-heated when is used to cool the PV panel. It was observed that the daily yield of the modified hybrid solar still was six times greater than that of the passive conventional still. El-Sebaii and El-Naggar [36] conducted theoretical and experimental studies on the performance of basin type solar stills with finned basin liners made of different materials. The results showed that the daily productivity of the conventional solar still was improved by around 16% with using the finned liner. However, the effect of the type of the fins material on the performance of the still was not significant.

Absorber

El-Sebaii et al. [37] investigated theoretically and experimentally the utilization of a metal plate floating on the water surface in order to increase the saline water temperature and consequently to decrease the time required for water to evaporate. The results obtained

showed that there was an improvement in daily productivity by about 20% over that of the ordinary still. Likewise, Valsaraj [38] fabricated and studied experimentally the performance of a single-slope basin still with a suspended aluminium plate. It was reported that distillate production was markedly enhanced. Montazeri et al. [39] carried out a theoretical and experimental investigations on the enhancement of an ordinary cascade or a step-type solar still by using Aluminium sheet as an absorber plate as shown in Figure 2.6. They stated that in the summer time, the productivity of the modified cascade solar still enhanced by 16% compared to that of the ordinary cascade solar still.

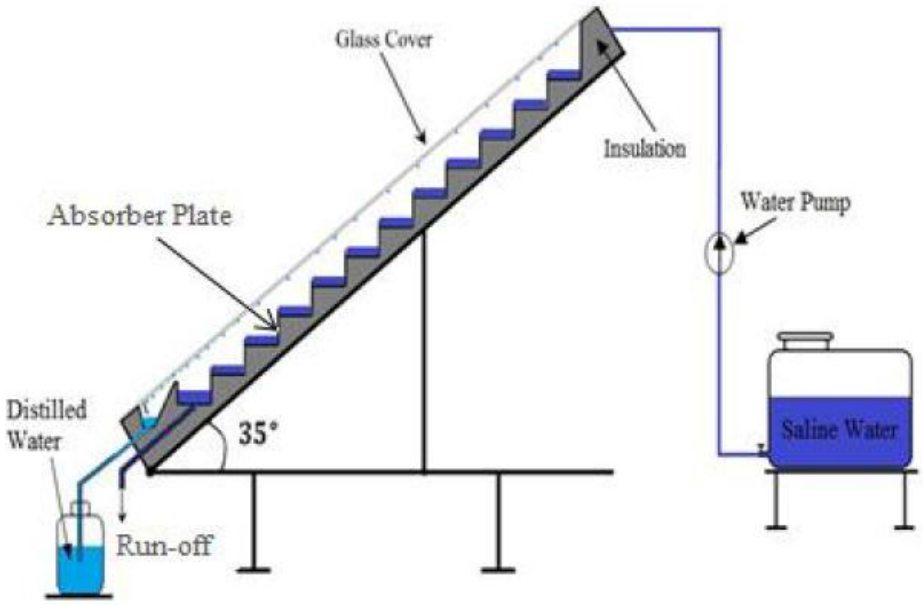

Figure 2.6 Schematic diagram of step-type solar still with absorber plate [39].

Furthermore, Hansen and Murugavel [40] presented results of the experimental study on the performance of a single basin solar still integrated with a hot water storage tank and an inclined solar still. Experiments were conducted for three types of absorber namely flat

absorber, grooved absorber and fin shaped absorber. It was observed that the integrated still with fin shaped absorber produced the greatest distillate yield.

Use of Internal and External Reflectors

A theoretical study of a single basin solar still with internal and external reflectors was carried out by Tanaka and Nakatake [41]. They reported that the average daily water productivity throughout the year was considerably increased when the internal and external reflectors were utilized. Similarly, Tanaka [42, 43] investigated experimentally and theoretically the performance of a single basin solar still augmented by internal and external reflectors. It was observed that using internal and external reflectors could improve the still's daily distillate yield by around 70%-100%. However, Khalifa and Ibrahim [44] evaluated experimentally the effect of internal and external reflectors at various inclination angles on the performance of a traditional solar still in different seasons, and they stated that the reflectors had a negative effect on still productivity in summer. A typical basin-type solar still with internal and external reflectors is illustrated in Figure 2.7.

A number of studies were conducted to enhance the performance of the basin type water stills. Gnanaraj and Ramachandran [45] presented an experimental investigations of single slope solar still combine with a mini solar pond and with reflectors installed on the top of the still and pond. It was reported that these modifications significantly enhanced the overall performance of the solar still (by about 96%) compared to that of the conventional still.

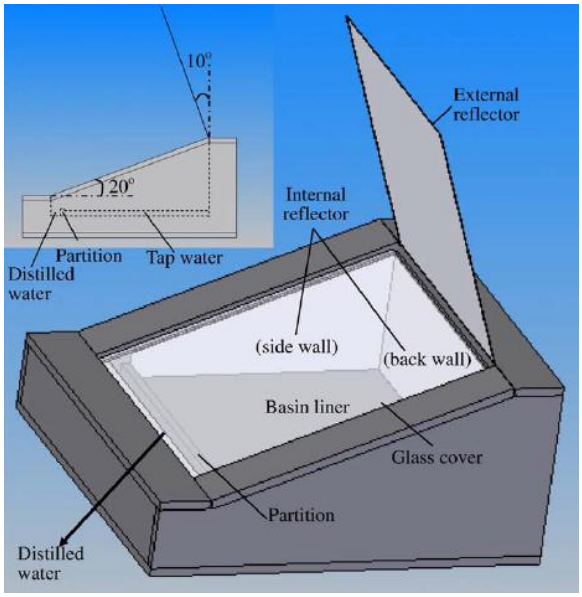

Figure 2.7 Typical basin-type solar still with internal and external reflectors [42]

Omara et al. [46] performed experimental and theoretical studies on the performance of the stepped solar still with internal reflectors and of the conventional solar still. The effect of installation of mirrors on the vertical sides of all steps was investigated. The results indicated that the daily productivity of the step-type solar still with and without internal mirrors was greater than the daily productivity of conventional still by around 75% and 57%, respectively.

Use of Heat Storage Medium

An experimental and mathematical modelling study was conducted by Sakthivel and Shanmugasundaram [47] to analyse the performance of basin-type solar still with black granite gravel as a heat storing material. It was observed that values of productivity and efficiency of the modified still were higher than those of a conventional still by 17% and 8%, respectively. Harris Samuel et al. [48] carried out a theoretical and experimental

investigation into the enhancement in yield of a conventional single basin still with two low-cost energy storage materials which were sponges and plastic balls filled with salt. Figure 2.8 presents a schematic diagram of a conventional single-basin solar still with salt balls.

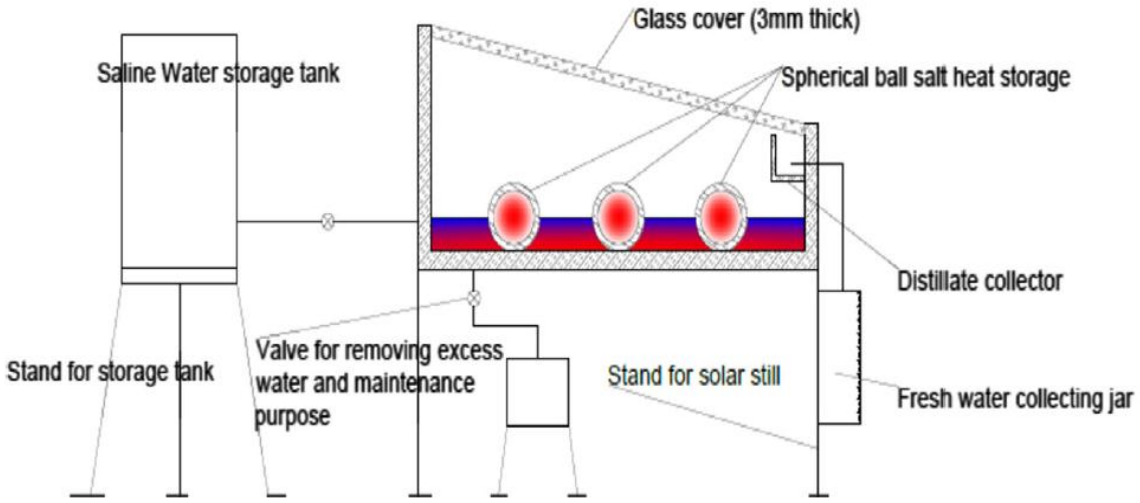

Figure 2.8 Schematic diagram of a single basin solar still with salt-filled balls [48].

It was reported that the conventional solar still with salt-filled balls produced the maximum yield of 3.7 kg/m^2 compared to 2.7 kg/m^2 for the still with sponges and 2.2 kg/m^2 for the conventional solar still. Moreover, a conventional solar still and solar still augmented by a phase-change material as a heat storage medium were designed, fabricated and tested by Kabeel and Abdelgaied [49]. The results obtained showed that the daily productivity of the conventional solar still was increased by around 67% when the heat storing material was added.

Panchal et al. [50] studied theoretically and experimentally the performance of the solar still with two different heat energy storage materials, namely, sandstones and marble

pieces. They claimed that using the sandstones and the marble pieces as a heat storage material inside the basin of the conventional solar still increases the daily yield by 30% and 14%, respectively. Kabeel et al. [51] presented results of the experimental investigation on improving the productivity of conventional single basin solar still by utilizing the heat storage material wrapped in jute cloth. It was found that the productivity and waterbed temperature were higher when the heat storage material was used compared to that of conventional single slope solar still.

Use of Nanoparticles

Experimental attempts have been made to improve solar still performance by utilizing Nano-fluids, which are suspended Nano-sized solid particles in saline water. Adding nanoparticles to the water enhances the heat transfer characteristics and the evaporative properties of the saline water, and consequently increases the productivity of the solar still. Kabeel et al. [52] studied experimentally the performance enhancement of a single basin solar still integrated with an external condenser when aluminium oxide nanoparticles were added to the basin water. The results showed that the productivity of the basin still could be improved by 16% when nanoparticles were added to the basin water.

Elango et al. [53] compared experimentally the performance of basin type solar still with different types of Nano-particles of Zinc, Aluminium, Tin and Iron oxides of various concentrations. They indicated that the productivity of solar stills with Nano-fluids were increased and the solar still with aluminium oxide produced highest yield with about 30% increment compared to the same solar still without Nano-fluids. Furthermore, theoretical study on the effect of using aluminium oxide nanoparticles with three concentrations on the performance of passive single basin double slope solar still was carried out by Sahota

and Tiwari [54]. It was determined that the daily productivity of the solar still increased with the rise in the aluminium oxide concentration in the waterbed.

Recently, Sharshir et al. [55] conducted experimental investigation to enhance the performance of solar still by using two Nano-flakes, namely, graphite and copper oxide with different concentrations. They reported that the improvement of modified still yield with cooling the glass cover was approximately 54% and 45% for the graphite and copper oxide, respectively.

The Main Advantages and Drawbacks of Basin-type Solar Stills

In spite of that the significant benefits of conventional basin-type solar stills, various disadvantages prevent the widespread adoption of these types of stills. The main advantages and drawbacks of low-temperature passive solar stills are as follows:

- Simple system requires only basic skills for construction and operation which is suitable for remote areas [56].
- Minimum maintenance and operational costs [13].
- Productivity of the system is limited by the large thermal capacity of the saline water in the still basin [44].
- The horizontal surface of the saline water receives lesser solar radiation [44].
- The system is not economical for large-scale applications because of high initial costs and low daily production rates of about 4-5 L/m^2 [6].
- The system's thermal efficiency is low with a maximum value being around 52% [45].

- The increase of salt sedimentation in the basin leads to a considerable decrease in the productivity [43].
- These require larger land area for construction [46].
- Sensitivity to extreme weather conditions and the state of the transparent cover of the still [46].

Wick Solar Stills

The wick solar still is one of the most commonly used techniques which have been adopted in order to address some of the disadvantages of the single basin still and to enhance performance. The operating principle of the wick still is based on lowering the saline water depth in the basin-type still to significantly improve the rate of distillate production, mainly due to the decreased volumetric heat capacity and increase in water basin temperature which enhances the evaporation process [57]. As illustrated in Figure 2.9, the wick still comprises a blackened wet wick material (jute, cotton, metal, etc) which acts as the liquid surface. The main advantage of using the wick is that the basin water remains as shallow as possible whilst avoiding dry spots. Wick solar stills can be classified in three types: the single wick, tilted wick or multiple wick solar still [58].

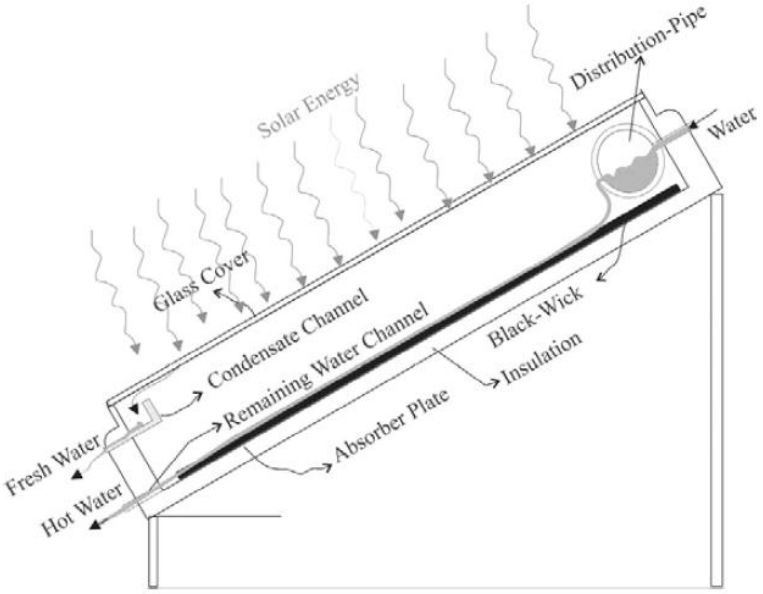

Figure 2.9 Schematic diagram of wick solar still [59].

Single Wick Solar Still

Matrawy et al. [60] carried out theoretical and experimental studies of the performance of a single corrugated-shape black clothe wick solar still augmented by an external inclined reflector aligned with a basin-type still. Authors reported that the productivity of the proposed wick still was greater by about 34% than that of the simple still. The enhancement of the performance of a single basin solar still by using a corrugated wick and internal reflectors on all side walls was experimentally investigated by Omara et al. [46]. Their experimental results showed that the productivity of the modified solar still was enhanced by about 146% compared to the ordinary solar still. Alaian et al. [61] conducted experimental research on the effect of applying a pin-finned wick on the productivity of the conventional solar still. He reported that productivity was increased by more than 23%.

Murugavel and Srithar [62] studied experimentally and theoretically the augmentation of the freshwater yield of a single basin double slope solar still with rectangular aluminium fins covered with various wick materials, as illustrated in Figure 2.10. They stated that the performance of the modified still was significantly improved, especially when the fins were covered by cotton cloth. Kaliappan et al. [63] carried out an experimental investigation of the performance of single and double basin solar stills with various wick materials made of either Jute cloth, cotton and clay pots. It was reported that the provision of wick materials improves the daily productivity of the solar stills. Moreover, Omara et al. [64] conducted an experimental investigation of the effect mixing various types of nanoparticles with the basin water of a corrugated wick solar still.

Tilted Wick Solar Still

In this type of stills, the liquid surface, which is a blackened wet jute cloth, can be inclined to receive maximum solar radiation so that a lesser mass of water will be heated up to a higher temperature and will evaporate rapidly. Aybar [59] carried out an experimental study and mathematical simulation of the effects of solar intensity and feed water flow rate on the performance of a tilted wick solar still, and there was a good agreement between the experimental and simulation results. The improvement in the performance of a tilted wick solar still for the case, in which a flat plate external reflector was added, was investigated by Tanaka and Nakatake [65]. They found that the average daily productivity of the still with the vertical external reflector was 9% greater than that of conventional tilted wick still.

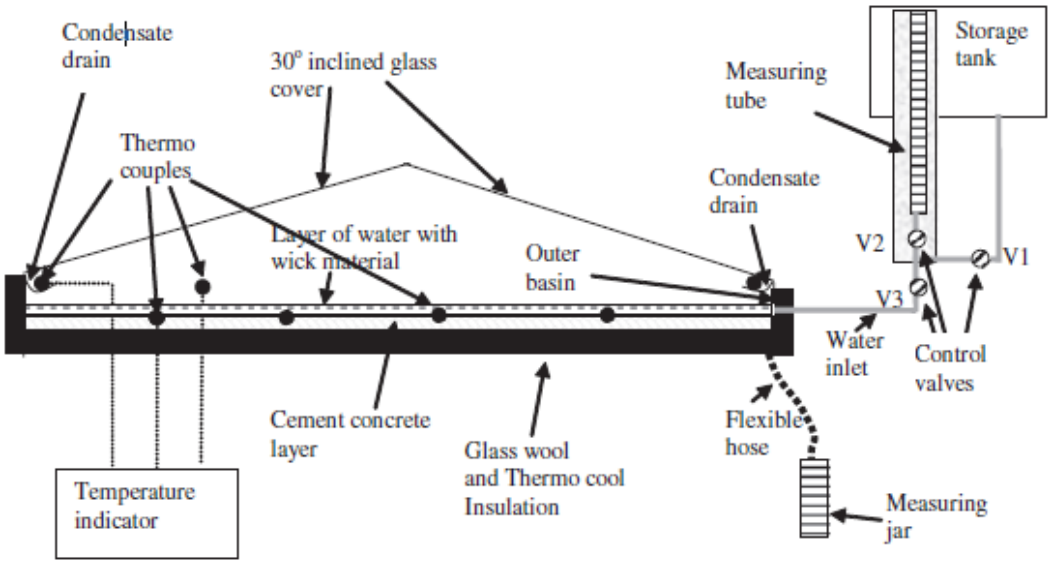

Figure 2.10 Schematic diagram of a basin type double slope wick solar still [62].

Moreover, in order to increase the productivity of the tilted wick solar still with a vertical flat plate reflector, a manually-operated azimuth tracking system was utilized by Tanaka and Nakatake [66]. The theoretical results showed that using the tracking system had a significant influence on the productivity of the tilted wick still (the enhancement was about 57% on a summer solstice day). To enhance the freshwater production rate of the tilted wick solar still, the same authors later in [67] conducted an analytical study on the inclination angle of the external flat plate reflector for the tilted wick solar still. They reported that the daily productivity of the still with an inclined reflector was greater than that of a still with a vertical reflector by 27%.

Tanaka [68] presented a theoretical investigation into the optimum inclination angles of the titled wick still and external reflector. It was found that the productivity of the still could be improved, when the external reflector was inclined forwards in summer and

backwards in winter. The same author then carried out a theoretical investigation in [69] on the performance of a tilted wick still with a flat plate bottom collector. The theoretical results showed that the average daily productivity of the proposed still could be increased by around 13% over the simple tilted wick still. Moreover, Mahdi et al. [70] experimentally studied the influence of feed water salinity and input flow rate on the performance of a tilted solar still with an absorber/evaporator wick, made of charcoal cloth.

Munisamy et al. [71] conducted an experimental investigation of the performance of a tilted wick solar still with different wick materials, namely, terry cloth, jute cloth, polyester cloth and fur fabric. It was indicated that the productivity of the tilted wick solar still was maximum for fur fabric. Sharon et al. [72] performed experimental and theoretical studies on the performance, economic and environmental benefits of a tilted solar still with stepped basin and a tilted solar still with blackened wick. They found that titled solar still with stepped basin demonstrated better performance and was more beneficial, compared to that of the titled solar still with wick in economic terms.

Multi-wick Solar Still

Here the upper ends of wicks are immersed in a saline water reservoir. Suction by the capillary action of the fiber supplies liquid to the surface and the configuration ensures that all the liquid surfaces, exposed to the solar radiation, are always wet. The parts of the cloth which are covered by the polythene sheets will not contribute to evaporation, and as a consequence, the exposed parts of the cloth remain wet [47].

The main difference between the multi-wick and single wick solar stills is that the liquid

surface in the former consists of series or layers of wick materials. Sodha et al. [73] designed and constructed a simple multi-wick solar still in which the wet surface consisted of layers of blackened jute cloth separated by thin layer of polythene sheets. In their experimental and theoretical investigation, they observed a significant improvement in the productivity of the wick stills. Tiwari [74] installed a demonstration plant of a multiple wick solar still and investigated its performance over one year period. It was concluded that the average lifespan of the still could be increased to 20 years by using fibreglass pipes.

Moreover, the effect of increasing the temperature difference between the wet surface of multiple wick solar still and the condensation surface, produced by a thin layer of water flowing over the still cover, was investigated by Dhiman and Tiwari [75]. They reported that distillate production was increased by about 10%. Kumar and Anand [76] carried out a theoretical study on a tubular multi-wick solar still and it was observed that the daily productivity of the proposed tubular multi wick still was 13% greater than that of the traditional multi wick still and 8% higher than that of a simple tubular solar still. Ohshiro et al. [77] studied theoretically and experimentally the performance of a multi-wick solar still which included layers of wick separated by PTFE nets. They reported that productivity was considerably enhanced compared with the conventional wick still.

Pal et al. [78] presented an experimental study to enhance the performance of basin type double slope multi-wick solar still by utilizing various types of wicks. It was observed that for same operational conditions the maximum productivity was obtained in the multi-wick solar still with black cotton wick.

New Designs and Technology

Numerous novel designs have been proposed in order to improve the performance of single basin solar stills. Abdallah et al. [79] investigated experimentally three different amendments to the conventional solar still: the installation of mirrors on the inner walls, the replacement of the traditional flat basin with a step-wise basin and the use of a sun-tracking mechanism with a conventional solar still. The conventional solar still augmented by the sun-tracking system had the maximum productivity improved by 280% compared to the conventional still. Velmurugan et al. [80] also suggested some modifications to augment the evaporation process in order to improve the productivity of simple solar still. They tested the solar still with finned basin and with sponges, and a wick-type still. The increment rise in productivity was 46% when fins were used in the design.

In addition, a number of other attempts were made in order to enhance the performance of the wick solar still. Kabeel [81] designed, constructed, and examined a new pyramid-shaped solar still. The basin of this still is concave with a square aperture and it is covered by a blackened jute wick. The main benefit of this design is that it increases both the evaporation surface area (concave wick surface) and the condensation surface area (pyramid cover) which consequently leads to increasing distillate production. A schematic diagram of a concave wick solar still is presented in Figure 2.11. The experimental results showed that the productivity of the proposed concave wick solar still could reach about the double of that of a conventional solar still.

A new design of a double-sloped single basin still with a rotating cylinder installed in the still cavity was introduced by Ayoub et al. [82]. They reported that the proposed

modification significantly influenced the still's performance and the average daily yield was doubled.

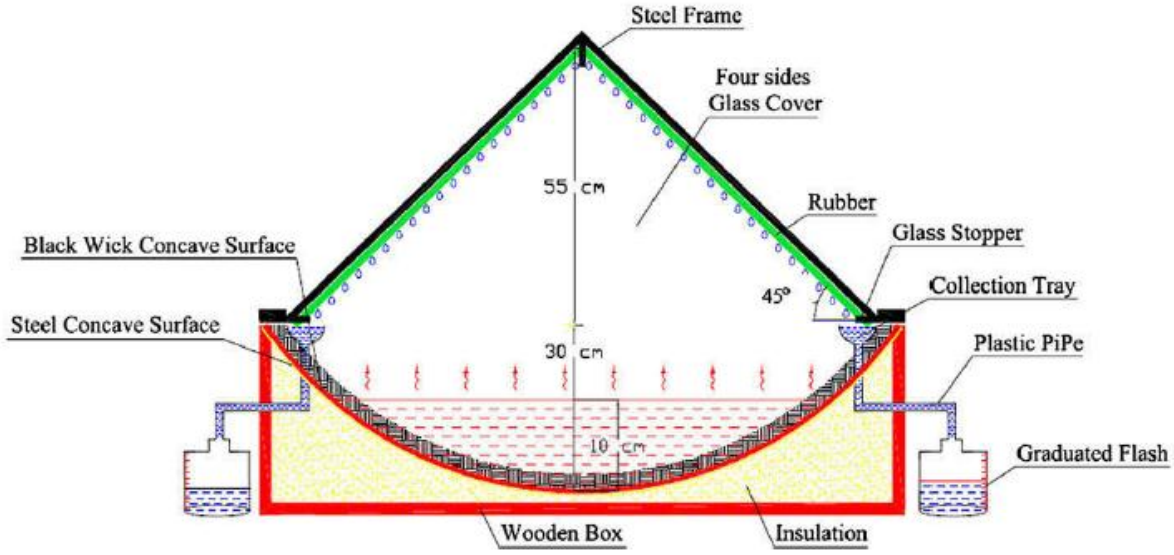

Figure 2.11 Schematic diagram of a concave wick solar still [81].

Furthermore, the effect of utilizing various types of nanoparticles on the productivity of corrugated wick solar stills with internal mirrors and external condensers was investigated experimentally by Omara et al. [64]. Experiments were conducted using two types of nanoparticles: aluminium oxide and cuprous oxide. These were mixed with the basin saline water, and it was found that adding the nanoparticles leads to a considerable enhancement in the productivity of the modified corrugated wick solar still. Productivity increased to 285% when using cuprous oxide and 255% with the addition of aluminium oxide, compared to the productivity of the conventional solar still.

The Main Advantages and Drawbacks of the Wick Solar Stills

The main advantages and drawbacks of utilizing wick solar stills are as follows:

- Improvement in productivity by 20-50% compared to conventional solar stills [1].

- Reduction in the saline water volume leads to increasing basin temperature and improves the evaporation process [61].
- Inclined evaporation surface leads to receiving more solar radiation [25].
- Higher overall efficiency compared to typical basin solar stills [61].
- Natural water supply by the capillary action of fibers [61].
- In the absence of reflectors, the production rate decreases [83].
- Continuous supply of saline water is needed [83].
- High risk of contamination due to the nature of wick materials [83].

Diffusion Solar Stills

The multiple-effect diffusion type solar stills have significant potential because of its simple design and high distillate yields. A simple basin-type, multiple-diffusion solar still is schematically presented in Figure 2.12.

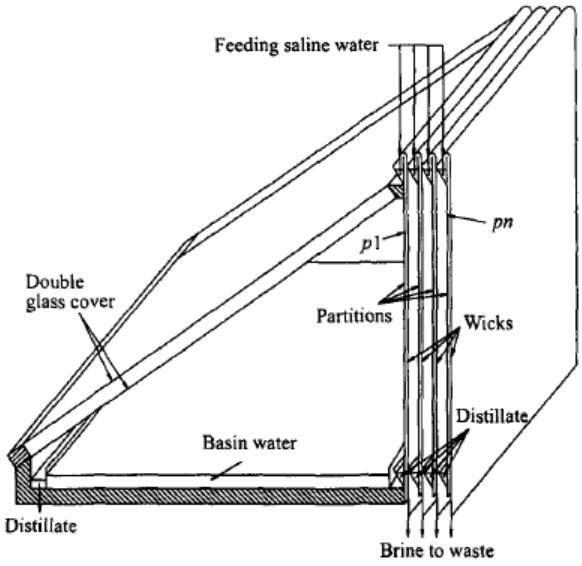

Figure 2.12 Schematic diagram of basin-type, multiple-diffusion solar still [83].

This design consists of a tilted glass cover, a flat blackened surface basin and a number of closely spaced vertical partitions covered with saline-soaked wicks. Solar radiation passes through the double glass cover, leading to the evaporation of the water in the basin, and water vapour condenses on the inner surface of the glass cover and diffuses through the air gap between the partitions to condense on the front surface of the next partition. Latent heat from condensation leads to further evaporation from the saline water soaked wick of the second partition. In this manner evaporation-diffusion-condensation processes are repeated on all gaps and partitions of the multiple-diffusion type solar still and, as a result, the productivity of the still is increased [83].

The performance of a simple basin-type, multiple-effect diffusion solar still of 10 vertical partitions with 5-mm air gaps was examined theoretically and experimentally by Tanaka et al. [84]. The results showed that the efficiency of the proposed still was significantly higher than that of the conventional solar still. The same authors extended their previous work and performed a parametric analysis [85]. They studied the influence of various design and operational parameters on the performance of the still, including the number of partitions, the thickness of air gaps, feeding rate of saline water supplied to wicks, and the initial water depth in the basin. They reported that the distillate yield of a multiple-effect still with 13 partitions and 5-mm diffusion gaps was four times greater than that of the basin-type still and about 40% more than typical multiple-effect solar stills.

Tanaka et al. [83] constructed and carried out an experimental investigation of the performance of a single basin, multiple-effect, diffusion solar still with 5-mm and 10-mm diffusion gaps. The experimental results showed that the productivity of the still with 5-mm gaps was greater than that of 10-mm gaps. Furthermore, an indoor experimental investigation of a vertical multiple-effect diffusion solar still augmented by a heat pipe

solar collector was subsequently carried out by Tanaka et al. [86]. The experimental results showed that the average daily productivity of this still was around 93% of the predicted productivity.

On the other hand, Tanaka and Nakatake [87] introduced a new design of the diffusion solar still, called a vertical multiple-effect diffusion still, as shown in Figure 2.13. In this new design, the solar collector was replaced by a flat-plate mirror in order to concentrate more sunrays on the vertical partitions. They studied theoretically the effect of the inclination angle of the flat mirror and the azimuth angle of the still on productivity, and it was found that these angles both have sizable influences. This theoretical study was then broadened by the same authors in [88]. They presented a parametric investigation examining the influence of various factors on the performance of the proposed system. Their results demonstrated that the daily yield of the new design was considerably higher than that of single effect stills.

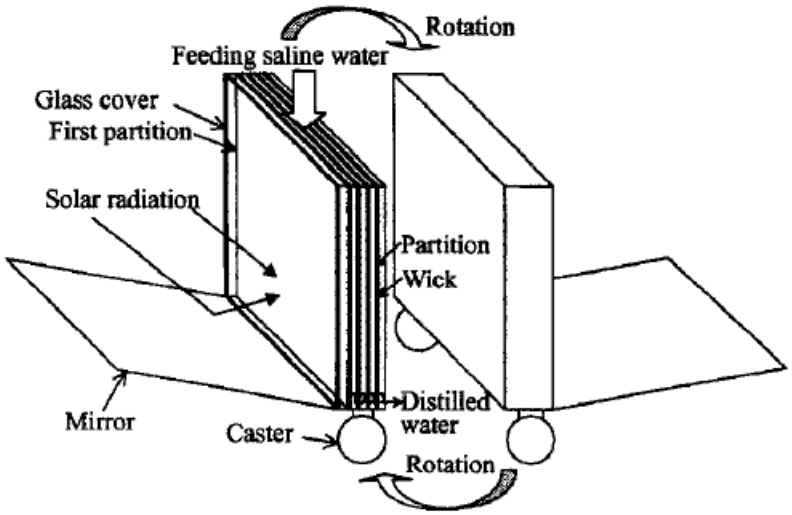

Figure 2.13 Schematic diagram of multiple-diffusion still with mirror [87].

Tanaka and Nakatake [89, 90] carried out a theoretical and experimental investigation of a vertical diffusion solar still with a flat plate solar reflector in order to assess the optimum reflector angle and the most advantageous orientation of the proposed diffusion still at various latitudes and in different months of the year. They reported that the inclination angle of the reflector and the orientation angle of the still should be adjusted according to the season and latitude, and also found that the daily productivity of the vertical multiple-effect diffusion still was 6 times greater than that of a simple single-effect solar still.

In addition, Tanaka [91] performed an outdoor experimental investigation on the performance of a vertical multiple-effect diffusion still with four or six effects and with a stainless steel plate reflector. The experimental apparatus is schematically shown in Figure 2.14. The experimental results showed that the distillate yield of the proposed diffusion still was 5.5 times greater than that of the basin-type solar still.

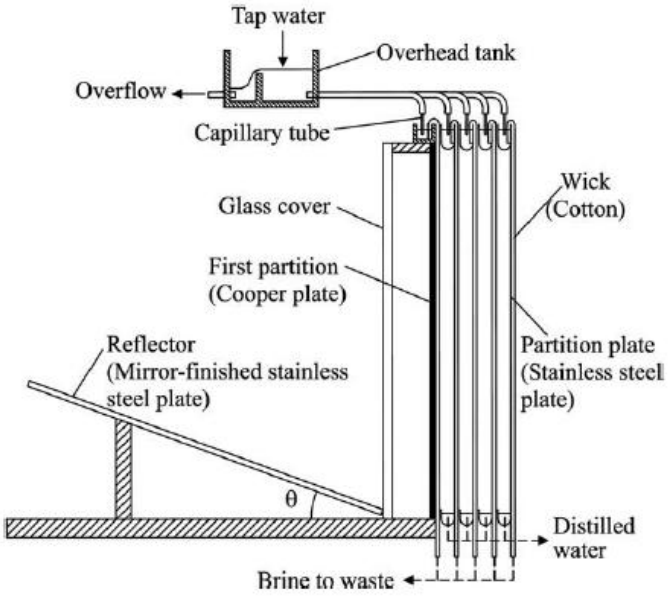

Figure 2.14 Schematic diagram of the experimental apparatus [91]

The same author then analyzed theoretically in [92] the effect of a bottom reflector on the

productivity of a vertical multiple-effect diffusion still coupled with a single basin still. It was demonstrated that using the external reflector has a great influence on the daily productivity of the still.

Tanaka and Iishi [93] carried out an experimental study on the performance of a vertical single-effect diffusion still coupled with a tilted wick still. They investigated whether natural convection can adequately transport water vapor from tilted wick still to the single-effect diffusion still. It was found that the maximum daily yield could reach around 5 kg/m^2. Kaushal et al. [94] performed an experimental and theoretical techno-commercial feasibility study on the design and operational parameters of a basin-type wick still combined with a multiple-effect diffusion solar still and waste heat recovery.

The Main Advantages and Drawbacks of the Diffusion Solar Stills

The use of diffusion solar stills has led to significant improvements in the productivity of solar stills; yet there are some constraints which hinder the employment of these types of solar stills. The main advantages and drawbacks of low-temperature passive solar stills are:

- Simple structure and easily operated system [95]
- Productivity and thermal efficiency of this system are higher than those of other solar stills [95].
- Numbers of partitions and air gaps have the significant influence on system productivity [95].
- Productivity is very sensitive to the size of the diffusion gaps between partitions [95].

Special Designs of Solar Stills:

Many innovative designs have been implemented with a view to improve the performance of solar stills but these configurations are not commonly used. However, in this section, some of the special designs, which are widely recognised, are briefly highlighted.

Greenhouse-type Solar Still

The simplest type of greenhouse-cum-solar still consists of basin-type solar stills, mounted on the roof of a glasshouse for the purpose of providing partial independence in supply of energy and freshwater. The working principle of this combination is that the saline water in the basins is heated up and evaporation starts by means of the absorption of solar radiation. Fresh water vapour then condenses on the surface of the glass cover of the roof and is eventually collected to be used for irrigation purposes in the greenhouse. The remaining absorbed solar energy is transferred to the greenhouse and hence provides the desired environment for the cultivation of plants [95].

The performance of the greenhouse-type solar still has been evaluated by Srivastava et al. [95] and Chaibi [96]. They carried out numerical analyses to study the effect of design and climatic parameters. It was revealed that this still can provide adequate distillate yields and the appropriate temperature and humidity needed for plant growth. Ghosal et al. [97] investigated theoretically the influence of different design and climatic parameters on the performance of a solar still integrated with a greenhouse for the climate of India. He reported that these variables have important effects on the productivity of the system, which is higher in areas with lower ambient temperature. Radhwan [98] also presented a

numerical transient analysis of a stepped solar still used for the purpose of heating and humidifying greenhouses.

Moreover, Radhwan et al. [99] constructed and experimentally investigated the thermal performance of a greenhouse with a set of 24 basin-type solar stills mounted on its roof. This experimental investigation was conducted in Jeddah, Saudi Arabia. They listed various design and operational measures, which can lead to the improved system performance. In similar manner, but for Mediterranean climatic conditions, Mari et al. [100] carried out a performance analysis of 28 single basin stills integrated with a greenhouse, and it was noted that freshwater production occurred even after the daytime hours.

Recently, Salah et al. [101] conducted a theoretical investigation on the enhancement of transparent single basin solar stills integrated with greenhouse. An aluminium metal net with area equal to 20% of the basin area was immersed in the still basin. The solar stills were placed on the roof of the greenhouse. Authors reported that the integrated simple stills-greenhouse system was capable to produce the amount of water required for irrigation and the productivity was increased by 50% when the aluminium net was used.

Tubular Solar Stills

The structure of a simple tubular solar still is presented in Figure 2.15. It is formed from a blackened semi-circular trough which contains saline water, and installed inside a larger transparent tube. The operating principle of the tube-type still is the same as that of a simple basin solar still: the bed water evaporates by receiving and absorbing solar radiation

and eventually vapour condenses on the inner surface of the outer tube and is collected [102].

Murase et al. [102] and Murase et al. [103] presented experimental and theoretical investigations of a tubular solar still for desert cultivation purposes, and they stated that the system can provide sufficient water supplies in desert areas. Ahsan and Fukuhara [104] proposed a new simulation model for the performance of a tube-type solar still taking into consideration water-air mixture properties. Ahsan et al. [105] and Ahsan et al. [106] then designed, constructed and carried out outdoor experiments with the tubular solar still and listed important parameters, influencing its productivity.

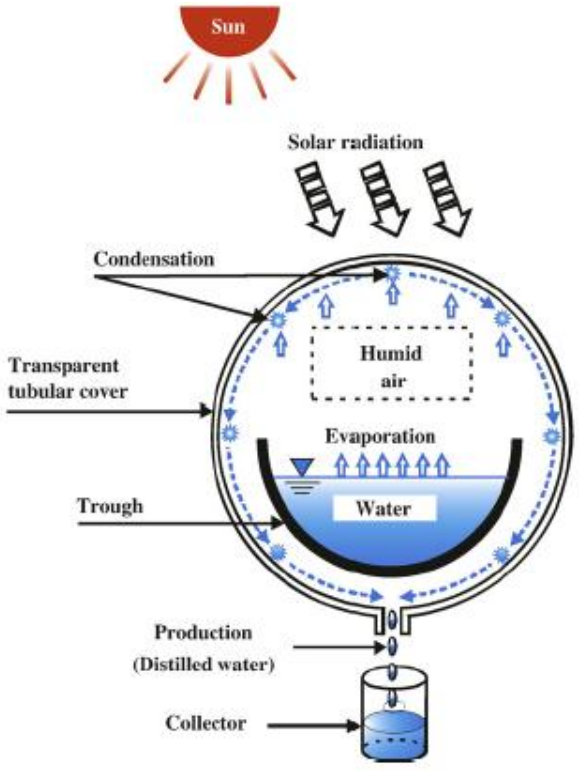

Figure 2.15 Simple tubular solar still [105].

An analytical and experimental study of a three-effect tubular solar still was conducted by Chen et al. [107], see Figure 2.16. It was concluded that an appropriate combination of design and operational parameters can markedly improve the still's performance. Rahbar et al. [108] studied the theoretical performance of tubular solar stills. They presented results of the CFD simulation of mass and heat transfer processes inside the still, and the numerical results indicated that vapour condensation takes place mainly on the upper transparent surface of the tubular still. Arunkumar [109] theoretically and experimentally investigated the performance of a tubular still augmented by a parabolic concentrator collector and coupled with a single basin still with an energy storage material.

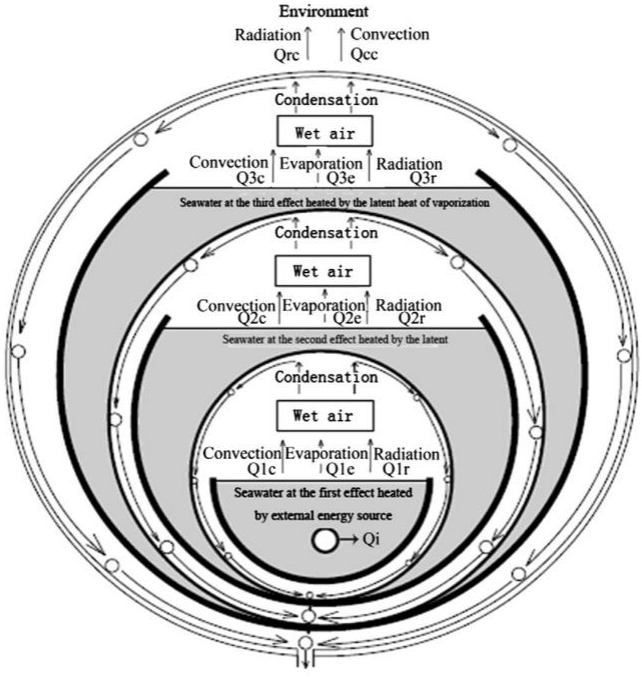

Figure 2.16 The operating principle of a three-effect tubular solar still [107].

Plastic or Fibre-reinforced Plastic (FRP) Solar Stills

The most commonly used materials in the construction of solar stills are wood, aluminium and galvanised iron. In order to eliminate the problems associated with these materials when in contact with saline water, plastic can be used to build the stills. Cappelletti [110] constructed and tested the performance of a two-basins plastic solar still. The influence of water depth on the productivity of the plastic solar still was investigated by Phadatare and Verma [111] and they reported that the productivity of the unit is inversely proportional to water depth. Furthermore, the same authors in [112] studied the effect of various cover materials on the performance of the plastic solar still.

Recently, Bhardwaj et al. [113] presented an inflated plastic solar still that can supply one family with fresh water. In order to increase the productivity of the still, a passive condenser, made of three plastic channels, was added. The results showed that this design might be an adequate alternative to supply freshwater for a single family. Panchal et al. [50] performed an experimental investigation of the effect of two low-cost heat storage materials, namely sandstones and marble pieces, on the performance of a simple basin-type solar still made of fibre reinforced plastic sheets. It was revealed that the productivity of the still with sandstones was higher compared to that with marble pieces and without materials inside the solar still.

Hemispherical Solar Stills

A schematic diagram of a hemispherical solar still is presented in Figure 2.17. It can be seen that the system mainly consists of a circular basin with a hemispherical transparent cover.

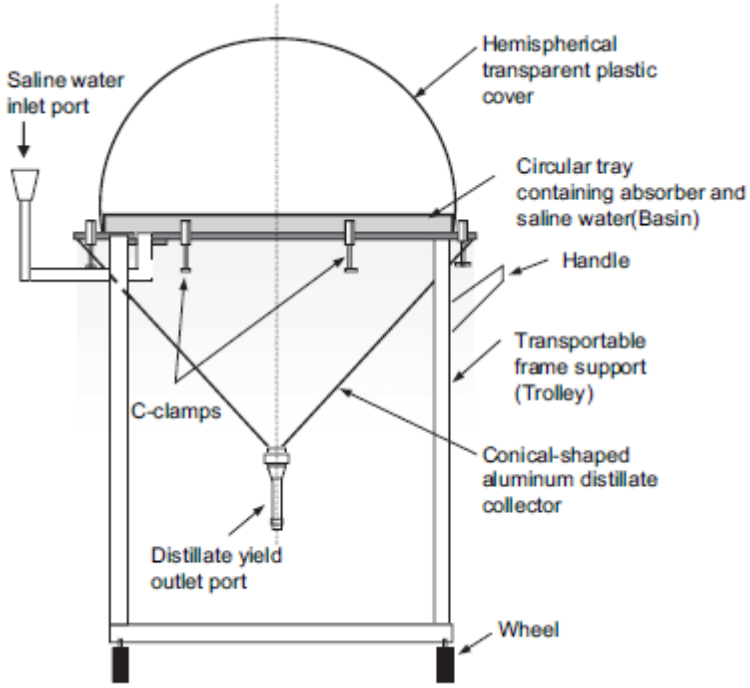

Figure 2.17 Schematic diagram of the new transportable hemispherical solar still [114].

Several researchers studied the performance of hemispherical solar still. Thus Ismail [114] constructed and conducted outdoor experiments on the performance of a simple hemispherical still with a circular basin. He reported that the average daily yield can reach 5.7 l/m^2. Arunkumar et al. [115] experimentally investigated the effect of flowing water on the transparent cover of a hemispherical solar still. The results showed that still efficiency was increased by 12%, as a results of water flowing over the top cover.

Inverted Absorber Solar Stills

A simple inverted absorber solar still is schematically presented in Figure 2.18. Similar single-effect inverted absorber solar still was introduced by Suneja and Tiwari [116]. The main feature of this type is that the solar radiation reflector or inverted absorber, which is

usually a concave mirror, is located underneath the saline water basin and therefore the water mass receives solar radiation from the bottom of the water basin and also through the glass cover.

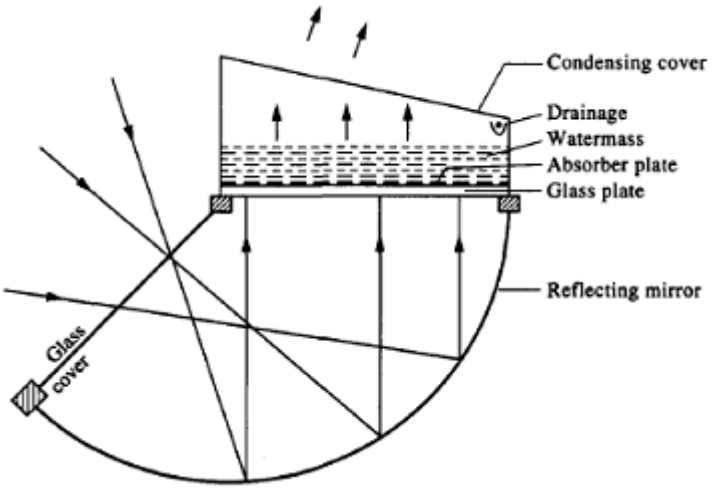

Figure 2.18 Schematic diagram of an inverted absorber solar still [117].

The performance of a single basin inverted absorber solar still was theoretically evaluated by Tiwari and Suneja [117]. They reported that the productivity of the still was about twice of that for a conventional solar still. A number of studies have been conducted in order to examine the optimum number of saline water basins for an inverted solar still. Suneja et al. [118] and Suneja and Tiwari [119] presented a parametric study of a double-effect inverted absorber still. The performance of a triple-effect inverted absorber solar still was then assessed by Suneja and Tiwari [120]. The results showed that the freshwater production of a triple-effect inverted absorber still is significantly greater than that of the single- and double-effect inverted absorber stills.

Furthermore, Abdul-Wahab and Al-Hatmi [121] carried out an experimental investigation of an inverted absorber solar still coupled with a refrigeration unit for various saline water

depths. The condenser of the refrigeration unit was immersed in the saline water basin while the condensation surface of the solar still was cooled by the evaporator of the refrigeration unit. They concluded that, as a result of adding the refrigeration unit, the productivity of the inverted absorber solar still was substantially increased.

Vertical Solar Stills

This type of the still consists of a vertical blackened absorbing plate which acts as an evaporating surface. The two sides of the plate are covered with transparent covers, which are the condensing surfaces. Brackish water is fed from the top of the still and flows by gravity downwards onto the absorbing plate. It then evaporates and condensation subsequently takes place on the internal surface of the transparent cover [122].

The performance of a vertical solar still in the Algerian desert was investigated experimentally by Boukar and Harmim [123-126]. They stated that their work had led to an improvement in the performance of the still. Moreover, Kaushal et al. [127] presented an improved combination of a single basin still and a vertical solar still, as shown in Figure 2.19. It was found that the overall efficiency of the improved still was about 10–15% greater than that of the conventional basin type still of the same design.

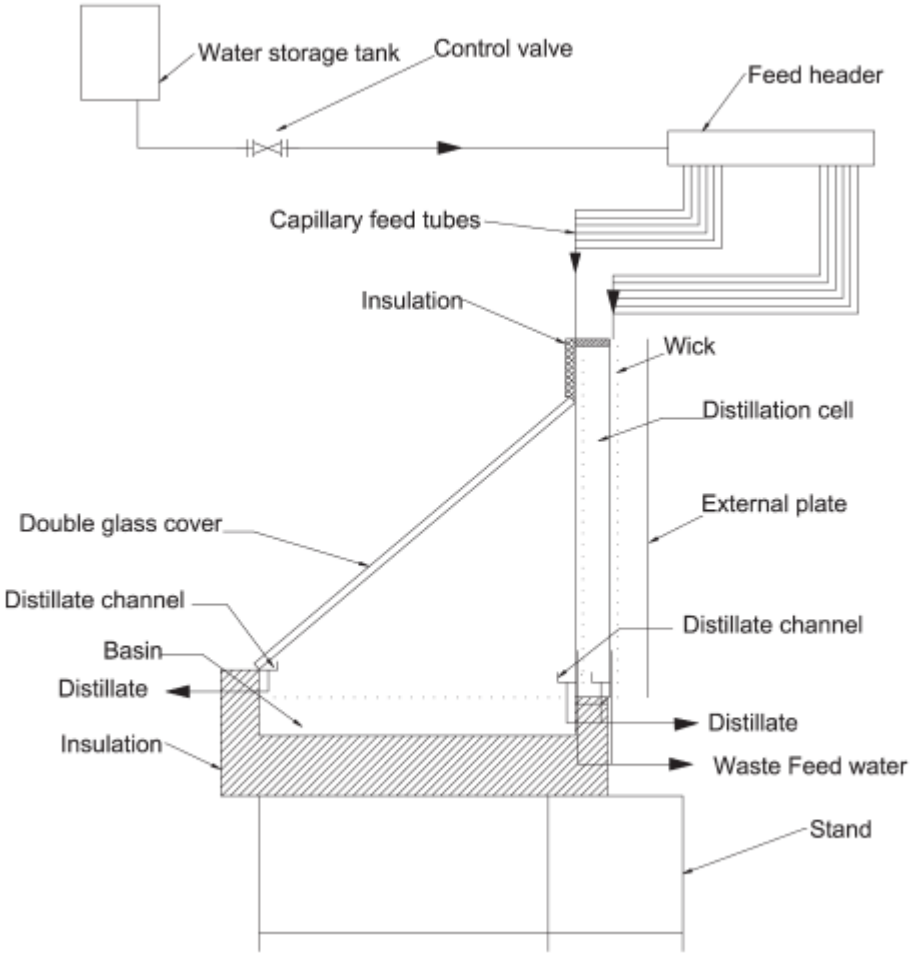

Figure 2.19 Schematic diagram of improved basin type vertical solar still [127].

2.3.1.2 *High Temperature Active Solar Stills*

The productivity of solar stills is determined by the temperature difference between the saline water and the inner surface of the transparent cover. This is the main drawback of passive solar stills, where the saline water is heated up only by direct solar radiation which results in the relatively low productivity. The high temperature active solar still is mainly composed of a conventional passive solar still coupled with an external heat source to supply auxiliary thermal energy to the saline water and therefore augment the evaporation process. The operating temperature of conventional solar stills is between 20-50 ^{o}C and, by

supplying additional thermal energy, the saline water temperature can reach 70-80 ^{o}C which enhances the water evaporation process and improves the productivity of the still. The external heat can be provided by solar collectors, solar concentrators or a heat recovery system. The circulation of saline water through the system can be accomplished either through thermosiphoning (natural circulation) or by means of a pump (forced circulation) [14].

- ***Solar Stills Coupled with Flat Plate Solar Collectors***

A simple active basin-type solar still coupled with a flat plate collector (FPC) is schematically presented in Figure 2.20. The system consists of a passive basin-type still connected to a flat plate collector (FPC) via an insulated pipe. A small circulating pump is used to keep the saline water flowing through the system. Therefore, the saline water gets heated up by the direct solar radiation transmitted through the glass cover and also by the added heat acquired in the flat plate collector.

Yadav [128] carried out a transient performance analysis of a basin-type solar still integrated with a flat plate collector. The system was operated under thermosiphon circulation mode and its performance was compared with that of a system using forced circulation. It was observed that the freshwater yield of the system operating in the forced mode was 5-10% greater than that with natural circulation and 30-35% higher than that of the conventional solar still. Tiris et al. [129] performed an experimental study on the performance of a twin-basin solar still equipped with a storage tank and coupled with two flat plate collectors for Turkish climatic conditions. They found that the productivity of their system was double of that for the conventional solar still.

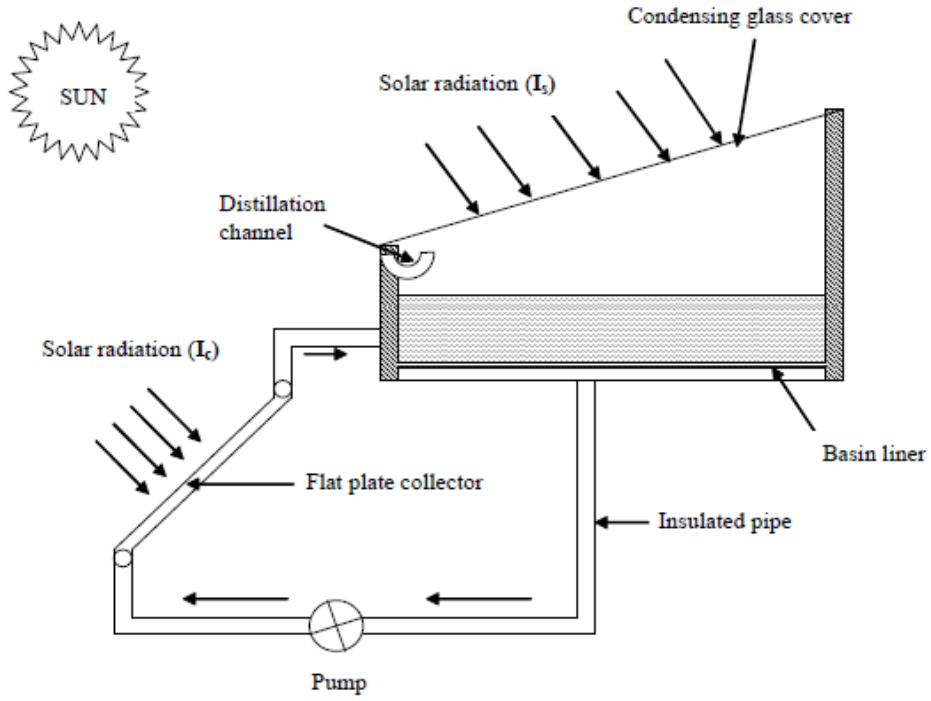

Figure 2.20 Active single basin solar still coupled with flat plate collector [130].

In order to examine the optimum inclination angles of the still cover and solar collector, Kumar et al. [131] carried out a numerical analysis of the performance of an active solar still augmented by a flat plate collector under Indian climatic conditions. They found that the maximum yearly productivity could be obtained when the inclination angles were 20^{o} and 15^{o} for the collector and glass cover, respectively.

Furthermore, Schwarzer et al. [132] presented a numerical simulation and experimental laboratory investigation of a distillation tower with six stages, using a multi-effect basin-type solar still coupled with a flat plate collector. The results showed that the production rate of the proposed system was five times higher than that of a conventional still. The performance of an asymmetric greenhouse-type solar still integrated with a storage tank and a field of 24 flat plate solar collectors was experimentally investigated by Voropoulos

et al. [133]. They reported that the productivity of this integrated system was about twice of that for a still-only desalination system.

The enhancements gained from coupling a flat plate solar collector with various designs of conventional solar still have been the focus of attention of many researches. Singh and Tiwari [134] theoretically evaluated the monthly performance of a basin-type solar still augmented by a flat plate collector. Badran et al. [135] stated that the yield of a single basin still with reflectors fixed on its inner walls was increased by 36% when a flat plate solar collector was coupled with the still. Similarly, Badran [136] carried out experiments on the performance of a single-basin, pyramid-shaped solar still with a transparent cover and integrated with a flat plate collector, and they noted an increase in still productivity of 52%. Dwivedi and Tiwari [137] presented a theoretical and experimental investigation of a symmetrical double-slope active solar still integrated with a flat plate collector operating with natural circulation. The results showed that the productivity of the active still was 51% greater than that of the passive still.

Moreover, several authors have examined the effect of various design and operational parameters on the performance of active solar stills. Tripathi and Tiwari [138] experimentally examined the effect of the water depth in a basin-type solar still coupled with a flat plate collector. The results showed that basin water depth has an important effect on still performance. The effect of the materials used for the condensing cover on the daily productivity of an active solar still was investigated by Dimri et al. [139]. They claimed that a copper cover resulted in a higher productivity compared to glass and plastic due to its higher thermal conductivity.

A parametric study of a single-basin solar still coupled with a flat plate collector was performed by Tiwari et al. [130]. They carried out energy and exergy analyses to evaluate the influence of water depth, the temperature of the inner and outer condensing surface, number of solar collectors, cover material and wind velocity on daily productivity. Correspondingly, Mousa and Arabi [140] investigated experimentally the performance of a single-basin still, and it was observed that the productivity is directly proportional to cooling water flow rate and ambient temperature. Taghvaei et al [141] studied experimentally the long-term influence of the depth of water in the basin on the performance of a single-basin still coupled with a flat plate collector as illustrated in Figure 2.21. They stated that, contrary to previous research results, increasing saline water depth led to an improvement in the productivity and efficiency of the system.

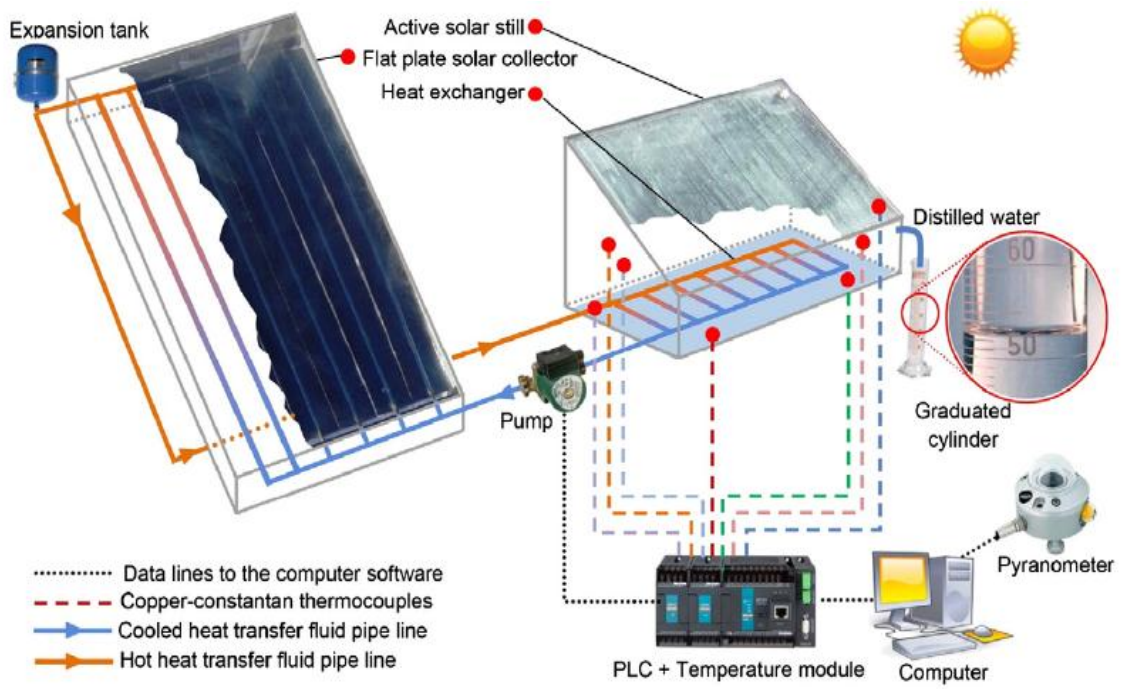

Figure 2.21 Schematic view of basin type solar still coupled with flat plate collector [141].

Moreover, the effect of utilizing a thermal energy storage medium, which was a thin layer of sand underneath the basin liner, in an active solar still coupled with a flat plate collector was investigated numerically under Saudi Arabia climatic conditions by El-Sebaii et al. [142].

It was reported that the yearly average daily production of the still with the storage medium was increased by about 24% compared to a still with no storage medium. Rajaseenivasan et al. [143] performed an experimental investigation on an active solar still having a basin of six small compartments and integrated with a flat plate solar collector. They observed that the proposed system produced 60% greater yield than the conventional still with the same basin.

On the other hand, some researchers have introduced further modifications to enhance the performance of active solar stills integrated with flat plat collectors (FPCs). One important innovation is a hybrid photovoltaic and thermal solar collector (PV/T) which simultaneously generates electrical power and thermal energy. In other words, the PV/T solar collector was introduced to convert solar radiation into electricity which is used to operate equipment such as pumps and motors. Meanwhile thermal energy is utilized for saline water heating [144]. Kumar and Tiwari [145] and Kumar et al. [146] conducted experimental and theoretical studies of a hybrid PV/T active solar still. They developed a mathematical model to predict the internal heat transfer coefficient and cover temperature of the still, which both have a significant effect on freshwater productivity.

Furthermore, Kumar and Tiwari [147] designed and constructed a hybrid PV/T single-slope active solar still. The experimental results showed that the productivity of the proposed system was 5.5 times greater than that of the passive still. Similarly, Singh et al.

[148] developed and fabricated a hybrid PV/T double-slope solar still integrated with flat plate solar collectors. The system is schematically illustrated in Figure 2.22. They investigated the performance of the system for Indian weather conditions and reported that the productivity of the proposed still was 140% greater than that of a hybrid PV/T single-slope still.

In addition, Gaur and Tiwari [149] carried out a numerical computation to estimate the optimum number of hybrid flat plate PV/T collectors for a single-basin active solar still. They concluded that the optimum number of collectors increased with increasing the saline water depth. Morad et al. [150] presented an experimental and theoretical investigations to enhance the performance of a double slope solar still by utilizing flat plate solar collectors. It was found that the maximum daily productivity of the passive system was about 8 liter/m^2 while it was 10 liter/m^2 for the active solar still.

Recently, Al-harahsheh et al. [151] conducted an experimental study of the performance of a single basin solar still with phase change material and augmented by flat plate solar collector. Figure 2.23 shows the schematic diagram of the experimental setup. They reported that the productivity of the modified system was remarkably improved and the major enhancement observed at night time due to using PCM.

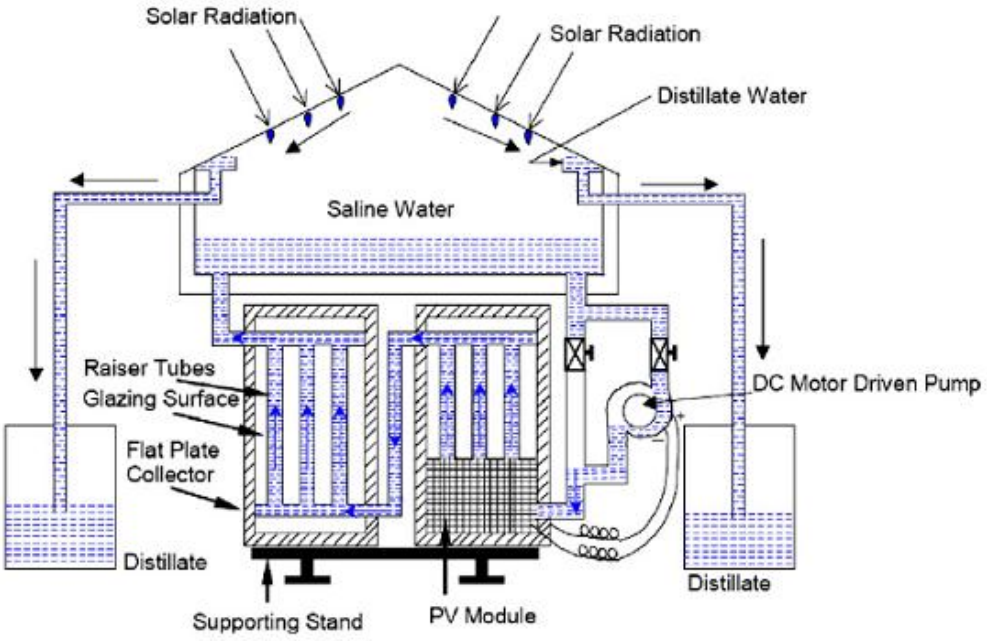

Figure 2.22 Schematic view of a hybrid (PV/T) double slope active solar still[148].

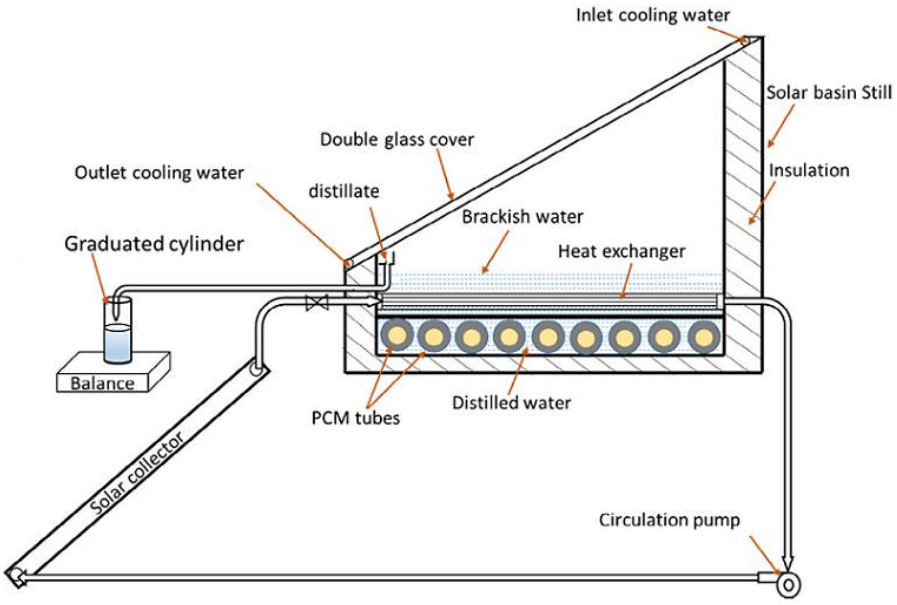

Figure 2.23 Schematic diagram of single basin solar still with PCM and FPC [151].

- ***Solar Stills Coupled with Evacuated Tube Solar Collectors***

Generally, the design and the operating principles of evacuated tube collector (ETC) active solar stills are to some extent similar to those of flat plate collector stills. The main advantage of using evacuated tube collectors is their higher efficiency compared to flat plate collectors, especially at low angles of solar radiation incidence. This is due to their cylindrical shape and also because the vacuum inside the tube reduces heat losses. However, the ETC is relatively expensive and this prevents the wider use of this type of solar collectors. Consequently less research has been conducted with evacuated tube active solar stills [152].

Tanaka and Nakatake [153] investigated theoretically the performance of a multiple-effect, vertical diffusion-type solar still integrated with a heat pipe solar collector. They stated that the productivity of the proposed diffusion still was 13% higher than that of the conventional basin-type diffusion still. Tanaka et al. [154] theoretically conducted a parametric analysis of a vertical multiple effect diffusion solar still augmented by a heat pipe collector. It was noted that the performance of the still is strongly influenced by many design and operational parameters.

A newly developed multistage solar still coupled with evacuated tube solar collectors (ETCs) was presented by Mahkamov and Akhatov [155]. Experiments were carried out under laboratory conditions, and the theoretical and experimental results demonstrated that the productivity of the multistage solar still was double that of the conventional greenhouse-type still. In similar manner, Shatat and Mahkamov [156] performed a theoretical and experimental parametric investigation into a multi-stage solar still coupled with an evacuated tube solar collector, and a schematic diagram of the proposed system is

presented in Figure 2.24. They stated that using the evacuated tube collector considerably increased still productivity compared with a still integrated with a flat plate collector.

Moreover, the performance of a single-slope basin-type solar still integrated with an evacuated tube collector (ETC) and storage tank was investigated theoretically and experimentally by Sampathkumar and Senthilkumar [157]. The results obtained revealed that the freshwater production rate increased by 77% compared to the yield of a passive single-basin still. Kabeel et al. [158] carried out theoretical and experimental comparative investigations of the performance of a conventional single-basin still and a stepped still, with both augmented by an evacuated tube collector. It was found that the maximum yield of the stepped still was around 57% greater than that of the conventional solar still.

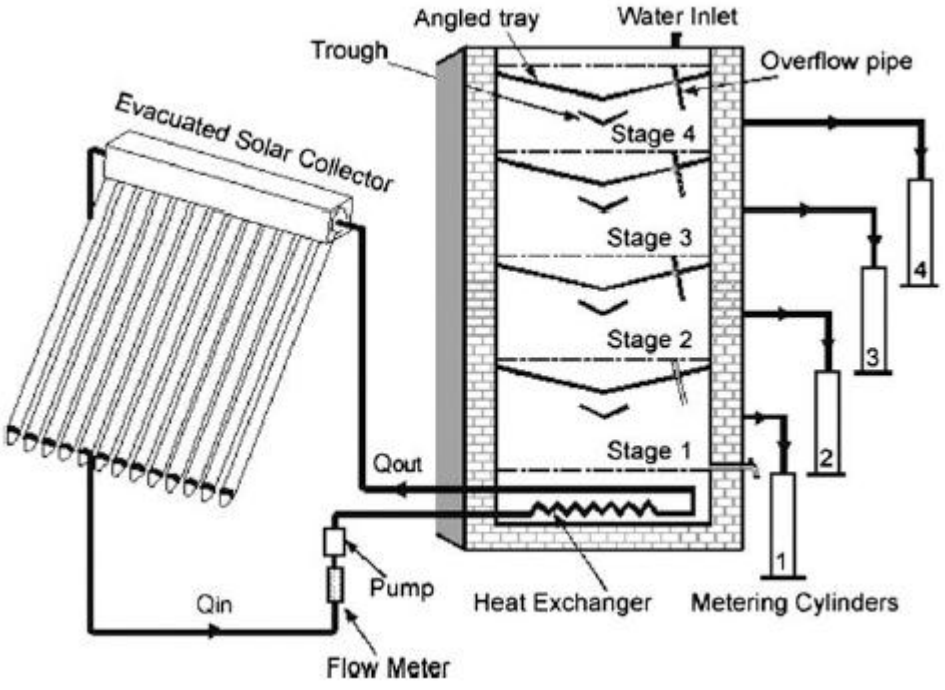

Figure 2.24 Schematic view of multi-stage solar still with evacuated tube collector [156].

Panchal and Shah [159] performed an experimental analysis to investigate the effect of various operational parameters and climatic conditions on the performance of a double-basin still coupled with an evacuated tube collector.

Furthermore, Singh et al. [160] presented a thermal model to evaluate the performance of a single-basin still, attached to an evacuated tube collector in natural operating mode, and it was observed that the utilization of the evacuated tube solar collector enhanced the still's performance. Previous work was expanded by Kumar et al. [161]. Authors performed a thermal analysis of a single-basin still, coupled with an evacuated tube collector in forced operation mode. They stated that the use of forced mode led to a greater productivity compared to the natural mode.

- ***Solar Stills Coupled with Solar Concentrators***

The solar concentrator is a point-focus collector that is always oriented towards the sun and concentrates solar energy on its focal point, and thereby solar concentrators are the most efficient of all collector types. Consequently, the performance of active solar stills could be further enhanced by utilizing solar concentrators instead of solar collectors. This distillation system consists of a simple passive solar still integrated with a solar concentrator [162].

Prasad and Tiwari [163] performed a numerical analysis to investigate the performance of a single-basin solar still coupled with a solar parabolic concentrator and using a circulating pump in the forced mode of operation. It was observed that water temperature and still productivity markedly increased due to the utilization of the concentrator. The performance of a double-slope solar still integrated with a parabolic concentrator in the

forced operation mode was theoretically investigated by Kumar and Sinha [162]. They reported that the performance of the proposed concentrator-assisted solar still was significantly higher than any other passive or active distillation systems.

Singh et al. [164] presented an analytical comparative study of active basin-type solar stills, where the first still was coupled with a solar collector and the second being concentrator-assisted. The results showed that the concentrator-assisted solar still produced the better performance. Abdel-Rehima and Lasheen [165] carried out a theoretical and experimental investigation of the performance of a modified active solar still under Egyptian climatic conditions. The modified system consisted of a passive single-basin solar still augmented by a solar concentrator (parabolic trough) connected to a sun tracking system. The authors stated that this modification led to an increase in the freshwater production rate of about 18%.

Moreover, Arunkumar et al. [166] conducted experiments to investigate the effect of adding a phase change material (copper balls filled with paraffin wax) on the performance of a hemispherical basin still coupled with a solar concentrator. It was found that the productivity of the proposed concentrator-coupled still increased by 26% because of the inclusion of the phase change material. Another attempt to improve the performance of this system further via the use of cold water flowing over the glass cover was made by Arunkumar et al. [167], as presented in Figure 2.25. They observed that freshwater productivity was directly proportional to the cooling water flow rate.

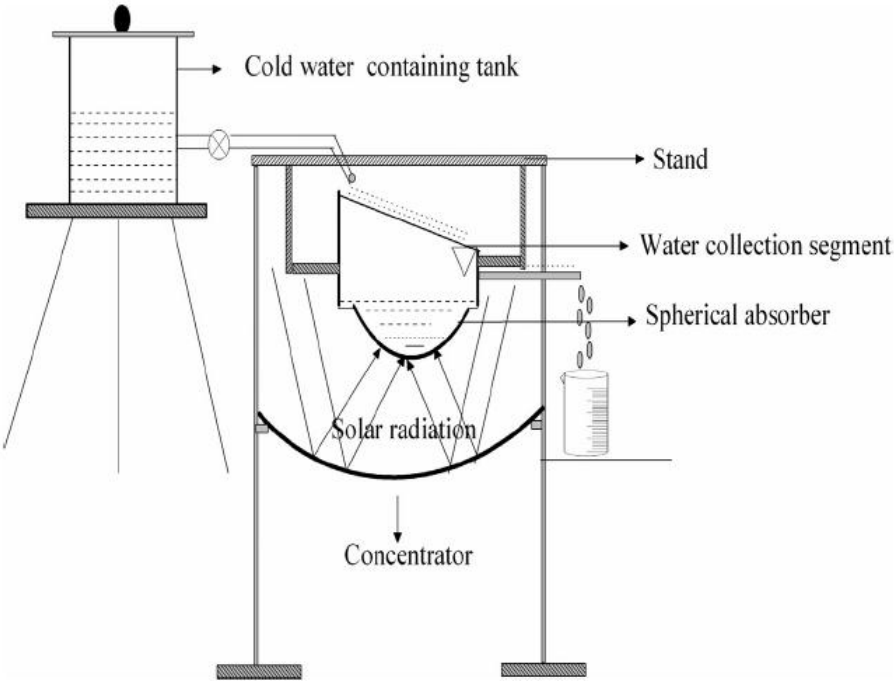

Figure 2.25 Schematic diagram of concentrator-assisted solar still [167].

In addition, Arunkumar et al. [168] presented experimental results for a newly-designed rectangular basin tubular solar still with a parabolic concentrator. The effect of the cooling water and air flow rates over the still cover was investigated and were found to significantly improve the daily yield, where the cooling water flow rate had the greater effect.

Arunkumar et al. [169] experimentally investigated the performance of a parabolic concentrator-assisted tubular solar still augmented by two types of solar stills: a single slope or pyramid-shaped solar still. Kabeel and Abdelgaied [170] carried out an experimental study on the performance of conventional solar still with Phase change material and coupled with cylindrical parabolic concentrator. The developed system is schematically presented in Figure 2.26.

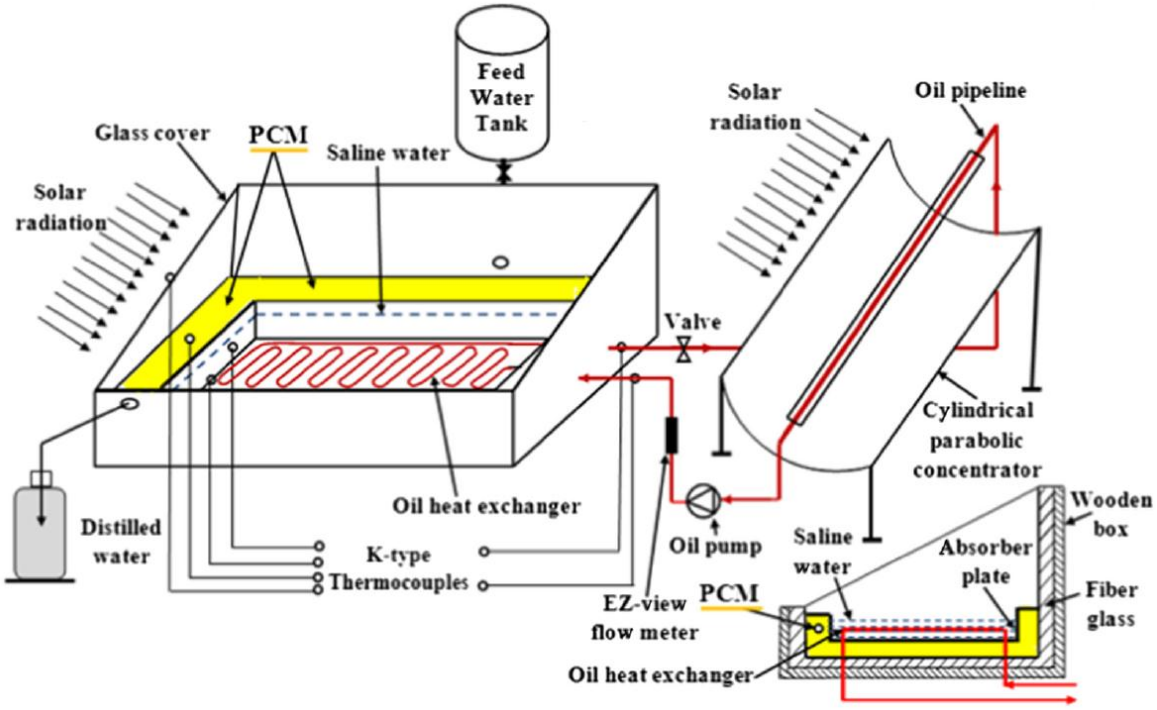

Figure 2.26 Simple solar still with PCM coupled to parabolic concentrator [170].

They used in the modified system oil heat exchanger and Paraffin wax (PCM) as a heat storage material. It was stated that the productivity of the developed system was around 140% greater than that of the conventional system.

- ***Solar Stills Utilizing Waste Heat***

Recovering heat, rejected from various industrial systems, is an important alternative source of the thermal energy needed to operate solar stills. This type of thermal distillation system consists of a passive solar still coupled with a waste heat recovery system, which usually consists of heat source, a heat exchanger or heat storage tank.

Voropoulos et al. [171] conducted an experimental study of a greenhouse-type solar still integrated with a hot water tank. They reported that the basin water temperature increased,

leading to the enhanced still productivity. Tanaka and Park [172, 173] experimentally and theoretically investigated the performance of a vertical multi-effect diffusion solar still utilizing thermal energy through a heat pipe connected to the exhaust gas system of a small electric generator, and a boost in productivity was observed. Maheswari et al. [174] presented an experimental analysis of the use of waste thermal energy from the exhaust gases of a five-horsepower diesel engine to improve the performance of a desalination unit. The results demonstrated that the freshwater production rate was considerably increased. Furthermore, Park et al. [175] carried out experiments on a hybrid distillation unit consisting of a single-basin still and a vertical wick-type multiple diffusion solar still utilizing the waste thermal energy from a small electric generator and solar radiation, as shown in Figure 2.27. The authors stated that utilizing the waste heat significantly improved still productivity.

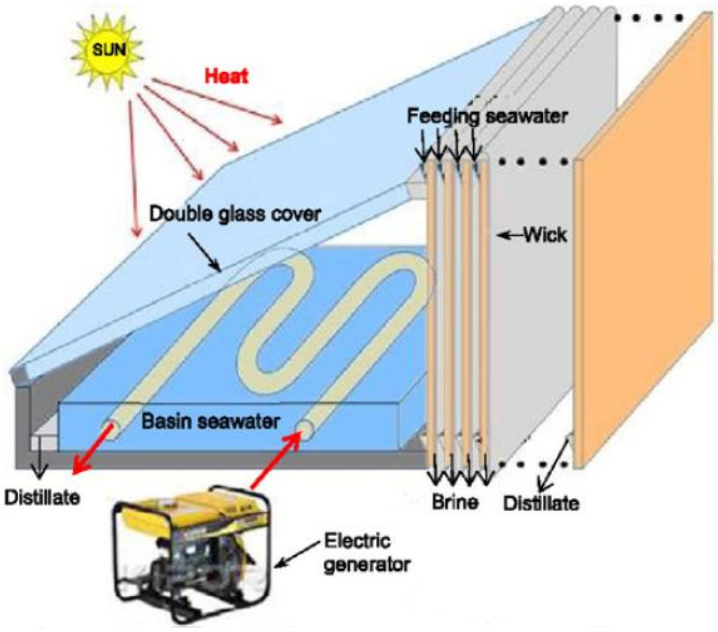

Figure 2.27 Schematic view of a hybrid solar still utilizing waste heat [175].

Advantages and Drawbacks of High Temperature Active Solar Stills

High temperature active solar stills have been employed to overcome some of the drawbacks of low-temperature passive solar stills and consequently to improve performance. The main advantages and drawbacks of high temperature active solar stills are as follows:

- Evaporation process is enhanced due to the rise in operating temperature from about 20-40 ^{o}C to around 80 ^{o}C [14].
- Significant enhancements in the yield of the system are observed in comparison to passive solar stills [157].
- Ability to be simultaneously used for desalination and heating purposes makes the system economically useful [14].
- Needs power to operate the circulation pump for the forced circulation mode [14].
- High risk of scaling and corrosion in heating surfaces due to the high temperature [14].
- Solar collector systems are an expensive technology and require additional space for installation [1].

2.3.1.3 *Evacuated Solar Stills*

Reducing the pressure inside the still is a new concept and has become one of the most effective techniques to increase the rate of distillate production. The operating principle of evacuated solar stills is based on the fact that, when the air inside the system is evacuated, saline water boils at a low temperature. In other words, the evaporation rate increases under vacuum conditions, and consequently still productivity increases. In general, a

vacuum pump is used to reduce the pressure inside the still, but it can also be passively accomplished by balancing the atmospheric and hydrostatic pressures in the supply and discharge pipelines [176]. However, there is an obvious interest in carrying out research into evacuated solar stills.

Al-Hussaini and Smith [177] and Abu-Jabal et al. [178] studied the theoretical effect of reducing the pressure inside a solar still. They stated that operating the still under vacuum conditions should lead to a significant improvement in daily productivity and the efficiency of the solar still. A solar desalination system with the passive vacuum technique was introduced by Al-Kharabsheh and Goswami [176], and the performance of a basin-type solar still with vacuum conditions was theoretically and experimentally investigated by Gnanadason et al. [179]. A schematic view of their evacuated single basin still is presented in Figure 2.28. The results showed that the productivity of the modified solar still was considerably improved by providing a vacuum inside the still.

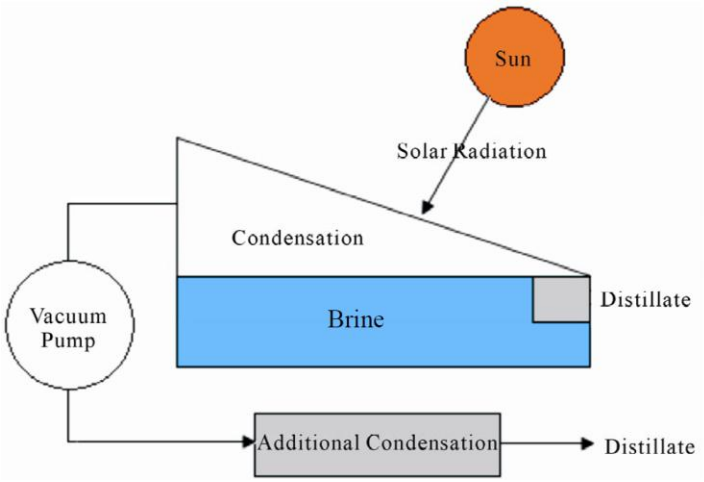

Figure 2.28 evacuated basin-type solar still [179].

Multi-stage solar stills have been proven to produce the superior performance compared to conventional solar stills, and extensive studies have been conducted with the evacuated

multi-stage solar still in order to provide further improvements. Abakr and Ismail [180] designed and constructed a multi-stage solar still with a solar collector and utilized a vacuum pump to create vacuum conditions inside the still. They theoretically and experimentally investigated the performance of the proposed system and it was revealed that that the daily production rate of the evacuated system can reach about 14 kg/m^2 which is about three times greater than the maximum rate of the simple solar still. In the same context, Ahmed et al [181] performed theoretical and experimental studies of the performance of an active multi-stage solar still. A vacuum pump was connected to the multi-stage still to reduce the internal pressure, and a substantial improvement in the production rate of distilled water was demonstrated.

Furthermore, Kumar et al. [182] conducted an optimization study of the performance of an evacuated multi-stage solar still. They evaluated theoretically and experimentally the effects of various design and operational parameters on the productivity of the system, and concluded that a system made of four stages is the optimal system configuration to achieve the maximum productivity. Similarly, Reddy et al. [183] presented a transient mathematical model of an evacuated multi-stage solar still. They investigated the influence of reducing internal pressure and different design parameters on the productivity and thermal performance of the system. The results indicated that an evacuated desalination unit consisting of four stages with an internal pressure equal to 0.3 bar can reach the daily yield of about 53 kg/m^2. Kabeel et al. [184] conducted an experimental investigation to enhance the performance of simple solar stills by utilizing nanoparticles and using a vacuum fan. Two types of nanoparticles were used in this investigation, namely cuprous oxide and aluminium oxide with different concentrations. It was observed that the maximum enhancement of the distillate yield with using the vacuum fan was 134% and

125% for cuprous and aluminium oxide nanoparticles, respectively, as compared to the conventional still.

Reddy and Sharon [185] presented an enviro-economic feasibility study of multi-effect active vertical solar still. The schematic diagram of the system is shown in Figure 2.29. They reported that the evacuated multiple effect vertical solar stills was found to be more beneficial in terms of daily productivity, CO_2 emission alleviation and production cost, compared to traditional multi-effect vertical solar stills.

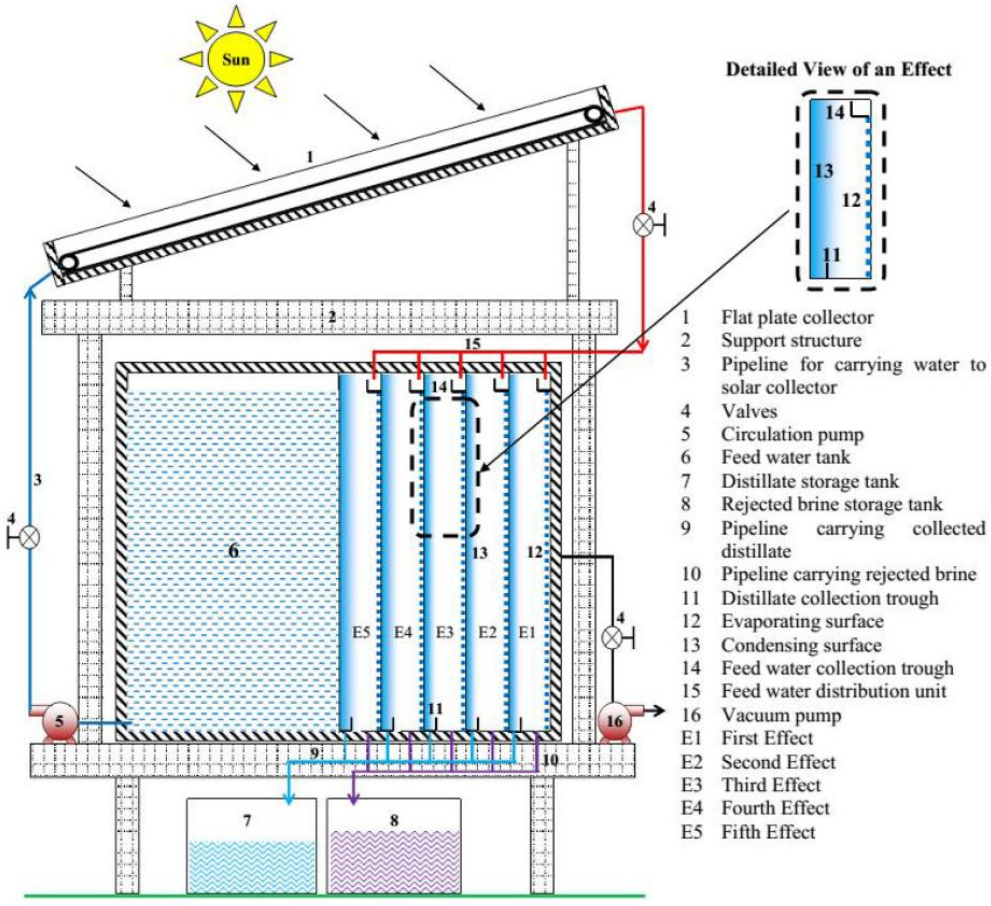

Figure 2.29 Evacuated active multi-effect vertical solar still [185].

Advantages and Drawbacks of the Evacuated Solar Stills

The use of evacuated solar water stills has led to remarkable enhancement in the performance of these systems. However, there are various drawbacks which prevent the

widespread adoption of these types of stills. One of the important challenges in this technology is the lack of detailed research conducted on evacuated solar stills. The main advantages and drawbacks of high temperature active solar stills are as follows:

- Significant enhancement in the performance of evacuated systems compared to that operating at atmospheric pressure [181].
- Natural vacuum desalination system is usually suitable for a small-scale application [11].
- The use of a vacuum pump to provide vacuum conditions requires electrical power [11].

2.3.2 Solar Humidification-Dehumidification Desalination

The humidification-dehumidification (HD) process is one of promising techniques for small production using solar seawater desalination systems. The working fluid in the HD process is air and the process is based on the fact that dry air is capable of carrying considerable amounts of water vapour and this capability increases with air temperature. When contact between the dry air and seawater occurs, the air is saturated with a substantial quantity of vapour and becomes humid, and subsequently distilled water is produced when the humid air is dehumidified and water vapour condenses onto a cooling surface [186].

The main components of a solar HD desalination system are a heat source, which is usually a solar collector, an air humidifier and an air dehumidifier with a cooling surface. In addition, solar humidification-dehumidification desalination systems can be classified into two types: simple HD and multi-effect humidification (MEH) systems [187].

2.3.2.1 Basic Solar Humidification-Dehumidification (HD) Desalination Systems

The basic solar HD system operation consists of three stages. In the first stage, solar radiation is used to heat up an air stream, and in the next stage, the hot air is mixed with seawater so that the air becomes humidified. In the third stage, the humid air is cooled (dehumidified) and distilled water is collected as a condensate. Figure 2.30 presents a simple solar HD desalination process.

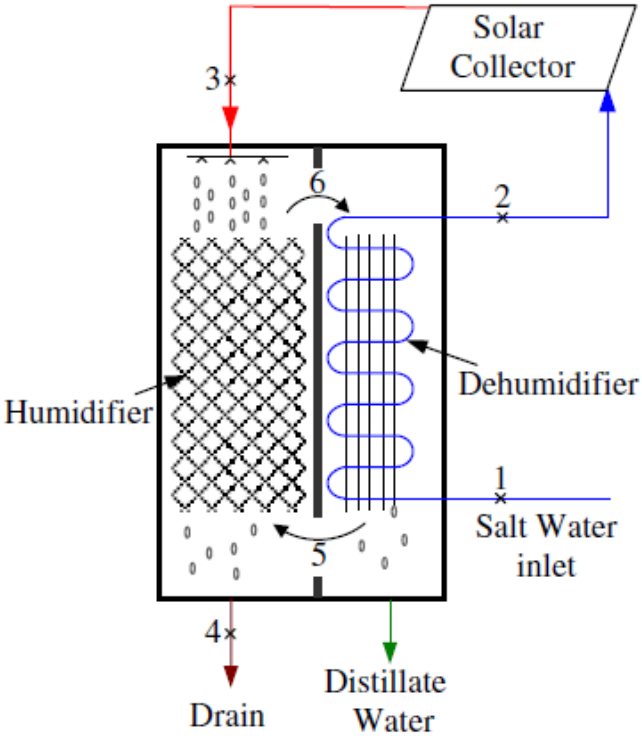

Figure 2.30 Simple solar HD desalination process [188].

Orfi et al. [189] carried out a theoretical and experimental investigation into a solar HD desalination system. The results showed that, for maximum productivity, an optimum air-seawater flow rate ratio is required. A mathematical analysis and experimental study of a solar desalination system based on the HD technique was presented by Hermosillo et al. [190]. Abdel Dayem [191] conducted experimental tests on a prototype of a solar HD

system for various weather conditions in Makah, Saudi Arabia and it was concluded that the temperature of the saline water has an important effect on system productivity.

Recently, Tabrizi et al. [192] performed an outdoor experimental study of a solar HD system integrated with a cascade solar still. They investigated the influence of various design and operational parameters on the daily productivity and thermal efficiency of the proposed combination, and reported that the performance of the system was significantly enhanced. A hybrid solar HD desalination system coupled with a set of conventional basin-type solar stills was presented by Sharshir [193]. The single basin stills were fed by the warm water draining from the HD system. It was observed that the overall efficiency of the hybrid solar system and the single-basin stills increased by 50% and 90% respectively.

2.3.2.2 Solar Multi-Effect Humidification (MEH) Desalination Systems

The operation principle of the multi-effect humidification desalination system (MEH) is based on the multiple reuse of the latent heat of condensation. The saline water in the first effect is heated and evaporated by means of external source and the water in the second effect is heated and evaporated due to the condensation of the water vapour from the first effect. A simple MEH desalination unit is schematically presented in Figure 2.31.

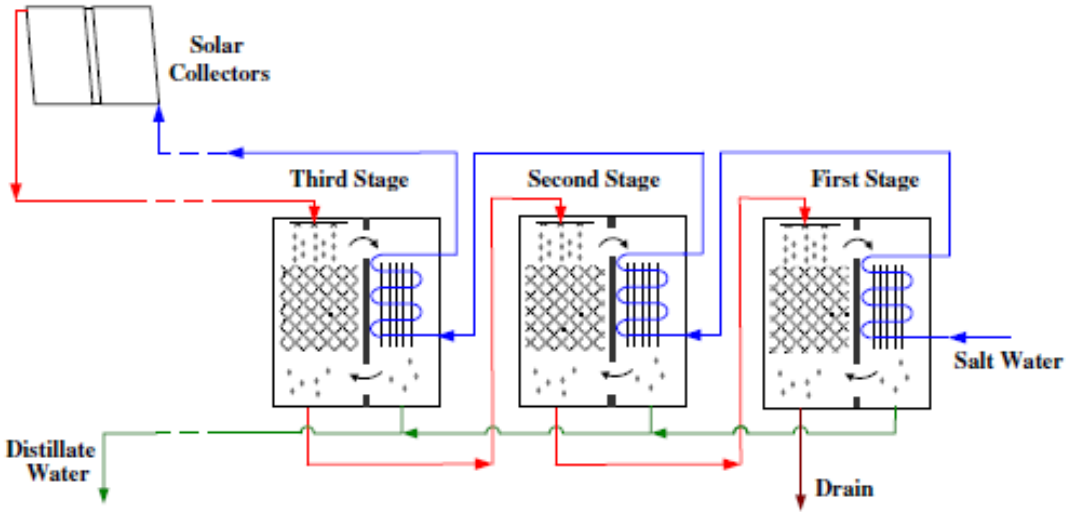

Figure 2.31 A simple MEH desalination unit [188].

The term (multi-effect) does not necessarily refer to the number of stages of a MEH system, but instead indicates the ratio between the heat input and the heat used for the desalination process. Moreover, MEH desalination systems are categorized into two types: those based on an open water/closed air cycle or systems based on a closed water/open air cycle, as shown in Figure 2.32. In the former system heat recovery takes place via air circulation between the humidifier and condenser, whereas in the second type heat is recovered by the circulation of water [194].

Numerous studies of multi-effect humidification desalination system have been conducted, attempting to enhance the productivity of such systems. Orfi et al. [195] performed a numerical analysis of a MEH desalination system with open and closed air cycles. The results showed that the productivity of the system can reach 43 litres per day per square metre of the solar collector.

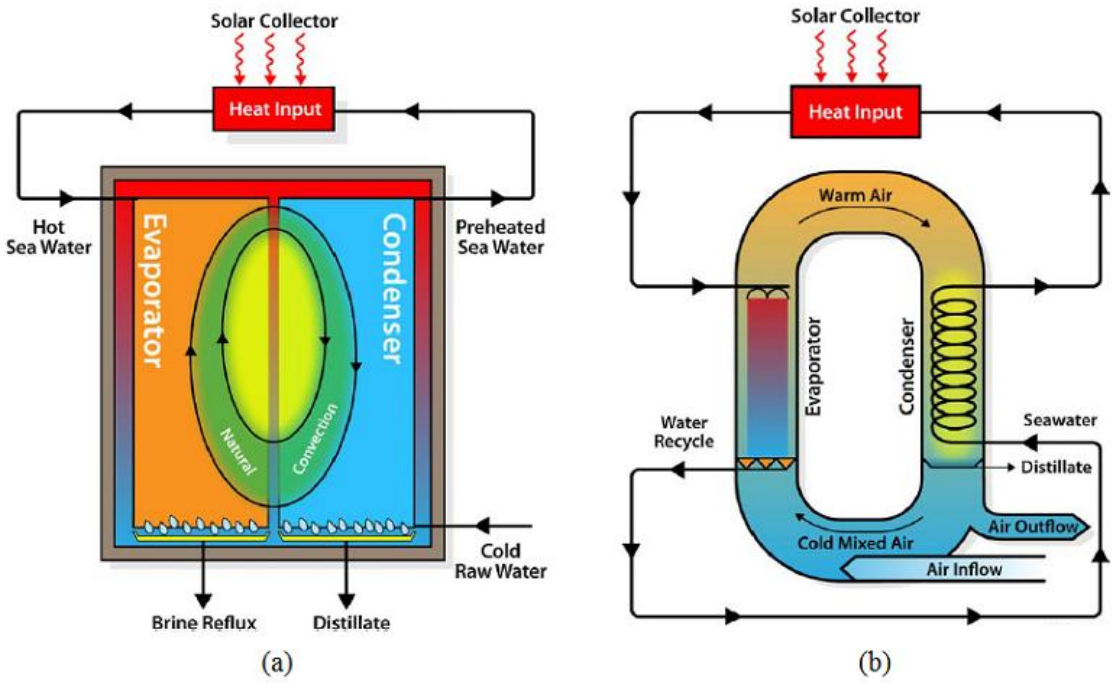

Figure 2.32 MEH unit: (a) open water/closed air cycle; (b) open air/closed water cycle [196].

Yuan and Zhang [197] described results of the theoretical investigation of a closed-air cycle MEH system. They studied the effect of design and operational parameters on the system's productivity. Further parametric studies were conducted by Yamali and Solmus [198, 199], who investigated theoretically and experimentally the influence of various design and operational parameters on the performance of a solar MEH system with double pass flat plate solar air heater. They reported that the productivity of the proposed system was greater by 8% than the productivity of the same system with a one-pass air heater.

Moreover, Hou and Zhang [200] presented a hybrid desalination system consisting of a solar MEH unit and a single-basin solar still coupled with evacuated tube solar collector. They claimed that the proper utilization of latent heat and the recirculation of water rejected from the solar MEH unit for reuse in the basin stills significantly enhanced the performance of the hybrid system. Also, the influence of integrating a cooling tower with

various configurations of an air-closed cycle MEH desalination unit was theoretically investigated by Marmouch et al. [201] and it was found that the maximum daily productivity of the system of six effects and cooling tower can reach 37 L/m2.

In addition, Zamen et al. [188, 202] and Kang et al. [203] carried out theoretical and experimental investigations into multi-stage humidification-dehumidification desalination systems, and concluded that a multi-stage technique leads to considerable enhancements of the desalination process enhancement. Kang and Zheng [204] presented a comparative performance analysis of an air-extraction multi-stage HD unit and a regenerative multi-stage HD desalination unit.

Main Advantages and Drawbacks of Solar HD Desalination Systems

- Simple technology, flexible system with moderate installation and operation costs [11].
- Utilizing various sources of low grade energy [11].
- System operates at the low temperature and air is the working fluid; therefore the problems of scaling and corrosion in the heating surface are reduced [205].
- Requires too many stages to improve the system performance [11].
- Consumes a large amount of power since there is the need in compressing a large volumes of air [206].

2.3.3 Solar Desalination Systems Integrated with Solar Chimney

A solar chimney is an alternative technique to harness solar energy for seawater desalination. The solar chimney system is used to drive a power generation plant and to produce freshwater. The desalination process in the solar chimney occurs based on a natural phenomenon in which air temperature decreases when the air rises into the atmosphere, and as a result its relative humidity increases. Subsequently, at a certain level, called the lifting condensation level, the air temperature goes down below the dew point and water vapour begins to condense on any available cold surface. Clouds are formed as a result of the same process, and the principle of the solar chimney desalination process in nature is shown in Figure 2.33.

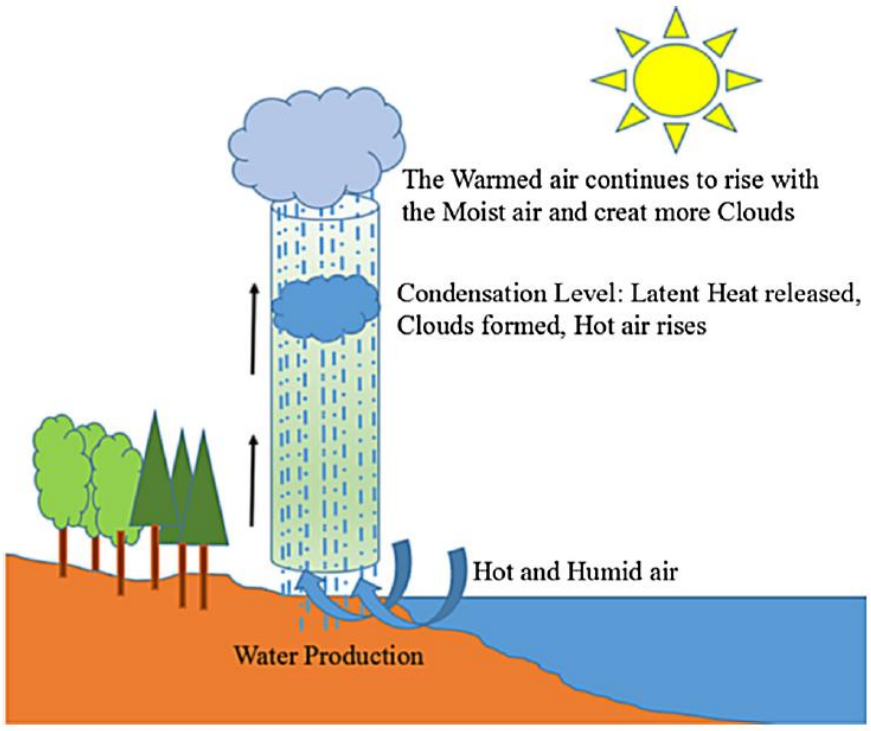

Figure 2.33 Principle of the solar chimney desalination process [207].

Recently, many studies have been conducted to evaluate the potential of utilizing solar chimneys in seawater desalination. Zhou et al. [208] and Zuo et al. [209] introduced two mathematical models for a classical solar chimney and an integrated solar chimney for power generation and seawater desalination. A schematic diagram of the solar chimney integrated system is presented in Figure 2.34. The results obtained demonstrated that the integrated solar chimney system considerably improved the efficiency of solar energy utilization and has great ecological and economic benefits. Zuo et al. [210] conducted outdoor experiments on the performance of a small-scale prototype device of an integrated solar chimney system. They concluded that the integrated system can simultaneously produce energy and potable water required.

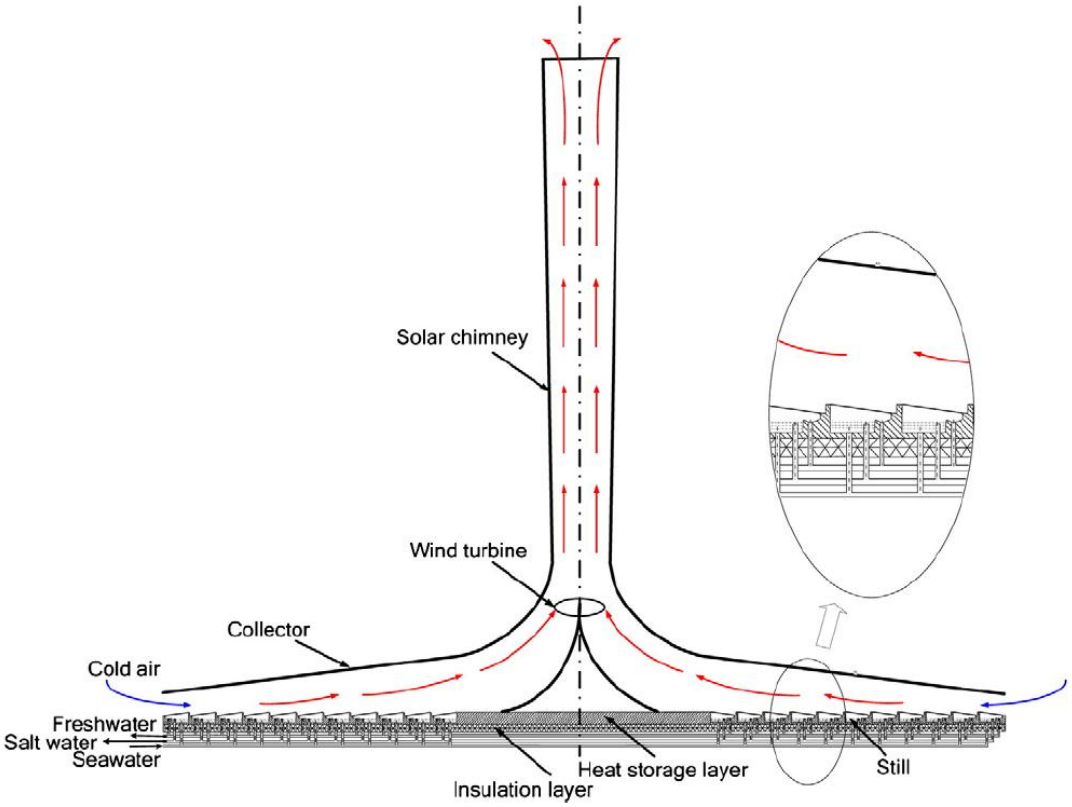

Figure 2.34 Schematic diagram of the solar chimney integrated system [210].

Moreover, a solar chimney integrated with a humidification-dehumidification desalination system was theoretically investigated by Niroomand and Amidpour [211]. It was found that the water flow rate and temperature at the inlet of the humidifier significantly affected the performance of the integrated system. Refalo et al. [212] performed an experimental investigation into the performance of a modified single-basin solar still coupled to a solar chimney and a water-cooled condenser, as shown in Figure 2.35. The experimental results revealed that the performance of the integrated basin-type solar still system was considerably enhanced. Also, in this context, Rajesh and Choudary [213] carried out theoretical and experimental studies of the performance of a solar chimney desalination system augmented by a solar collector made of recycled aluminium cans for energy and freshwater production.

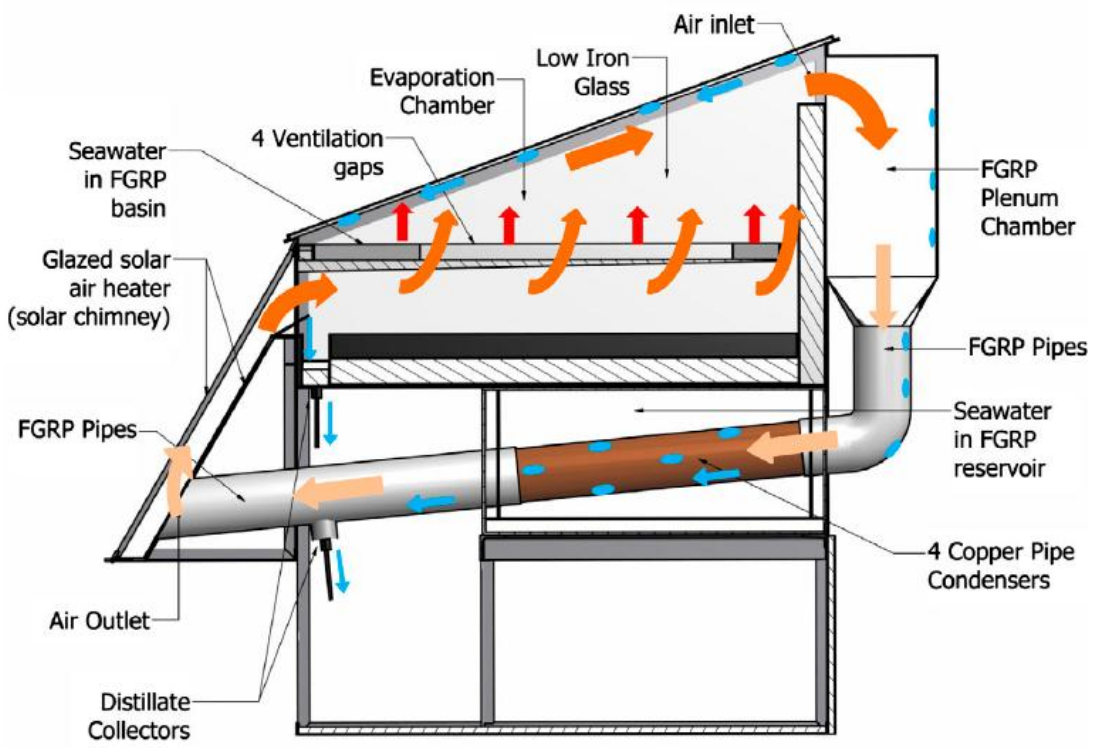

Figure 2.35 Schematic diagram of solar still with solar chimney and condenser [212].

Main Advantages and Drawbacks of Solar Chimney Desalination systems

- Ability to treat various kinds of saline water [209].
- Significant ecological benefits [209].
- Inexpensive water production [11]
- Feasible capital costs [11].
- Needs large space [209].
- Complicated processes require skilled operators [209].

2.4 Mathematical modelling in solar water desalination systems

Mathematical models are developed to simulate the processes that occur in reality in all components of the real system. The main advantages of the mathematical modelling is that it typically offers convenience and cost advantages over the experimental investigation in obtaining the required data. Therefore, the mathematical modelling was widely utilized in the theoretical investigations related to water desalination systems.

Setoodeh et al. [214] presented the calculation of heat transfer coefficient in a basin-type solar still by using computational fluid dynamic (CFD) method. They developed a three-dimensional, two-phase model to simulate the processes of the system. The simulation results were compared with previously published experimental results and there were a good agreement between both sets of results. In similar context, Rahbar et al. [108] investigated the ability of a two-dimensional CFD simulation in estimation of convective heat transfer coefficient in a tubular solar still. It was reported that the simulation results showed an acceptable agreement with experimental data reported in the open literature. Khare et al. [22] developed a 3-dimentional, 2-phase CFD model of a simple single slope

solar still using ANSYS FLUENT. They conducted a parametric study to improve the productivity of the system and claimed that there was a good agreement between their results and obtained experimental data.

Mathematical modelling was used to study the performance of multi-stage solar desalination systems. Shatat and Mahkamov [156] carried out a parametric analysis of a four-stage solar water still by ANSYS FLUENT. It was found to be unfeasible to use CFD technique for modelling the heat transfer and the flow in all four stages of the still as the computational time and computer memory requirements restricted the intensive application of CFD technique for analysis and design of the distillation stills. Therefore, FLUENT CFD software was used to simulate the condensation and evaporation processes only inside the first stage. In addition, they developed a lumped-parameter mathematical for a transient numerical simulation of a multi-stage solar water still. Theoretical estimation and experimental results obtained were found to be in a good agreement.

Similarly, Kumar et al. [182] developed a transient mathematical model for a multi-stage evacuated solar desalination system in MATLAB. Two separate programs were written for calculating outlet temperature from flat plate collectors and productivity of desalination system. The outlet temperature from the flat plate collectors that calculated in the first program was given as input to the multi-stage desalination program. They reported that there was a good agreement for the distillate yield between the present model and the experimental results.

It can be concluded that the CFD is appropriate to be used with single-stage or a simple basin-type solar still though it is not trivial to write a program code which can simulate simultaneously the solar radiation and the desalination process of a multi-stage solar stills. Therefore, in this research, the simulation of the operation of the multi-effect solar water

stills coupled with evacuated tube solar collectors was conducted in a Matlab/Simulink environment as it is presented in Chapter 3. A Simulink model was developed in order to overcome the restrictions of the ANSYS FLUENT.

2.5 Conclusions Based on Literature Review

From the literature review, the desalination systems driven by solar energy can be considered as a promising alternative to reduce the continuous increase in energy demand caused by the utilization of conventional desalination systems and to alleviate the negative environmental impacts of fossil fuel.

Despite the fact that the small scale solar desalination systems have low performance in terms of productivity and thermal efficiency and they are still at the laboratory stage of development, it can be concluded from the performed review that there is an increasing interest in developing and improving its performance in order to make them more efficient and commercially competitive. Furthermore, the literature review shows that a number of attempts were made to enhance the performance of small scale desalination systems. The modifications proposed are mainly focused on introducing new design features, enhancing the evaporation processes and using advanced techniques such as nano-particles addition. Unfortunately, the above-mentioned modifications require sometime service of highly qualified operators and extra materials and equipment, which negatively affects the cost of the solar desalination systems.

The literature review conducted also reveals that the previous studies of the small-scale solar desalination systems concentrated on the units, operating under atmospheric pressure and few attempts were made on creation of the systems working in reduced pressure

conditions. The effect of the pressure level inside the system is very important and needs further investigations. Finally, the literature review demonstrates that the performance of the multi-stage solar stills is greater than that of the single basin solar stills; moreover the evacuated tube solar collectors have higher efficiency compared to the efficiency of the flat plate solar collectors.

Therefore, the main aim of this PhD study is to investigate theoretically and experimentally the performance of a solar desalination system consisting of multi-effect solar still, coupled with fluid piston energy converter for reduction of the pressure and driven by evacuated tube solar collectors. The performance of the proposed system is to be examined for different internal pressure levels.

Chapter 3 Mathematical Modelling of the Dynamic Multi-Effect Solar Water Still

In this chapter, the system's configuration and operation principles of the evacuated multi-effect solar desalination stills are described. The thermodynamic mathematical model of the proposed system is presented, which is a system of mass and energy balance equations applied to each stage of the desalination system. Thereafter, the developed dynamic simulation model is used to solve the governing equations in the Matlab/Simulink environment. Finally, the theoretical results obtained on performance of the system are presented and validated.

3.1 Design and Operational Principles of the System

The proposed system in this study is a novel solar thermal desalination system developed by Professor K. Mahkamov. The system configuration is schematically presented in Figure 3.1 and it consists of two subsystems. The first includes multi-effect water stills which are made up of four stills arranged one on the top of another. Each unit, which is called an effect or stage, comprises two V-shaped trays which represent the evaporating and condensing surfaces. The condensing surface at the bottom of one stage acts as the evaporating surface for the stage above.

The other system is the heat supply system, which includes an evacuated tube solar collector, a solar radiation simulator, and a small fluid piston energy converter. The solar collector is used to provide heating for the saline water in the stills and also to drive the

fluid piston converter. This converter operates as a vacuum pump to evacuate air from the stills and reduce their pressure, which should intensify the evaporation rate of saline water.

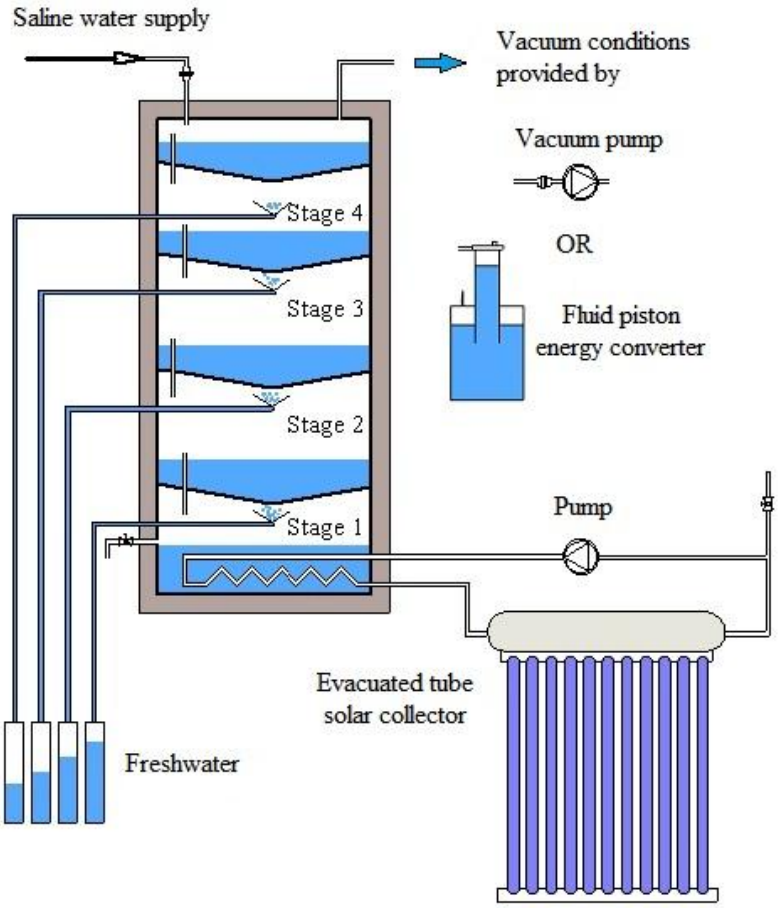

Figure 3.1 Schematic diagram of the multi-effect solar desalination system.

The heat energy is supplied to the system through the solar collectors, making the system to operate in active mode in order to enhance the rate of production of fresh water. As shown in Figure 3.1, the solar radiation is absorbed by the solar collector and the thermal energy generated is transferred into the closed loop between the solar collector manifold and the heat exchanger which is immersed in the waterbed of the first (bottom) stage. Thus, the heat energy is provided that is utilized to increase the temperature of the saline water in this stage, and consequently the saline water evaporates.

The water vapour in the first stage condenses on the bottom surface of the second stage and, as a consequence of this, the latent heat of condensation is passed to the second stage and thus the latent heat rejected from the condensation process is used to progressively increase the temperature of the saline waterbed in the second stage, leading to further evaporation and condensation. Similarly, the saline waterbeds in the tray of the third and fourth stages are heated by utilizing the latent heat released from the condensed water vapour of the previous stages.

The fresh water droplets condense on the bottom surfaces of all stages and flow into the inclined trough due to the gravity towards the stage outlet and are collected separately from each stage.

3.2 Description of the Thermodynamic Mathematical Model

Aiming to derive the thermodynamic mathematical model for the multi-effect water stills, each effect or stage of the desalination system was considered as a control volume. The mathematical model is obtained by applying energy and mass balance equations for each stage of the system separately, as shown in Figure 3.2. The overall mathematical model of the multi-effect water still is interconnecting all of the stages together.

The mathematical model developed takes into consideration the influence of variation in the thermo-physical properties of the binary mixture of dry air and water vapour, the partial pressure of the vapour on the evaporating and condensing surfaces, and also variations in the average distance between these two surfaces. The heat losses from the system is also considered in this model.

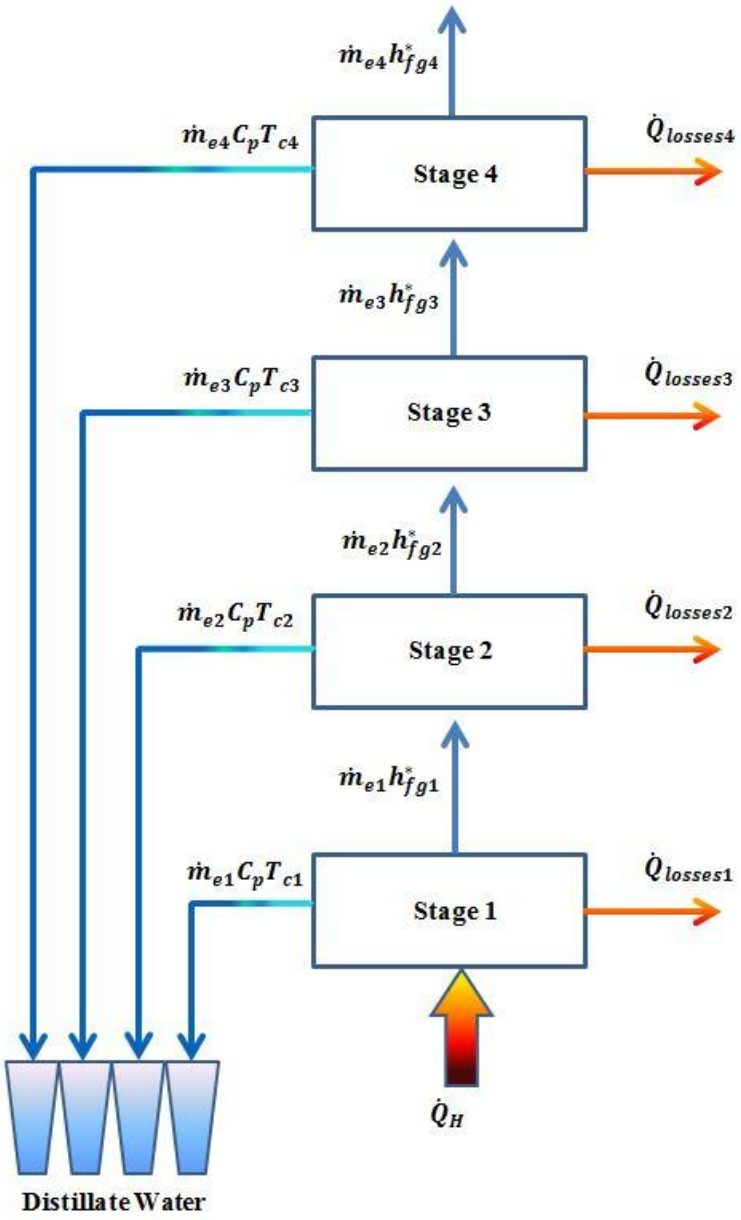

Figure 3.2 Energy balance diagram for a multi-effect solar stills.

3.2.1 Assumptions of the Thermodynamic Mathematical Model

To reduce the complexity of the calculations, the following assumptions have been made when deriving the model:

- Heat is transmitted between the hot saline waterbed and the condensation surface by processes of evaporation and condensation.
- Heat transfer by natural convection and radiation can be considered as negligible due to the absence of non-condensable gases and the low temperature difference between adjoining stages.
- All evaporated water is condensed and is equal to the distillate yield in the every stage.
- The distillate leaves the stage with the same temperature as the condensing surface.

3.2.2 Governing Equations

To calculate the variations in the waterbed temperature and freshwater productivity of each stage in the system, the energy and mass conservation equations were written in the form of ordinary differential equations. The dynamic mathematical model of the multi-effect solar still is presented as a combination of the following equations:

First stage:

$$\dot{Q}_H - \dot{m}_{e1}\left(h^*_{fg1} + c_p T_{c1}\right) = M_{s1} C_{ps1} \frac{dT_{s1}}{dt} + \dot{Q}_{losses1} \tag{3.1}$$

Second stage:

$$\dot{m}_{e1} h^*_{fg1} - \dot{m}_{e2}\left(h^*_{fg2} + c_p T_{c2}\right) = M_{s2} C_{ps2} \frac{dT_{s2}}{dt} + \dot{Q}_{losses2} \tag{3.2}$$

Third stage:

$$\dot{m}_{e2} h^*_{fg2} - \dot{m}_{e3}\left(h^*_{fg3} + c_p T_{c3}\right) = M_{s3} C_{ps3} \frac{dT_{s3}}{dt} + \dot{Q}_{losses3} \tag{3.3}$$

Fourth stage:

$$\dot{m}_{e3}h^*_{fg3} - \dot{m}_{e4}\left(h^*_{fg4} + c_p T_{c4}\right) = M_{s4}C_{ps4}\frac{dT_{s4}}{dt} + \dot{Q}_{losses4} \tag{3.4}$$

The mass conservation equation for each stage is:

$$\frac{dM_{si}}{dt} = -\dot{m}_{ei} \tag{3.5}$$

The latent heat of vaporization of water in each stage is calculated, as suggested in [156]:

$$h_{fgi} = 1000 \times [3161.5 - 2.41(T_{av} + 273.15)] \tag{3.6}$$

where:

$$\mathrm{T_{av}} = \frac{\mathrm{T_{si}} + \mathrm{T_{ci}}}{2} \tag{3.7}$$

The most significant improvement takes into consideration the nonlinear temperature profile in the condensation film and refinements to the energy balance to include the additional energy needed to reduce the film temperature below the saturation point. Both above effects can be taken into account by substituting h_{fgi} with h^*_{fgi}, where h^*_{fgi}, is the modified latent heat of vaporization of the water at the condensing surface for each stage, and it is determined in [215]:

$$h^*_{fgi} = h_{\mathrm{fgi}} + 0.68 \times C_{pi}(T_{si} - T_{ci}) \tag{3.8}$$

The specific heat capacity of water for each stage can be given as a function of its temperature as proposed in [216]:

$$C_{pi} = 1000 \times [4.2101 - 0.0022T_{si} + 5 \times 10^{-5}T_{si}^2 - 3 \times 10^{-7}T_{si}^3] \quad (3.9)$$

The specific heat capacity of saline water at constant pressure can be determined as proposed in [217]:

$$C_{ps} = a + bT_{si} + cT_{si}^2 + dT_{si}^3 \quad (3.10)$$

where the values of the constants a, b, c, and d are estimated according to the degree of salinity of the water S, (mg/kg or ppm) as follows:

$$a = 4206.8 - 6.6197\,S + 1.2288 \times 10^{-2}S^2 \quad (3.11)$$

$$b = -1.1262 + 5.4178 \times 10^{-2}S - 2.2719 \times 10^{-4}S^2 \quad (3.12)$$

$$c = 1.2026 \times 10^{-2} - 5.3566 \times 10^{-4}S + 1.8906 \times 10^{-6}S^2 \quad (3.13)$$

$$d = 6.8777 \times 10^{-7} + 1.517 \times 10^{-6}S - 4.4268 \times 10^{-9}S^2 \quad (3.14)$$

The above correlations are valid for a range of water salinity between 20,000 ppm and 160,000 ppm and a saline water temperature which varies between 20 ^{o}C and 180 ^{o}C.

The walls of the stills are insulated and the heat losses through the walls of each stage, $\dot{Q}_{lossesi}$, can be estimated based on the thermal conductivity of the insulation material used, the temperature of the saline water bed and the ambient temperature as follows:

$$\dot{Q}_{\text{lossesi}} = U_{ti} \times A_{wsi} \times (T_{si} - T_a) \quad (3.15)$$

where

$$U_t = \left[\left(\frac{1}{h_{cvi}}\right) + \frac{insulation\ thickness, m}{insulation\ thermal\ conductivity}\right]^{-1} \quad (3.16)$$

The natural convection heat transfer induced by the temperature difference ΔT between two fluids is estimated by the value of the ordinary Grashof number, *Gr*. However, due to the extremely intricate phenomena of combined mass and heat transfer inside the evacuated multi-effect desalination system, the mass transfer takes place due to a fluid density differential, which is a function of temperature and its composition. Since the water vapour is lighter than dry air, the evaporation actually increases the driving buoyancy force, represented by ΔT, which leads to the definition of the modified Grashof number which is defined as follows [218]:

$$Gr_i^* = \frac{g B_i \rho_{mi}^2 L^3\, \Delta T_i^*}{\mu_{mi}^2} \quad (3.17)$$

where:

$$\beta_i = (T_{ci})^{-1} \quad (3.18)$$

ΔT_i^* is the modified temperature difference for each stage, which it is higher than ΔT and given by

$$\Delta T_i^* = (T_{si} - T_{ci}) + \frac{T_{si}(P_{vsi} - P_{vci})(M_a - M_v)}{M_a P_o - P_{vsi}(M_a - M_v)} \quad (3.19)$$

Here, P_v is the partial saturation pressure of water vapour. In spite of the fact that P_v is available as classical correlations in the several previously published articles, these are not valid for the entire temperature range of this research. Therefore for this purpose, the following correlation was derived by fitting the numerical values of the partial saturation

pressure of water vapour in kPa in the temperature range between 10 and 110 ^{o}C (available from the thermodynamic tables of properties of water). Thus, the partial saturation pressure of the water vapour inside each stage of the system can be calculated as suggested in [183]:

$$P_{vi} = 1.131439334 - 3.750393331 \times 10^{-2} T_{av} + 5.591559189 \times 10^{-3} T_{av}^{2} - 6.220459433 \times 10^{-5} T_{av}^{3} + 1.10581611 \times 10^{-6} T_{av}^{4} \quad (3.20)$$

The convective heat transfer coefficient for the enclosed space can be calculated using the following correlation proposed in [219]:

$$Nu = C\,(Ra)^{n} \quad (3.21)$$

Here the constants *C* and *n* can be assumed to be equal to 0.2 and 0.26 respectively, as suggested in [183], and these values are valid for a suitably broad range of values of Rayleigh number, Ra, between 3.5×10^{3} and 10^{6}.

Also,

$$Nu = \frac{h_{cvi}\, L}{k_{mi}} \quad (3.22)$$

and

$$Ra = Gr.Pr \quad (3.23)$$

Thus, equation 3.21 can be written as:

$$\frac{h_{cvi}\,L}{k_{mi}} = 0.2(Gr_i^*\,Pr_i)^{0.26} \tag{3.24}$$

Also,

$$Pr_i = \frac{\nu_{mi}}{\alpha_{mi}} \tag{3.25}$$

Accordingly, the convective heat transfer coefficient for each stage can be calculated as follows:

$$h_{\text{cvi}} = Ck_{mi}L^{3n-1}\left(\frac{g\rho_{mi}\beta_i}{\mu_{mi}\alpha_{mi}}\right)^n\left[(T_{si}-T_{ci}) + \frac{T_{si}(P_{vsi}-P_{vci})(M_a-M_v)}{M_aP_o - P_{vsi}(M_a-M_v)}\right]^n \tag{3.26}$$

The distillate production rate for each stage can be calculated using the following expression presented in [219]:

$$\dot{m}_{\text{ei}} = \frac{A_s h_{cvi}}{(\rho_{mi}c_{pmi})}\frac{P_o}{P_{AMi}}\frac{M_v}{R}\left(\frac{P_{vsi}}{T_{si}} - \frac{P_{vci}}{T_{ci}}\right)Le_i^{-2/3} \tag{3.27}$$

Here, P_{AMi} is the arithmetic mean pressure, Pa, which is [219]:

$$P_{AMi} = P_o - \frac{P_{vsi}-P_{vci}}{2} \tag{3.28}$$

$$Le_i = \frac{\alpha_{mi}}{D_i} \tag{3.29}$$

All values of the thermo-physical properties of the vapour-air mixture in equations 3.17 to 3.29 can be estimated as proposed in [218, 219], see Appendix B.

3.3 Global Solar Resources

The sun radiates energy into outer space and, as this radiation passes through the earth's atmosphere, a certain amount of the radiation is backscattered into space and a proportion of the sun's rays are absorbed and scattered by the atmosphere. The remaining solar radiation is directed towards the Earth's land-sea surface from various directions, as shown in Figure 3.3. The amount of radiation scattered, absorbed, and reflected depends on the conditions in the local atmosphere that the incident radiation passes through; for example, the percentages of water vapour, dust, and pollution. In addition, the latitude of a particular location and the time of a certain day of the year have important effects on the amount of the sun's rays incident on the Earth's surface [220].

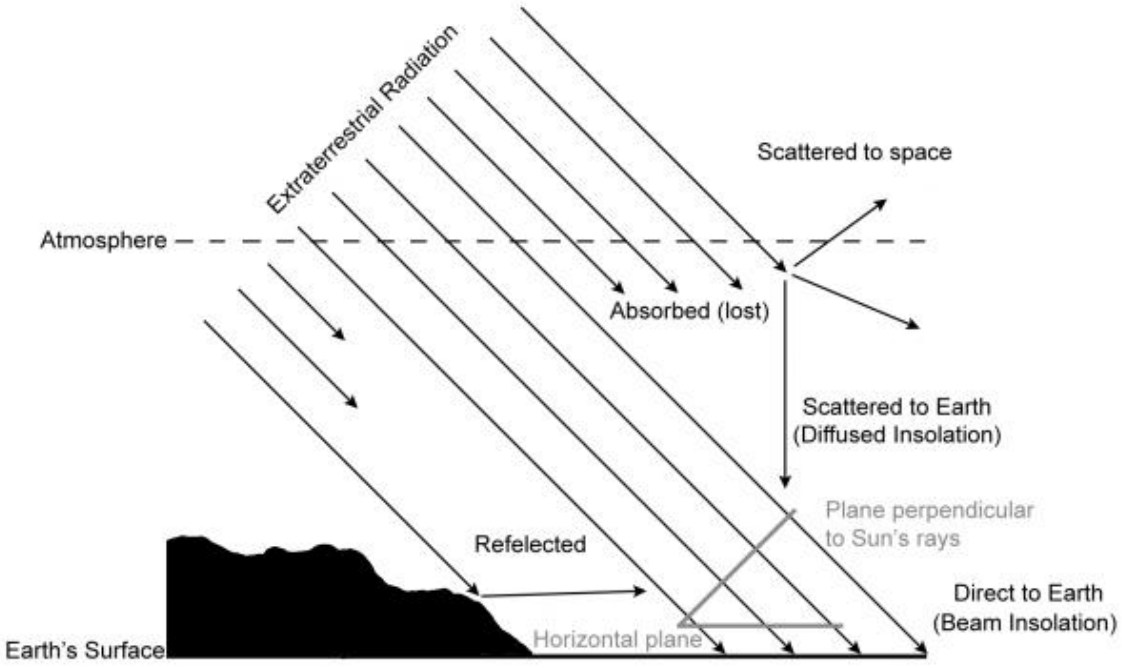

Figure 3.3 Solar radiation reaching the Earth

The total solar radiation, often called the global solar radiation received at the earth's surface (G_{tot}), is the sum of direct or beam radiation (G_B), diffused radiation (G_D), and reflected radiation (G_R) [220].

$$G_{tot} = G_B + G_D + G_R \tag{3.30}$$

3.3.1 Beam Radiation (G_B)

Beam radiation is the solar radiation received from the sun which passes straight through the earth's atmosphere and is incident on a surface. It can be calculated as:

$$G_B = G_0 * \tau_b * R_b \tag{3.31}$$

where G_0 is the solar radiation flux from outside the earth's atmosphere which is incident perpendicularly on a horizontal plane, and R_b a geometric factor which is the ratio of beam solar radiation on a tilted surface to that on a horizontal surface at a specified time. The atmosphere transmittance factor, τ_b, represents the variation in the effects of the atmospheric conditions on the scattering and absorbing of solar radiation. Throughout any day of the year, the value of G_0 for a horizontal surface can be estimated as:

$$G_0 = G_{sc}\left(1 + 0.033\cos\frac{360n}{365}\right)\cos\theta_z \tag{3.32}$$

where n is the number of the day in the year

Meanwhile:

$$\tau_b = a_0 + a_1 exp\left(\frac{-k}{\cos\theta_z}\right) \tag{3.33}$$

where a_0, a_1 and k are factors which take into account the location's latitude and the sky's transmittance.

And:

$$R_b = cos\,\theta / \cos\theta_z \tag{3.34}$$

3.3.2 Diffused Radiation (G_D)

Solar radiation which is scattered in all directions in the atmosphere and hits the earth's surface from various directions is called diffused radiation. The diffused solar radiation on a surface, G_D, can be calculated as:

$$G_D = G_0 * \tau_d * \left(\frac{1+\cos\beta}{2}\right) \tag{3.35}$$

where τ_d is the atmospheric transmittance of the diffused solar radiation and β is the inclination angle of the surface or the solar collector.

Also,

$$\tau_d = 0.271 - 0.294(\tau_b) \tag{3.36}$$

3.3.3 Reflected Radiation (G_R)

This is the beam and diffused solar radiation that is reflected from surfaces other than the atmosphere, such as by trees, buildings, hills, and incident on a plane such as a solar collector. The reflected solar radiation on a surface, $G_{R,}$ is given by:

$$G_R = G_0(\tau_b + \tau_d) * \rho_g \left(\frac{1-\cos\beta}{2}\right) \tag{3.37}$$

where ρ_g is the reflectance of the ground.

3.4 Heat Energy Supplied to the Desalination System

As mentioned above, the total amount of solar radiation received from the sun and incident upon the solar collector depends on many factors such as the latitude, longitude and position of the sun in the sky at a particular time of day throughout the year. Likewise, the direction and inclination angle of the solar collector have important consequence effects on the amount of thermal energy that can be collected. The thermal energy of solar radiation provides the heat used to operate the desalination system, and the heat input can be calculated as described in [220]:

$$\dot{Q}_H = G_{tot} \times A_{SC} \times \eta_{SC} \tag{3.38}$$

where:

G_{tot} is the total solar irradiation incident on the surface area of the solar collector, given by equation 3.30, A_{SC} is the absorber area of the solar collector; and η_{SC} is the thermal efficiency of the solar collector which can be calculated as in [152] as:

$$\eta_{SC} = c_0 - c_1 \frac{(T_f - T_a)}{G_{tot}} - c_2 \frac{(T_f - T_a)^2}{G_{tot}} \tag{3.39}$$

Here T_f and T_a are the fluid and ambient temperatures respectively. The efficiency coefficients c_0, c_1 and c_2 are defined by the manufacturers of solar collectors during performance tests. Examples of the efficiency coefficients of evacuated tube solar collectors from three manufactures are presented in Table 3.1.

Table 3.1 Efficiency coefficients of different evacuated tube solar collectors [221].

Manufacturer	c_0	c_1 [W/m^2.K]	c_2 [W/m^2.K^2]
Solar UK	0.753	1.54	0.0099
Solar Tube Company	0.649	1.487	0.014
Thermo Technologies	0.81	1.23	0.0122

3.5 MATLAB/Simulink Environment

The set of governing equations describing the operation of the multi-effect solar water desalination, described in sections 3.2 - 3.4 were solved in a Matlab/Simulink environment. In order to simulate the performance of the proposed system, a dynamic Simulink model was developed in the Matlab/Simulink environment based on the above mathematical model as shown in Figure 3.4. This Simulink model was developed as a closed-loop, and it consists of three main subsystem blocks.

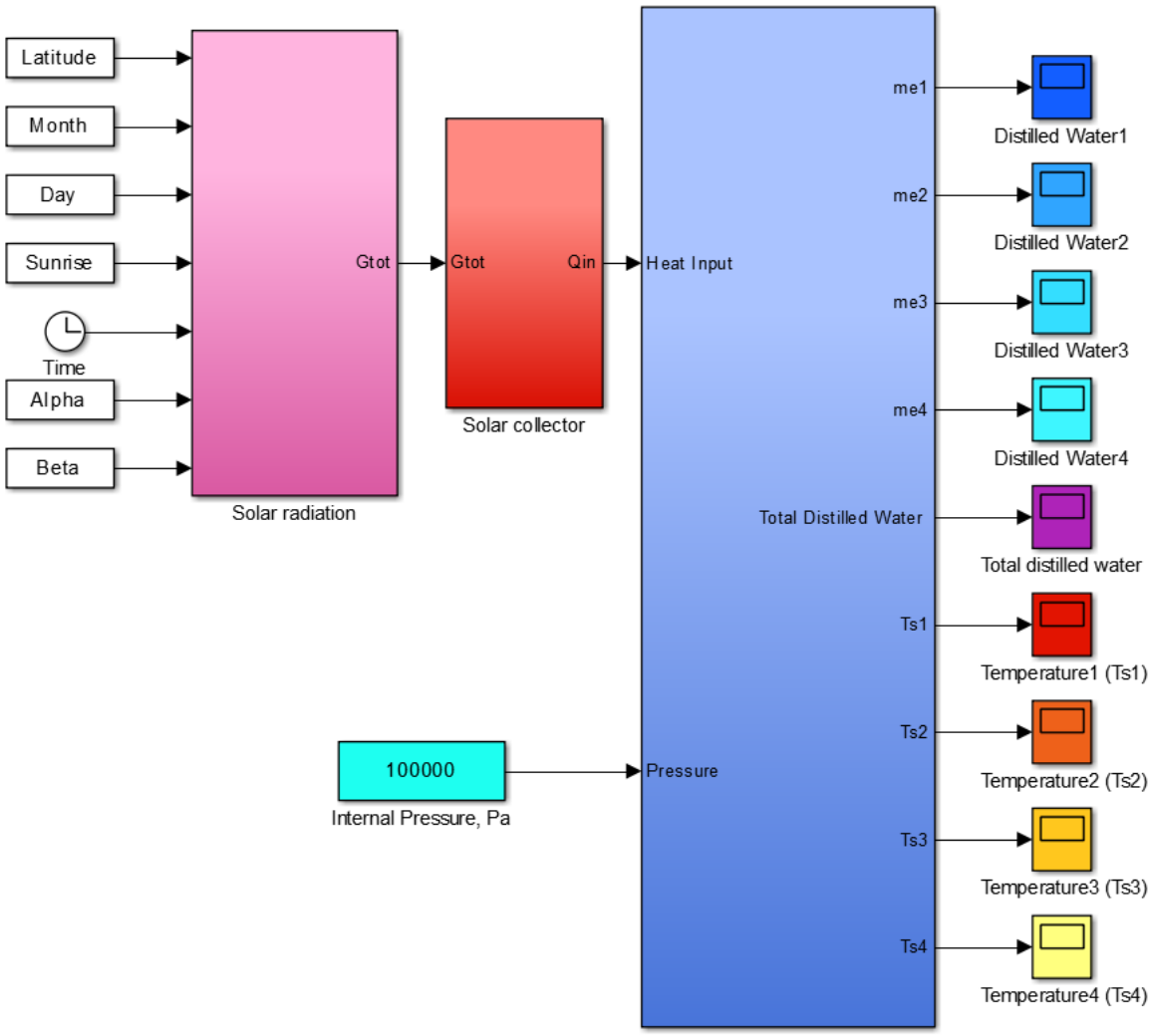

Figure 3.4 Simulink model of the multi-effect solar still.

The first block on the left in Figure 3.4 represents the thermal energy source, in which the simulation of the available solar irradiance throughout the day is executed. Afterwards, the solar irradiation produced is used as input data for the second block. This block contains the evacuated tube solar collector (ETC) model, in which the useful heat energy supplied to the desalination system is computed based on the efficiency of the ETC. The third main block represents the multi-effect desalination system. Detailed Simulink models of the desalination system are illustrated in Figures 3.5 to 3.8.

Figure 3.5 represents the four stages of the multi-effect solar water desalination unit. It can be seen that all stages are linked to each other in the appropriate sequence.

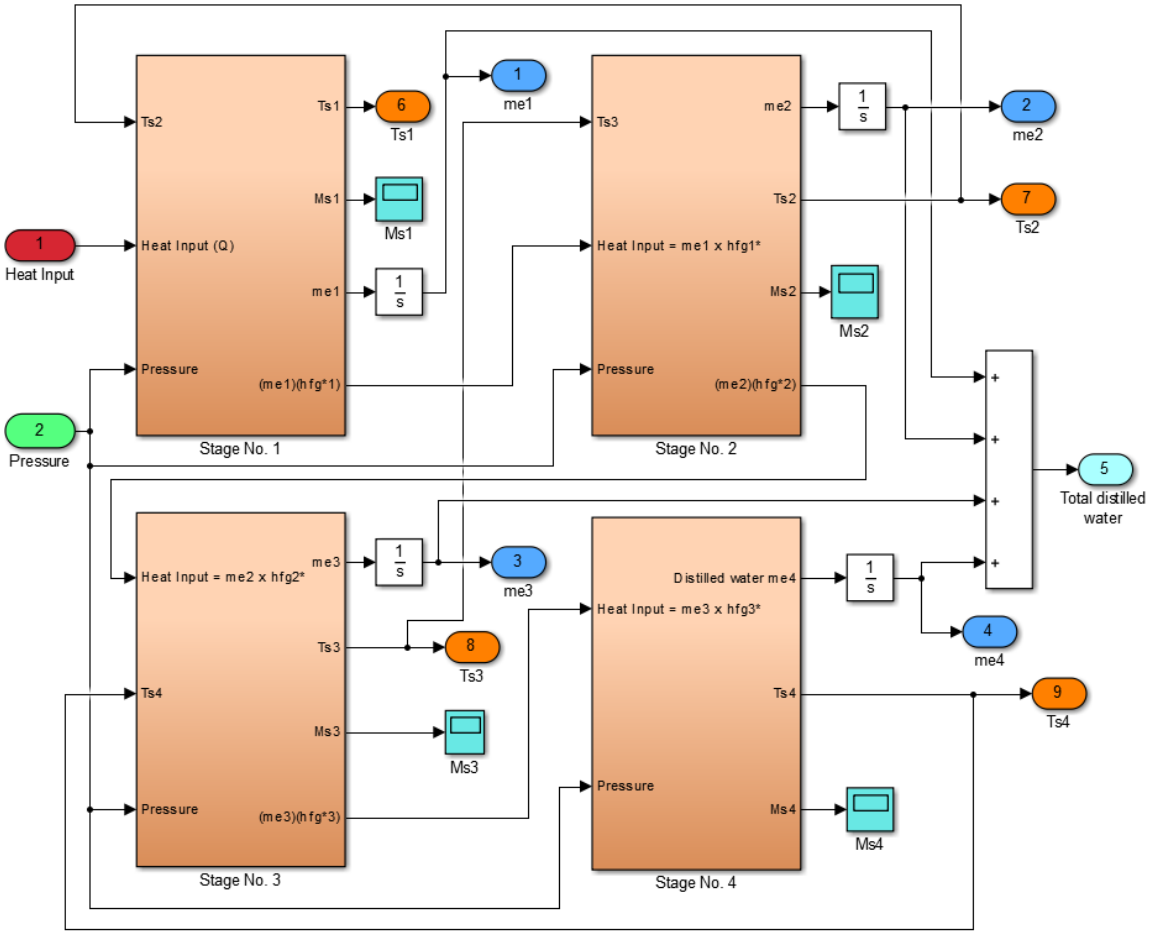

Figure 3.5 Stgaes of the still.

In this block, the cumulative freshwater yield of all stages is calculated. Figure 3.6 shows the Simulink model of the first stage of the still, which is used to determine variations in the temperature and the productivity of the stage. The internal pressure and heat input, which is pre-calculated, are used as input data for the stage model.

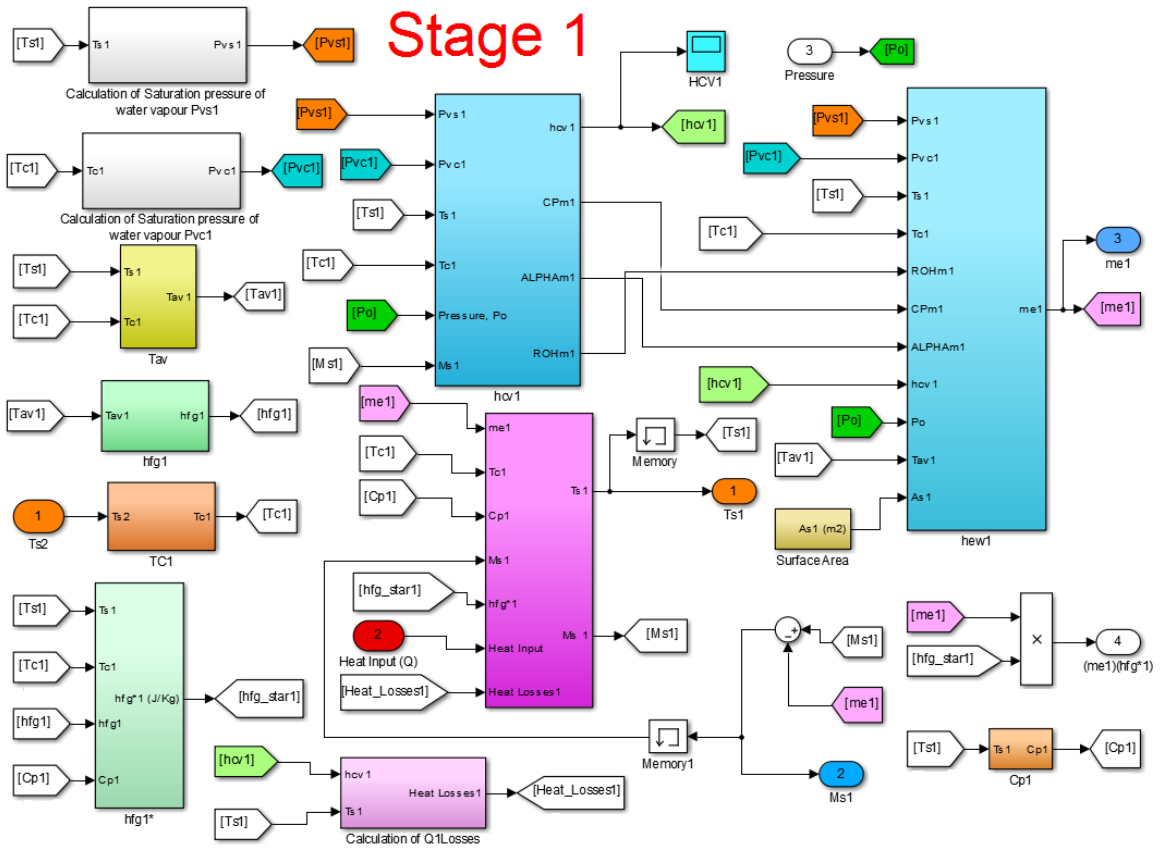

Figure 3.6 Simulink model of the first stage of the solar stills.

The Simulink model presented in Figure 3.7 is used to compute the convective heat transfer coefficient in the stage. In this block, all the thermo-physical properties of the vapour-air mixture are calculated and used to determine the convective heat transfer coefficient. Finally, as shown in Figure 3.8, the stage's productivity is computed using the value of the convective heat transfer coefficient calculated from the previous block.

These calculations were repeated for each value of solar irradiance throughout the day from the sunrise until sunset, in order to simulate the operation of the solar desalination system and to evaluate its performance for several values of internal pressure.

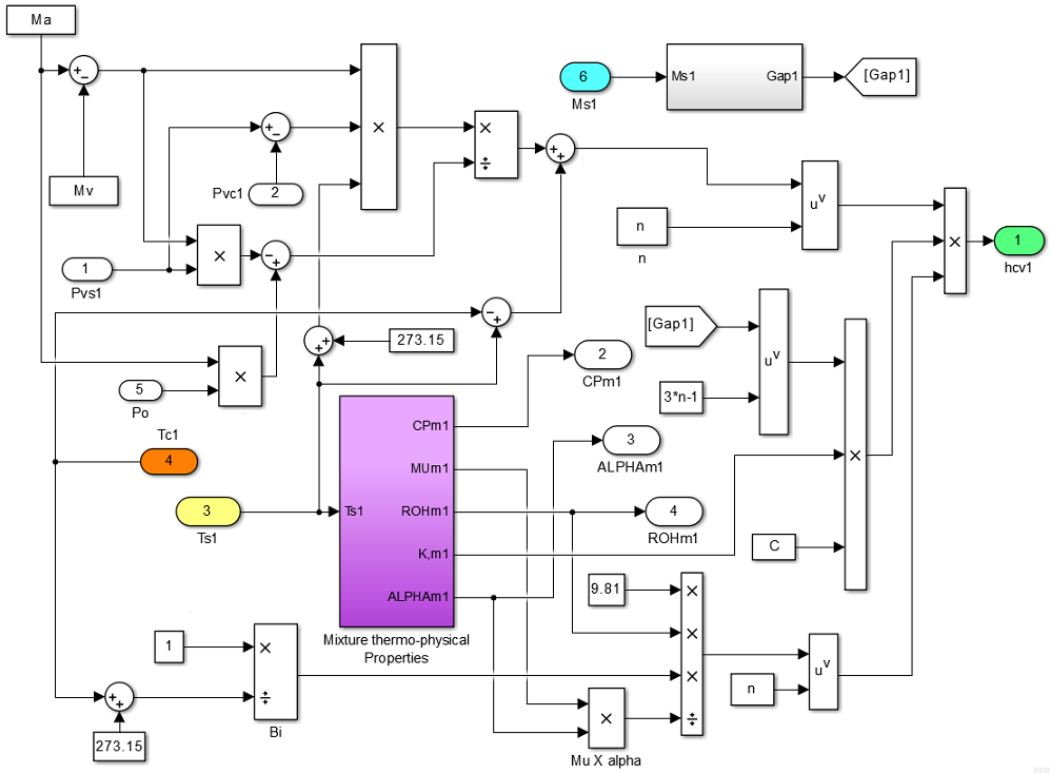

Figure 3.7 Simulink block for calculating the convective heat transfer coefficient.

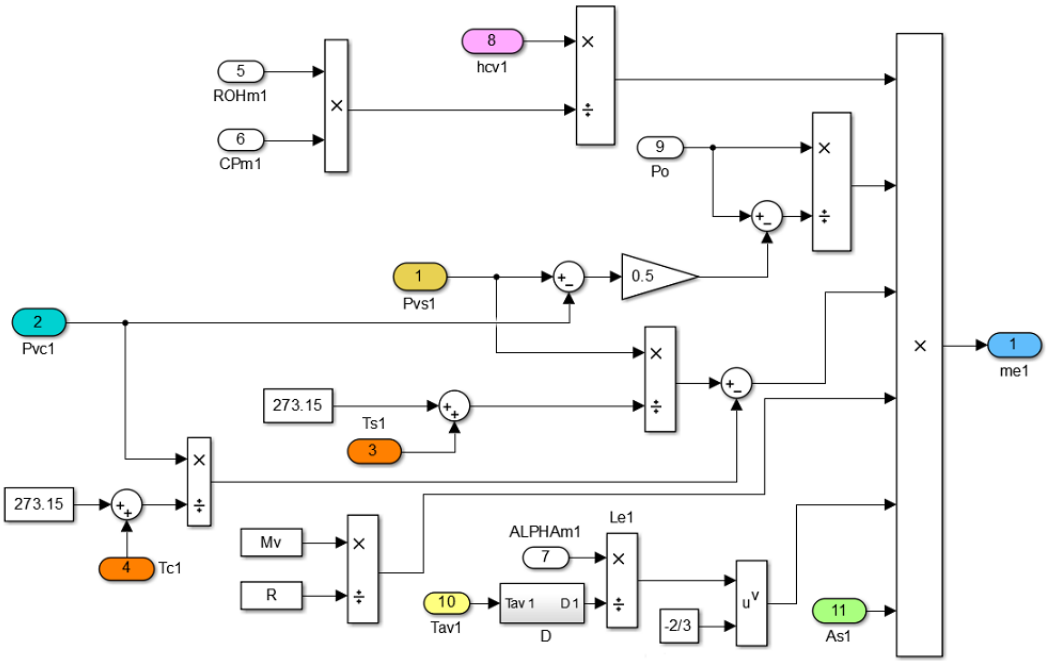

Figure 3.8 Simulink block for calculating the productivity of the still.

3.6 Validation of the Simulation Model using Published Theoretical Results

The degree of accuracy of the simulation model in predicting the physical performance of the actual system is the main concern in mathematical modelling. For that reason, the results of the current developed Simulink model were validated against the theoretical results, published in open literature. This comparison was conducted for the cumulative distillate productivity, the productivities of stages and their temperatures. The relative absolute deviation between parameters, being compared, was calculated as follows:

$$Relative\ deviation\ = \left|\frac{X_p - X_{ref}}{X_{ref}}\right| \times 100 \tag{3.40}$$

here Xp is a particular result predicted by the present simulation model and $Xref$ is the reference value of the corresponding result obtained from published sources.

3.6.1 Validation against Theoretical Case Study (1)

In this section the theoretical results obtained from the simulation model were validated against the theoretical results presented by Shatat and Mahkamov [156] and Shatat [222]. The simulation was performed for the same operating conditions, including the initial temperature of the waterbeds in all stages and internal pressure, and also by employing the same solar irradiation of a typical summer day in Middle Eastern countries as shown in Figure 3.9.

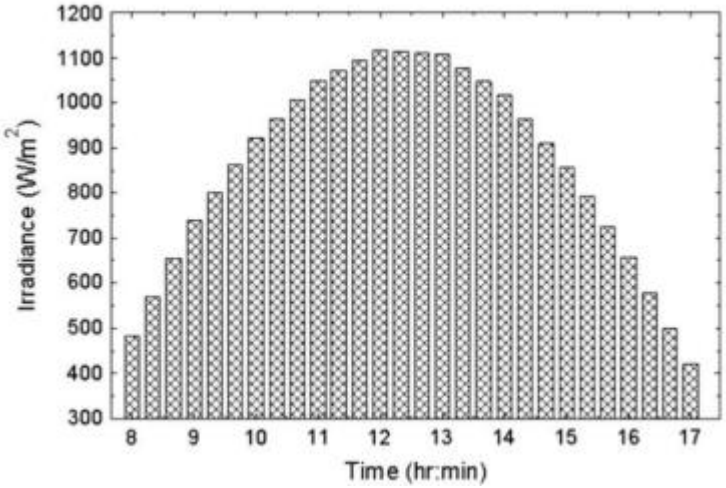

Figure 3.9 Solar irradiation of a mid-summer day in the Middle East [156].

The initial values of waterbed temperatures were set to be 12.5 ^{o}C, 12.4 ^{o}C, 12.3 ^{o}C, 12.2 ^{o}C for the first, second, third and fourth stages respectively, while the condensation surface temperatures were calculated as stated by Shatat and Mahkamov [156, 222] as follows:

$$T_{c1} = T_{s2} - 2 \tag{3.46}$$

$$T_{c2} = T_{s3} - 2.7 \tag{3.47}$$

$$T_{c3} = T_{s4} - 1.11 \tag{3.48}$$

$$T_{c4} = T_{s4} - (0.00007T_{s4}^{3} - 0.015T_{s4}^{2} + 0.9763T_{s4} - 10.324) \tag{3.49}$$

Table 3.2 shows the correspondence between day time and the time on graph. The current model's results and those published in the previous studies [156, 222] for variations in the temperature at each stage are shown in Figure 3.10 and Figure 3.11. It can be seen that

there is a very good agreement in terms of the magnitude and trend of the theoretical results obtained from the developed model with those of prior research [156].

Table 3.2 Correspondence between day time and the time on graph

Time on graph (min)	Corresponding time (hr:min)
0	08:00
200	11:20
400	14:40
600	18:00
800	21:20
1000	00:40
1200	04:00
1400	07:20
1440	08:00

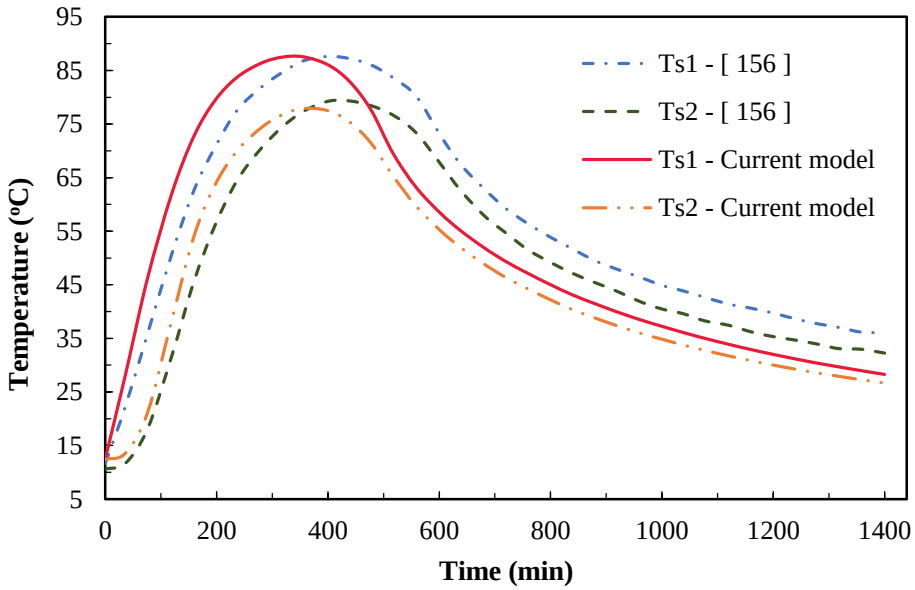

Figure 3.10 Variations in temperature in the first and second stages.

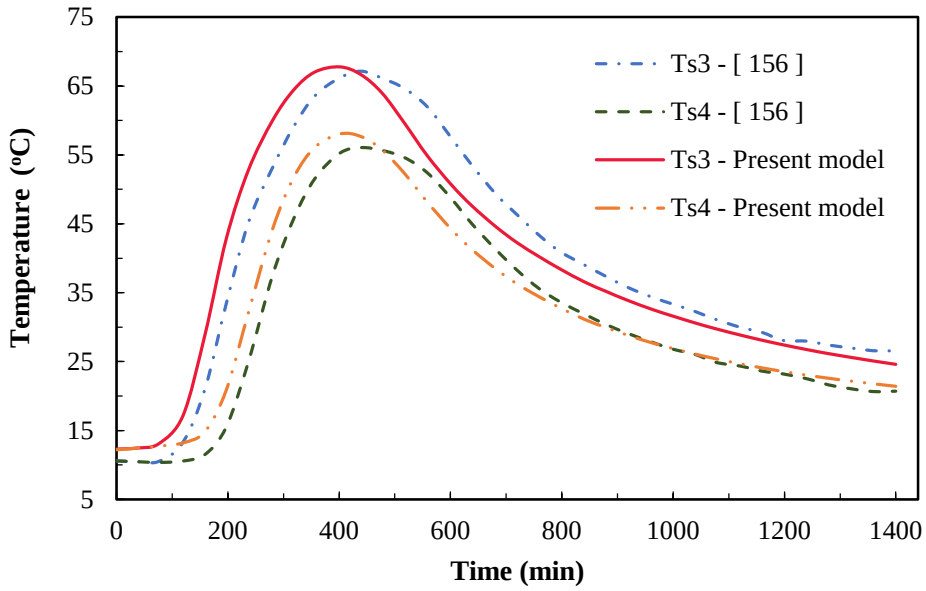

Figure 3.11 Variations in the temperature in third and fourth stages.

The maximum relative deviations between the temperature curves are 22.4%, 20.6%, 21.8% and 19.9% respectively, for the first, second, third and fourth stages.

The comparisons between the present Simulink model's results and the theoretical results [156, 222] for the distillate productivities of each stage and the total cumulative productivity are demonstrated in Figures 3.12 to 3.14.

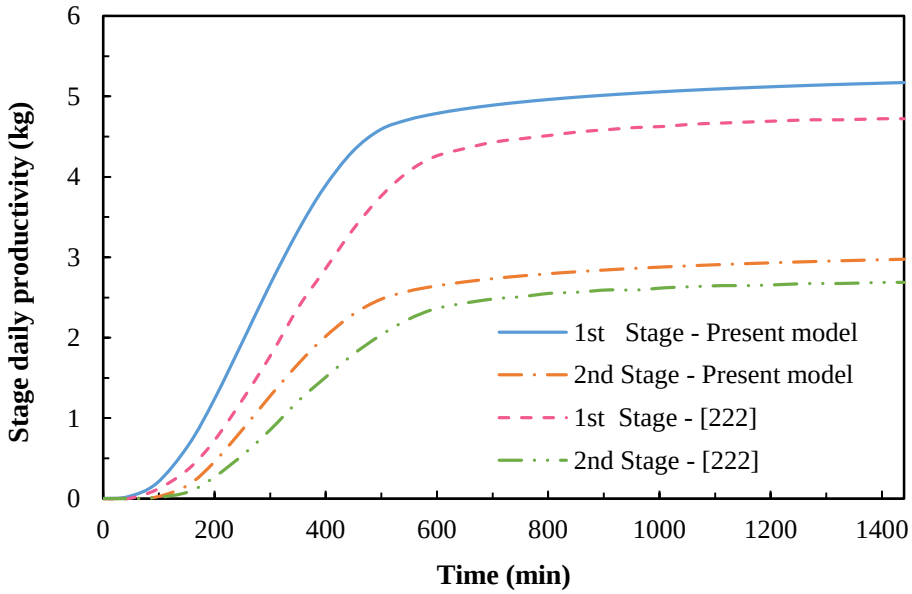

Figure 3.12 Theoretical daily productivity of the first and second stages.

It is obvious that the results predicted by the present model and the theoretical results from other research [156, 222] are in very good agreement in terms of the magnitude and trend. The maximum relative deviations between the two sets of results for daily productivity in the first, second, third, and fourth stages are 22.4%, 27.8%, 17.9%, 9.1% respectively, with 18.8% for the deviation in total cumulative distillate productivity.

This deviation between the theoretical results obtained from the present simulation model and those previously published [156, 222] can be attributed to the fact that the present model takes into account the thermo-physical properties of the binary mixture of dry air and water vapour.

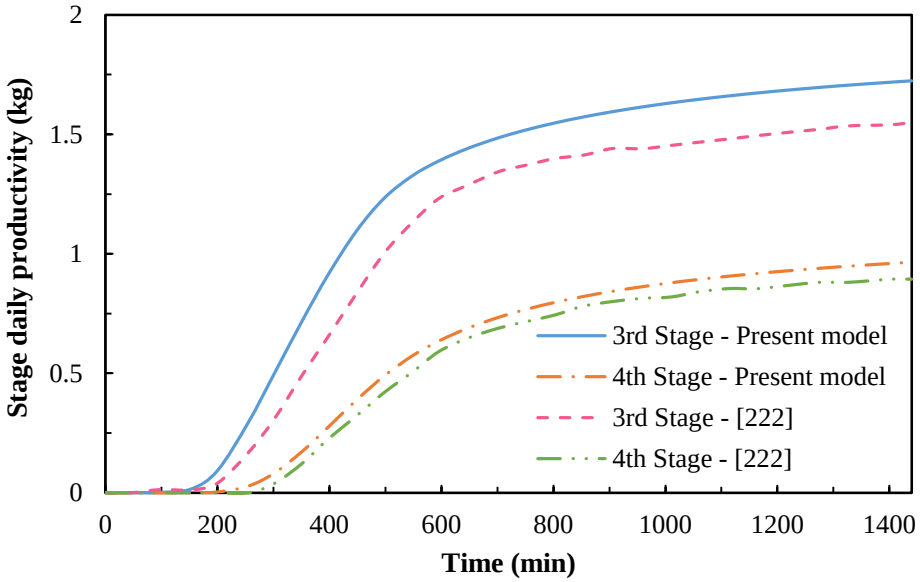

Figure 3.13 Theoretical daily productivity of the third and fourth stages.

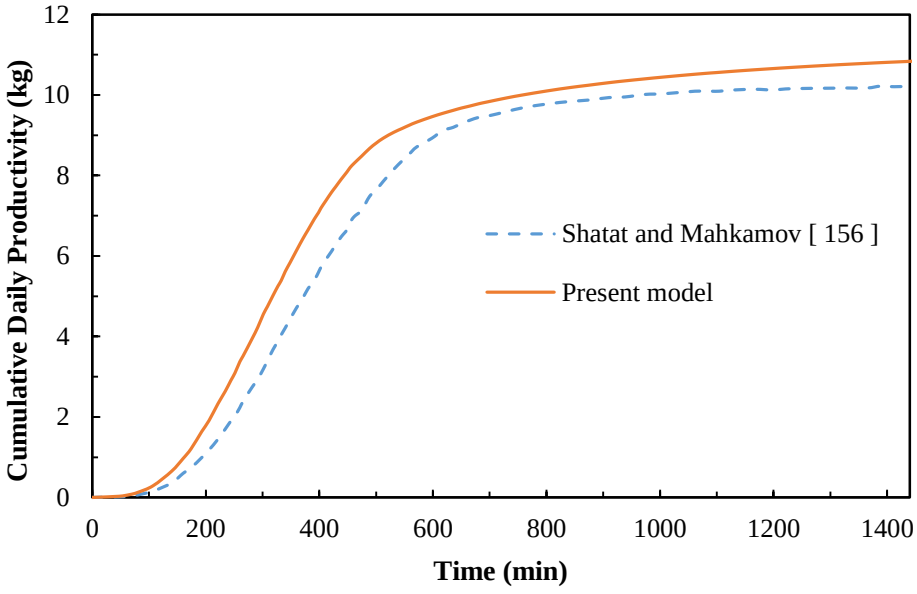

Figure 3.14 Theoretical total cumulative daily productivity.

3.6.2 Validation against Theoretical Case Study (2)

This section presents the validation of the results from the developed simulation model against the results of the theoretical investigation carried out by Reddy et al. [183]. A comparison was conducted between the total cumulative distillate productivity predicted by the present model and that presented in [183] as shown in Figure 3.15. It can be seen that there is very good agreement in terms of magnitude and trend between the two curves, and the total cumulative daily distillate productivity predicted by the present model deviates by a maximum of 6.1 % compared to that of [183].

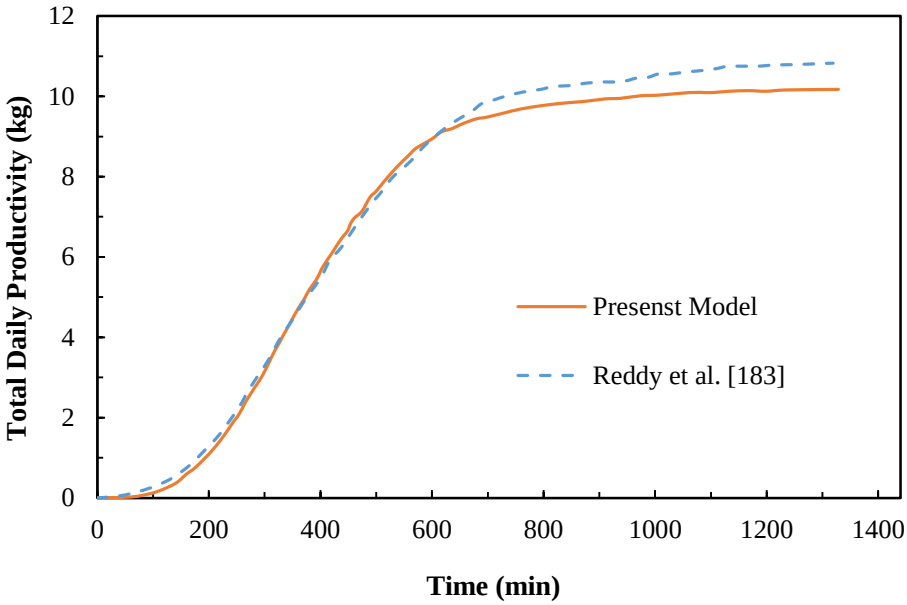

Figure 3.15 Theoretical total cumulative daily productivity.

Thus, it can be concluded that the present simulation model accurately predicts the performance of the multi-effect solar water desalination still.

3.7 Discussion of Numerical Results

The theoretical simulations of the proposed dynamic solar desalination system were conducted by utilizing the previously described Simulink model. In this simulation process, variations in solar irradiation throughout the day were assumed as input data to predict the overall performance of the system. All the physical dimensions of the multi-effect solar water desalination system were identical to the dimensions of the test rig in the laboratory. These results were obtained for the operating conditions mentioned in section 3.6.1 with an internal pressure equal to atmospheric pressure.

3.7.1 Variations in Waterbed Temperature in the Different Stages

The theoretical variations in waterbed temperatures for the four stages of the proposed multi-effect solar water desalination still are illustrated in Figure 3.16.

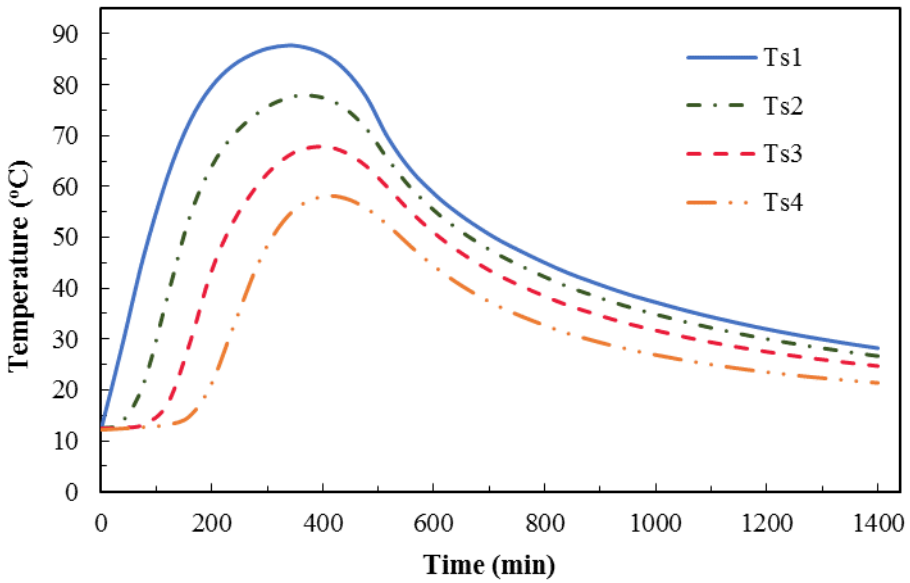

Figure 3.16 Theoretical variations in waterbed temperatures.

It can be seen that the waterbed temperature curves follow the same trend of variation but have different maximum temperature and phasing. The waterbed temperature in each stage increases with increasing solar irradiation until reaching the maximum value around the mid-day and thereafter decreasing as solar irradiation decreases. In addition, the first stage has a maximum waterbed temperature of about 87.5 ^{o}C, and those for the second, third and fourth stages are 78 ^{o}C, 67.8 ^{o}C and 58 ^{o}C respectively. Changes in phasing is the results of time necessary for heating and evaporating water in each bed.

3.7.2 Daily Distillate Productivity of the Stages

Figure 3.17 shows the predicted distillate yield of each stage of the proposed desalination system over the 24 hour period. It is obvious that the freshwater production rate is markedly high in the first 8 hours of the desalination process and then the production rate becomes lower for the rest of the day. This noteworthy high levels in distillate yield is due to the increase in solar radiation.

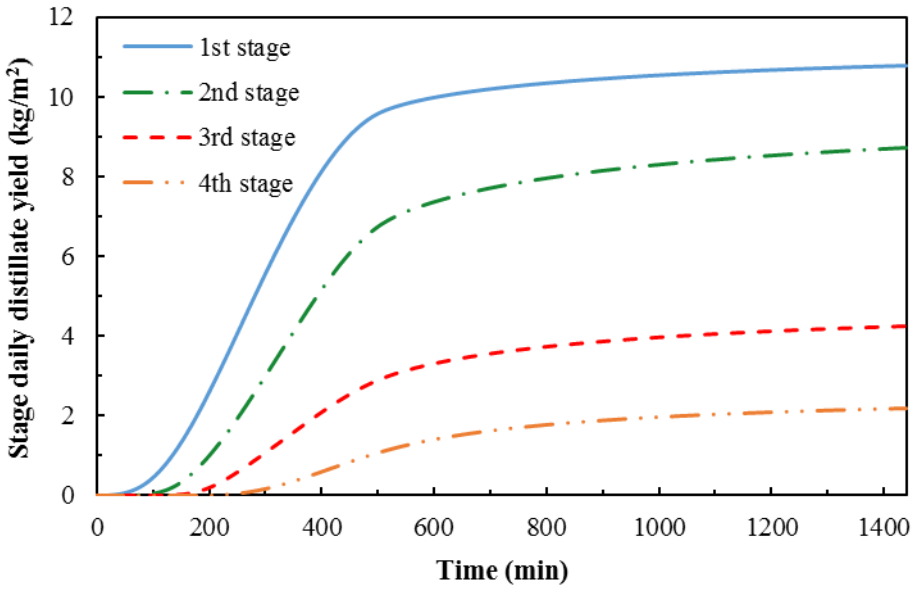

Figure 3.17 Theoretical daily productivity of the stages.

It was found that the first stage produces a maximum freshwater yield of about 10.8 kg/m^2/day and the fourth stage has the lowest daily productivity of 2.2 kg/m^2, while the second and third stages produce 8.7 kg/m^2/day and 4.3 kg/m^2/day respectively.

3.7.3 Variation in the Total Cumulative Daily Productivity

The theoretical variation in the total cumulative distillate yield calculated using the proposed simulation model is depicted in Figure 3.18. It can be seen that the rise in total cumulative distillate yield is more noticeable during the initial hours of the day. The total cumulative yield was found to be around 26 kg/m^2/day.

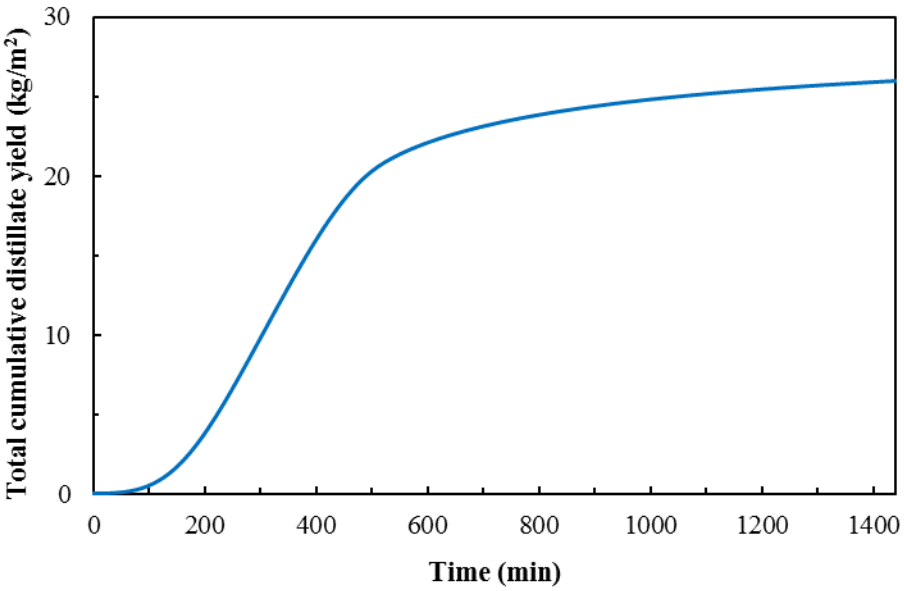

Figure 3.18 Theoretical total cumulative distillate yield.

3.7.4 Effect of Solar Radiation on the Distillate Yield

Figure 3.19 presents the variation in the hourly total cumulative distillate yield over the 24 hour period. It can be seen that the maximum hourly distillate output was obtained during the daytime due to the high value of the solar radiation.

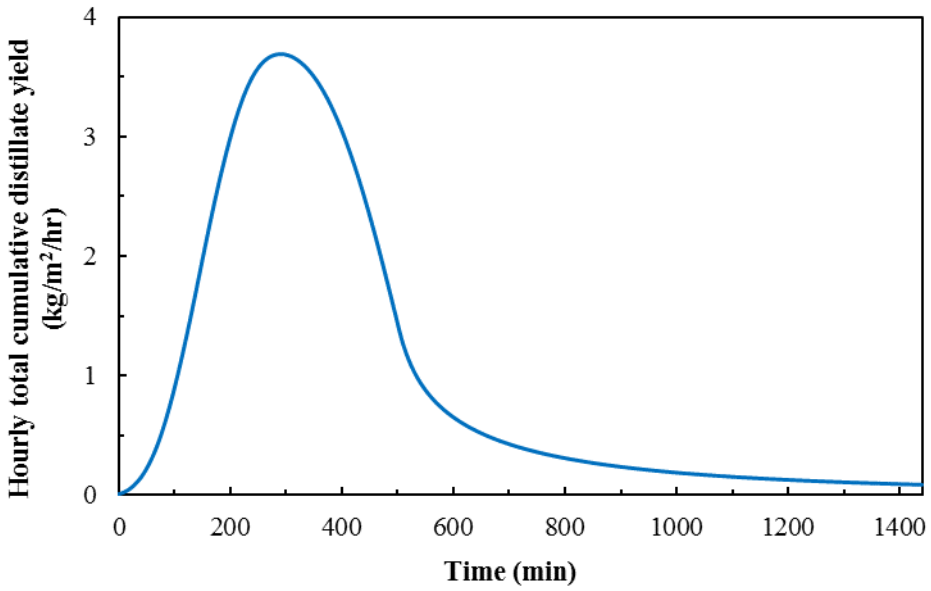

Figure 3.19 Variation in the hourly total cumulative distillate yield.

The hourly total cumulative distillate yield and solar radiation are directly related. Figure 3.20 shows the variation in the hourly total cumulative distillate yield and changes in the solar radiation from 08:00 o'clock to 17:00 o'clock during the day. It was observed that the increase in solar radiation leads to increasing hourly total cumulative yield. It was also observed that the maximum hourly cumulative yield of about 3.69 kg/m^2/hr was obtained around 13:00 o'clock while the maximum solar radiation of 1115 W/m^2 occurred at 12:00 o'clock. This time difference between the production of maximum hourly cumulative distillate and the time of maximum solar radiation is due to the time lag

between the evaporation and condensation processes and the influence of the heat storage in the waterbed.

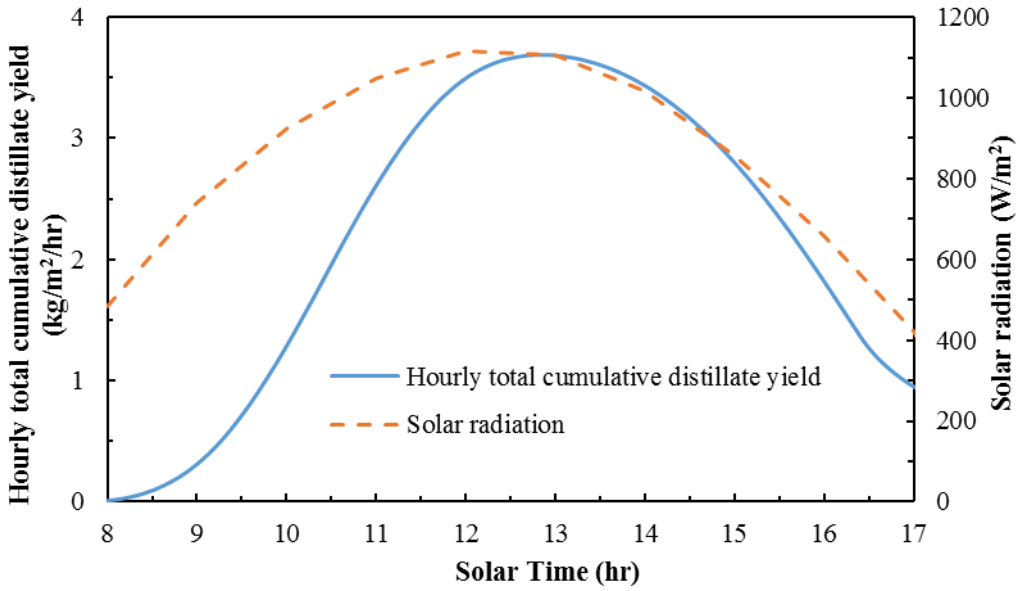

Figure 3.20 Effect of solar radiation on hourly total cumulative distillate yield.

3.7.5 Variation in Convective Heat Transfer Coefficient

The variation in the convective heat transfer coefficient, *hcv*, over the time for all stages was investigated and the results are illustrated in Figure 3.21. It was noticed that the convective heat transfer coefficient for all stages increases from minimum values at the beginning of operation until reaching maximum values of 2.76 W/m^2 K, 2.57 W/m^2 K, 2.43 W/m^2 K and 2.01 W/m^2 K for the first to fourth stages respectively. Afterward the values gradually decrease to approximately equal values of about 1.51 W/m^2 K. The low values during the initial hours of the desalination process can be attributed to the low temperature differences between the waterbeds and the condensing surfaces.

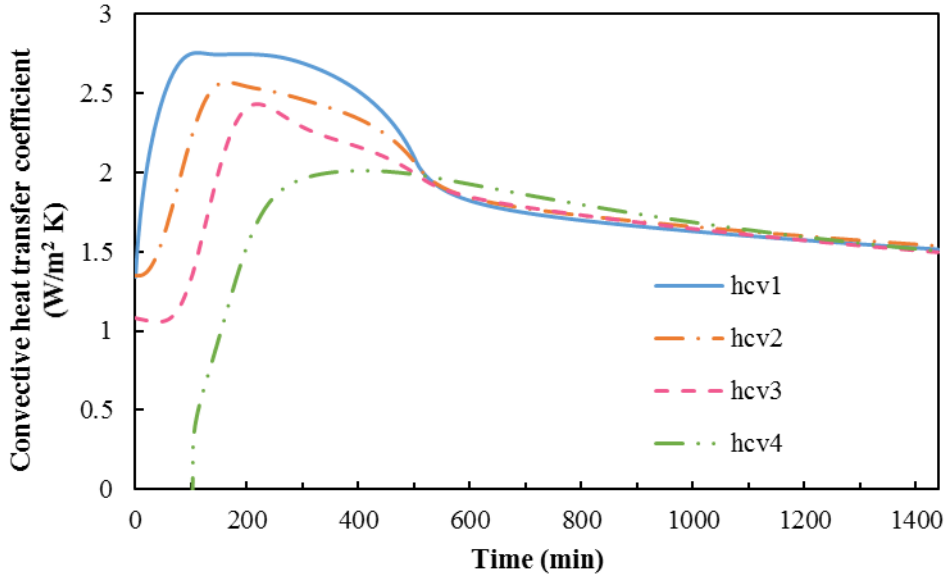

Figure 3.21 Variation in convective heat transfer coefficient (hcv) with time.

Data presented in Figures 3.22 to 3.25 can be examined with a view to understand the relationship between the variations in the convective heat transfer coefficient and the temperature difference between the evaporation surface and the condensation surface (Ts-Tc).

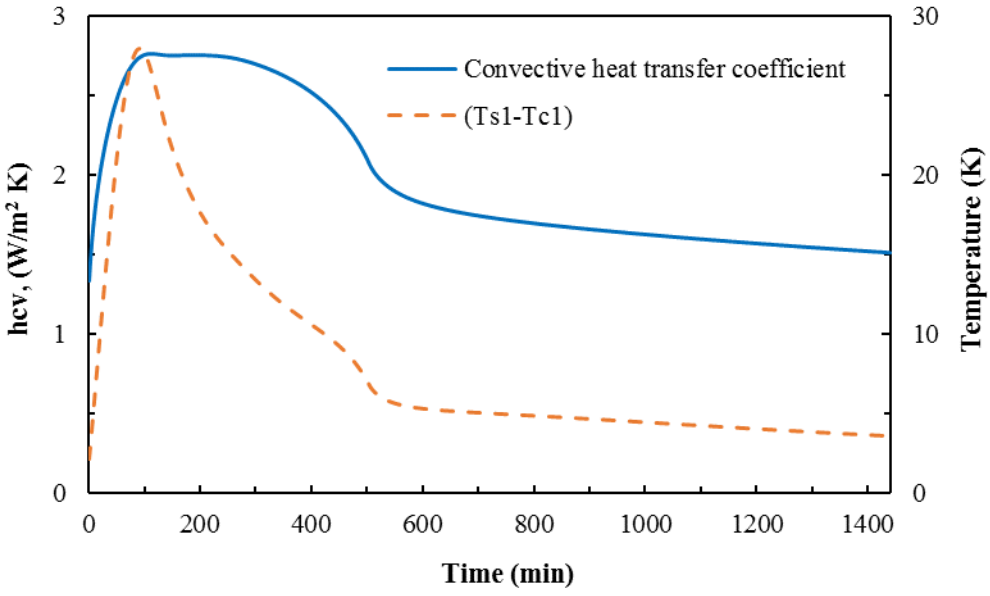

Figure 3.22 Variation in convective heat transfer coefficient with (Ts1-Tc1).

It is evident from these graphs that the convective heat transfer coefficient for all stages increases with the difference between the temperatures of the evaporation and condensation surfaces and vice versa.

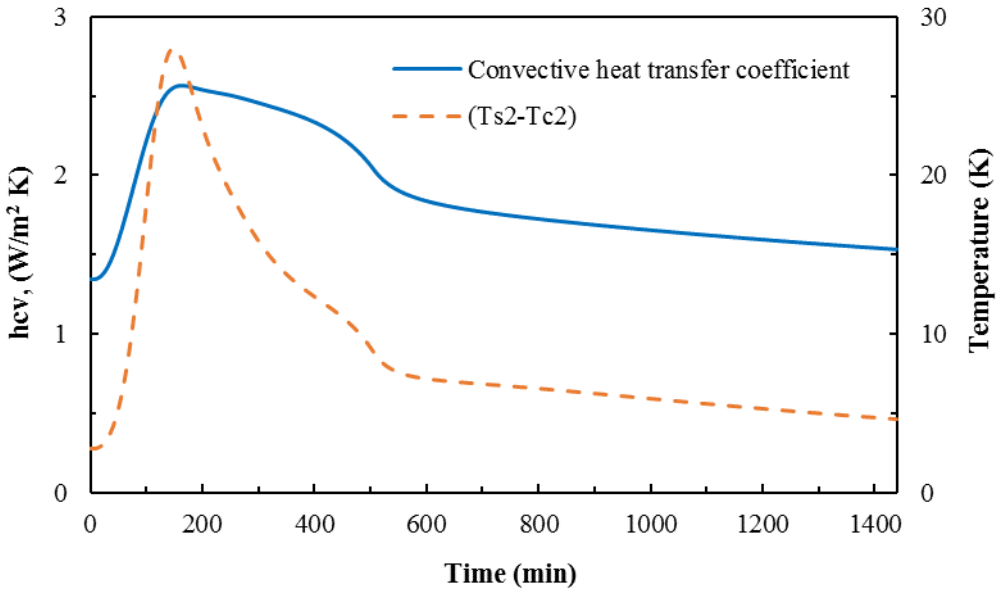

Figure 3.23 Variation in convective heat transfer coefficient with (Ts2-Tc2).

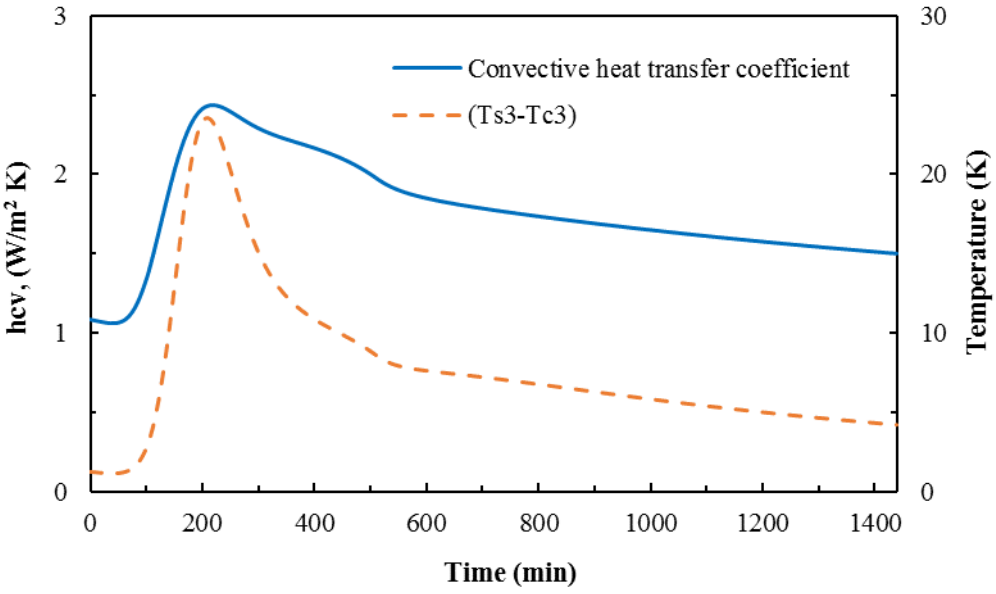

Figure 3.24 Variation in convective heat transfer coefficient with (Ts3-Tc3).

It is also clearly seen in Figure 3.25 that the convective heat coefficient of the fourth stage has a negative value at the beginning of the desalination process, and this can be explained by the fact that, during the beginning of the operation of the system, the temperature of the waterbed is lower than that of the condensing surface.

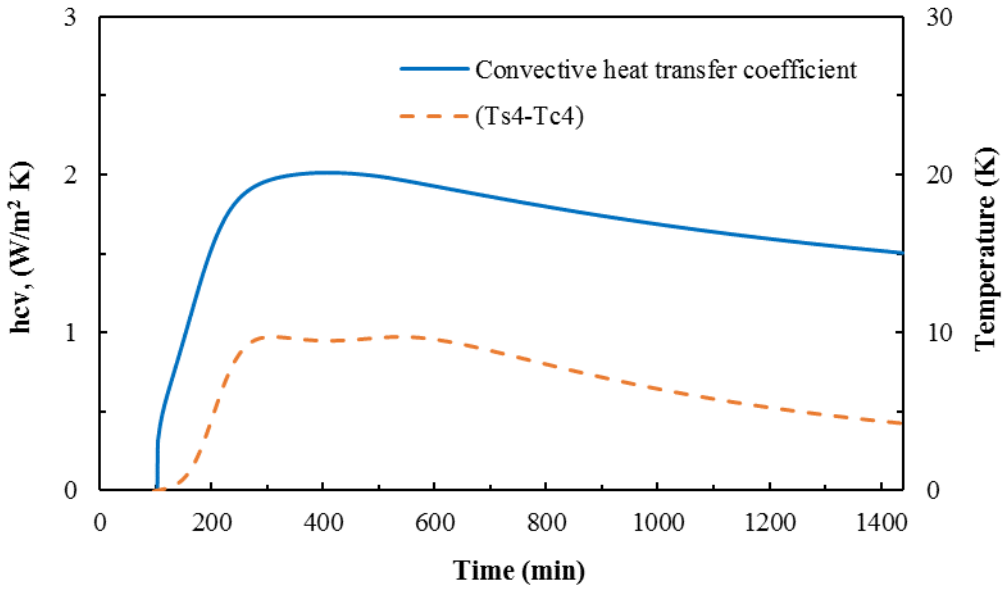

Figure 3.25 Variation in convective heat transfer coefficient with (Ts4-Tc4).

It is worth mentioning that the variations in the convective heat transfer coefficient and the temperature difference for all stages are in good agreement with the results for the daily distillate yield of the different stages, as presented in Figure 3.17.

3.7.6 Variation of Solar Collector Efficiency

The variation in the collector efficiency with changing levels of solar radiation throughout the daytime was investigated and the results are depicted in Figure 3.26. It can be seen that the collector efficiency is proportional to the solar radiation during the day, and the highest efficiency of 63.3% was observed in the period between mid-day and 13:00 o'clock.

Moreover, Figure 3.27 presents the variation in the hourly total cumulative distillate yield against the collector efficiency.

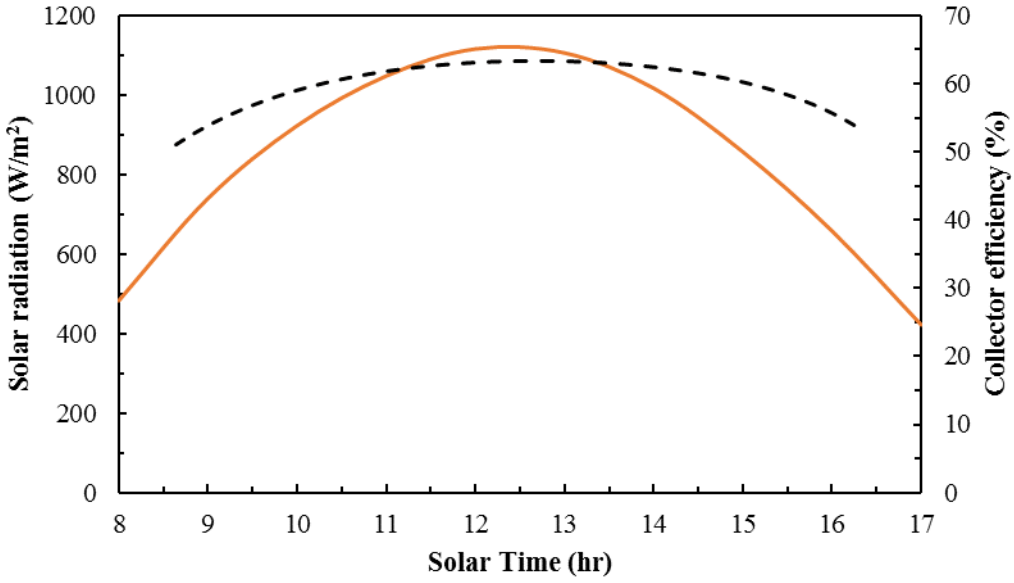

Figure 3.26 Variation in collector efficiency with solar radiation.

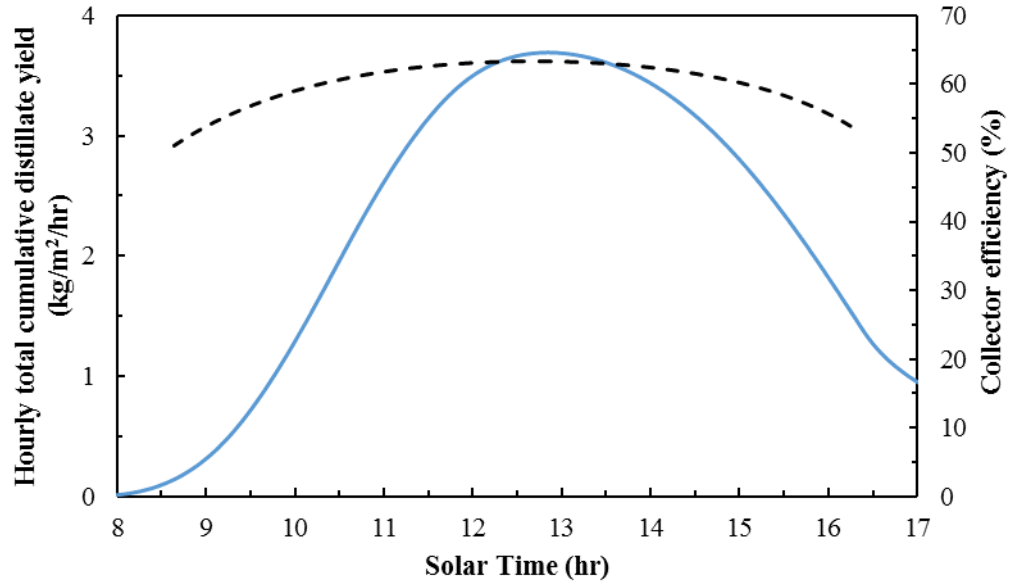

Figure 3.27 Variation in hourly total cumulative distillate yield with collector efficiency.

It can be seen that the maximum hourly total cumulative yield is achieved during the period of the highest collector efficiency, and this maximum productivity is attributed to the fact that the solar collector efficiency reaches its maximum during the time of maximum solar radiation.

3.8 Summary

In this Chapter the design and operational principles of the multi-effect solar water still were described. The dynamic simulation model of the proposed system was developed based on application of mass and energy balance equations in the form of ordinary differential equations written for each component of the system. This model, as well as the model of the solar radiation, were implemented in the Matlab/Simulink environment in order to simulate the operation of the solar desalination system. Subsequently, the numerical results obtained were examined and compared with theoretical results, published in the open literature and the validation shows that the simulation model developed in this work can accurately predict the performance of the multi-effect solar water desalination still. However, this simulation model also needs to be validated by experimental data in order to fully prove its accuracy. Finally, the theoretical results obtained on the performance of the desalination system throughout the day using the developed dynamic simulation model were presented and discussed.

Chapter 4 Experimental Investigation of the Dynamic Multi-Effect Solar Water Still

The theoretical results obtained from the mathematical model of the evacuated multi-effect solar desalination system, as presented in Chapter 3, need to be examined against experimentally acquired results in order to evaluate their validity and the accuracy of the simulation model. The experimental investigation was conducted on the prototype of the multi-effect solar desalination unit which was originally designed, constructed and examined for reliability by Professor Khamid Mahkamov at Northumbria University.

In this experimental part of the PhD study, the test rig was configured in such a way so to obtain data on the performance of the proposed self-evacuating solar desalination system, which is composed mainly of the multi-effect desalination unit coupled with an evacuated tube solar collector and the small fluid piston energy converter. Furthermore, this chapter provides the detailed description of all components of the experimental prototype of the suggested desalination system. Finally, an analysis and discussion of the experimentally obtained results are presented.

4.1 Experimental Set-up

The experimental set-up consists of two systems. The desalination system comprises the water desalination still with four stages or effects. The second system is the thermal energy-supply system, which is made up of the evacuated tube solar collector, solar radiation simulator, and heat exchanger. In addition, the small fluid piston energy converter is used to provide vacuum conditions inside the system.

In this section the detailed description of the main components of the experimental set-up of the proposed solar desalination system, with essential specifications of various sensors and data collection devices that were used to record the performance of the system are also described.

4.1.1 The Water Desalination System

This section presents a detailed description of the proposed multi-effect water desalination system in which the desalination process takes place and freshwater is produced.

4.1.1.1 *Multi-Effect Water Still (four stages)*

The solar water still consists of four stages placed one on the top of other. The three upper stages of the still are fabricated of rectangular hollow cages and the bottom stage is a rectangular basin. All stages are made of steel and have dimensions of 1200 mm in the length and 400 mm in the width, and they are covered with an angled tray, as presented in Figures 4.1 to 4.3. The heights of the bottom basin and cages are 160 and 125 mm respectively. Moreover, the bottom case has the largest volume and contains the major quantity of saline water with a depth of approximately 40 mm to cover a serpentine heat exchanger which is fixed at the bottom of the basin.

All the trays have a similar design and are made of steel sheets angled at 8^{o} from the centre line and welded to the sidewalls of a rectangular cage. A simple triangular trough is located in each stage case just beneath the ridge of the angled tray, running along the bottom of the tray to ensure the collection of freshwater and its conveyance to the freshwater collection containers.

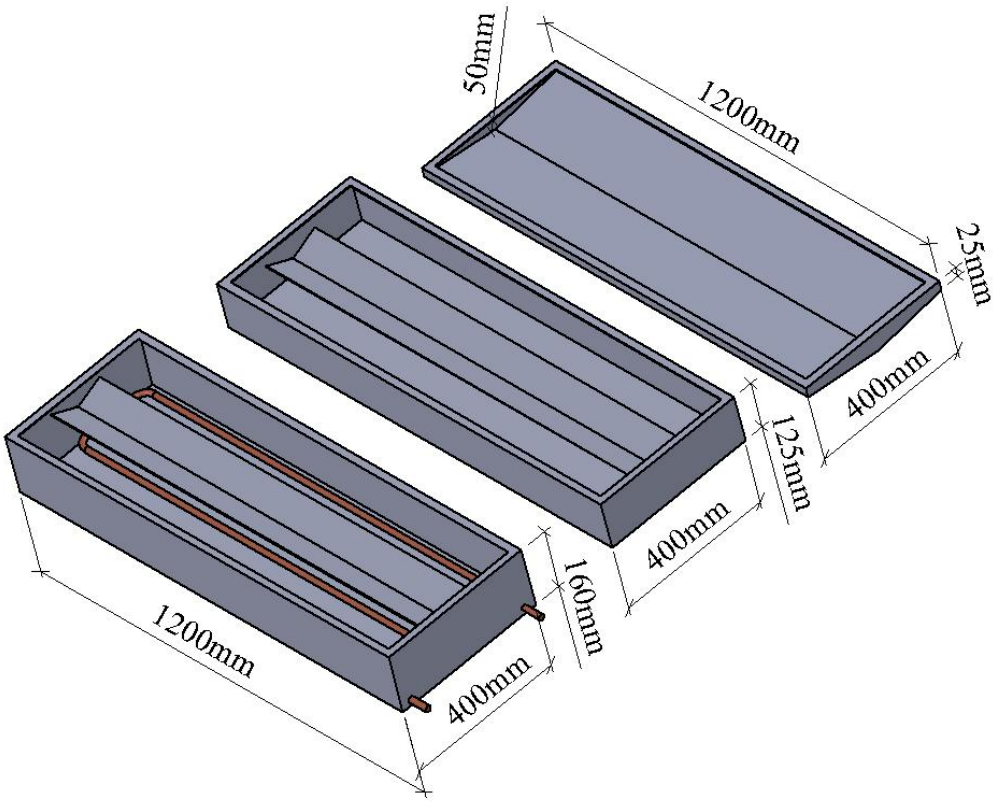

Figure 4.1 Multi-effect water still components and heat exchanger.

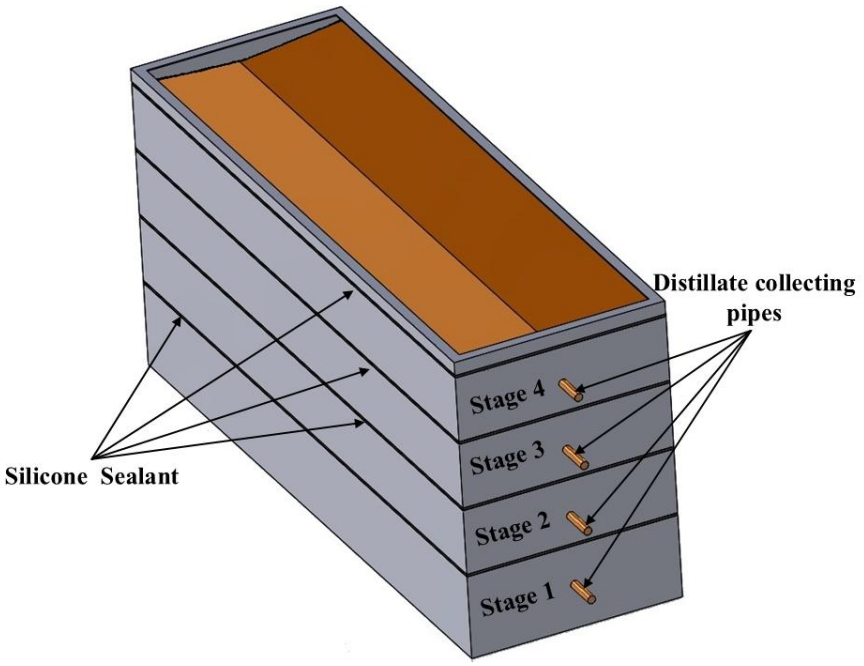

Figure 4.2 Assembled multi-effect water still.

The troughs are positioned in such a way as to ensure that the fresh water collected flows out of the stage due to gravity, and the two ends of the trough are welded at different levels with respect to the corresponding opposite sidewalls of the cage. The lower edge is welded at the area adjacent to the stage outlet which is connected to the collecting container via a copper pipe of 15 mm in the diameter.

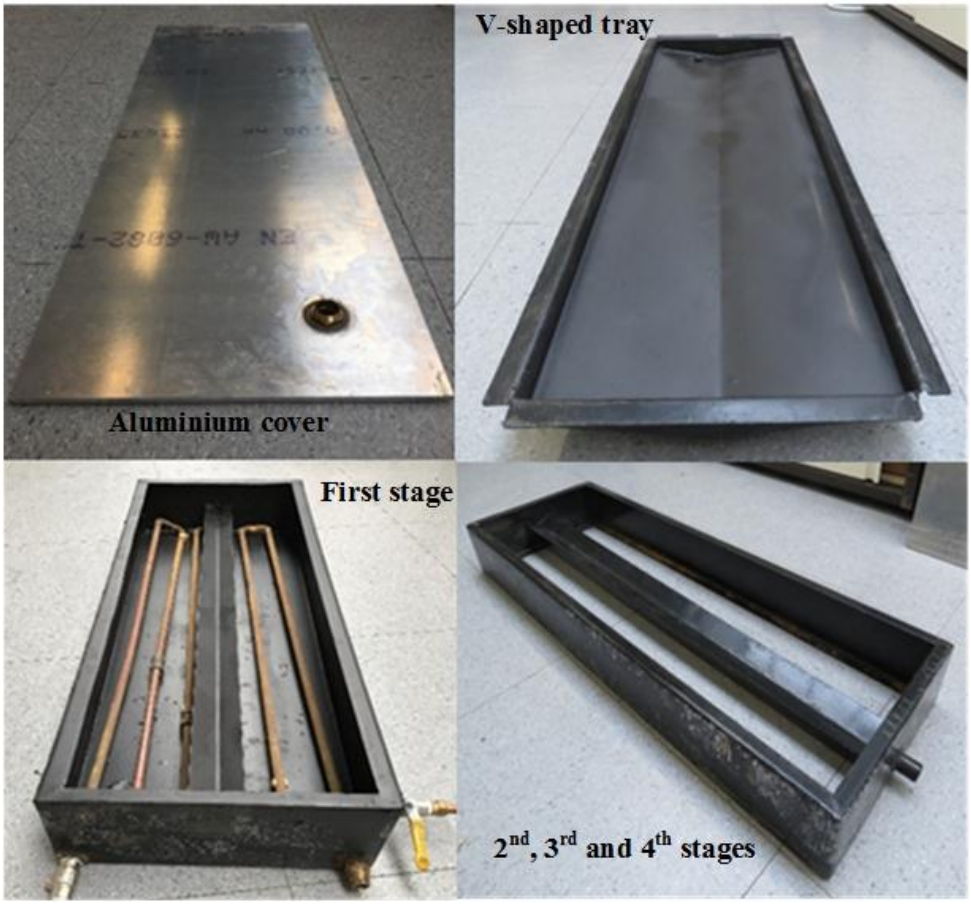

Figure 4.3 Components of multi-stage water still.

All trays are prepared with a coating of a polyolefin-based alloy, PLASCOAT PPA 567. This was firstly applied as finishing paint on the undercoating of all trays and subsequently subjected to high temperature by placing all parts in an electrical thermal furnace. As a

result of this treatment, the coating alloy produces a thin protective layer which is not prone to cracks due to high temperature or hot vapour environment.

In order to prevent any leakage of air or vapour from or into the system through the contact surfaces, self-adhesive backed foam strips, which are 6 mm thick and 19 mm wide and made of EPDM/Chloroprene [223], are placed between all stages. Furthermore, a cyanoacrylate adhesive suitable for use with EPDM foam strips [224] is used to join the strips at the corners to create rectangular loops around all edges of the stages, as shown in Figure 4.4. The specifications of the foam strip are presented in Table 4.1.

Figure 4.4 Foam strips and adhesive

In addition, to ensure that the system is hermetic and no leakages are possible from or into the system, the gaps between all stages are filled with a heat-resistant silicone sealant that can withstand temperatures up to 300 °C. Also, three aluminium beams with six steel-threaded rods are used to force the stages to each other, as shown in Figure 4.5. Strips of an encapsulated thermal insulation material made of glass mineral wool with the thickness of 20 cm and thermal conductivity of 0.044 W/m.k are used to minimize heat losses from the top, bottom and side walls of the system.

Table 4.1 Specifications of the foam gasket

Parameter	Description
Colour	Black
Material	EPDM/Cholorprene
Maximum temperature (°C)	120
Minimum temperature (°C)	-20
Density (g/cm³)	110
Elongation at break (%)	150

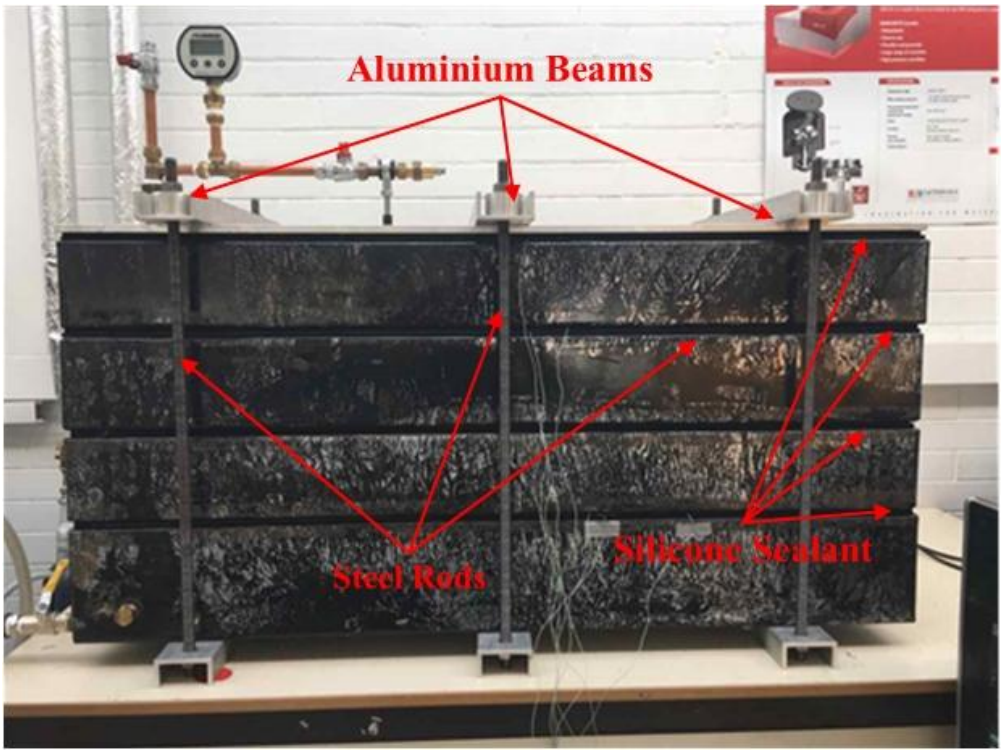

Figure 4.5 Aluminium beams and threaded steel rods

4.1.1.2 *Serpentine Heat Exchanger*

A serpentine heat exchanger made of copper pipe is horizontally placed at the bottom of the first stage and fastened using plastic clips inside the first stage box, as shown in Figure 4.3. The outer diameter of the copper pipe is 15 mm and it has the total length of 7 metres. The heat exchanger is connected to the solar collector and both are integrated as the closed loop by connecting the inlet of the heat exchanger via copper pipes to the outlet of the manifold header pipe of the solar collector, while the inlet of the header pipe is connected to the outlet of the heat exchanger. All pipes and pipe joints are thermally insulated using a polyethylene foam insulation material.

The freshwater passes through the heat exchanger and the solar collector works in the forced circulation mode, and the hot water circulating pump is utilized to circulate the hot water inside this loop. Consequently, the heat is transferred to the saline water and its evaporation takes place. The hot water flow rate in the system can be controlled by changing the speed of the circulation pump.

4.1.2 The Thermal Energy Supply System

In this section, the configuration of the thermal energy supply system, including the evacuated tube solar collector, solar radiation simulator and the hot water circulating pump, is described.

4.1.2.1 *Evacuated Tube Solar Collector*

A set of twenty evacuated tube solar collectors are arranged and installed on the steel structure, as presented in Figure 4.6. These evacuated tubes receive the heat generated

from the solar irradiation simulator, which is installed directly above the evacuated tubes, and subsequently, the heat produced is transferred to the water in the first stage via the serpentine heat exchanger. It is worth mentioning that the evacuated tube solar collectors were selected to be used in the experiments due to their relatively high performance compared to flat plate solar collectors, because the vacuum envelope minimizes the conduction and convection losses. Besides this, the surface coating is highly selective [225].

The evacuated tube solar collector is schematically presented in Figure 4.7. It is composed of a heat pipe made of copper placed inside a vacuum-sealed glass tube. The heat pipe contains a small quantity of the working fluid, for example, methanol, and the top side of the heat pipe, which is the condensing zone, is inserted into a manifold header pipe through the cylindrical housing port.

Figure 4.6 Evacuated tube solar collector.

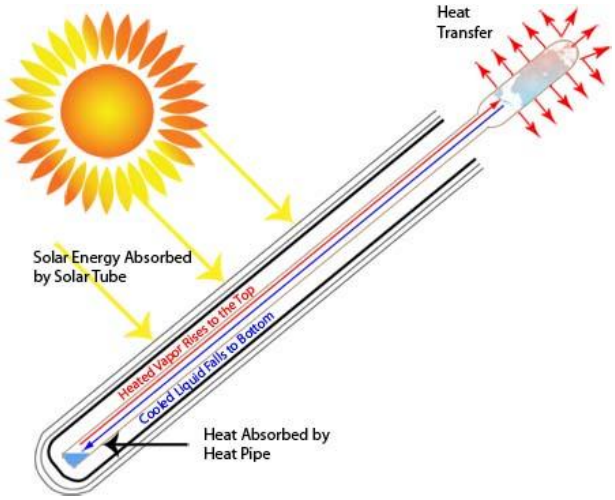

Figure 4.7 Schematic diagram of the evacuated tube solar collector [226].

Solar radiation is absorbed by the dark inner absorption surface of the evacuated tube, and it consequently heats up the external surface of the heat pipe. The working fluid inside the heat pipe vapourises and hot vapour moves under the effect of the density difference to the top of the heat pipe. Thereafter the heat is absorbed by the water in the manifold header pipe, and as a result, the cold vapour liquefies and returns to the bottom of the heat pipe (the vapourization zone) to repeat the cycle [152]. The detailed specifications of the evacuated tube solar collectors utilized in this research are presented in Table 4.2.

A long horizontal cylinder made of copper is used as a manifold header pipe. It has a volume of approximately 425 ml with dimensions of 150 cm in the length and 6 cm in the diameter. As shown in Figure 4.8, the manifold header pipe has twenty heat pipe housing ports with axes normal to the main flow direction in the header pipe. The top of each heat pipe is inserted into a housing port and a sufficient thermal contact between the housing ports and the tops of the heat pipes is secured by applying a special high thermal conductivity metallic glue compound. As a result, the heat energy received from the solar

simulator is transferred to the water in the manifold header pipe and then is passed to to the saline water in the first stage still by means of the serpentine heat exchanger.

Table 4.2 Specifications of the evacuated tube solar collectors

Parameter	Description
Collector type	Evacuated tube heat pipe
Number of tubes	20 tubes
Tube length	1.74 m
Outer tube diameter	0.047 m
Collector area	2.250 m^2
Absorber area	1.80 m^2
Dimensions L×W×H	1760×1500×130 (mm)
Weight	55 kg
Maximum operating temperature	190 ˚C
Stagnation temperature	247 ˚C

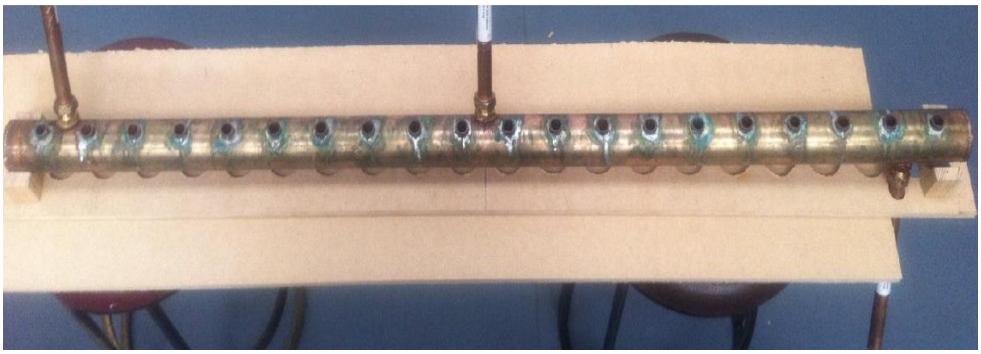

Figure 4.8 Manifold copper header pipe.

Additionally, in order to reduce the heat losses to the surroundings, a thermal insulation material, made of glass wool, is wrapped around the manifold pipe header and placed in the wooden box.

4.1.2.2 *The Solar Radiation Simulator*

The main purpose of using the solar radiation simulator is to mimic the solar irradiation so as to examine the performance of the dynamic solar water desalination still with various levels of solar irradiance independent of outdoor weather conditions. Figure 4.9 presents the solar radiation simulator and the variable voltage transformer. The solar simulator is made up of 110 tungsten halogen floodlighting lamps each with 150 watts of electrical power. These lamps are divided into three groups and arranged in rows on the steel frame to form a 10 x 11 array positioned parallel to the evacuated tube solar collectors.

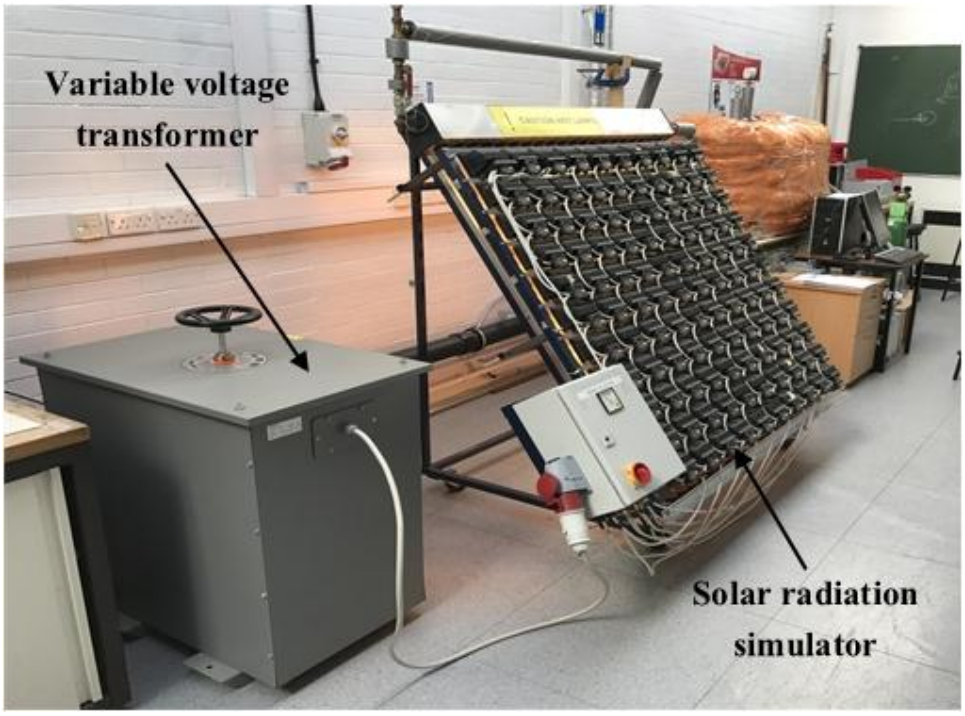

Figure 4.9 Solar radiation simulator and the variable voltage transformer.

Each of the three groups of lamps is connected to one phase of the three-phase variable voltage transformer. The main advantage of using this transformer is to vary the electrical power supplied to the lamps and consequently simulate different levels of solar radiation.

4.1.2.3 *Hot Water Circulating Pump*

A GRUNDFOS – UPS 15-50 N 130 hot water recirculation pump was utilized to circulate the hot water between the evacuated tube solar collectors and the heat exchanger in the still. This pump has a one-phase, canned rotor where the pump and motor are integrated. Figures 4.10 and 4.11 illustrate the circulation pump and its performance curves. This pump can safely supply hot water at the temperature up to 110 ^{o}C and maintain the pressure of 10 bar at a maximum ambient temperature of 40 ^{o}C.

Figure 4.10 Hot water circulating pump.

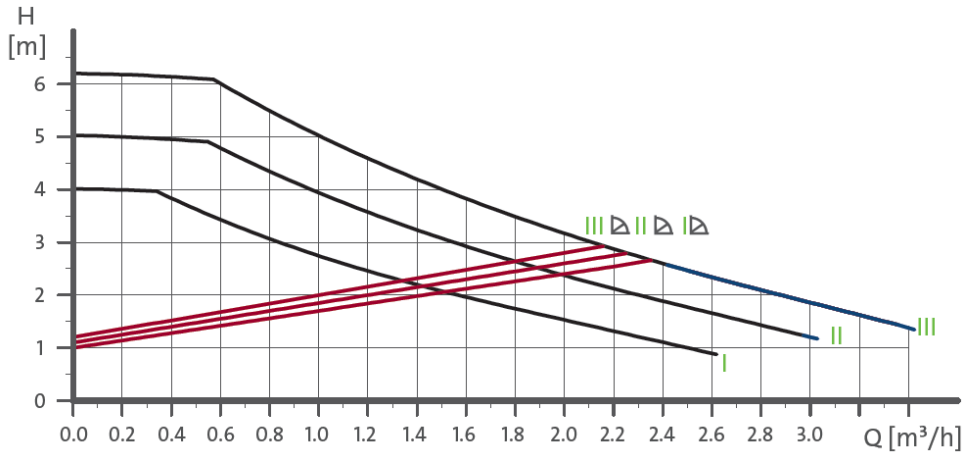

Figure 4.11 Circulation pump performance curves.

4.1.3 Fluid Piston Energy Converter

The fluid piston energy converter is used for the purpose of converting the part of the thermal energy produced by the solar collector into linear oscillations of the liquid column. The converter used in this investigation is made of two clear acrylic cylinders which are installed concentrically in the vertical position as shown in Figure 4.12. The two cylinders are tightly closed with aluminium flanges and filled up with water. The operational principle of the fluid piston energy converter is described in detail in [221, 227]. The converter operates at the pressure close to atmospheric one with the relatively low frequency of approximately 3 Hz.

The variation in the pressure inside the fluid piston is measured by the pressure sensor of model UNIK 5000, from GE [228]. As shown in Figure 4.13, the sensor is installed at the top of the upper cylinder of the energy converter. This sensor is the differential bi-directional gauge pressure transducer with a pressure range between -4 bar and 4 bar gauge.

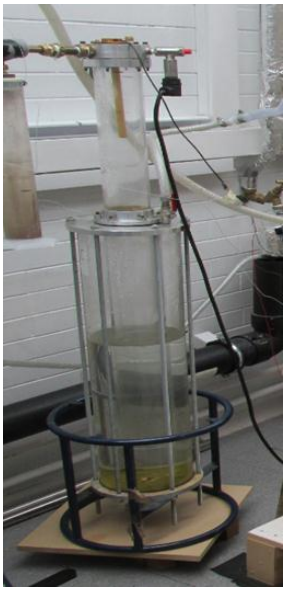

Figure 4.12 Liquid piston energy converter.

The pressure sensor was calibrated by the manufacturer and its accuracy is ±0.04% and the frequency response to the pressure change is up to 5 kHz at the temperature range between -20 to 80 ^{o}C, which is within the operational temperature range of the fluid piston.

Figure 4.13 Pressure sensor.

4.1.4 Condenser

A counter-flow double pipe heat exchanger was used in this investigation as the condenser for the fluid piston converter, as shown in Figure 4.14. It is composed of two concentric pipes, where the inner pipe has the diameter of 15 mm while the outer shell has the 50 mm diameter. This condenser was utilized to condense the hot water vapour and reduce its temperature prior to the entry into the energy converter.

Figure 4.14 Condenser.

4.2 Experimental Data Measurement and Collection

Various parameters were measured and recorded continuously throughout the experiments in order to examine the performance of the multi-effect solar still, including temperature, freshwater productivity, internal pressure and flow rate. In this work, particular emphasis was placed on the temperature and freshwater productivity measurements.

4.2.1 Temperature Measurements

Temperatures are measured at different positions of the system using standard K-type thermocouples made by TC Ltd [229], as shown in Figure 4.15. These thermocouples are PFA-insulated single pair twisted cables 0.2 mm in diameter with a maximum operating temperature of 250 ^{o}C. Eight thermocouples are inserted and fixed inside the still in each stage to measure the waterbed temperature and the condensing surface temperature. The temperatures of the hot water at the inlet and the outlet of the heat exchanger and solar collector (pipe header manifold) are also measured by means of four thermocouples. Another thermocouple is used to measure the room temperature. All thermocouples are connected to a data acquisition system which records the values of the temperatures every minute.

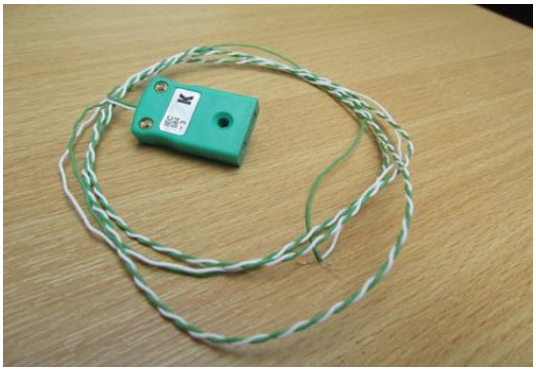

Figure 4.15 K-type single-pair twisted thermocouple cable.

4.2.2 Hot Water Flow Rate Measurement

In order to measure and monitor the hot water flow rate circulating between the solar collector and the heat exchanger, a FTB2005 turbine flow sensor from Omega [230] was connected to the pipeline at the point close to the heat exchanger inlet. The flow sensor is suitable for low-flow applications with a measurement range of 2 to 30 litres/min and its accuracy of readings is equal to ±3%, with the maximum operating temperature of 100 ^{o}C and maximum operating pressure of 13.7 bar. This flow sensor is connected to a 6-digit meter, model no. DPF702, made by Omega [231]. Figure 4.16 shows the flow sensor and the flow meter.

Figure 4.16 The flow sensor and the flow meter

4.2.3 Freshwater Productivity Measurement

Figure 4.17 shows the four collecting cylinders which were used to collect the distilled water produced from each stage. They are made of steel with a thickness of 2 mm and, to ensure that these cylinders are able to maintain vacuum pressure, an air leakage test was conducted with a pressure of 4 bar.

The volume of each cylinder was estimated based on the theoretical daily productivity of each stage. Table 4.3 presents the approximate dimensions of the collecting cylinders.

Figure 4.17 Distilled water collecting cylinders

Table 4.3 Dimensions of the collecting cylinders.

Cylinder	Diameter (mm)	Height (mm)	Volume (litre)
1	160	300	6.00
2	120	300	3.40
3	100	300	2.40
4	80	300	1.50

4.2.4 Water Test Meter

A portable water test meter from Omega [232], model HHWT-SD1, is used to conduct analyses of water samples collected before and after treatment, as shown in Figure 4.18. This instrument has the capability to measure pH, total dissolved salt (TDS) and the conductivity using TDS/conductivity probes and a pH electrode. The specifications of the HHWT-SD1 meter are presented in Table 4.4.

Figure 4.18 Water test meter.

Table 4.4 Specifications of HHWT-SD1 water test meter.

Measurement	Measurement range	Measurement accuracy
pH	0 to 14	+ 0.02
TDS	Up to 132,000 ppm	+ 2 %
Conductivity	Up to 200 mS	+ 2 %

4.2.5 Internal Pressure Measurement

A digital pressure gauge from OMEGA [233] was installed on the top cover of the multi-effect still to measure and monitor internal pressure, as shown in Figure 4.19. The gauge has a measurement range of -1.0 bar to 1.0 bar with an accuracy of ±0.25%.

4.2.6 Vacuum Pump

A single-stage vacuum pump made by CPS Products [234] is used to evacuate the multi-effect still in order to investigate any air leakage from the system and to reduce the internal

pressure level during experiments. The vacuum pump power is ¼ HP with 48 litres/min free air displacement, and is shown in Figure 4.20.

Figure 4.19 Digital pressure gauge.

Figure 4.20 Single-stage vacuum pump.

4.2.7 Other Instruments

This section describes the experimental instruments which were utilized to carry out these investigations.

4.2.7.1 *Photometer*

A standard photometer model PMA2200 from the Solar Light company [235] as shown in Figure 4.21 is utilized to measure and calibrate the radiation produced from the floodlights. This single-input photometer has the capability to detect and measure the full spectrum of radiation from ultraviolet to visible and even radiation with infrared wavelengths. The

sensor was calibrated by the manufacturer and has an accuracy of 0.5% of the full range of measurement with a sampling rate of 3 samples/sec.

Figure 4.21 Photometer.

4.2.7.2 *Stopwatch*

The solar irradiation was periodically changed by adjusting the percentage of the voltage in the transformer every 20 minutes. Also, the amount of freshwater collected was measured every hour. A digital stopwatch from RS [236] was used to specify when these measurements must be recorded, see Figure 4.22.

4.2.7.3 *Electrical Balance*

An electrical balance with a high range of 16 kg x 0.1 g made by ISG [237] was used to weigh the distilled water produced every hour, see Figure 4.22.

Figure 4.22 The stopwatch and the electrical balance.

4.3 Data Acquisition System

The variation of temperature during the experiment was monitored and recorded by means of the data acquisition system supplied by National Instruments. The components of the data acquisition system are schematically presented in Figure 4.23.

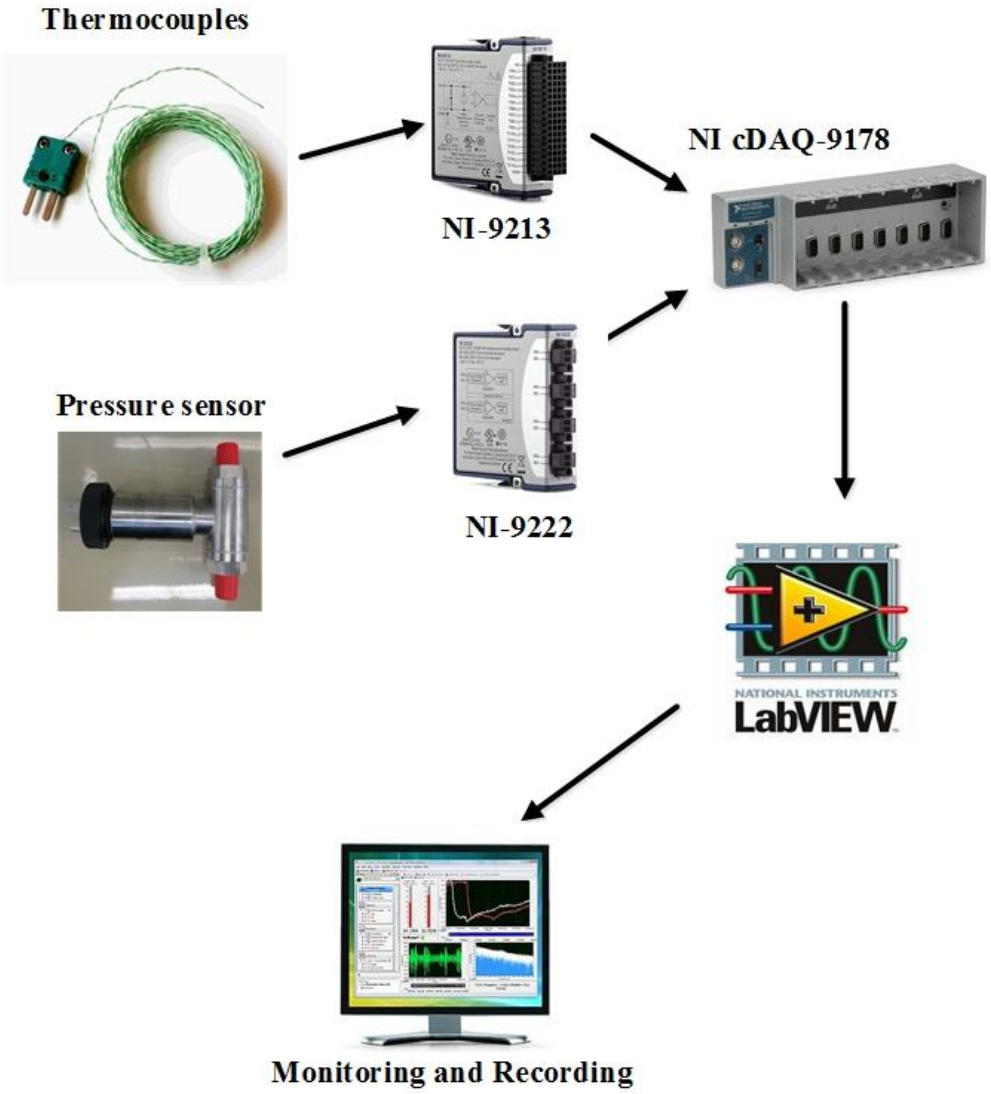

Figure 4.23 Arrangement used in the data acquisition system.

The system is composed of three modules, a NI-9222 module and two NI-9213 modules, and the three modules were installed on a compact DAQ chassis, namely the NI-cDAQ-9178 USB cDAQ model [238,239,240]. See Appendix C for more details about the data acquisition system. The thermocouples which measure the temperature of the waterbed and condensation surface of all stages inside the still are separately connected to the NI-9213 module and the second NI-9213 module is connected to the thermocouples used for measuring the temperature of the hot water circulating between the solar collector and the still.

The components of the data acquisition system are connected to the thermocouples and the cDAQ chassis is connected to a computer via a USB cable. In addition software from National Instruments, namely, LabVIEW software was installed on the computer and integrated with the acquisition system in order to monitor and record temperature variations during the experiments [241]. This software is a graphical programming language which is equipped with built-in engineering libraries of functions and a variety of tools and features for the simultaneous monitoring and recording of experimental data. A LabVIEW project was developed to conduct the experimental investigation. This project comprises two panels on the PC desktop, as shown in Figures 4.24 and 4.25. The first panel is the block diagram panel which is used to create or program the data analysis algorithm and the second panel is the front panel that enables the user to monitor and record the process and the experimental results.

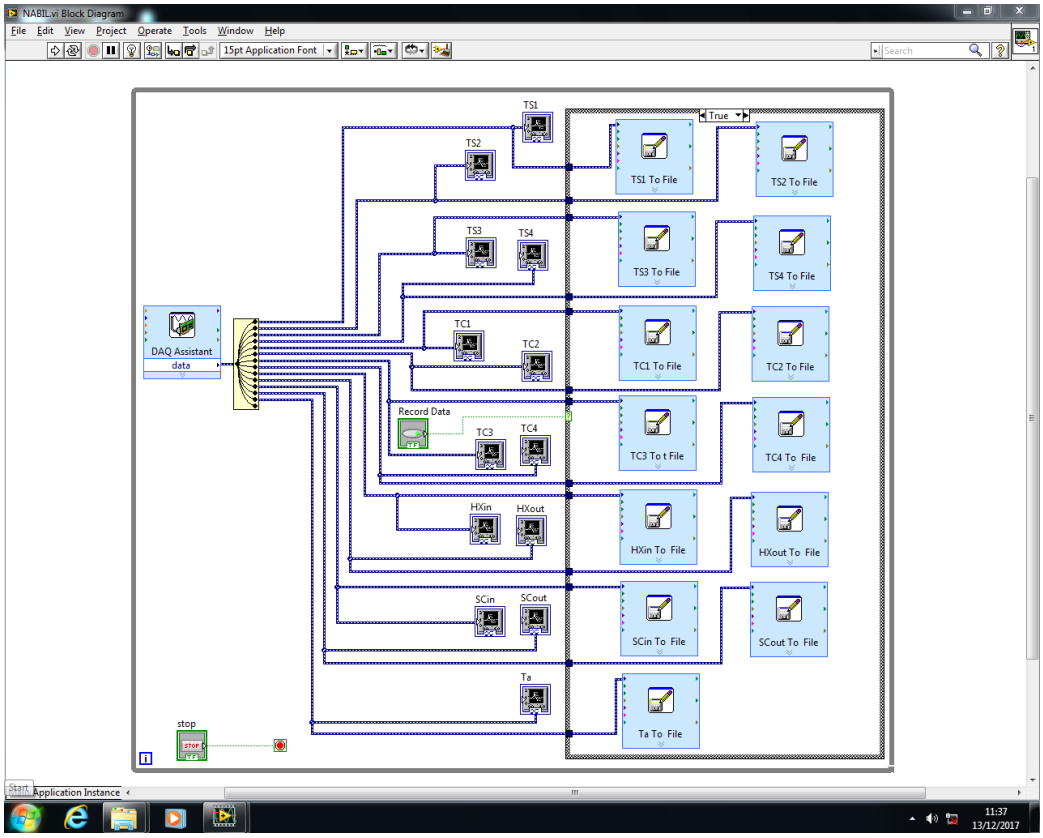

Figure 4.24 LabVIEW block diagram panel.

Figure 4.25 LabVIEW monitoring and recording of experimental data in the front panel.

4.4 Calibration of the Solar Radiation Simulator

Prior to conducting the experiments, the solar radiation simulator was calibrated to mimic the variation in solar irradiation throughout a typical summer day (15th of July), in Benghazi city in Libya. Figure 4.26 presents the variation in the total solar irradiance over a typical summer day in the region under investigation. The calibration procedure aims to calculate the average radiation emitted by the halogen floodlights at various values of electrical voltage produced by the three phase-variable voltage transformer.

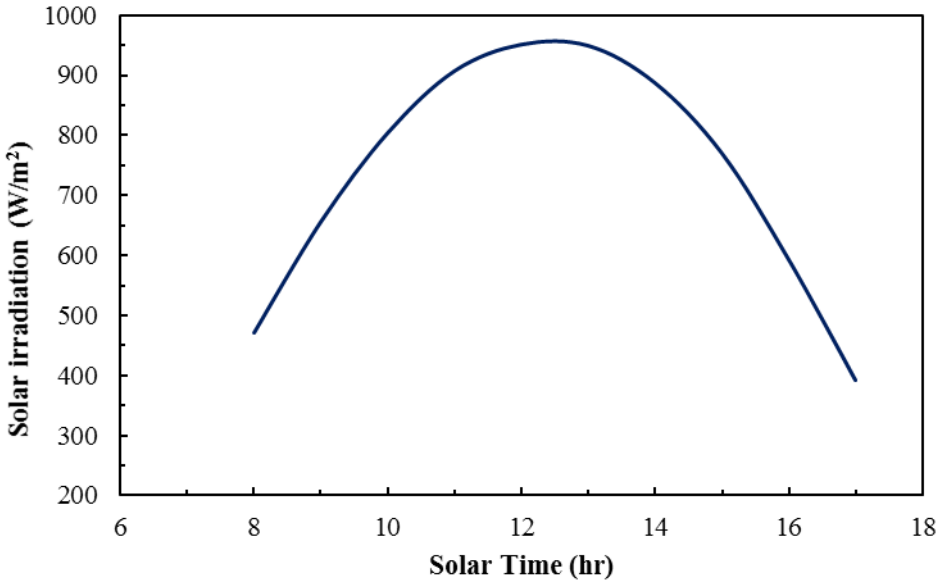

Figure 4.26 Total solar irradiance over a typical summer day in Benghazi, Libya.

The solar simulator area was partitioned into a grid of columns and rows of floodlighting lamps, as illustrated in Figure 4.27. The calibration process of the solar simulator was conducted by utilizing the previously described photometer PMA 2200. The emitted radiation has a maximum level at the centre of each lamp which diminishes in the zones far from the centre, and therefore the calibration process was carried out in two steps. The

amount of the radiation was first measured in the central point under each of the 110 lamps, and then the total average radiation was computed by multiplying the average radiation by the total area of the lamps.

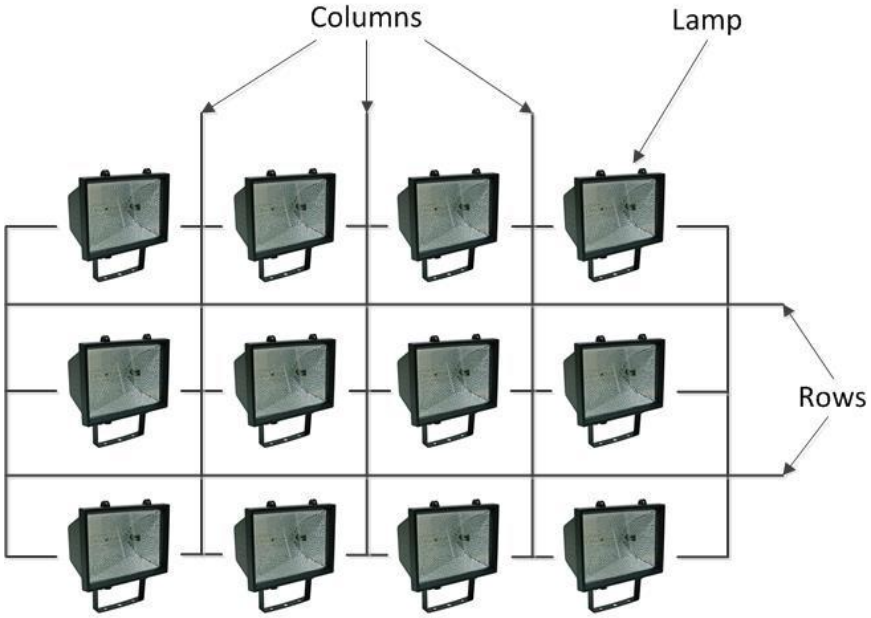

Figure 4.27 Part of the solar simulator.

The second step was to measure the average radiation at the areas between the rows and the columns of the floodlights, and this was performed in the same way as for the first step. The total average irradiation emitted from the entire area of the solar simulator is equal to the summation of the total radiation under all of the lamps and in the areas between the rows and the columns of the lamps divided by the total area of the solar simulator.

Finally, as a result of this calibration process, a curve of the relationship between the average total irradiation produced by the solar simulator and the percentage of electrical voltage from the transformer is plotted, as demonstrated in Figure 4.28. This calibration curve can be used to simulate any total solar irradiation level.

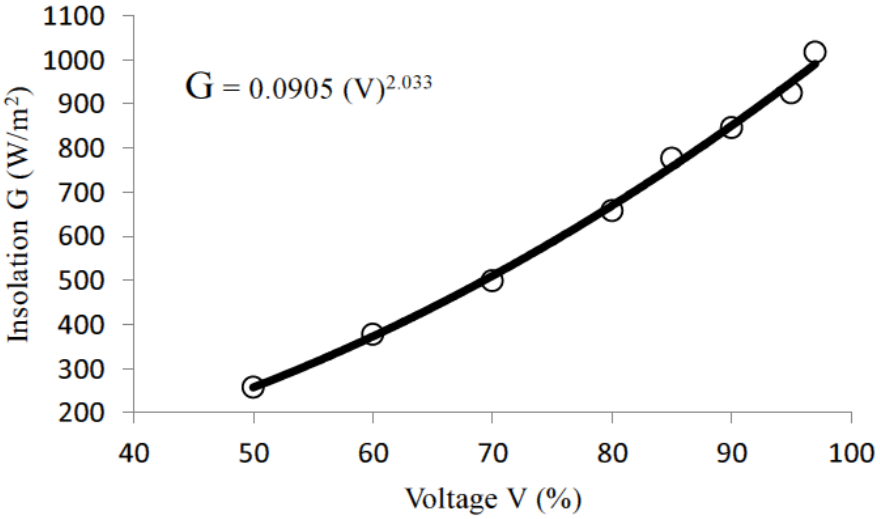

Figure 4.28 Average total irradiation versus transformer voltage.

4.5 Experimental Investigation Procedures

This section describes the experimental investigation conducted in this PhD research. This investigation includes two procedures. In the first experimental procedure, a fluid piston energy converter is used to reduce the internal pressure in a multi-effect solar water still. The performance of the proposed solar desalination system is experimentally investigated in the second procedure.

4.5.1 Utilizing the Fluid Piston Energy Converter with Multi-effect Water Still

Many studies have been conducted of evacuated desalination systems utilizing a vacuum pump. This section presents an attempt to reduce the pressure level inside the multi-effect solar water still without using the vacuum pump. In order to make the system self-evacuating and provide vacuum conditions without the external support from the vacuum pump, the fluid piston energy converter is utilized. The schematic diagram and photograph of the main components of the experimental set-up are presented in Figures 4.29 and 4.30.

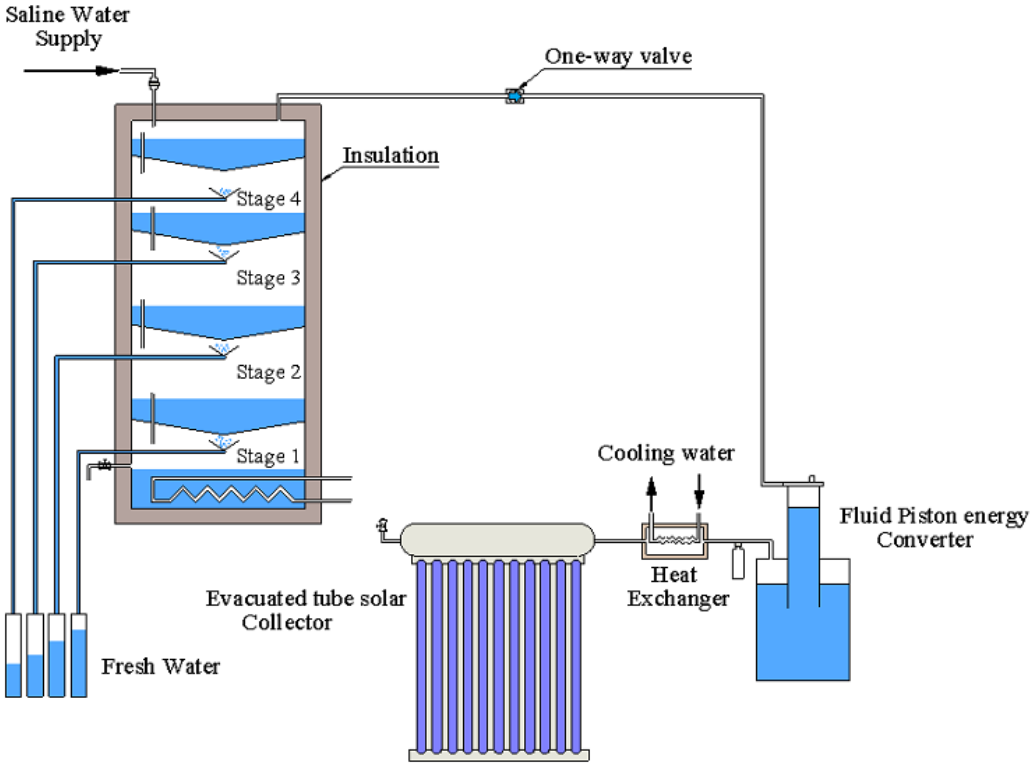

Figure 4.29 Schematic diagram of the fluid piston with the desalination unit.

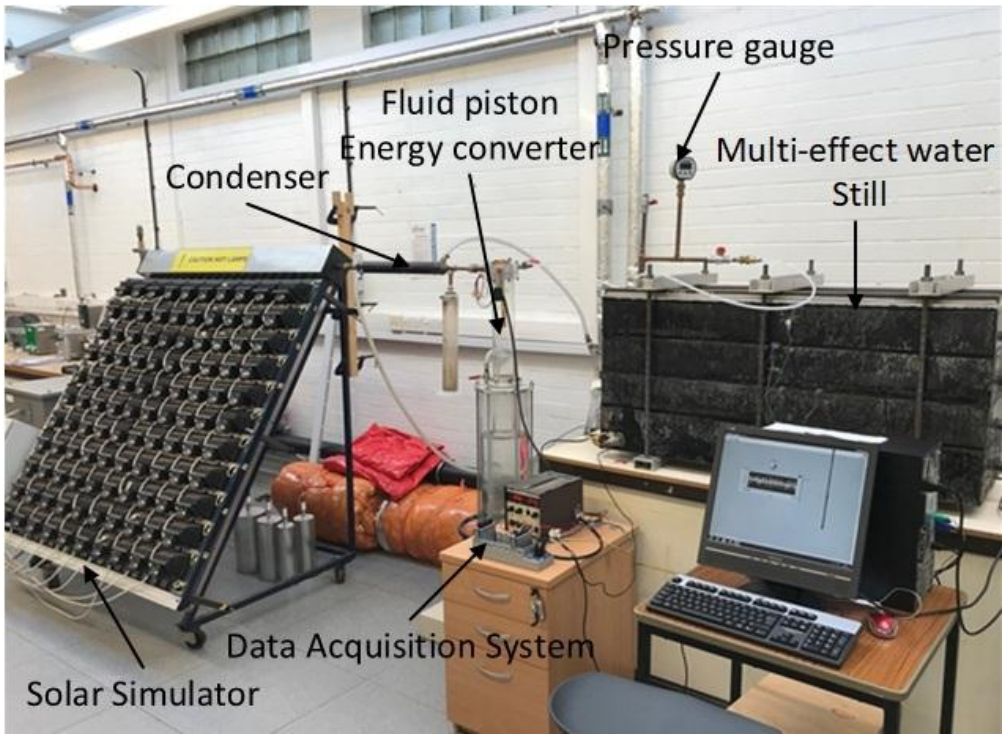

Figure 4.30 Utilizing the fluid piston to reduce the internal pressure level.

The experimental set-up consists of two systems. The first is a multi-effect solar water still. The second system is a novel modification allowing the operation of an internal pressure self-reduction technique, consisting of a small fluid piston energy converter connected to the evacuated tube solar collector, solar radiation simulator and heat exchanger. The solar collector is used to heat the saline water in the still and also to drive the fluid piston energy converter. This converter operates as the pump to evacuate air from the system, leading to the reduced internal pressure level which would result in the increased rate of saline water evaporation.

Before starting the experiments, the four stages of the multi-effect water still were arranged one on the top each other in a horizontally levelled position. All thermocouples were fixed in the designated locations and then the gaps between the stages were tightly sealed. The multi-effect still was evacuated by utilizing a vacuum pump in order to ensure that the system was hermetically sealed and that there were no air leakages from or into the system.

The thermal energy-supply system, including the solar radiation simulator, solar collector, the condenser and the fluid piston converter, were assembled and all pipes were connected. Moreover, a one-way valve was installed in the plastic tube which connects the fluid piston converter to the desalination unit. After assembling all components, the system was pressurized and then the pressure inside the system was monitored for 24 hours and also all pipe fittings were tested using a leakage detector to ensure that the system was fully hermetic. Finally, all pipes were thermally insulated to minimize heat loss.

The ability of the fluid piston converter to reduce the pressure level inside the system was investigated experimentally for various levels of solar irradiation. The experiments started by filling the evaporator with 450 ml of water. This evaporator is also the manifold pipe header shown in Figure 4.8. Then the cooling water flow rate in the condenser was adjusted. Finally, the solar radiation simulator was switched on and the electrical voltage supplied to the simulator was set at a certain value to simulate the necessary irradiation level in accordance with the curve, illustrated in Figure 4.28. The energy converter' liquid column starts to oscillate when the sufficient amount of hot water vapour produced in the evaporator. This occurred when the temperature in the evaporator approached boiling point. It took about 25 minutes for the converter to start to operate, after which the pressure in the system was monitored and recorded.

4.5.2 Performance of the Multi-Effect Solar Water Still

In this section, the performance of the multi-effect solar water still connected to the evacuated tube solar collector was investigated for different internal pressure levels. A schematic diagram and photograph of the main components of the experimental set-up are presented in Figure 4.31 and Figure 4.32 respectively.

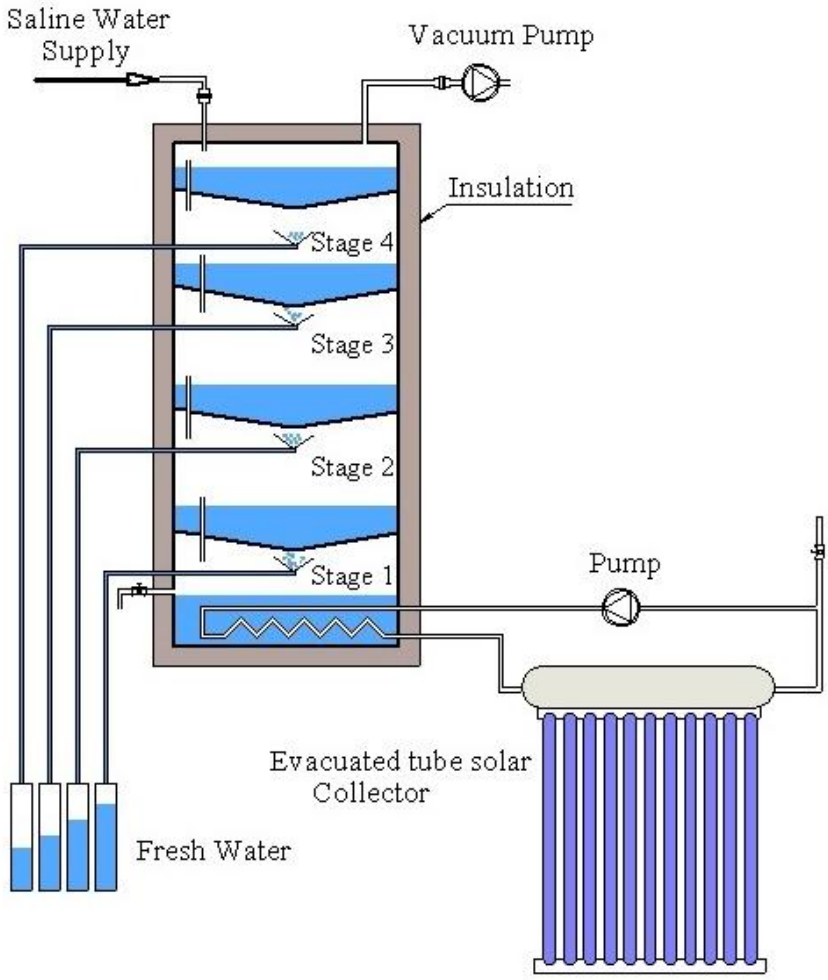

Figure 4.31 Schematic diagram of a multi-effect solar water still coupled to ETC.

Prior to the experiments, the four stages of the multi-effect water still were placed above each other in a horizontally levelled position. All thermocouples were fixed in the designated locations and then the gaps between the stages were tightly sealed.

The thermal energy-supply system, including the solar radiation simulator, solar collector and the hot water circulation pump, was assembled and all pipes were connected and tested for leakage.

The multi-effect still was evacuated by utilizing the vacuum pump in order to ensure that the system was hermetically sealed and that there were no air leakages in the system.

Finally, the whole water desalination system and all pipes were thermally insulated to minimize heat losses.

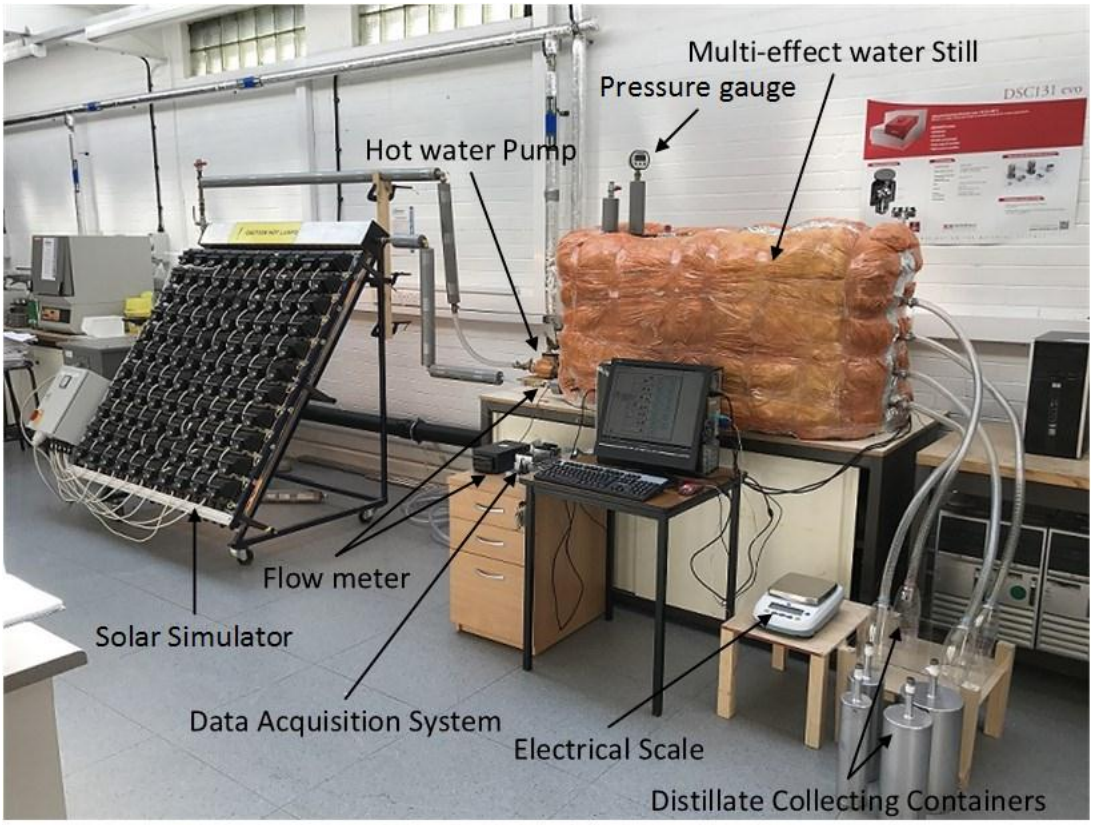

Figure 4.32 Main components of the experimental set-up.

The saline water was passed into the multi-effect still through the inlet at the top cover of the system. The by-pass pipe between each two stages is height-adjustable, and thus the amount of saline water in each effect could be adjusted by regulating the height of the bypass pipe. When the height of the saline water reached the desired level in the v-shaped tray, it overflowed into the following stage, and the following stages were similarly filled.

The first stage also was equipped with the overflow outlet at the height that maintained the saline water depth in the bottom stage to be 40 mm. When all the stages were filled with the desired amount of saline water, the overflow outlet valve was closed. The heights of the bypass pipes were adjusted so that the volumes of saline water in the second, third and fourth stages were 4.2 L, 4.5 L and 4.3 L respectively with the water depth varying from 0 mm at the edges to 25 mm at the tray's centre line. The volume of saline water in the first stage was equal to 18.4 L.

The internal pressure in the multi-effect still was controlled using the vacuum pump and monitored by the pressure gauge, as per previous description.

Experiments were carried out simulating the climatic conditions of a typical summer day (15^{th} July) in Benghazi, Libya. Active part of each experimental investigation was carried out for 540 min, corresponding to the start at 08:00 am and finishing at 17.00. However, the waterbed temperatures were measured and recorded for 24 hours and also the total cumulative distillate yield of all stages was weighed at the end of 24 hour period.

The electrical voltage supplied to the solar radiation simulator was adjusted every 20 minutes in order to simulate variations in solar radiation in accordance with the diagram in Figure 4.28. The rate of hot water flowing through the solar collector was maintained at the level of around six litres/min, as recommended by the manufacturer. The fresh water produced from each stage during the experiment was collected separately in four containers and the amount of collected distillate was weighed every hour and also after 24 hours of operation.

Each experiment was repeated several times in order to eliminate any human errors that might occur in measurements.

4.6 Discussion of Experimental Results

This section presents the results obtained from the experimental work conducted to investigate the influence of using the fluid piston energy converter with the desalination system and also to evaluate the performance of the multi-effect solar water still at and below atmospheric pressure. All experimental results obtained are presented and discussed below.

4.6.1 Reducing Pressure Level by Utilizing the Fluid Piston Energy Converter

The experimental investigation was conducted for various solar irradiation levels ranging between 500 and 950 W/m^2. In this section the experimental findings of 950 W/m^2, which corresponds to a percentage of the transformer's electrical voltage of 95%, are presented. The variations in pressure inside the fluid piston energy converter are shown in Figure 4.33. It can be seen that the internal pressure oscillates between just above the atmospheric (1.02 atm) and falls to approximately 89500 Pa (0.895 atm). This drop in the internal pressure inside the energy converter and in the desalination multi-effect solar water still leads to increase in the rate of the evaporation process, and consequently increases the system's distillate productivity.

During these experiments, it was noted that, when the frequency of the converter was higher than 3 Hz, this caused a distortion of the water surface in the inner cylinder during the fluid piston's oscillations, as shown in Figure 4.34. Such irregular fluctuations led to a considerable drop in the kinetic energy of the fluid piston oscillations and consequently reduced the effective power output of the energy converter. Figure 4.35 illustrates the smooth oscillations of the fluid piston energy converter with frequencies at or below 3 Hz.

This behaviour could be attributed to the fact that the water mass in the inner cylinder of the fluid piston was not sufficient to give the necessary movement inertia.

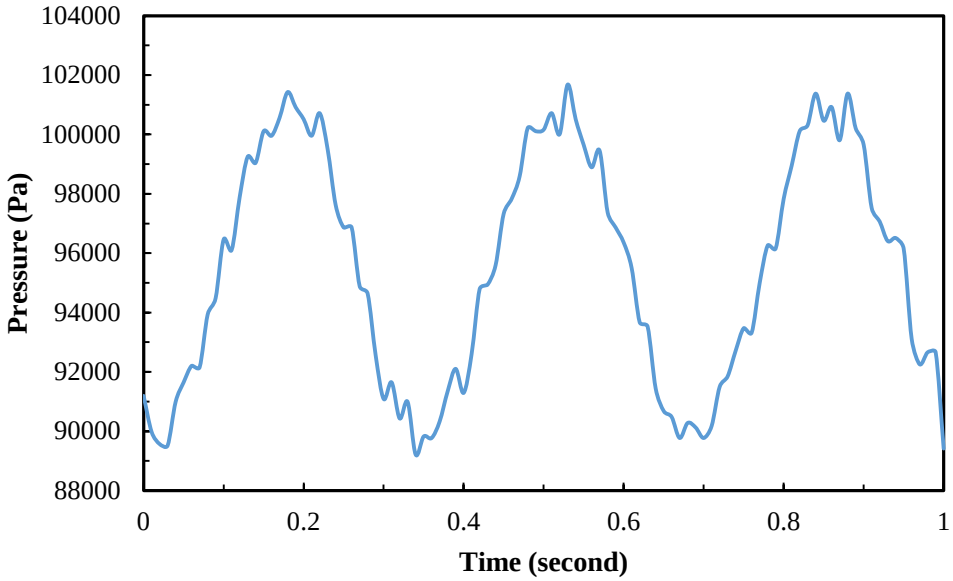

Figure 4.33 Experimental cyclic pressure inside the energy converter.

Figure 4.34 Water surface distortion during high frequency in the fluid piston.

Figure 4.35 Smooth oscillations of the energy converter.

The influence of the cooling water flow rate on the pressure inside the system was investigated for various solar irradiation levels and flow rates. The experimental results obtained for a solar irradiation of 700 W/m^2 and two flow rates, namely 4.0 and 2.0 litre/min are shown in Figure 4.36.

It was observed that increasing the cooling water flow rate led to shifting the pressure of the piston downwards, and this could be explained by the fact that decreasing the flow rate caused increase in the heat accumulated inside the fluid cylinder and consequently an the increase in pressure. The pressure level of the piston fluctuated between 93000 Pa and 102000 Pa for a cooling water flow rate of 4 litre/min, whilst it ranges between 96000 Pa and 105000 Pa for a flow rate of 2 litre/min. Therefore, the cooling water flow rate has a significant effect on the minimum pressure level inside the fluid piston and the whole desalination system, and consequently on the distillate productivity.

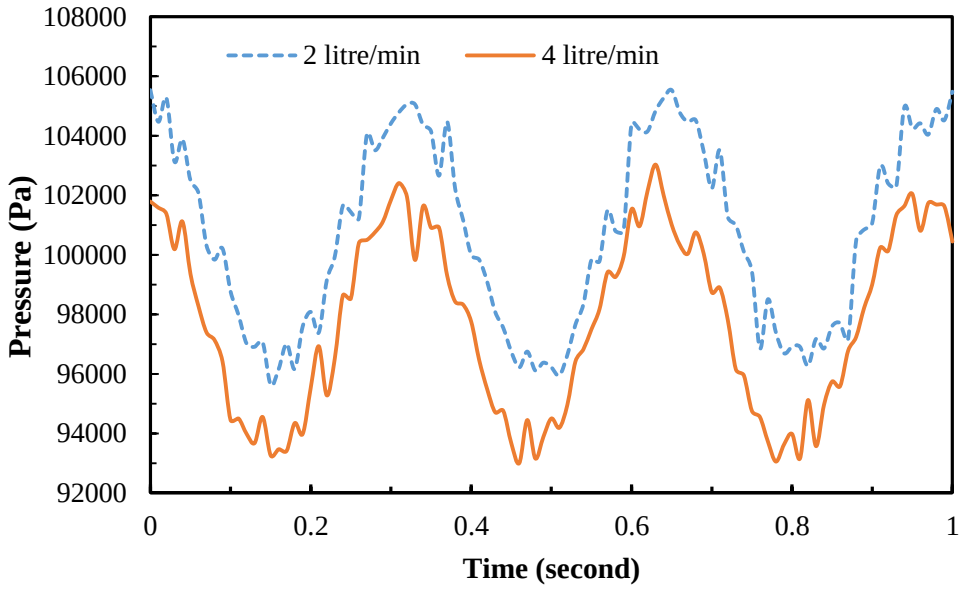

Figure 4.36 Influence of cooling water flow rate on the pressure level in the system.

4.6.2 Performance of Multi-Effect Solar Water Still

The experimental investigations of the performance of the proposed system were conducted for several internal pressure levels, namely 1.0, 0.9, 0.8, and 0.7 atm. In this section, the experimental results obtained when the system operated under atmospheric pressure are presented and discussed. The rest of the experimental results are discussed in Chapter 5. The experimental findings, including variations in the stage temperature, stage distillate yield and the total cumulative distillate yield, are presented in Figures 4.37 to 4.43.

4.6.2.1 *Fully Insulated Multi-Effect Water Still*

This experiment was conducted when the cover, bottom side, and all side walls of the multi-effect water still were thermally insulated. Figure 4.37 shows the variations in the temperatures of the waterbed in all stages for the fully insulated system. It can be seen that, after 360 minutes of operation, the waterbed temperatures in the first and second stages had the same value of approximately 93 °C. By the end of the experiment, the temperatures in all stages reached approximately the same level. The waterbed temperatures in all stages reduce tracking the corresponding reductions in levels of solar radiation; however, the decline in waterbed temperature in the first stage was faster than in the upper stages.

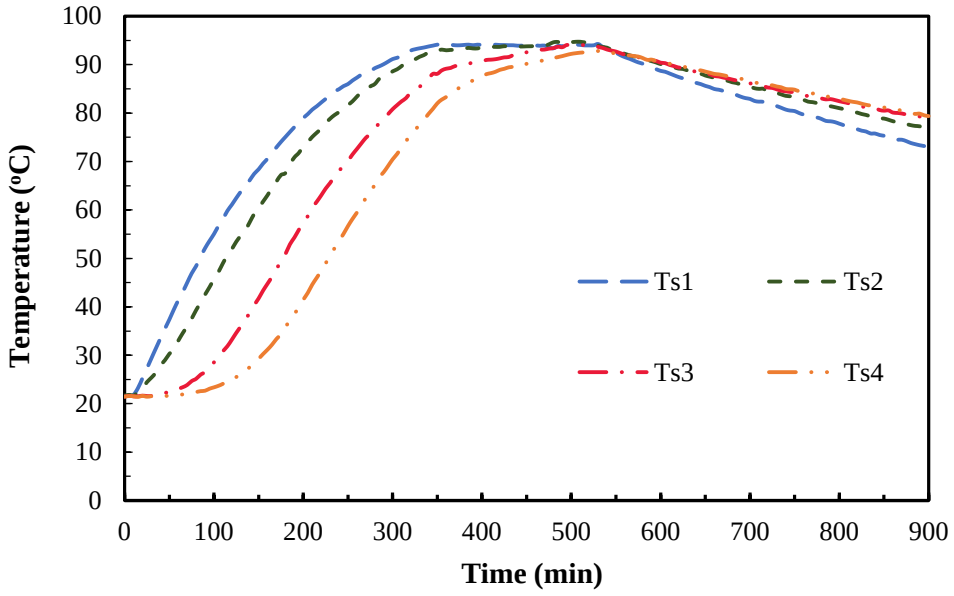

Figure 4.37 Variation in waterbed temperatures for fully-insulated still.

The experimental variation of the distillate yield for all stages is depicted in **Error! Reference source not found.**. It was observed that the desalination process stopped before the end of the experiment at the time corresponding to 480 minutes of operation.

This could be explained by the fact that when the waterbed temperatures in all stages of the fully insulated multi-effect had gradually reached the same level, this led to thermal damage conditions in which the temperature of the condensing surface exceeded that of the evaporation surface. Consequently, this caused the termination of condensation and evaporation processes.

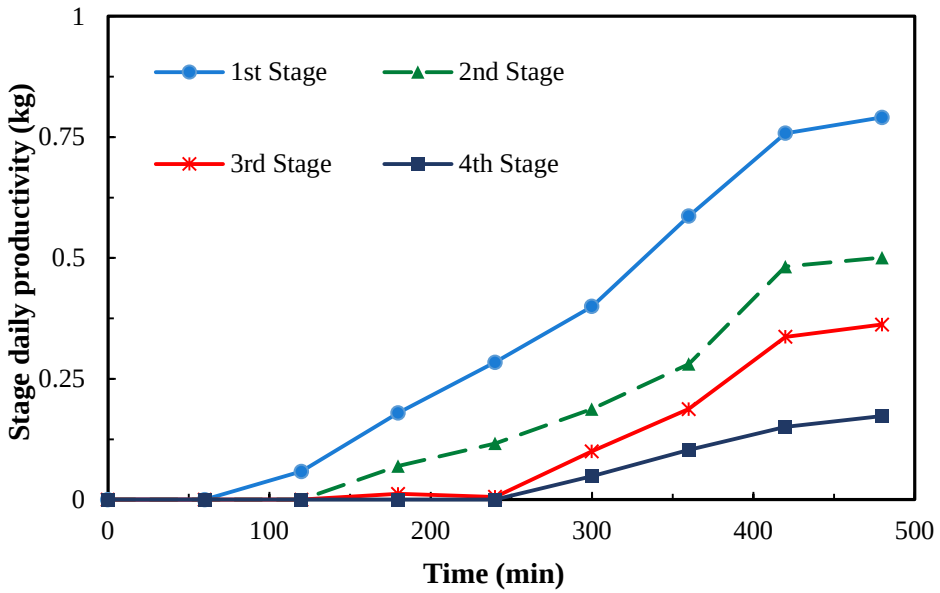

Figure 4.38 Experimental variation of distillate yield of all stages of fully-insulated still.

The total cumulative distillate yield collected from all stages during this experiment was found to be 1.83 kg, as demonstrated in Figure 4.39. These results demonstrate that, due to the high solar radiation available to the system, the evaporating surface area of each stage needs to be increased by being filled up with the adequate amount of saline water in order to sufficiently harness the thermal energy from solar radiation provided.

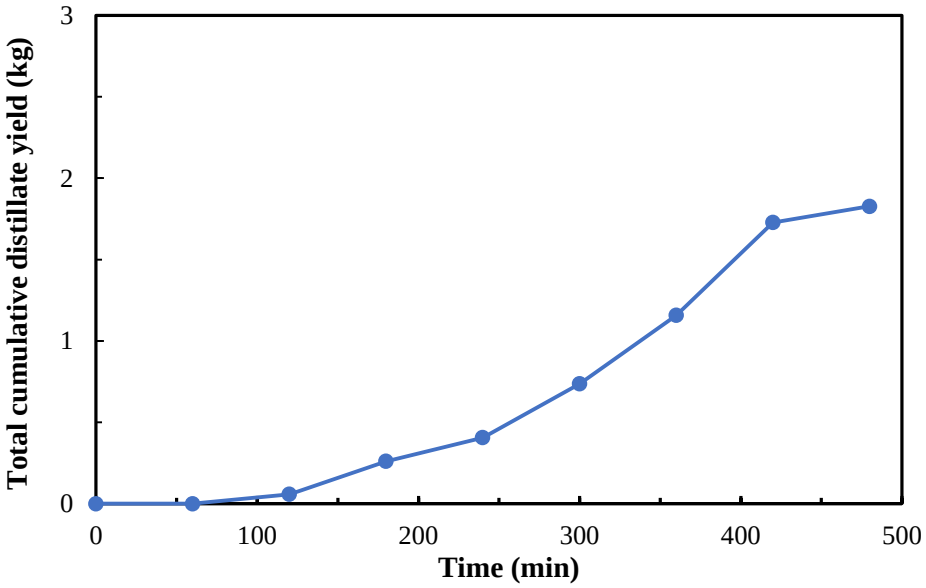

Figure 4.39 Experimental total cumulative distillate yield of fully-insulated still.

4.6.3 Partially Insulated Multi-Effect Water Still

It was observed that the multi-effect water still produced fresh water continuously throughout the day (24 hours) when the top cover of the system did not have the thermal insulation. The variations in the waterbed temperatures for the partially-insulated multi-effect water still are shown in Figure 4.40. It was noticed that the waterbed temperatures of all stages gradually increase with corresponding rise in the solar radiation, and then the temperatures gradually reduce with decreasing solar radiation.

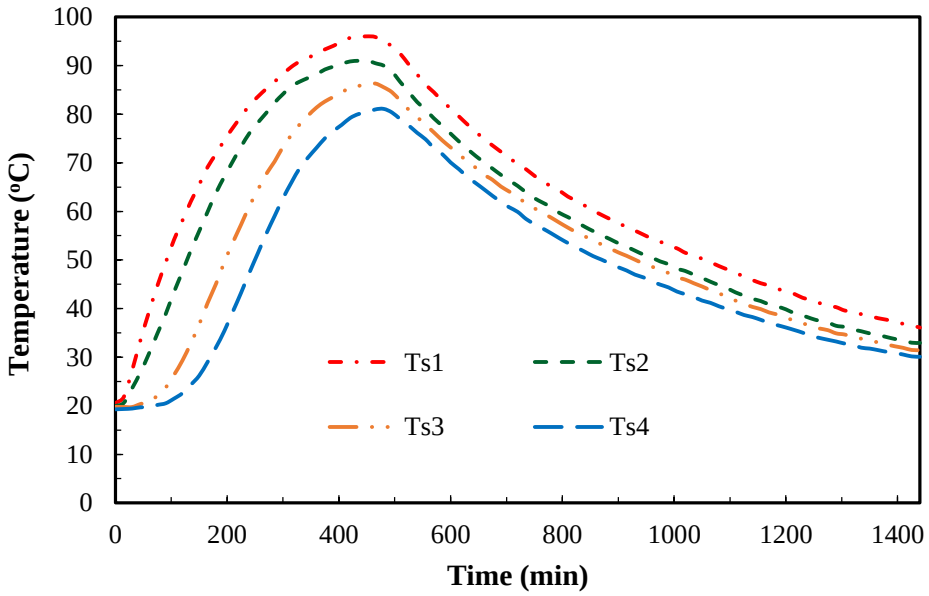

Figure 4.40 Variation in waterbed temperatures for partially-insulated still.

It was also found that the temperature in the first stage was considerably higher than that of other stages, with the maximum value of approximately 96 ^{o}C. The waterbed temperature in the fourth stage has the lowest level during the day and can reach the maximum value of 81 ^{o}C. This minimum level can be attributed to the significant heat losses from the uncovered top tray. The recording of the waterbed temperatures was stopped after 24 hours and it was observed that the waterbed temperatures in all stages of the system ranged between 30 °C and 36 °C at the end of the experiment.

Figure 4.41 presents the variations in the temperature difference between the evaporating surface and condensing surface in each stage of the system throughout the day. It can be noticed that these temperature differences increase as the solar radiation rises during the day and vice versa. The recorded maximum temperature differences were around 11, 19, 14 and 9 ^{o}C for the first, second, third and fourth stages respectively.

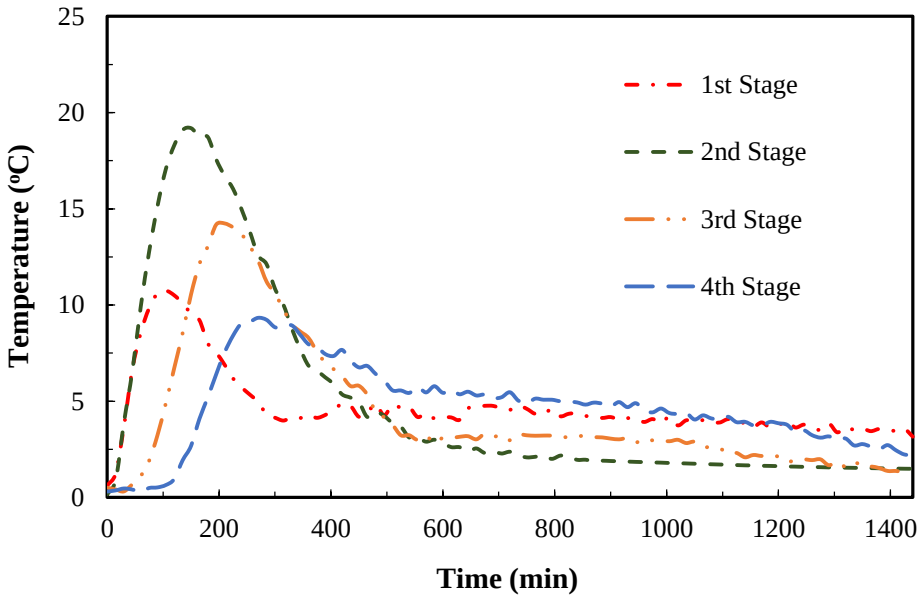

Figure 4.41 Temperature differences between the evaporating and condensing surfaces.

Figure 4.42 demonstrates the variation in the distillate water yield of the partially-insulated still throughout the day. It can be seen that, in the daytime during the initial nine hours of the experiment, the system produced the major amount of daily the distillate yield due to the high levels of solar radiation, and thereafter the production rate of all stages gradually decreased. The first stage produced a large proportion of the freshwater yield, with a maximum amount of approximately 4.1 kg/day. The lowest amount of distillate was produced by fourth stage, which was found to be less than 1.0 kg/day while the daily productivity of the second and third stages were 2.2 and 1.4 kg respectively.

The variations in the total daily cumulative distillate yield of the still are depicted in Figure 4.43. It is observed that the increase in the total cumulative distillate yield is more noticeable during the initial hours of the experiment. The experimental total daily cumulative yield was equal to 8.65 kg.

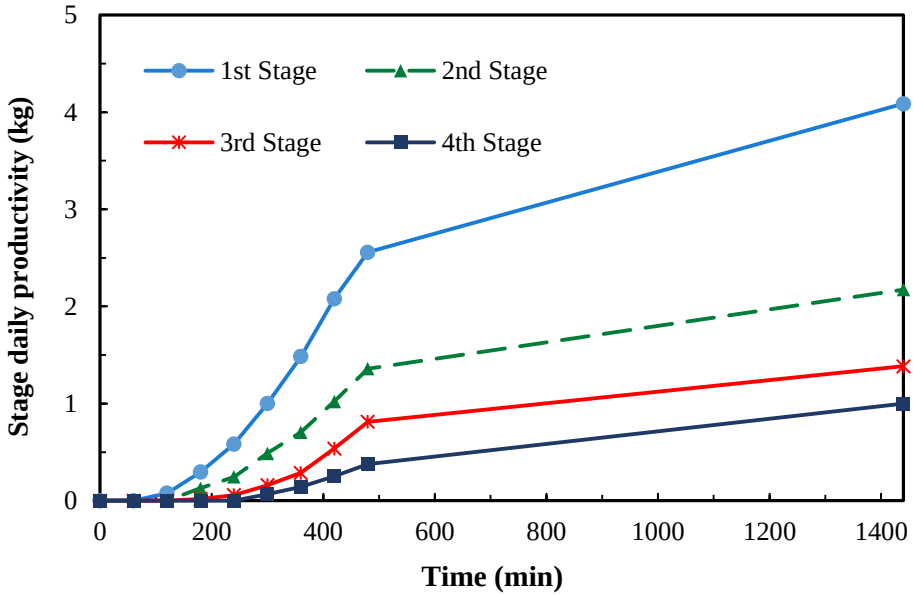

Figure 4.42 Experimental variation in distillate yields of partially-insulated still.

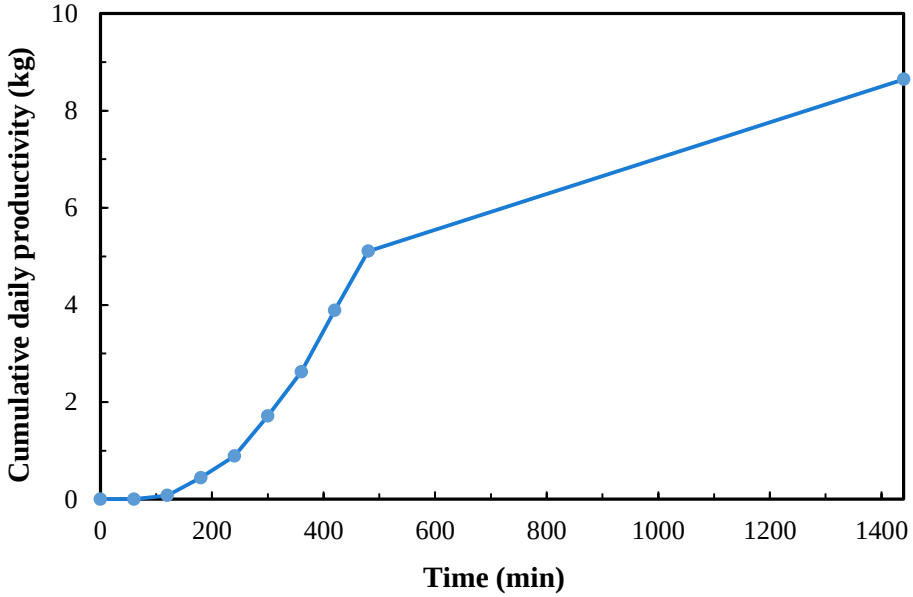

Figure 4.43 Experimental total cumulative distillate yield of partially-insulated still.

It is worth mentioning here that the highest freshwater production rates were observed when the solar radiation had reached the maximum level and this then was maintained for

some period of time during the day. This can be explained by the fact that the productivity rate of each stage is mainly influenced by the waterbed temperature in that stage and the temperature differences between each two adjacent stages, which both have the maximum levels when the solar radiation is at its maximum level. This behaviour is in a good agreement with the variation in the waterbed temperatures of all stages and the variation in the temperature difference between the stages as presented previously in Figures 4.40 and 4.41.

4.6.4 Water Quality Analysis

The freshwater produced from all stages was collected separately and water quality analysis was conducted at the end of each experiment using the water test meter described previously. Table 4.5 presents the average water quality measurements, including total dissolved solids (TDS), electrical conductivity, and pH. Accordingly, the analysis demonstrates that the distillate produced is significantly pure with average total dissolved solids ranging between 7.6 and 8.1 mg/L, an average conductivity of less than 60 µS and values of pH ranging between 6.38 and 7.07.

Table 4.5 Water quality parameter measurements.

Sample	TDS (mg/L)	Conductivity (µS)	pH
Before treatment	298	485	7.36
Distillate from stage 1	7.6	52.3	6.38
Distillate from stage 2	8.1	54.5	6.95
Distillate from stage 3	7.8	59.0	6.84
Distillate from stage 4	7.9	58.2	7.07

4.7 Summary

This chapter provided the detailed description of all components of the experimental prototype of the dynamic multi-effect water desalination still. The experimental instruments, various sensors and the data acquisition system utilized in this investigation were also presented. The experimental procedure and examples of the results obtained from the experiments were presented and discussed. In addition, experimental data obtained in this Chapter, will be used in Chapter 5 to validate the developed mathematical model of the system.

Chapter 5 Validation of Mathematical Model with Experimental Results

This Chapter introduces the further validation of the mathematical model of the dynamic multi-effect solar desalination still, as presented in Chapter 3. The theoretical results are examined against the experimental findings in this Chapter. The levels of agreement between the theoretical results and experimental data in term of waterbed temperatures, the daily productivity of stages and total cumulative distillate yield are presented and discussed for two levels of internal pressure, namely, 1.0 atm (atmospheric pressure) and 0.7 atm. The validation was performed for the same physical dimensions as in the system prototype and also by using the same operational conditions in the experiments, including the initial temperature of the waterbeds in all stages, internal pressure and solar radiation.

5.1 Development of the Mathematical Model

The mathematical model of the dynamic multi-effect water still described in Chapter 3 was further developed in order to be validated against experimental results. Experiments were conducted and repeated several times. During the experimental investigation, the temperature differences between the condensing surface and the evaporation surface in each stage were recorded. Subsequently, the temperature differences in all stages were taken into account in the developed mathematical model. The temperatures of the condensing surface for the first, second and third stages are calculated as follows:

$$T_{c1} = T_{s2} - 1.78 \quad (5.1)$$

$$T_{c2} = T_{s3} - 2.34 \quad (5.2)$$

$$T_{c3} = T_{s4} - 0.92 \quad (5.3)$$

The temperature of the condensing surface in the fourth stage was calculated as a function of the waterbed temperature based on the curve fitting of experimental temperature data as follows:

$$T_{c4} = T_{s4} - (0.000099T_{s4}^3 - 0.017T_{s4}^2 + 0.9911T_{s4} - 13.444) \quad (5.4)$$

The above experimental correlations are widely applicable in simulating the performance of the proposed multi-effect water stills and can be utilized for any operating conditions.

5.2 Validation of the Mathematical Model under Atmospheric Pressure

In this section the experimental results obtained from the operation of the multi-effect water still under atmospheric pressure are used to the test the theoretical results of the mathematical model.

5.2.1 Validation of the Waterbed Temperature in the Different Stages

The comparison between the experimental and theoretical results for the waterbed temperatures in all stages of the multi-effect water still for an internal pressure equal to 1.0 atm are demonstrated in Figures 5.1 to 5.4. It can be seen that the pattern of variation of the calculated waterbed temperature curves in all stages correspond with that of the

experimental results. However, the experimental results for the temperature reached higher values than in the theoretical results.

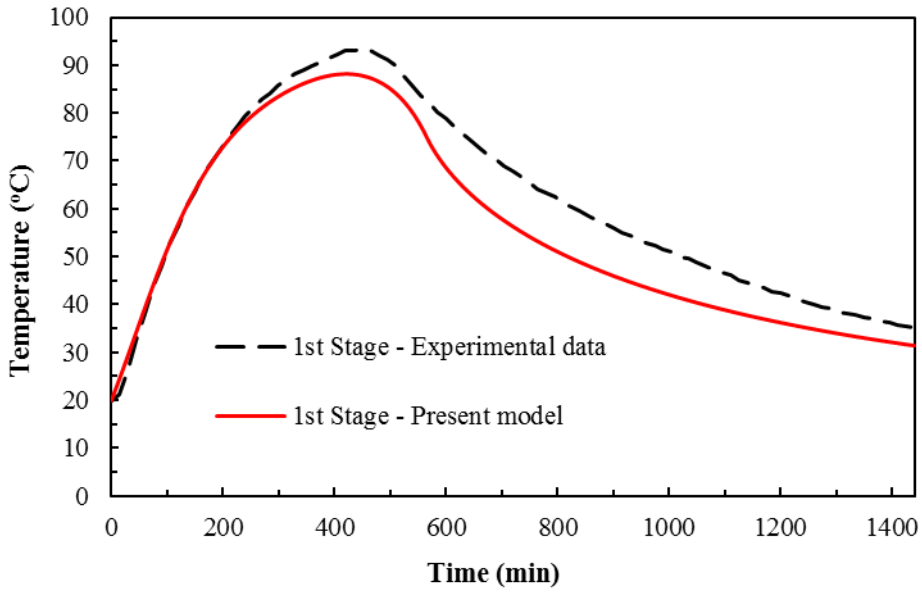

Figure 5.1 Comparison between experimental and theoretical temperature in the first stage at 1.0 atm.

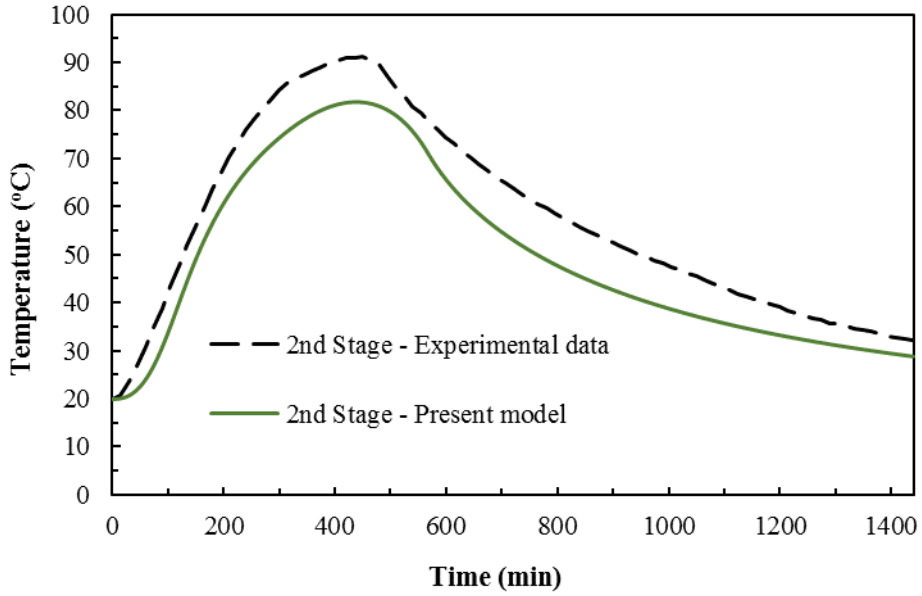

Figure 5.2 Comparison between experimental and theoretical temperature in the second stage at 1.0 atm.

The maximum deviations between the predicted and experimental values of the waterbed temperatures are 17.2%, 17.9%, 26.7% and 18.2% for the first to fourth stages respectively.

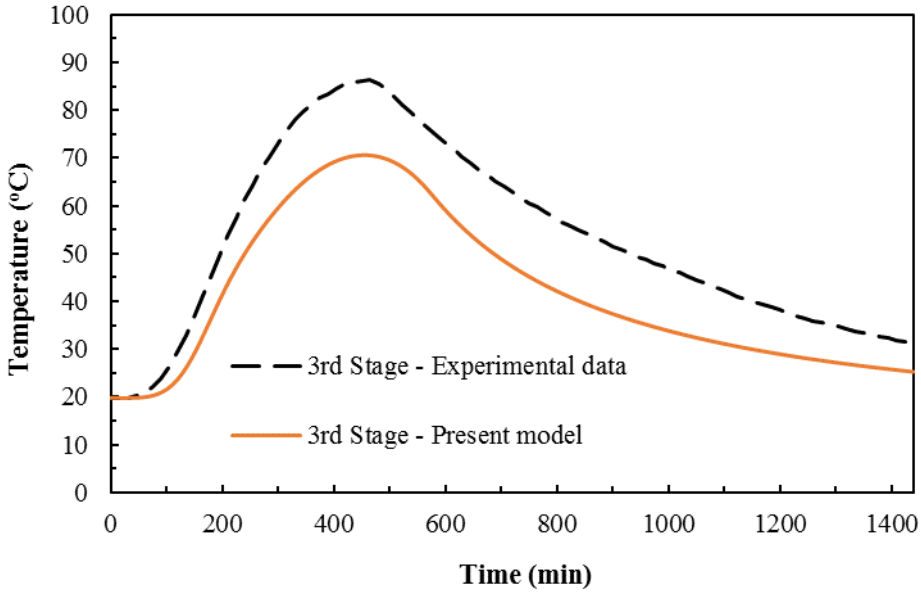

Figure 5.3 Comparison between experimental and theoretical temperature in the third stage at 1.0 atm.

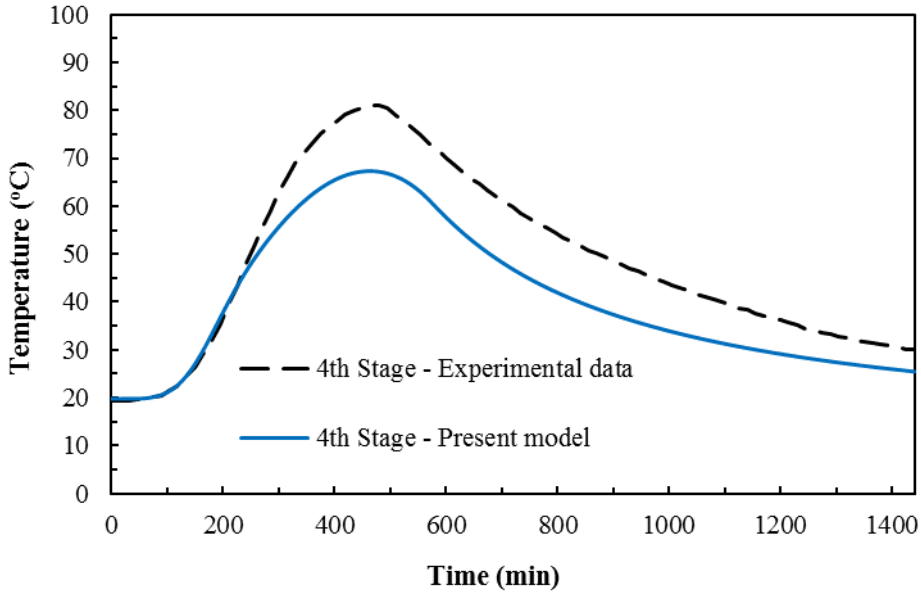

Figure 5.4 Comparison between experimental and theoretical temperature in the fourth stage at 1.0 atm.

This discrepancies in the results can be explained by the lack of accuracy in determining the input heat in each stage and the heat losses from the system.

5.2.2 Validation of the Freshwater Daily Productivity

Figures 5.5 to 5.9 present the comparisons between the experimental and theoretical results for the freshwater productivity of the multi-effect water still for an internal pressure equal to 1.0 atm. Although the daily productivity curves have similar trends, it was noticed that the mathematical model markedly overestimates daily productivity in all stages. The comparison of the values of theoretical and experimental daily productivity of the first stage is shown in Figure 5.5.

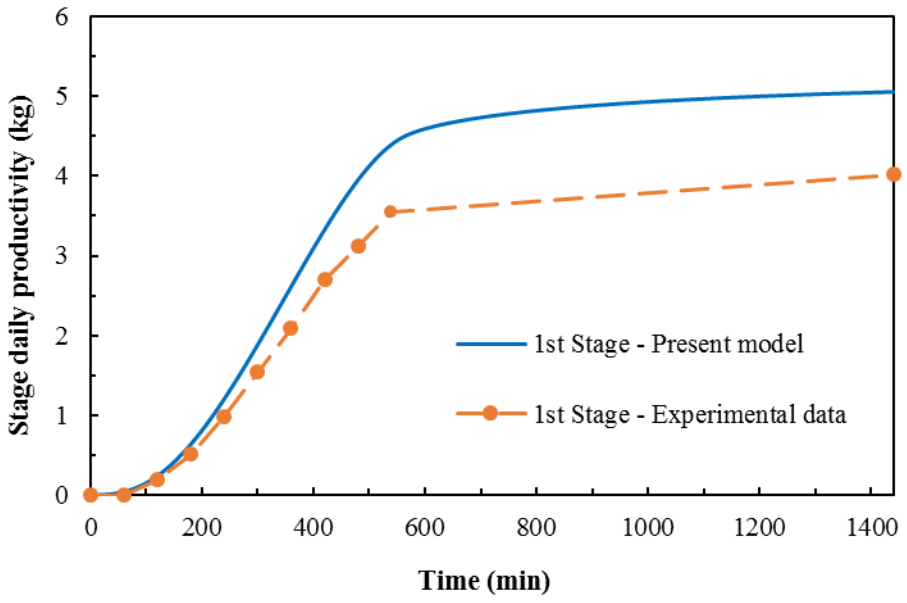

Figure 5.5 Comparison between experimental and theoretical daily yield in the first stage at 1.0 atm.

It can be noticed in this figure that the actual quantity of distillate produced after 24 hours is 4.02 kg, while the theoretical daily production is equal to 5.05 kg. The maximum

relative deviation between the experimental and the calculated results was found to be 26.5%

Figure 5.6 demonstrates the comparison between experimental and theoretical daily productivity produced by the second stage. In this figure, the maximum relative deviation is 25.2% while the theoretical and experimental distillate yields are 2.28 and 2.92 kg/day, respectively.

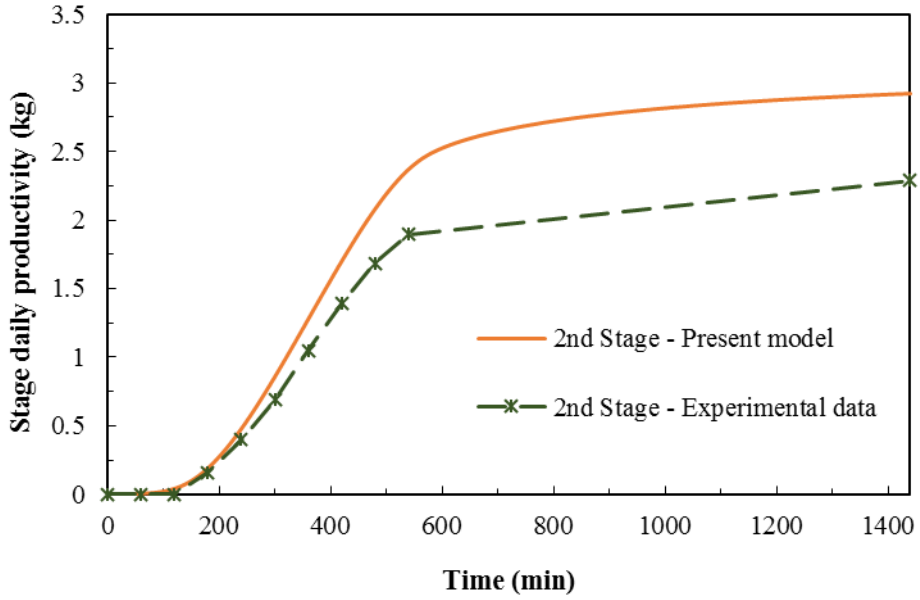

Figure 5.6 Comparison between experimental and theoretical daily yield in the second stage at 1.0 atm.

The comparisons between experimental and theoretical daily productivities of the third and fourth stages are depicted in Figure 5.7 and Figure 5.8. It can be seen that the theoretical and experimental daily yield of the third stage are 1.36 and 1.72 kg respectively, with a maximum relative deviation is 27.7%. For the fourth stage, the theoretical distillate yield, experimental distillate yield and maximum relative deviation are 0.78 kg/day, 1.0 kg/day and 28.3% respectively.

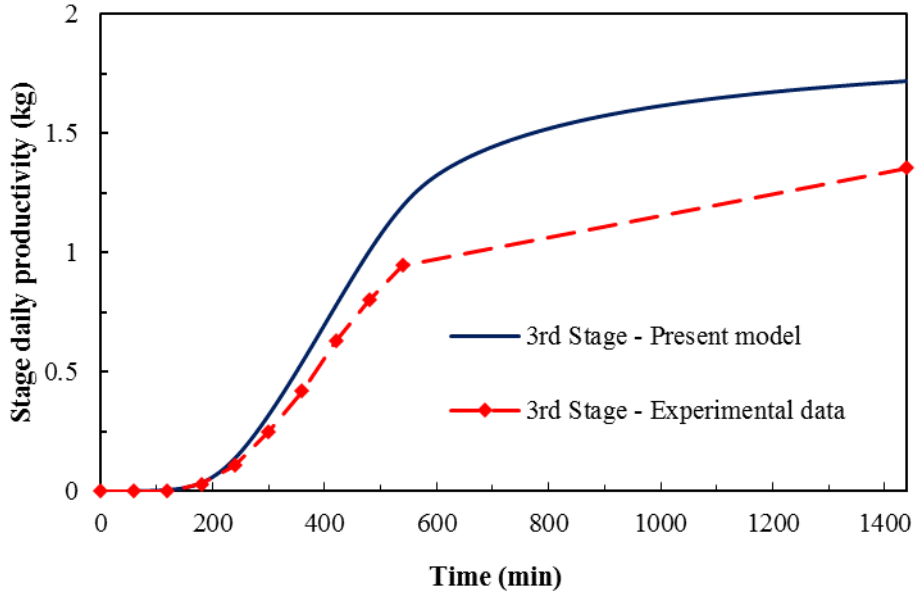

Figure 5.7 Comparison between experimental and theoretical daily yield in the third stage at 1.0 atm.

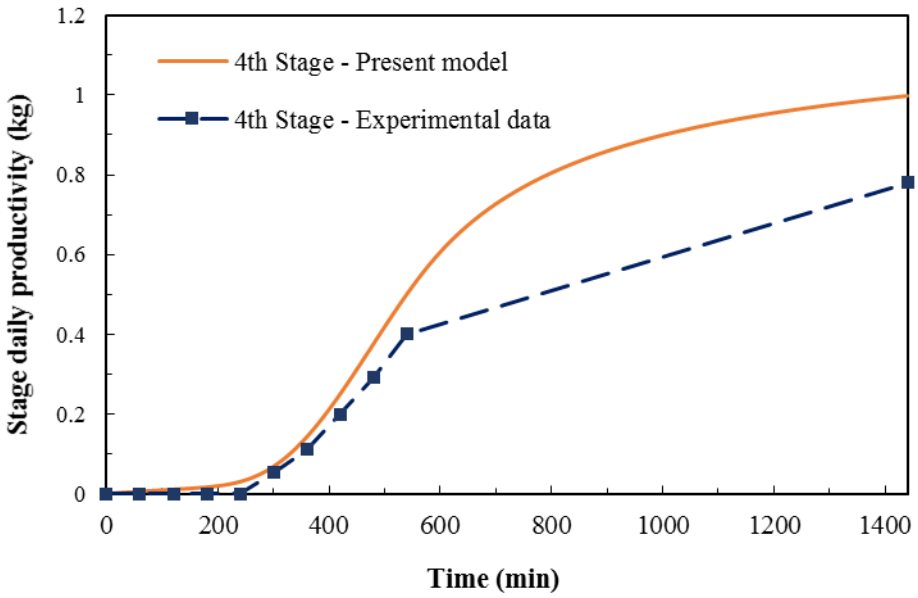

Figure 5.8 Comparison between experimental and theoretical daily yield in the fourth stage at 1.0 atm.

Figure 5.9 presents the comparison between experimental and theoretical cumulative daily productivity of the multi-effect water still. It is obvious that the trends in the values of

experimental cumulative daily yield corresponds to the curve of the theoretically obtained curve. However, similar to the results for the productivity of stages, the theoretical quantity of cumulative daily productivity is considerably higher than the actual values. It can be noticed that the actual quantity of cumulative distillate produced after 24 hours is 8.44 kg while the theoretical daily production equals 10.69 kg. The maximum relative deviation between the experimental and the calculated results was found to be 27.1%.

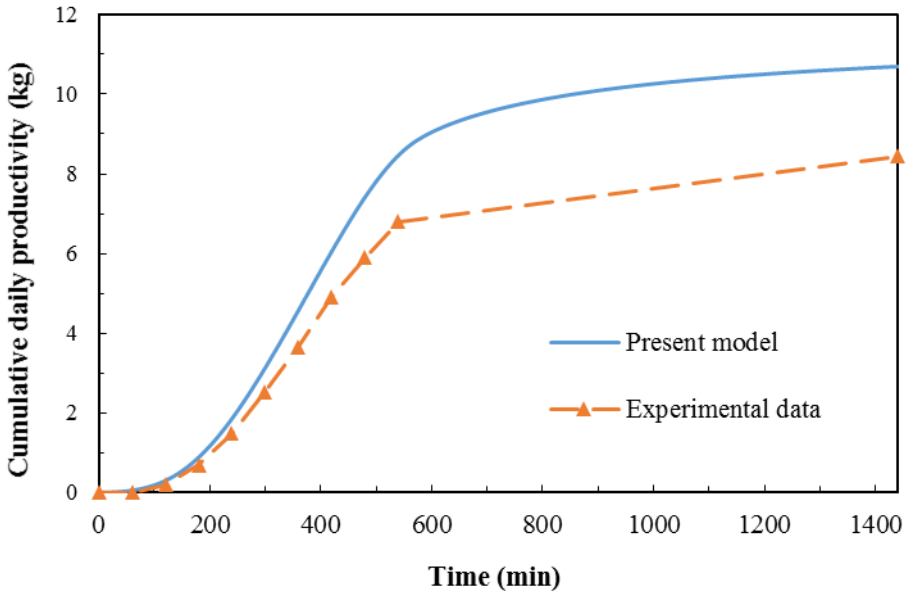

Figure 5.9 Comparison between experimental and theoretical cumulative yield at 1.0 atm.

It is worth mentioning here that the low quantities of experimental daily productivity could be attributed to the fact that it was assumed in the mathematical model that the total quantity of evaporated water in each stage is condensed, whereas in fact it is not. Other reasons which could lead to this inaccuracy in the theoretical results are errors in the measurement of the actual volume of the saline waterbed in each stage and also the adjustment of the horizontal position of all trays.

5.3 Validation of the Mathematical Model under Vacuum Pressure

Experiments on the performance of the evacuated multi-effect water still were conducted for various values of internal pressure; namely, 0.9, 0.8, and 0.7 atm. During the experimental investigation it was noticed that the effect of the reduction of the internal pressure became profound when the pressure was 0.7 atm. Therefore, the focus in this section is given to the validation of the results for an internal pressure equal to 0.7 atm. As mentioned in Chapter 4, the internal pressure in the system was controlled using a vacuum pump and it was monitored by a pressure gauge. The experiments were conducted for nine hours starting at 09:00 am, and the whole system was switched off at 06:00 pm. The waterbed temperatures and freshwater productivity were measured and recorded during the operating time of 540 min.

5.3.1 Validation of the Waterbed Temperature in the Stages

Figure 5.10 to 5.13 present the comparison between the experimental and theoretical results of the waterbed temperatures in all stages of the multi-effect water still for an internal pressure equal to 0.7 atm. It is evident that the waterbed temperature curves of both experimental and theoretical results are remarkably consistent. However, the theoretical results for temperature showed a lower value compared to the experimental results, and this accords with the observations mentioned earlier of the waterbed temperature curves under atmospheric pressure.

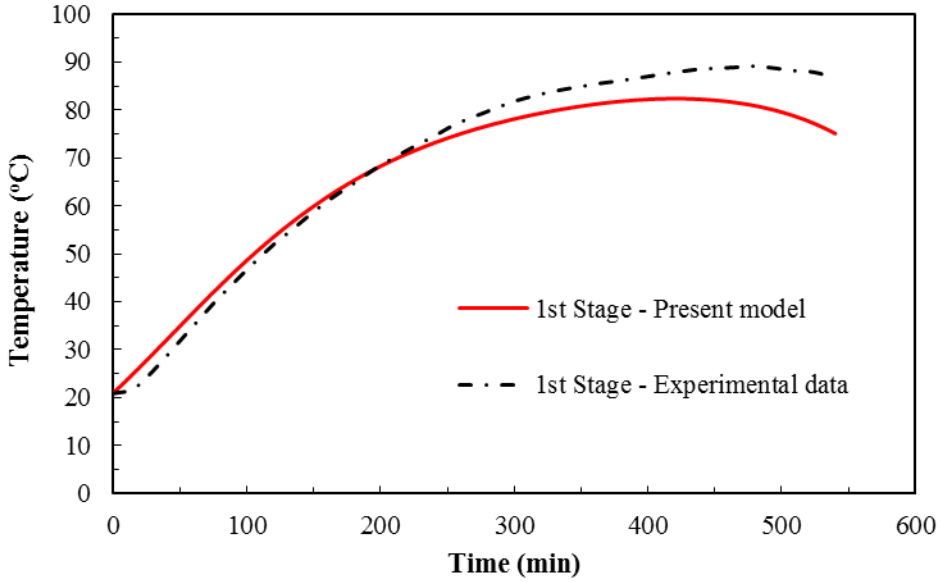

Figure 5.10 Comparison between experimental and theoretical temperature in the first stage at 0.7 atm.

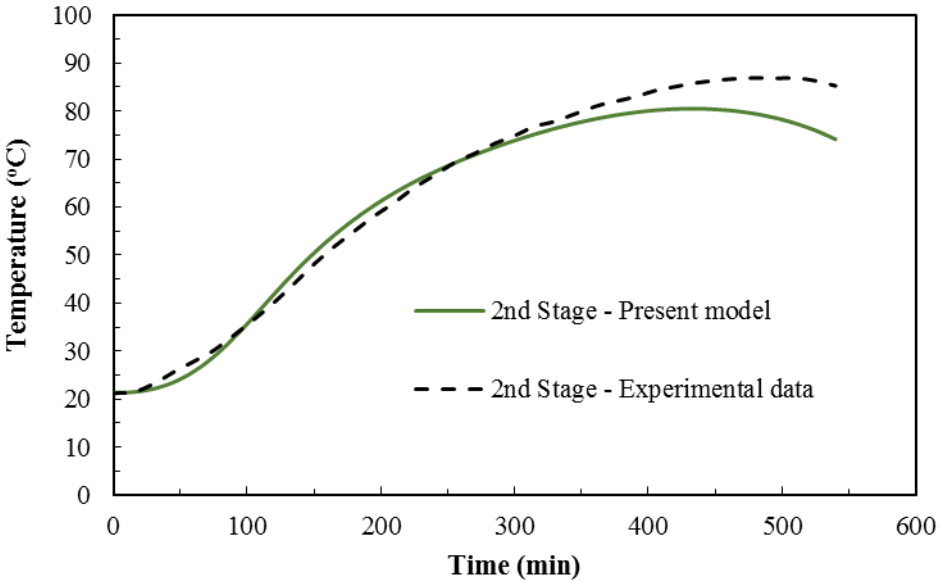

Figure 5.11 Comparison between experimental and theoretical temperature in the second stage at 0.7 atm.

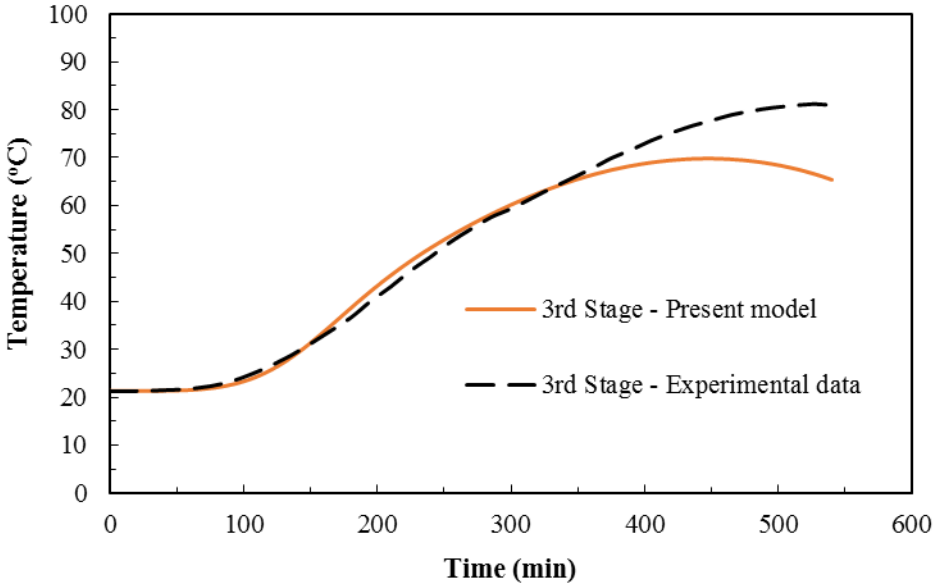

Figure 5.12 Comparison between experimental and theoretical temperature in the third stage at 0.7 atm.

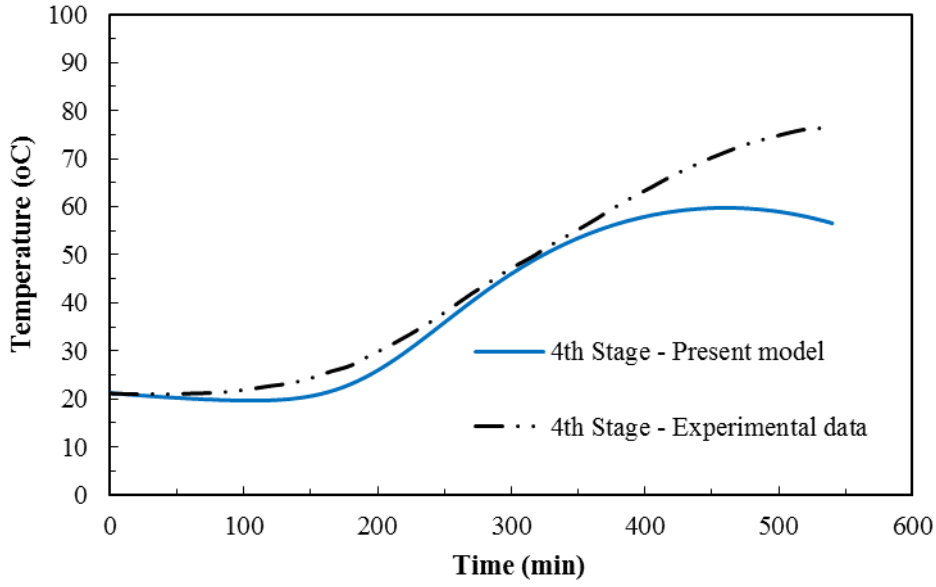

Figure 5.13 Comparison between experimental and theoretical temperature in the fourth stage at 0.7 atm.

The maximum relative deviations between experimental and theoretical results of the waterbed temperatures for the first, second, third and fourth stage are 13.4%, 13.1%, 19.2% and 25.8% respectively. The high deviation between the calculated and experimental results for the fourth stage waterbed temperature could be explained by the inaccuracy in calculating the heat losses from the uncovered top tray.

5.3.2 Validation of Freshwater Productivity

The comparisons between the experimental and theoretical results of the distillate productivity of all stages of the multi-effect water still with an internal pressure equal to 0.7 atm are illustrated in Figures 5.14 to 5.17. Similar to the findings, reported in Section 5.1.2, the experimental and theoretical productivities increase in an identical pattern, although the theoretical distillate productivity is a notable overestimated.

Figure 5.14 presents the comparison between the experimental and theoretical productivity of the first stage. It was found that the actual distillate yield of this stage during the experimental period was 3.60 kg while the theoretical daily production is 4.43 kg. The maximum relative deviation between the experimental and theoretical curves is 25.4%.

The comparison between experimental and theoretical productivity produced by the second stage is demonstrated in Figure 5.15. It can be seen that the theoretical and experimental distillate productivities are 2.41 kg and 1.92 kg respectively. The maximum relative deviation is 26.5%.

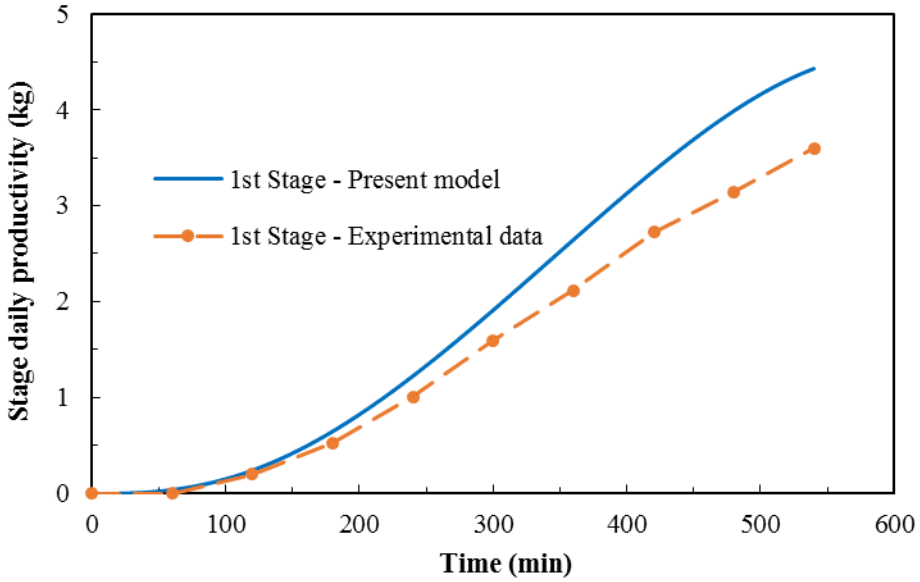

Figure 5.14 Comparison between experimental and theoretical yield in the first stage at 0.7 atm.

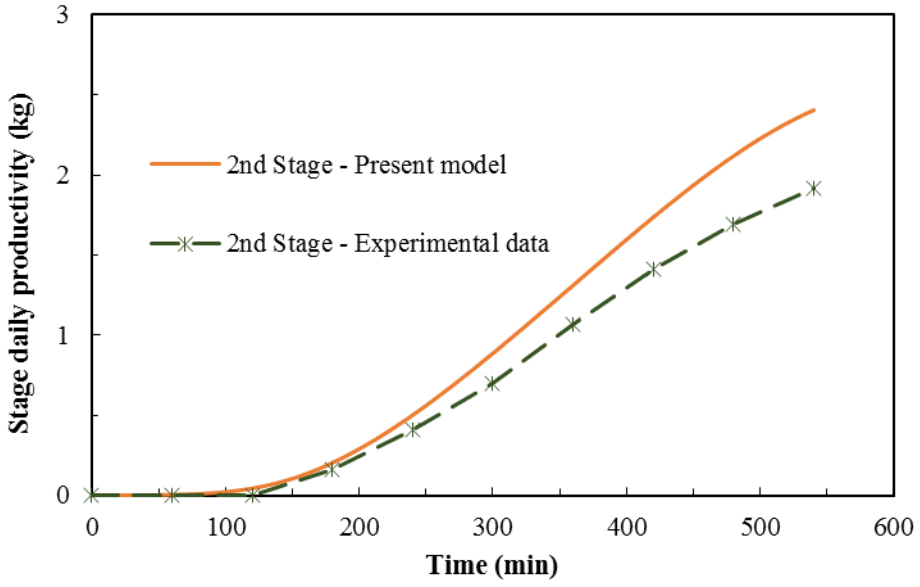

Figure 5.15 Comparison between experimental and theoretical yield in the second stage at 0.7 atm.

Figure 5.16 and Figure 5.17 show the comparisons between experimental and theoretical productivities of the third and fourth stages. It was noticed that the theoretical and

experimental yields of the third stage were 1.23 kg and 1.01 kg respectively, while the maximum relative deviation was 27.2%. For the fourth stage, the theoretical distillate yield, the experimental distillate yield and the maximum relative deviation are 0.53 kg, 0.44 kg and 28.1% respectively.

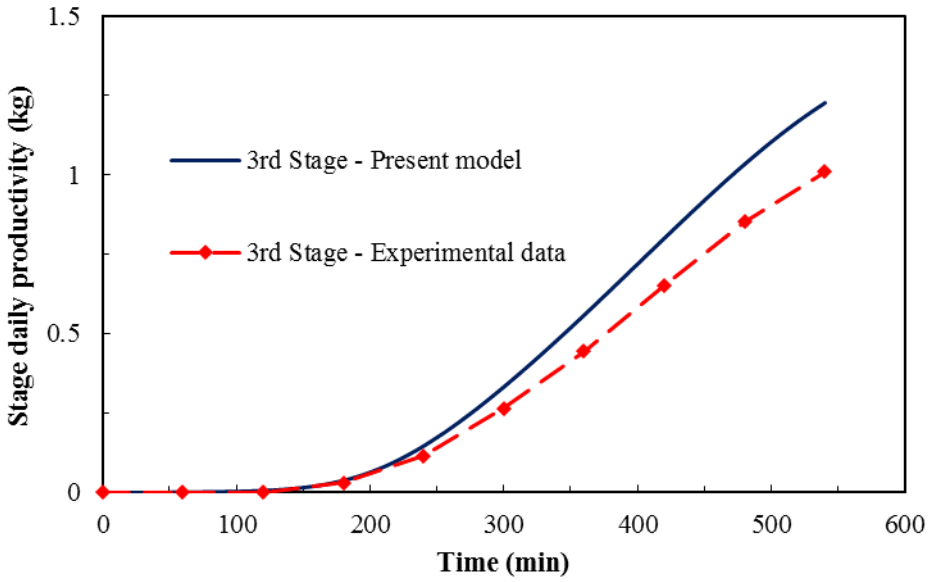

Figure 5.16 Comparison between experimental and theoretical yield in the third stage at 0.7 atm.

The comparison between the experimental and theoretical cumulative productivity of the multi-effect water still is depicted in Figure 5.18. It can be seen that the pattern of the experimental cumulative yield curve corresponds to that of the theoretically obtained yield. However, the experimentally obtained quantity of cumulative distillate is considerably lower than the estimated quantity. The values of theoretical and actual cumulative productivity during the experiment time are 8.60 kg and 6.97 kg, while the maximum relative deviation between the experimental and calculated results is 26.9%.

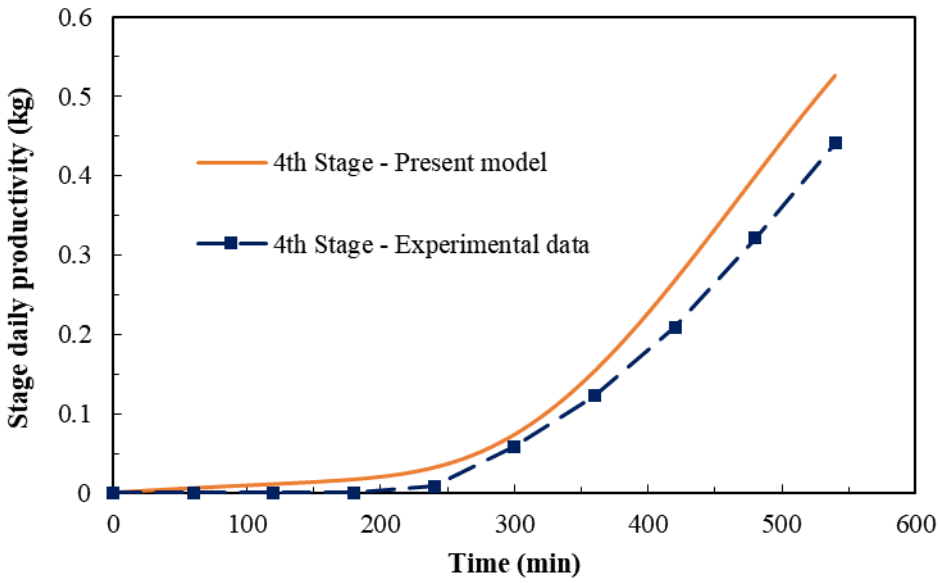

Figure 5.17 Comparison between experimental and theoretical yield in the fourth stage at 0.7 atm.

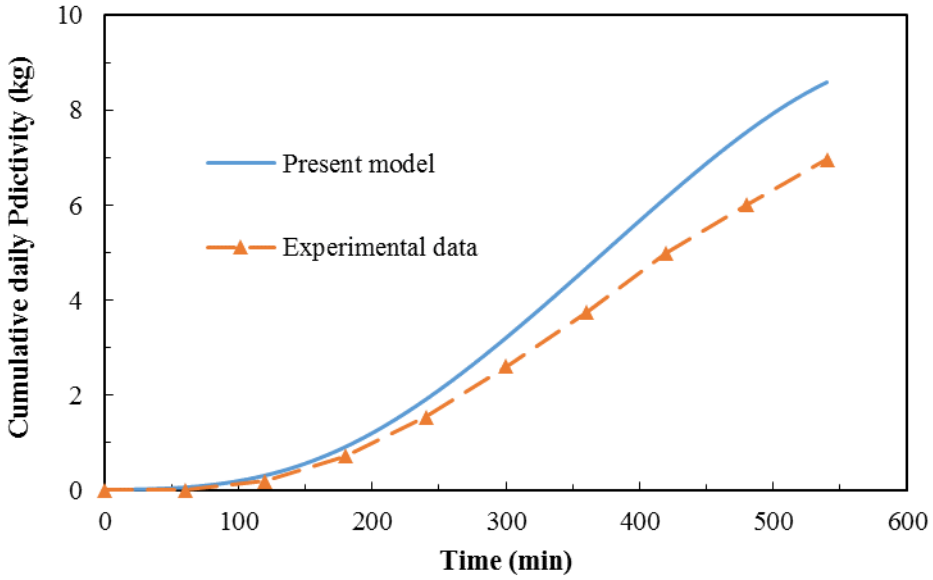

Figure 5.18 Comparison between experimental and theoretical cumulative yield at 0.7 atm.

This disagreement between experimental and theoretical results could be explained by the fact that the mathematical model calculates the system productivity based on inaccurate

assumptions the distillate yield is the condensed vapour and inaccurate measurements of the initial volume of the saline waterbed. Furthermore, this discrepancy could also be attributed to the level of internal pressure during the experiment not being stable, whereas it was assumed in the mathematical model to be a constant value.

5.4 Summary

In this Chapter the experimental results were used to examine the accuracy of the mathematical model in predicting the performance of the multi-effect solar water desalination still. The examination of the mathematical model was conducted for the operation of the proposed system under atmospheric pressure and an internal pressure of 0.7 atm. The investigation includes comparisons of waterbed temperatures, stage distillate productivity and the cumulative total yield of the system. For atmospheric pressure, it was found that the maximum relative deviation of the waterbed temperatures ranged between 17.2% and 26.7%, while the maximum relative deviation between the experimental and theoretical results of distillate productivity is between 25.2% and 28.3%. For an internal pressure equal to 0.7 atm, the maximum relative deviation between the experimental results and the calculated results ranges between 13.1% and 25.8%. For the results of stage distillate productivity, the maximum relative deviation is in the range between 25.4 and 28.1%. Accordingly, the comparison between the experimental and theoretical results demonstrates that the developed simulation model can predict the performance of the multi-effect solar water desalination sufficiently well and can be used to conduct further investigation into the effects of reducing the internal pressure.

Chapter 6 Influence of Internal Pressure Level on the Performance of the Multi-Effect Solar Water Still

This Chapter describes a detailed theoretical investigation of the performance of a dynamic multi-effect solar water still with the reduced internal pressure. The enhancement in the proposed system productivity when coupled to a small fluid piston energy converter is presented. The effects of the level of internal pressure on the temperature of the stages, their daily productivity and the total cumulative daily distillate yield are demonstrated and discussed.

6.1 Introduction

The performance of the dynamic multi-effect solar water still is influenced by several design and operational parameters. The effect of the design parameters on the performance of the proposed system has been investigated previously by Shatat and Mahkamov [156]. Therefore, in this Chapter, attention is drawn to the influence of internal pressure on the performance of the still. The theoretical analysis presented in the following sections was conducted using the mathematical model developed for different values of internal pressure.

The purpose of this investigation is to find out how the system's performance is enhanced by reducing the internal pressure level. This investigation was performed for the same physical dimensions as those of the experimental prototype. During the investigation, all of

the operational parameters, including the total solar irradiance presented in Figure 4.26 and the initial temperatures of the waterbeds in all stages, were kept constant and only the internal pressure was changed. The initial temperatures of the first, second, third and fourth stages were assumed to be 20.97, 21.32, 21.35 and 21.25 ^{o}C respectively.

6.2 Productivity Enhancement using a Fluid Piston Energy Converter

This section presents the theoretical prediction of the distillate productivity when the small fluid piston is coupled to a multi-effect solar water still. As mentioned in Section 4.6.1, the fluid piston converter is able to produce vacuum conditions inside the system of about 0.895 atm. Figure 6.1 shows the enhancement in the total cumulative distillate yield when the system is coupled with the fluid piston. It can be seen that reducing the internal pressure level affects the system productivity positively, since the lower pressure level intensifies the evaporation process and leads to higher distillate production rates.

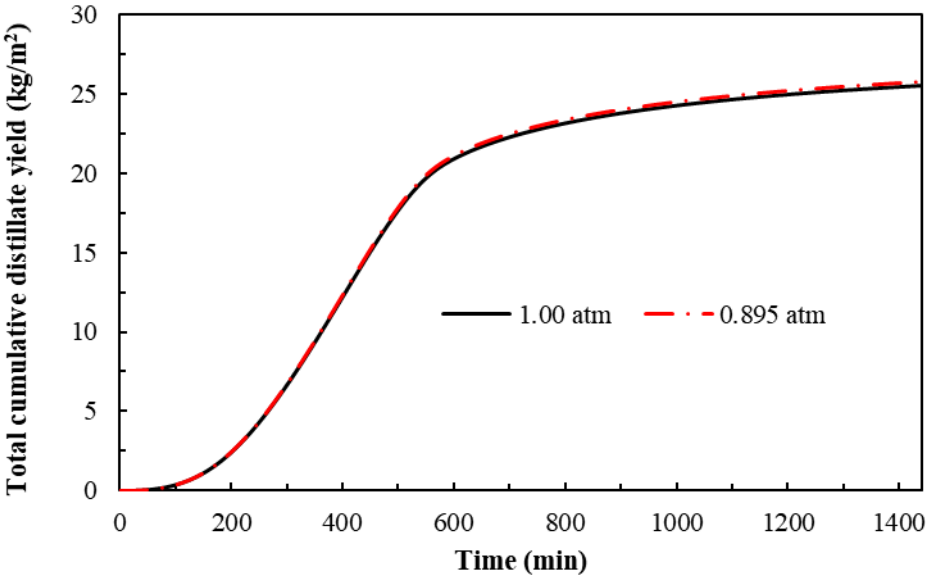

Figure 6.1 Enhancement in distillate productivity using fluid piston.

It was also found that the total cumulative distillate yield over 24 hours is equal to 25.55 kg/m^2 for atmospheric pressure and it could reach about 25.80 kg/m^2 at 0.895 atm. The percentage of the improvement in the system productivity is about 1.0 %. However, this low performance can be improved by conducting further investigation for a better understanding of the design and operational principles of the fluid piston energy converter which might lead to a significant enhancement in the performance of the proposed desalination unit.

6.3 Effect of Internal Pressure on the Temperatures of the Stages

Figures 6.2 to 6.5 demonstrate variations in the waterbed temperatures in all stages of the proposed system at different internal pressure levels. Figure 6.2 presents the effect of internal pressure on the variation in waterbed temperature for the first stage. It can be seen that decreasing the pressure below the atmospheric level strongly affects the temperature variation. The stage's temperature decreases with internal pressure. But this effect becomes more obvious when the internal pressure drops to 0.7 atm or below. The waterbed temperature in this stage can reach the maximum values of around 85.9 and 56.9 ^{o}C for internal pressure levels of 1.0 and 0.05 atm respectively.

The effects of changing the internal pressure on the variation in waterbed temperature of the second and third stages are depicted in Figure 6.3 and Figure 6.4. Although the waterbed temperature curves have a trend similar to that in the first stage, the maximum temperature in the second stage has a lower value. It ranged between 76.9 ^{o}C for atmospheric pressure and 55.5 ^{o}C for 0.05 atm. In the third stage the waterbed temperature can reach maximum values of 65.8 and 47.9 ^{o}C for 1.0 and 0.05 atm.

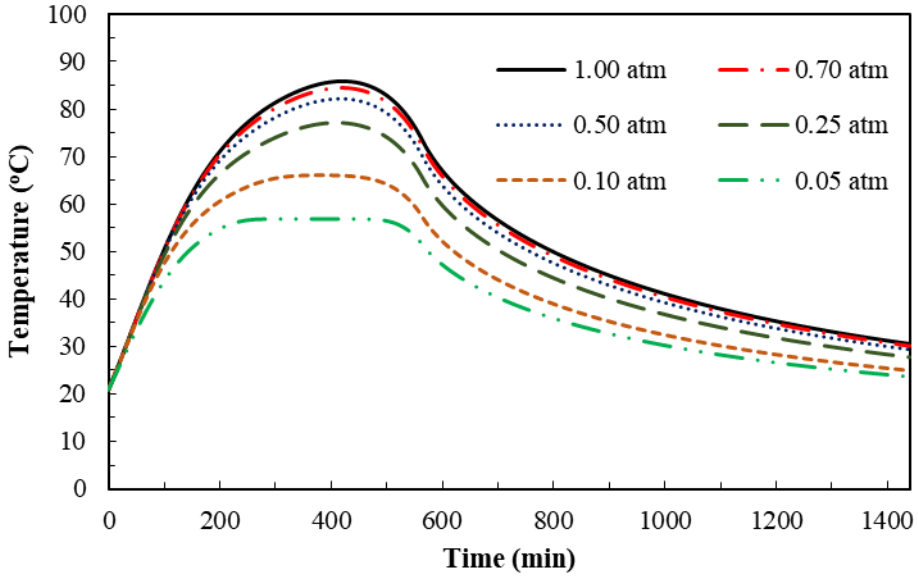

Figure 6.2 Effect of internal pressure level on the first stage temperature.

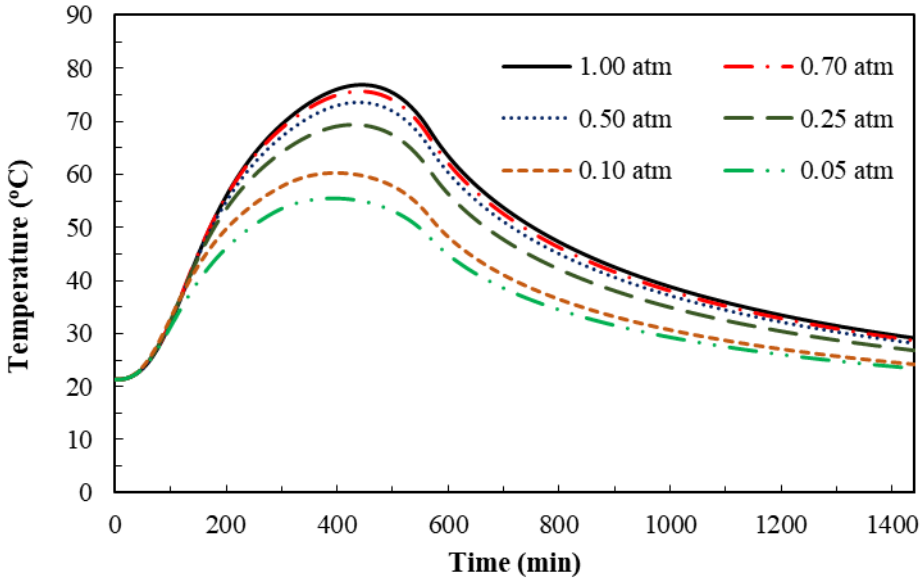

Figure 6.3 Effect of internal pressure level on the second stage temperature.

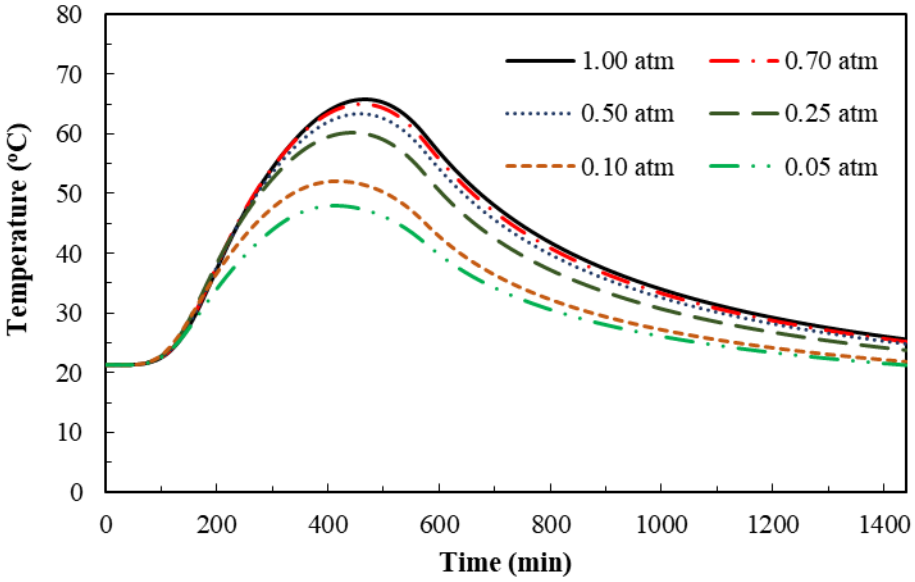

Figure 6.4 Effect of internal pressure level on the third stage temperature.

Figure 6.5 illustrates the variation in waterbed temperature with the internal pressure level in the fourth stage. The fourth stage is characterized by the lower waterbed temperature, and in this stage, the maximum temperature is 56.0 ^{o}C for the atmospheric pressure while it can reach 36.9 ^{o}C for 0.05 atm.

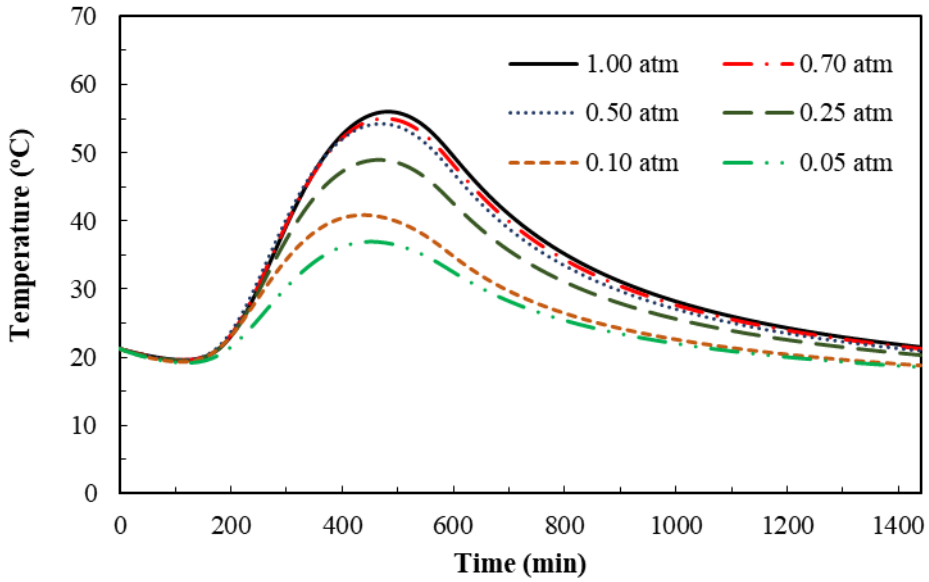

Figure 6.5 Effect of internal pressure level on the fourth stage temperature.

The variations in temperature difference between the condensing and evaporation surfaces in all stages with the reduced internal pressure were calculated and the results are presented in Figures 6.6 to 6.9. Similar to the temperatures graphs, the effect of the pressure level is most apparent at the 0.7 atm level and below. Figure 6.6 demonstrates the effect of the change in internal pressure on variations in the temperature difference in the first stage. It is obvious that the temperature difference between the evaporating and condensing surfaces increases until it reaches the maximum value and then decreases to approximately the initial value at the end of the day.

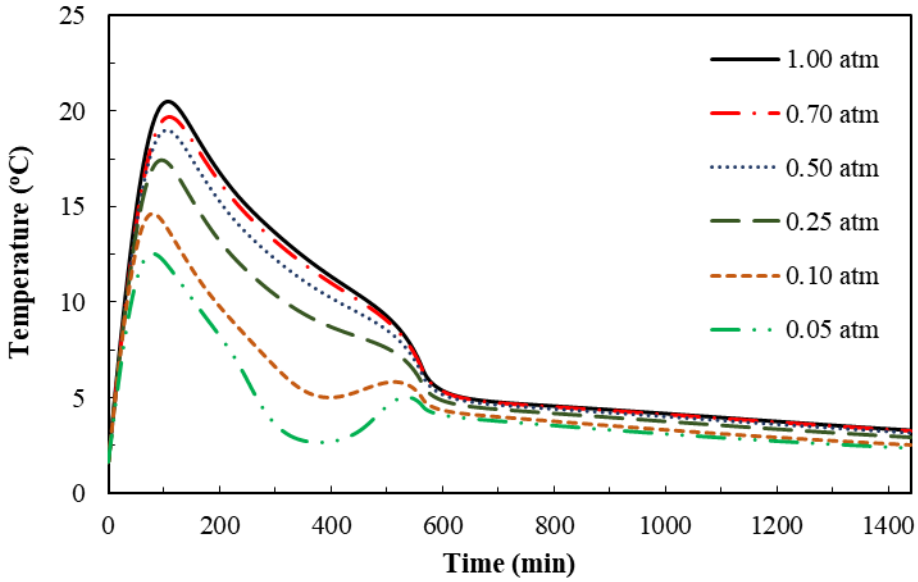

Figure 6.6 Variations in temperature difference with pressure level in the first stage.

However, this variation is slightly different at very low pressures, namely at 0.1 and 0.05 atm, as the temperature difference after reaching the maximum value decreases and then fluctuates around the final value. It can also be seen that the temperature difference at 0.05 atm first decreases to the minimum value and then increases and again starts decreasing to its final value. In this stage, the maximum temperature differences between the two

surfaces were found to be 20.5 and 12.6 ^{o}C for the atmospheric pressure and 0.05 atm respectively.

The variations in temperature difference between the evaporating and condensing surfaces with the change in internal pressure for the second and third stages are depicted in Figure 6.7 and Figure 6.8. It was noticed that, for atmospheric pressure, the temperature differences can reach maximum values of 19.3 and 17.2 ^{o}C for the second and third stages respectively, while they were found to be 11.8 and 10.8 ^{o}C for 0.05 atm.

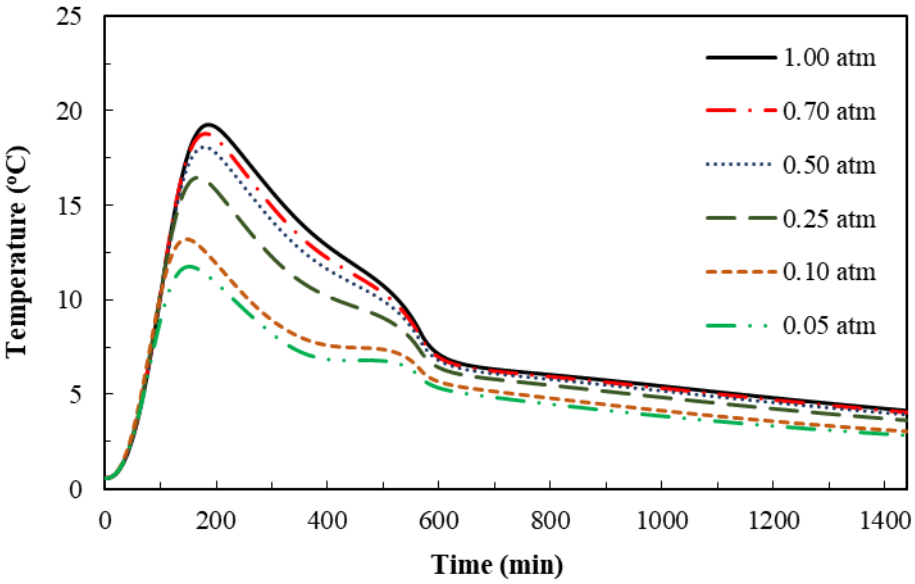

Figure 6.7 Variations in temperature difference with pressure level in the second stage.

Figure 6.9 shows the influence of the internal pressure level on the variation in the temperature difference of the condensing and evaporating surfaces in the fourth stage. It is obvious that, for all pressure levels, the temperature difference decreases at the beginning of the desalination process and then increases until reaching the maximum value before decreasing to its minimum value. This decrease in temperature difference of 1 ^{o}C at the beginning of the process could be attributed to the fact that the temperature of the evaporating surface decreases because of the low temperature of top cover, and also

because the effect of the latent heat of condensation is not sufficient to raise the waterbed temperature.

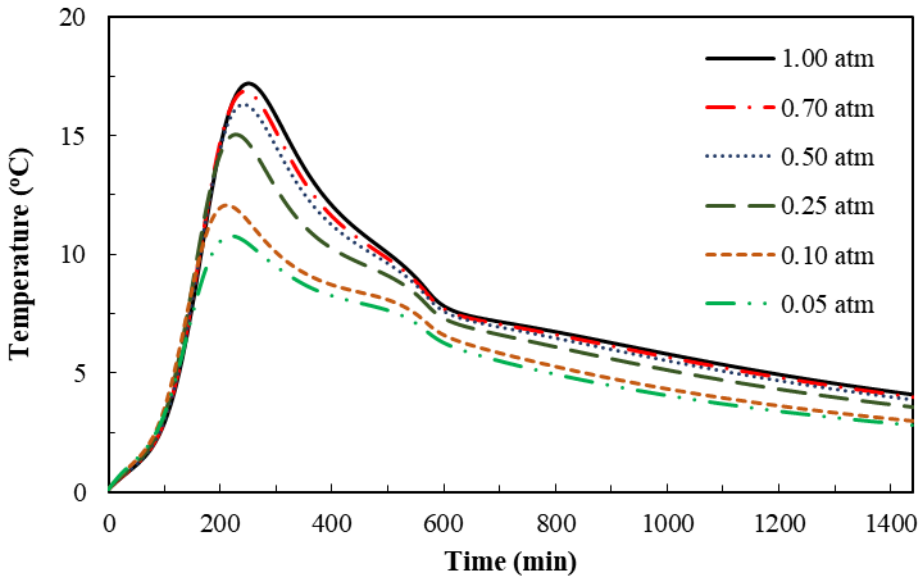

Figure 6.8 Variations in temperature difference with pressure level in the third stage.

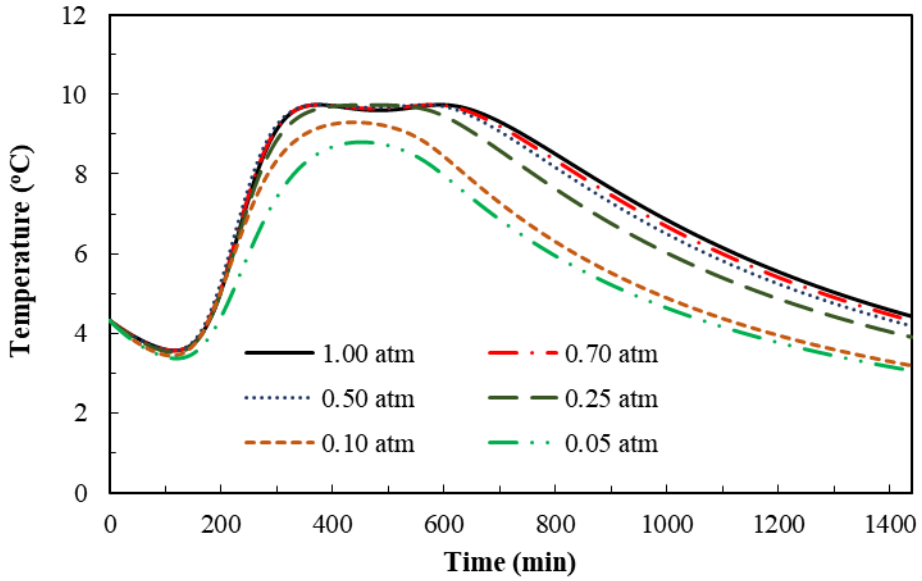

Figure 6.9 Variations in temperature difference with pressure level in the fourth stage.

Later, as the solar radiation increases and due to the evaporation and condensation processes between all stages, the temperature of the evaporating surface in the fourth stage increases leading to the rise in the temperature difference. As the solar radiation decreases the temperature difference also decreases to the lower value. The maximum temperature differences between two surfaces were found to be 9.7 and 8.8 ^{o}C at the atmospheric pressure and 0.05 atm, respectively.

6.4 Effect of Internal Pressure on Convective Heat Transfer Coefficient

The effect of changing the internal pressure level on the variations in the convective heat transfer coefficient, *hcv,* was investigated for a range of pressure levels, and the results are illustrated in Figures 6.10 to 6.13. A similar trend for the convective heat transfer coefficient was observed in all stages as it increases towards the maximum value then decreases to approximately the same low value.

Figure 6.10 presents the variation in convective heat transfer coefficient in the first stage for different pressure levels. It was noticed that, for all pressure levels, the convective heat transfer coefficient increases from the minimum value of about 1.15 W/m^2 K at the beginning of the process. The low convective heat transfer coefficient during the initial hours of the desalination process can be attributed to the low temperature differences between the evaporating and condensing surfaces during this period. Thereafter it reaches the maximum value and then decreases to the lower value ranging between approximately 1.57 and 1.81 W/m^2 K. It can also be seen that the maximum value of the convective heat transfer coefficient varies from 2.64 W/m^2 K for the atmospheric pressure to 8.18 W/m^2 K for 0.05 atm.

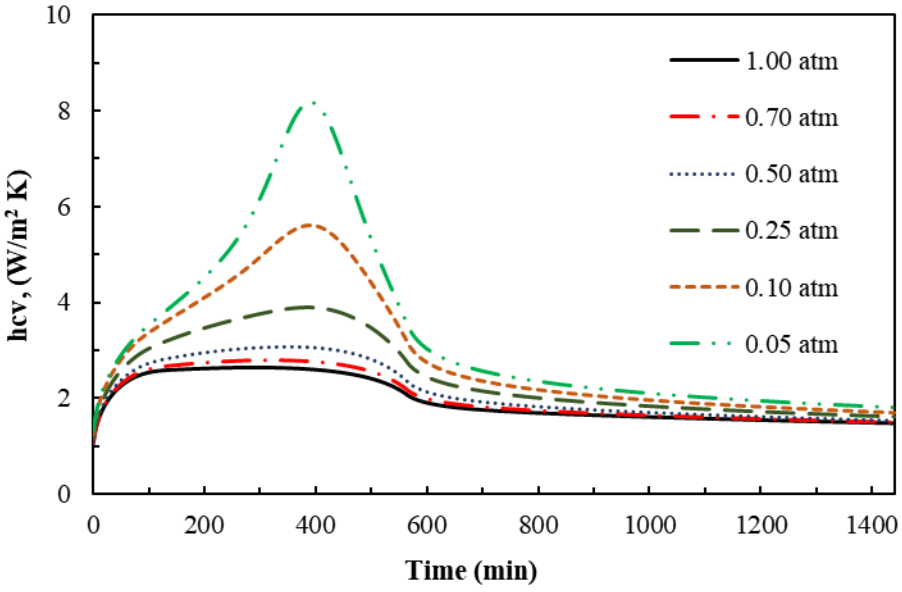

Figure 6.10 Variations in *hcv* with internal pressure level in the first stage.

The effect of reducing the internal pressure level on the variation in the convective heat transfer coefficient in the second stage is depicted in Figure 6.11. The convective heat transfer coefficient in this stage starts with values similarly ranging between approximately 1.0 – 1.2 W/m^2 K and after reaching the maximum value decrease to low values between 1.5 and 1.8 W/m^2 K. The maximum values of the convective heat transfer coefficient were found to be 2.41 and 5.30 W/m^2 K for atmospheric pressure and 0.05 atm, respectively.

Figure 6.12 demonstrates the variations in the convective heat transfer coefficient with the internal pressure in the third stage. It was observed that the initial values of the coefficient were around 1 W/m^2 K and the low final values were found to be between 1.5 and 1.8 W/m^2 K, while the maximum values for atmospheric pressure and 0.05 atm were 2.28 and 3.82 W/m^2 K, respectively.

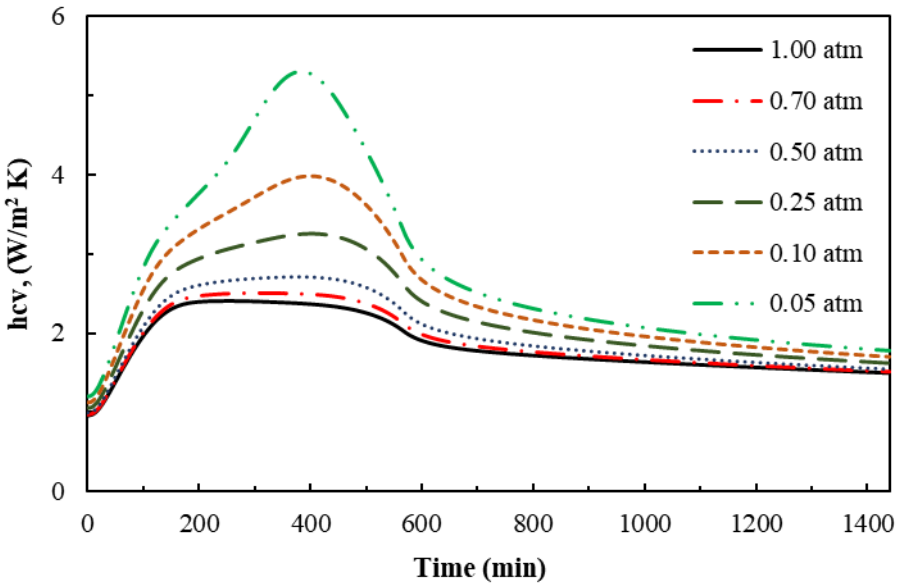

Figure 6.11 Variations in *hcv* with internal pressure level in the second stage.

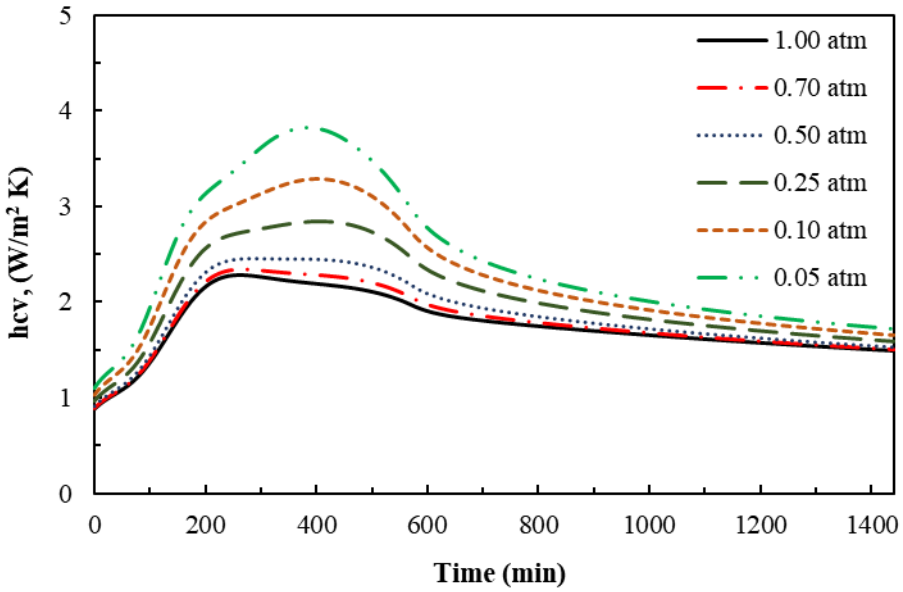

Figure 6.12 Variations in *hcv* with internal pressure level in the third stage.

The variation in the convective heat transfer coefficient with the reduced internal pressure level in the fourth stage is shown in Figure 6.13. It can be seen that the convective heat

transfer coefficient decreases at the beginning of the desalination process until it reaches the minimum value and this decrease was noticed at all pressure levels. This drop is attributed to the lower temperature difference between the evaporating and condensing surfaces during this phase of the process. Then the convective heat transfer coefficient increases as the solar radiation rises and the maximum values equal to 2.01 W/m^2 K for atmospheric pressure and to 3.23 W/m^2 K for the pressure level of 0.05 atm.

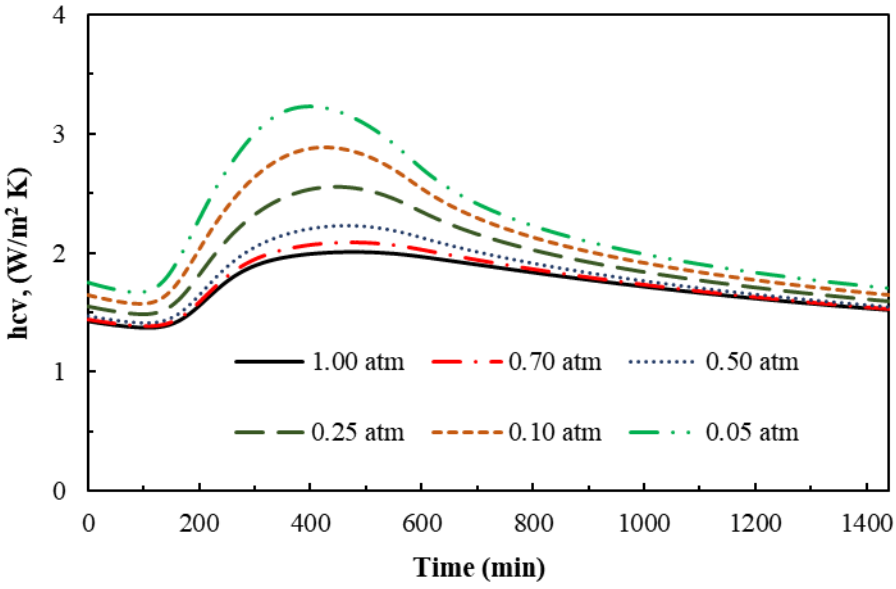

Figure 6.13 Variations in *hcv* with internal pressure level in the fourth stage.

At the end of the process, it was noticed that the maximum values of the convective heat transfer coefficient were between 1.51 and 1.70 W/m^2 K for the atmospheric pressure and 0.05 atm, respectively.

It is evident from these graphs that the convective heat transfer coefficient for all stages increases with reductions in the internal pressure level, which could lead to improvements in the daily productivity of the system.

6.5 Effect of Internal Pressure on Productivity

The variations in the daily productivity of the multi-effect solar water still at different internal pressure levels were investigated and the results are discussed in this section. Figure 6.14 shows the variations in daily productivity with changing internal pressure for the first stage. It can be seen that reducing the internal pressure level affects the stage's productivity positively, since the minimum pressure level intensifies the evaporation process and leads to the higher freshwater production rates. It can also be noticed that, in this stage, the effect of reducing pressure is profound when the pressure is equal to 0.7 atm.

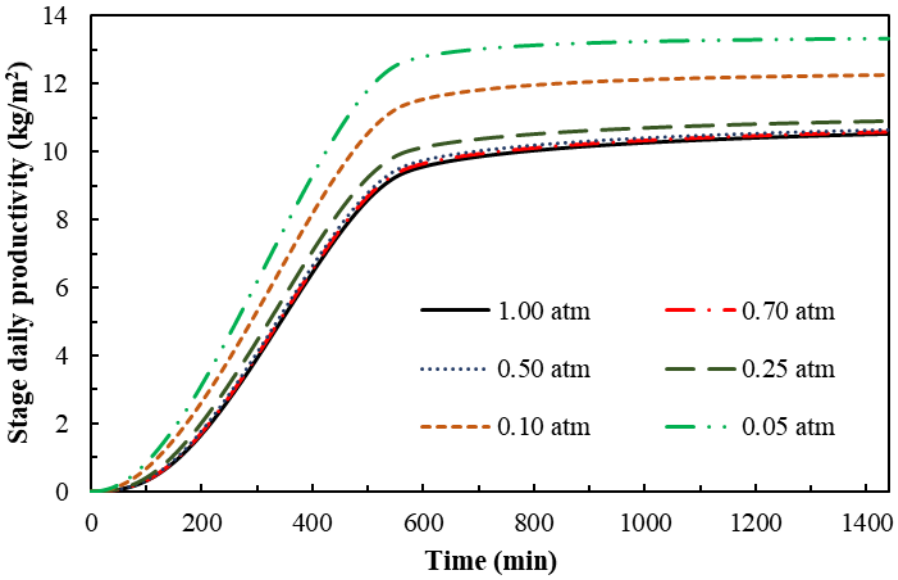

Figure 6.14 Variations in the daily productivity with internal pressure of the first stage.

The cumulative distillate yield over 24 hours was found to be equal to 10.53 kg/m^2 for the atmospheric pressure and it could reach about 13.34 kg/m^2 at 0.05 atm. The freshwater productivity of the first stage at 0.05 atm was found to be higher than that at the atmospheric pressure by 26.7%.

The effect of changing the internal pressure level on the variation in distillate production rates in the second and third stages is demonstrated in Figure 6.15 and Figure 6.16. It was found that, although in these stages the effect of reducing the pressure level is apparent when the pressure is equal to 0.7 atm, this effect becomes more profound at 0.10 atm. The daily cumulative productivities of the second and third stages for the atmospheric pressure level were around 8.50 and 4.25 kg/m^2 respectively, whereas for the pressure level of 0.05 atm these were 14.41 and 7.0 kg/m^2. The percentages of enhancement in the daily productivity of the second and third stages were equal to approximately 41.01% and 64.71% respectively, when the internal pressure was 0.05 atm.

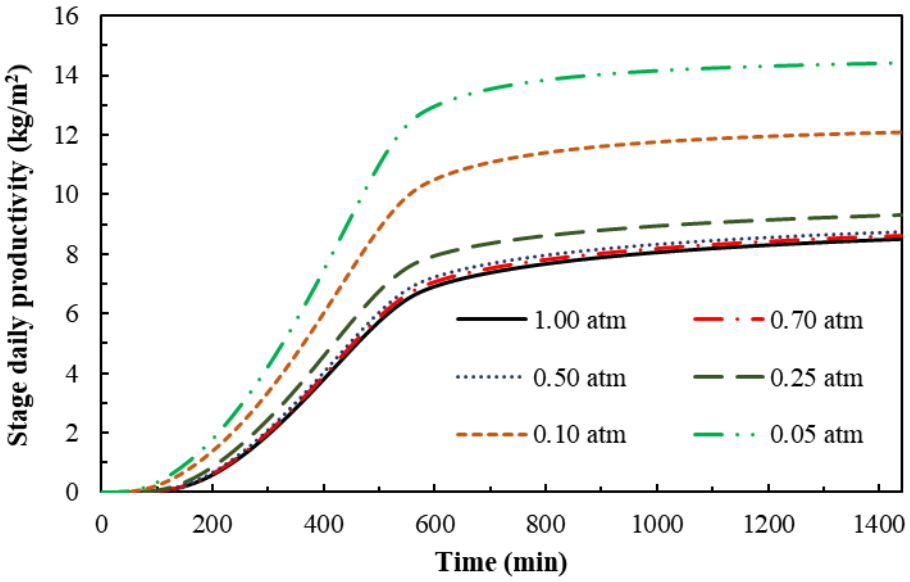

Figure 6.15 Variations in the daily productivity with internal pressure of the second stage.

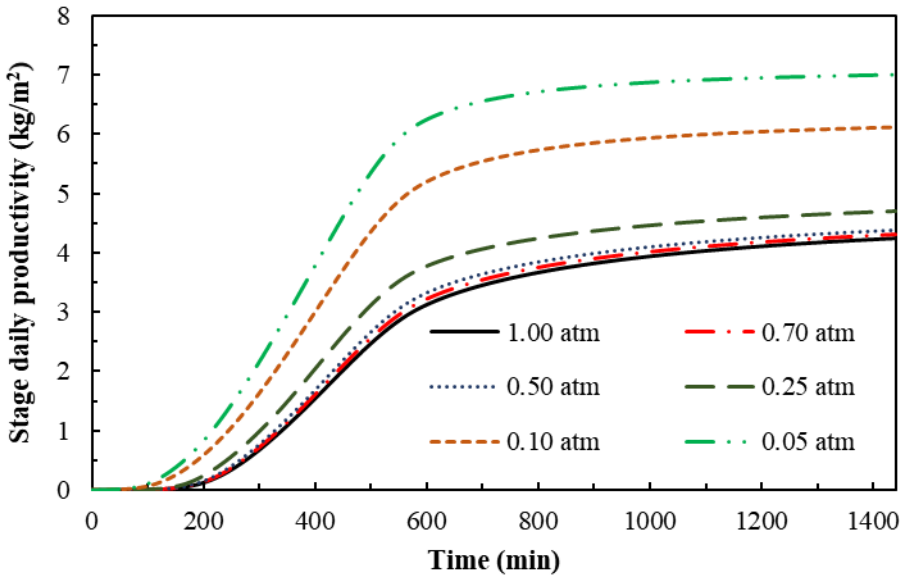

Figure 6.16 Variations in the daily productivity with internal pressure of the third stage.

Figure 6.17 presents the variations in the daily productivity of the fourth stage with the internal pressure level. It is obvious that the daily cumulative distillate yield is influenced by the pressure level and, similarly to the previous stages, the pressure effect is clearer at pressures below 0.7 atm. It was noticed that the cumulative productivity over the day reached around 2.28 kg/m^2 for atmospheric pressure and was about 4.06 kg/m^2 at 0.05 atm. The cumulative distillate productivity of this stage at 0.05 atm was improved by 78.07% compared to the productivity of the stage at the atmospheric pressure.

It is worth mentioning that the first stage obviously produces the maximum freshwater yield. However, it was noticed that in the case of the internal pressure of 0.05 atm the second stage produces higher distillate yield as shown in Figure 6.14 and Figure 6.15.

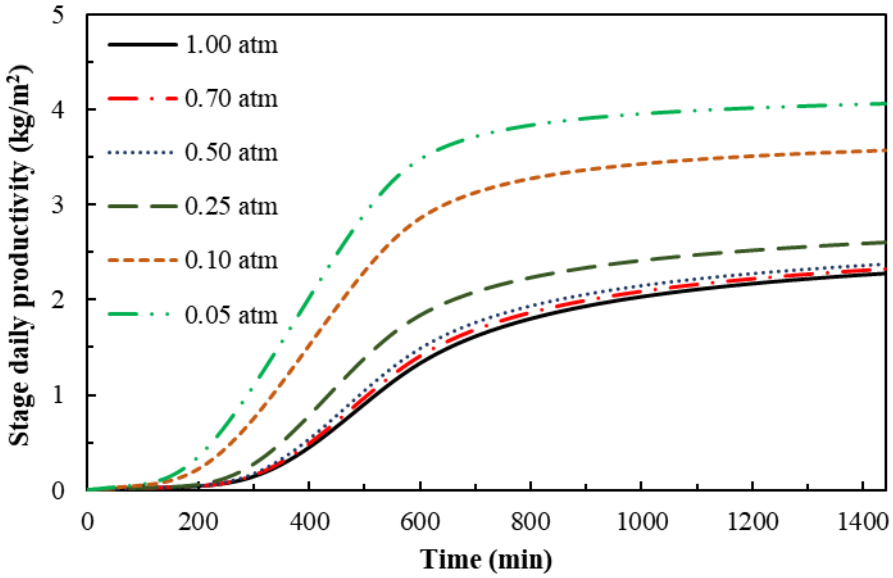

Figure 6.17 Variations in the daily productivity with internal pressure of the fourth stage.

In order to understand this discrepancy between the productivity of the two stages, Figure 6.18 shows the variations in convective heat transfer coefficient *hcv* and the temperature differences (Ts – Tc) of the first and second stages at the pressure level of 0.05 atm. The convective heat transfer coefficient and the temperature difference between the evaporating and condensing surfaces strongly affect the productivity in this stage. It can be seen that, although the first stage has a higher *hcv* compared to that of the second stage, its temperature difference is very low during the period when *hcv* is high. Meanwhile the convective heat transfer coefficient of the second stage is at its maximum value during the period of a relatively high temperature difference. It can also be seen that the convective heat transfer coefficients in both stages have approximately the same value at the time corresponding to 600 min and decrease to approximately the same low value, whereas the temperature difference in the second stage stays higher than that of the first

stage. As the consequence of this, the second stage produces a distillate yield greater than that of the first stage at the internal pressure of 0.05 atm.

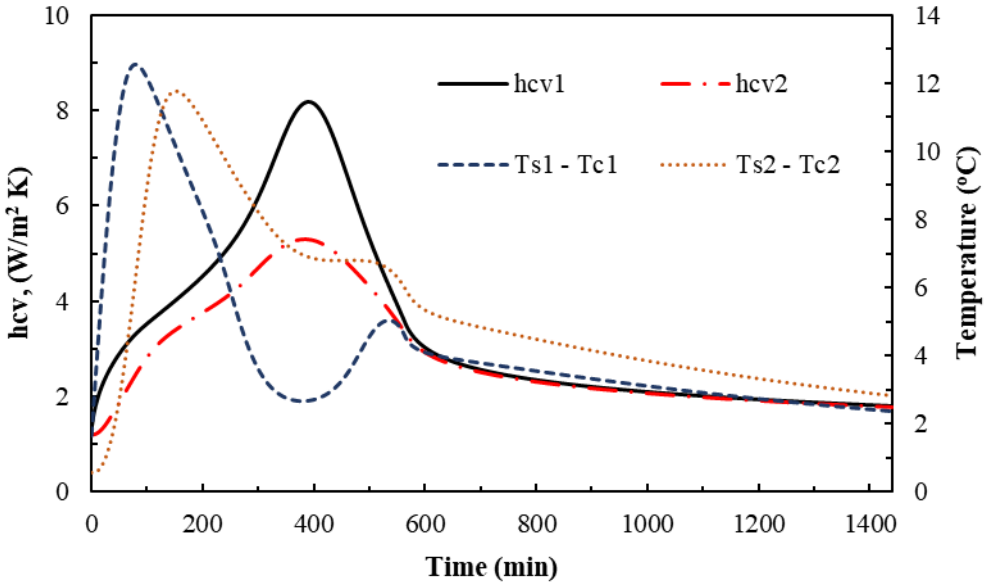

Figure 6.18 Comparisons of *hcv* and (Ts – Tc) of the first and second stages at 0.05 atm.

Figure 6.19 and Figure 6.20 demonstrate the effect of internal pressure on the total cumulative daily distillate yield. It is clear that the total yield increases with the decrease in the internal pressure level due to higher evaporation rates at the lower pressure. However, this influence is more obvious at pressure levels below 0.7 atm. The total cumulative daily distillate yield is found to be 25.55 kg/m^2 at the atmospheric pressure while it can reach 38.82 kg/m^2 at the pressure of 0.05 atm. The total daily productivity of the multi-effect solar still was enhanced by about 52% when it was operated at the pressure of 0.05 atm.

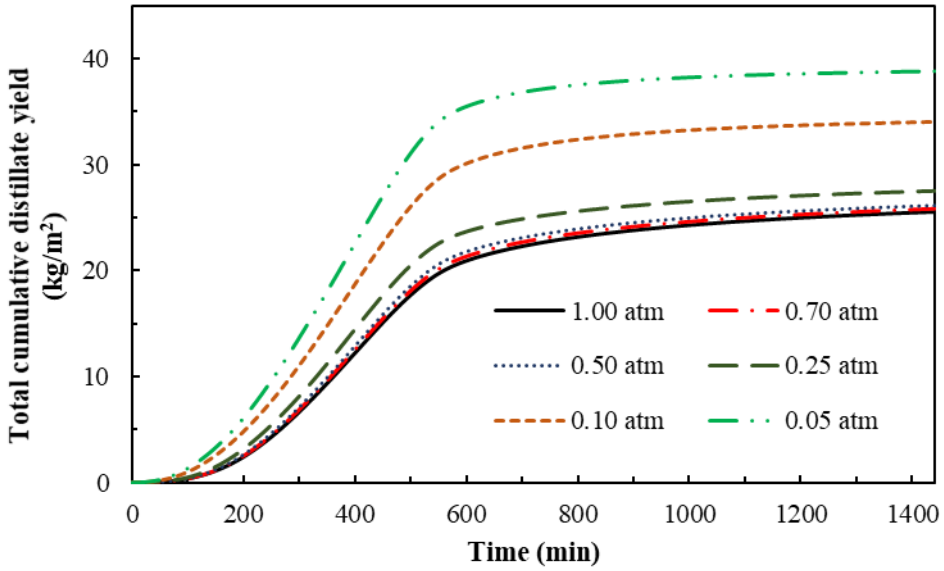

Figure 6.19 Variations in the total cumulative distillate yield with internal pressure level.

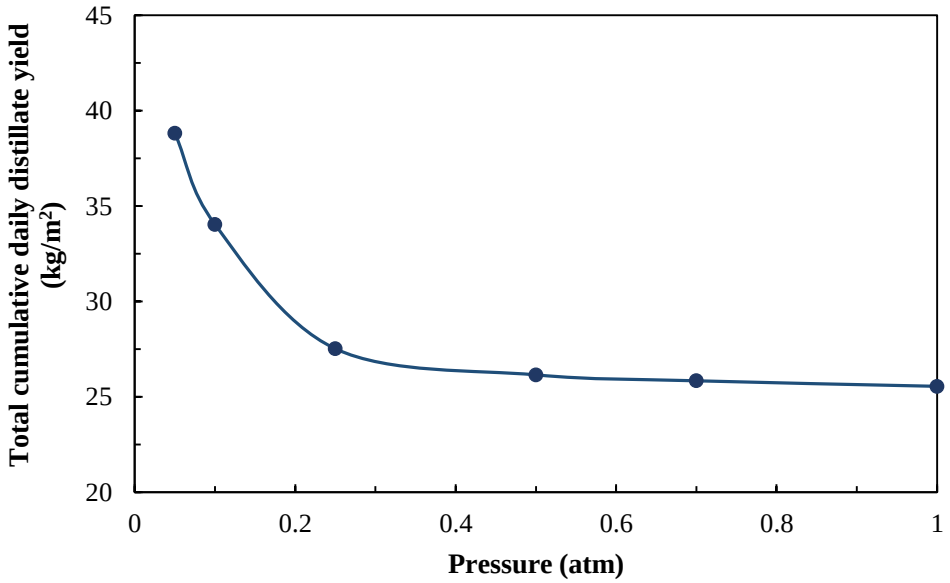

Figure 6.20 Effect of internal pressure level on the total cumulative daily distillate yield.

The variations in the hourly total cumulative distillate yield with the internal pressure level were also investigated and the results are depicted in Figure 6.21. It is obvious that the decrease of pressure leads to the increase in the hourly total cumulative distillate yield, and

it can reach the maximum values of 3.27 and 4.26 kg/m^2 for atmospheric and 0.05 atm pressures, respectively.

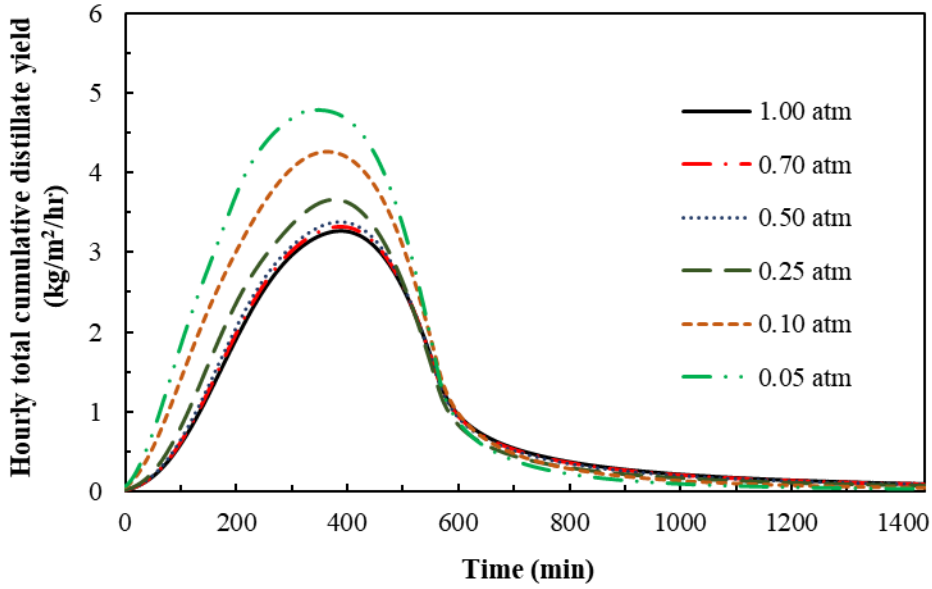

Figure 6.21 Variation in the hourly total cumulative distillate yield with internal pressure.

6.6 Summary

In this Chapter, the results of the comprehensive investigation of the performance of the dynamic multi-effect solar water stills were presented. The results of reducing the internal pressure level on the variations in temperature of the stages, their daily productivity and the total cumulative daily distillate yield were discussed. It can be concluded from this investigation that reducing the internal pressure positively affects the performance of the proposed system. It was found that the operating the multi-effect solar water still with the fluid piston converter could lead to the increase in the total cumulative distillate yield by about 1.0%. Whereas operating the proposed water still at an internal pressure level of 0.05 atm increases its total daily productivity by about 52%. Thus, one feasible approach to the enhancement of the performance of multi-effect solar water stills is to intensify the evaporation rate by reducing the internal pressure level.

Chapter 7 Conclusions and Recommendations for Future Work

The major conclusions and findings from this study are presented in this chapter. Recommendations for further improvements that should be introduced in theoretical and experimental investigations of the dynamic multi-effect solar water still are highlighted.

7.1 Conclusions

The performance of the multi-effect solar water still was investigated and the following conclusions can be drawn:

1. The literature review demonstrates that water desalination systems driven by solar energy are promising technologies to meet the continuous increase in drinking water demand and to mitigate the negative environmental impacts of using fossil fuels to operate conventional desalination systems. However, small-scale solar desalination systems still need further development and improvement.
2. A mathematical model of the dynamic solar multi-effect water still was developed based on differential equations of energy balance and mass conservation, written for each component of the system. Numerical simulations of the performance of the proposed system under various operational conditions were conducted in a MATLAB/Simulink environment.
3. A novel modification of the fluid piston energy converter was experimentally tested to demonstrate its capacity to produce vacuum conditions inside the multi-effect water still using solar energy. The experimental results obtained

demonstrated that the fluid piston converter was able to reduce the pressure inside the system below atmospheric pressure to the level of about 89500 Pa (0.895 atm). This reduction resulted in the improvement in the system productivity of about 1.0% compared to that at the atmospheric pressure.

4. Experimental investigations were carried out for various levels of internal pressure namely, atmospheric pressure, 0.9, 0.8, and 0.7 atm. It was observed that effect of internal pressure is profound starting at the pressure level of 0.7 atm.
5. Comparisons of the theoretical and experimental results showed that the developed mathematical model can accurately predict the performance of the solar multi-effect water still.
6. A water quality analysis of the distillate produced was conducted to measure levels of total dissolved solids (TDS), electrical conductivity and pH. The results demonstrated that it has high quality and is very pure.

7.2 Recommendations for Future Work

The simulation model of the dynamic solar multi-effect water still developed in this research can be effectively used to predict the performance of the system for various operational conditions. However, this theoretical model can be further improved to provide even more accurate predictions of the physical processes taking place in all stages of the dynamic solar water still. Moreover, the experimental prototype of the multi-effect water still can be further modified to provide better performance and higher productivity.

Recommendations for improvements to be carried out in future work can be summarized as follows:

1. The Mathematical model of the multi-effect water stills can be further improved to predict more accurately the performance of the proposed system by taking in consideration the effect of presence of non-condensable gases inside the system, calculating the temperature of condensing surfaces in each stage (Tc's), and the increase in the concentration of salts during the distillation process. Moreover, this dynamic model of the multi-effect water stills should be linked to an optimization code to determine the optimal design parameters of the system.

2. Further experimental investigation on the performance of the multi-effect solar water stills, when operated simultaneously with the fluid piston energy converter should be conducted.

3. Experimental work can be extended by modifying the laboratory prototype of the multi-effect water stills so that it can produce further reductions in the internal pressure.

4. Further study should be conducted for better understanding of the design and operational principles of the fluid piston energy converter using larger physical dimensions of the energy converter and deploying various working fluids instead of water, such as helium or hydrogen, in order to enhance its performance.

References

[1] H. M. Qiblawey and F. Banat, "Solar thermal desalination technologies," *Desalination,* vol. 220, pp. 633-644, 2008.

[2] UN-WATER. (2017, 11/05/2017). *UN-WATER KEY WATER INDICATOR PORTAL , KWIP*. Available: http://www.unwater.org/kwip/en/

[3] G. N. Tiwari, H. N. Singh, and R. Tripathi, "Present status of solar distillation," *Solar Energy,* vol. 75, pp. 367-373, 2003.

[4] A. D. Khawaji, I. K. Kutubkhanah, and J. M. Wie, "Advances in seawater desalination technologies," *Desalination,* vol. 221, pp. 47-69, 2008.

[5] L. García-Rodríguez, "Seawater desalination driven by renewable energies: A review," *Desalination,* vol. 143, pp. 103-113, 2002.

[6] F. Muhammad-Sukki *et al.*, "Solar photovoltaic in Malaysia: The way forward," *Renewable and Sustainable Energy Reviews,* vol. 16, pp. 5232-5244, 2012.

[7] *Renewables 2016 Global Status Report "Renewable Energy Policy Network for the 21st Century (REN21) ", Paris.* Available: http://www.ren21.net/wp-content/uploads/2016/06/GSR_2016_Full_Report.pdf

[8] J. L. Seitz and K. A. Hite, *Global Issues: An Introduction.*, fourth ed. Malden, USA: Blackwell, 2012.

[9] H. Z. Hassan, A. A. Mohamad, and R. Bennacer, "Simulation of an adsorption solar cooling system," *Energy,* vol. 36, pp. 530-537, 2011.

[10] F. Trieb and H. Müller-Steinhagen, "Concentrating solar power for seawater desalination in the Middle East and North Africa," *Desalination,* vol. 220, pp. 165-183, 2008.

[11] H. Sharon and K. S. Reddy, "A review of solar energy driven desalination technologies," *Renewable and Sustainable Energy Reviews,* vol. 41, pp. 1080-1118, 2015.

[12] S. Kalogirou, "Survey of solar desalination systems and system selection," *Energy,* vol. 22, pp. 69-81, 1997.

[13] B. Belgasim and K. Mahkamov, "Theoretical Modelling of a Dynamic Solar Thermal Desalination Unit with a Fluid Piston Engine," presented at the World Renewable Energy Congress Linkoping, Sweden, 8-13/ May, 2011.

[14] K. Sampathkumar, T. V. Arjunan, P. Pitchandi, and P. Senthilkumar, "Active solar distillation-A detailed review," *Renewable and Sustainable Energy Reviews,* vol. 14, pp. 1503-1526, 2010.

[15] H. B. Bacha and K. Zhani, "Contributing to the improvement of the production of solar still," *Desalination and Water Treatment,* vol. 51, pp. 1310-1318, 2013.

[16] A. K. Tiwari and G. N. Tiwari, "Thermal modeling based on solar fraction and experimental study of the annual and seasonal performance of a single slope

passive solar still: The effect of water depths," *Desalination,* vol. 207, pp. 184-204, 2007.

[17] G. N. Tiwari, A. Kupfermann, and S. Aggarwal, "A new design for a double-condensing chamber solar still," *Desalination,* vol. 114, pp. 153-164, 1997.

[18] A. A. El-Sebaii, "Thermal performance of a triple-basin solar still," *Desalination,* vol. 174, pp. 23-37, 2005.

[19] A. A. Al-Karaghouli and W. E. Alnaser, "Experimental comparative study of the performances of single and double basin solar-stills," *Applied Energy,* vol. 77, pp. 317-325, 2004.

[20] A. A. Al-Karaghouli and W. E. Alnaser, "Performances of single and double basin solar-stills," *Applied Energy,* vol. 78, pp. 347-354, 2004.

[21] Y. A. F. El-Samadony, W. M. El-Maghlany, and A. E. Kabeel, "Influence of glass cover inclination angle on radiation heat transfer rate within stepped solar still," *Desalination,* vol. 384, pp. 68-77, 2016.

[22] V. R. Khare, A. P. Singh, H. Kumar, and R. Khatri, "Modelling and Performance Enhancement of Single Slope Solar Still Using CFD," *Energy Procedia,* vol. 109, pp. 447-455, 2017.

[23] H. N. Panchal and N. Patel, "ANSYS CFD and experimental comparison of various parameters of a solar still," *International Journal of Ambient Energy,* pp. 1-7, 2017.

[24] M. Feilizadeh, M. Soltanieh, M. R. Karimi Estahbanati, K. Jafarpur, and S.-S. Ashrafmansouri, "Optimization of geometrical dimensions of single-slope basin-type solar stills," *Desalination,* vol. 424, pp. 159-168, 2017.

[25] I. Altarawneh, S. Rawadieh, M. Batiha, L. Al-Makhadmeh, S. Alrowwad, and M. Tarawneh, "Experimental and numerical performance analysis and optimization of single slope, double slope and pyramidal shaped solar stills," *Desalination,* vol. 423, pp. 124-134, 2017.

[26] A. Khechekhouch, a. Boukhari, Z. Driss, and N. Benhissen, "Seasonal effect on solar distillation in the El-Oued region of south-east Algeria," *International Journal of Energetica,* vol. 2, pp. 2543-3717, 2017.

[27] A. H. Bassam and H. Mousa, "Water film cooling over the glass cover of a solar still including evaporation effects," *Energy,* vol. 22, pp. 43-48, 1997.

[28] O. M. Haddad, M. A. Al-Nimr, and A. Maqableh, "Enhanced solar still performance using a radiative cooling system," *Renewable Energy,* vol. 21, pp. 459-469, 2000.

[29] I. Al-Hayeka and O. O. Badran, "The effect of using different designs of solar stills on water distillation," *Desalination,* vol. 169, pp. 121-127, 2004.

[30] H. E. S. Fath and H. M. Hosny, "Thermal performance of a single-sloped basin still with an inherent built-in additional condenser," *Desalination,* vol. 142, pp. 19-27, 2002.

[31] K. Hidouri, R. Ben Slama, and S. Gabsi, "Hybrid solar still by heat pump compression," *Desalination,* vol. 250, pp. 444-449, 2010.

[32] O. Mahian and A. Kianifar, "Mathematical modelling and experimental study of a solar distillation system," *Proceedings of the Institution of Mechanical Engineers, Part C: Journal of Mechanical Engineering Science,* vol. 225, pp. 1203-1212, 2011.

[33] Y. Taamneh and M. M. Taamneh, "Performance of pyramid-shaped solar still: Experimental study," *Desalination,* vol. 291, pp. 65-68, 2012.

[34] H. Hassan and S. Abo-Elfadl, "Effect of the condenser type and the medium of the saline water on the performance of the solar still in hot climate conditions," *Desalination,* vol. 417, pp. 60-68, 2017.

[35] B. Praveen kumar, D. Prince Winston, P. Pounraj, A. Muthu Manokar, R. Sathyamurthy, and A. E. Kabeel, "Experimental investigation on hybrid PV/T active solar still with effective heating and cover cooling method," *Desalination,* 2017.

[36] A. A. El-Sebaii and M. El-Naggar, "Year round performance and cost analysis of a finned single basin solar still," *Applied Thermal Engineering,* vol. 110, pp. 787-794, 2017.

[37] A. A. El-Sebaii, S. Aboul-Enein, and E. El-Bialy, "Single basin solar still with ba‚ffle suspended absorber," *Energy Conversion and Management,* vol. 41, pp. 661-675, 2000.

[38] P. Valsaraj, "An experimental study on solar distillation in a single slope basin still by surface heating the water mass," *Renewable Energy,* vol. 25, pp. 607-612, 2002.

[39] M. Montazeri, A. Banakar, and B. Ghobadian, "Enhancement of cascade solar still productivity with sloping absorber plate," *Maejo International*

Journal of Science and Technology, vol. 11, pp. 35-44, 2017.

[40] R. Samuel Hansen and K. Kalidasa Murugavel, "Enhancement of integrated solar still using different new absorber configurations: An experimental approach," *Desalination,* vol. 422, pp. 59-67, 2017.

[41] H. Tanaka and Y. Nakatake, "Theoretical analysis of a basin type solar still with internal and external reflectors," *Desalination,* vol. 197, pp. 205-216, 2006.

[42] H. Tanaka, "Experimental study of a basin type solar still with internal and external reflectors in winter," *Desalination,* vol. 249, pp. 130-134, 2009.

[43] H. Tanaka, "A theoretical analysis of basin type solar still with flat plate external bottom reflector," *Desalination,* vol. 279, pp. 243-251, 2011.

[44] A. J. N. Khalifa and H. A. Ibrahim, "Effect of inclination of the external reflector on the performance of a basin type solar still at various seasons," *Energy for Sustainable Development,* vol. 13, pp. 244-249, 2009.

[45] S. J. P. Gnanaraj and S. Ramachandran, "Optimization on performance of single-slope solar still linked solar pond via Taguchi method," *Desalination and Water Treatment,* vol. 80, pp. 27-40, 2017.

[46] Z. M. Omara, A. E. Kabeel, A. S. Abdullah, and F. A. Essa, "Experimental investigation of corrugated absorber solar still with wick and reflectors," *Desalination,* vol. 381, pp. 111-116, 2016.

[47] M. Sakthivel and S. Shanmugasundaram, "Effect of energy storage medium (black granite gravel) on the performance of a solar still," *International Journal of Energy Research,* vol. 32, pp. 68-82, 2008.

[48] D. G. Harris Samuel, P. K. Nagarajan, R. Sathyamurthy, S. A. El-Agouz, and E. Kannan, "Improving the yield of fresh water in conventional solar still using low cost energy storage material," *Energy Conversion and Management,* vol. 112, pp. 125-134, 2016.

[49] A. E. Kabeel and M. Abdelgaied, "Improving the performance of solar still by using PCM as a thermal storage medium under Egyptian conditions," *Desalination,* vol. 383, pp. 22-28, 2016.

[50] H. Panchal, D. K. Patel, and P. Patel, "Theoretical and experimental performance analysis of sandstones and marble pieces as thermal energy storage materials inside solar stills," *International Journal of Ambient Energy,* pp. 1-9, 2017.

[51] A.E. Kabeel, S.A. El-Agouz, T. Arunkumar, and R. Sathyamurthy, "Enhancing the performance of single slope solar still using jute cloth knited with sand heat energy storage," presented at the Twentieth International Water Technology Conference, Hurghada, Egypt, 18-20 May, 2017.

[52] A. E. Kabeel, Z. M. Omara, and F. A. Essa, "Enhancement of modified solar still integrated with external condenser using nanofluids: An experimental approach," *Energy Conversion and Management,* vol. 78, pp. 493-498, 2014.

[53] T. Elango, A. Kannan, and K. Kalidasa Murugavel, "Performance study on single basin single slope solar still with different water nanofluids," *Desalination,* vol. 360, pp. 45-51, 2015.

[54] L. Sahota and G. N. Tiwari, "Effect of nanofluids on the performance of passive double slope solar still: A comparative study using characteristic curve," *Desalination,* vol. 388, pp. 9-21, 2016.

[55] S. W. Sharshir *et al.*, "Enhancing the solar still performance using nanofluids and glass cover cooling: Experimental study," *Applied Thermal Engineering,* vol. 113, pp. 684-693, 2017.

[56] S. A. Kalogirou, "Seawater desalination using renewable energy sources," *Progress in Energy and Combustion Science,* vol. 31, pp. 242-281, 2005.

[57] A. F. Muftah, M. A. Alghoul, A. Fudholi, M. M. Abdul-Majeed, and K. Sopian, "Factors affecting basin type solar still productivity: A detailed review," *Renewable and Sustainable Energy Reviews,* vol. 32, pp. 430-447, 2014.

[58] A. K. Kaviti, A. Yadav, and A. Shukla, "Inclined solar still designs: A review," *Renewable and Sustainable Energy Reviews,* vol. 54, pp. 429-451, 2016.

[59] H. Ş. Aybar, "Mathematical modeling of an inclined solar water distillation system," *Desalination,* vol. 190, pp. 63-70, 2006.

[60] K. K. Matrawy, A. S. Alosaimy, and A. F. Mahrous, "Modeling and experimental study of a corrugated wick type solar still: Comparative study with a simple basin type," *Energy Conversion and Management,* vol. 105, pp. 1261-1268, 2015.

[61] W. M. Alaian, E. A. Elnegiry, and A. M. Hamed, "Experimental investigation on the performance of solar still augmented with pin-finned wick," *Desalination,* vol. 379, pp. 10-15, 2016.

[62] K. Kalidasa Murugavel and K. Srithar, "Performance study on basin type double slope solar still with different wick materials and minimum mass of water," *Renewable Energy,* vol. 36, pp. 612-620, 2011.

[63] S. Kaliappan, M. D. Rajkamal, V. G. Ganesan, and P. Manikandan, "Experimental investigation on single basin and double basin solar desalination," *Int. J. Chem. Sci.,* vol. 14, pp. 1-12, 2016.

[64] Z. M. Omara, A. E. Kabeel, and F. A. Essa, "Effect of using nanofluids and providing vacuum on the yield of corrugated wick solar still," *Energy Conversion and Management,* vol. 103, pp. 965-972, 2015.

[65] H. Tanaka and Y. Nakatake, "Improvement of the tilted wick solar still by using a flat plate reflector," *Desalination,* vol. 216, pp. 139-146, 2007.

[66] H. Tanaka and Y. Nakatake, "One step azimuth tracking tilted-wick solar still with a vertical flat plate reflector," *Desalination,* vol. 235, pp. 1-8, 2009.

[67] H. Tanaka and Y. Nakatake, "Increase in distillate productivity by inclining the flat plate external reflector of a tilted-wick solar still in winter," *Solar Energy,* vol. 83, pp. 785-789, 2009.

[68] H. Tanaka, "Tilted wick solar still with external flat plate reflector: Optimum inclination of still and reflector," *Desalination,* vol. 249, pp. 411-415, 2009.

[69] H. Tanaka, "Tilted wick solar still with flat plate bottom reflector," *Desalination,* vol. 273, pp. 405-413, 2011.

[70] J. T. Mahdi, B. E. Smith, and A. O. Sharif, "An experimental wick-type solar still system: Design and construction," *Desalination,* vol. 267, pp. 233-238, 2011.

[71] T. K. Munisamy, A. Mohan, and M. Veeramanikandan, "Experimental investigation of tilted wick solar still using fabrics," *Australian Journal of Mechanical Engineering,* pp. 1-6, 2017.

[72] H. Sharon, K. S. Reddy, D. Krithika, and L. Philip, "Experimental performance investigation of tilted solar still with basin and wick for distillate quality and enviro-economic aspects," *Desalination,* vol. 410, pp. 30-54, 2017.

[73] M. S. Sodha, A. Kumar, G. N. Tiwari, and R. C. Tyagi, "Simple multiple wick solar still- Analysis and performance," *Solar Energy,* vol. 26, pp. 127-131, 1981.

[74] G. N. Tiwari, "Demonstration Plant of a Multi Wick Solar Still," *Energy Conversion and Management,* vol. 24, pp. 313-316, 1984.

[75] N. K. Dhiman and G. N. Tiwari, "Effect of water flowing over the glass cover of a multi-wick solar still," *Energy Conversion and Management,* vol. 30, pp. 245-250, 1990.

[76] A Kumar and J. D. Anand, "Modelling and performance of a tubular multiwick solar still," *Energy,* vol. 17, pp. 1067-1071, 1992.

[77] K. Ohshiro, T. Nosoko, and T. Nagata, "A compact solar still utilizing hydrophobic poly(tetrafluoroethylene) nets for separating neighboring wicks," *Desalination,* vol. 105, pp. 207-217, 1996.

[78] P. Pal, P. Yadav, R. Dev, and D. Singh, "Performance analysis of modified basin type double slope multi–wick solar still," *Desalination,* vol. 422, pp. 68-82, 2017.

[79] S. Abdallah, O. Badran, and M. M. Abu-Khader, "Performance evaluation of a modified design of a single slope solar still," *Desalination,* vol. 219, pp. 222-230, 2008.

[80] V. Velmurugan, M. Gopalakrishnan, R. Raghu, and K. Srithar, "Single basin solar still with fin for enhancing productivity," *Energy Conversion and Management,* vol. 49, pp. 2602-2608, 2008.

[81] A. E. Kabeel, "Performance of solar still with a concave wick evaporation surface," *Energy,* vol. 34, pp. 1504-1509, 2009.

[82] G. M. Ayoub, M. Al-Hindi, and L. Malaeb, "A solar still desalination system with enhanced productivity," *Desalination and Water Treatment,* vol. 53, pp. 3179-3186, 2014.

[83] H. Tanaka, T. Nosoko, and T. Nagata, "Experimental study of basin-type multiple-effect diffusion-coupled solar still," *Desalination,* vol. 150, pp. 131-144, 2002.

[84] H. Tanaka, T. Nosoko, and T. Nagata, "A highly productive basin-type-multiple-effect coupled solar still," *Desalination,* vol. 130, pp. 279-293, 2000.

[85] H. Tanaka, T. Nosoko, and T. Nagata, "Parametric investigation of a basin-type-multiple-effect coupled solar still," *Desalination,* vol. 130, pp. 295-304, 2000.

[86] H. Tanaka, Y. Nakatake, and M. Tanaka, "Indoor experiments of the vertical multiple-effect diffusion-type solar still coupled with a heat-pipe solar collector," *Desalination,* vol. 177, pp. 291-302, 2005.

[87] H. Tanaka and Y. Nakatake, "A simple and highly productive solar still: a vertical multiple-effect diffusion-type solar still coupled with a flat-plate mirror," *Desalination,* vol. 173, pp. 287-300, 2005.

[88] H. Tanaka and Y. Nakatake, "Factors influencing the productivity of a multiple-effect diffusion-type solar still coupled with a flat plate reflector," *Desalination,* vol. 186, pp. 299-310, 2005.

[89] H. Tanaka and Y. Nakatake, "Numerical analysis of the vertical multiple-effect diffusion solar still coupled with a flat plate reflector: optimum reflector angle and optimum orientation of the still at various seasons and locations," *Desalination,* vol. 207, pp. 167-178, 2007.

[90] H. Tanaka and Y. Nakatake, "Outdoor experiments of a vertical diffusion solar still coupled with a flat plate reflector," *Desalination,* vol. 214, pp. 70-82, 2007.

[91] H. Tanaka, "Experimental study of vertical multiple-effect diffusion solar still coupled with a flat plate reflector," *Desalination,* vol. 249, pp. 34-40, 2009.

[92] H. Tanaka, "Theoretical Analysis of the Effect of a Bottom Reflector on a Vertical Multiple-Effect Diffusion Solar Still Coupled with a Basin-Type Still," *Advances in Mechanical Engineering,* vol. 5, pp. 1-11, 2015.

[93] H. Tanaka and K. Iishi, "Experimental study of a vertical single-effect diffusion solar still coupled with a tilted wick still," *Desalination,* vol. 402, pp. 19-24, 2017.

[94] A. K. Kaushal, M. K. Mittal, and D. Gangacharyulu, "Productivity correlation and economic analysis of floating wick basin type vertical multiple effect diffusion solar still with waste heat recovery," *Desalination,* vol. 423, pp. 95-103, 2017.

[95] N. S. L. Srivastava, M. Din, and G. N. Tiwari, "Performance evaluation of distillation-cum-greenhouse for a warm and humid climate," *Desalination,* vol. 128, pp. 67-80, 2000.

[96] M. T. Chaibi, "Analysis by simulation of a solar still integrated in a greenhouse roof," *Desalination,* vol. 128, pp. 123-138, 2000.

[97] M. K. Ghosal, G. N. Tiwari, and N. S. L. Srivastava, "Thermal modeling of a controlled environment greenhouse cum solar distillation for composite and warm humid climates of India," *Desalination,* vol. 151, pp. 293-308, 2002.

[98] A. M. Radhwan, "Transient analysis of a stepped solar still for heating and humidifying greenhouses," *Desalination,* vol. 161, pp. 89-97, 2004.

[99] A. M. Radhwan and H. E. S. Fath, "Thermal performance of greenhouse with a built-in solar distillation system: experimental study," *Desalination,* vol. 181, pp. 193-205, 2005.

[100] E. G. Marı, R. P. G. Colomer, and C. A. Blaise-Ombrecht, "Performance analysis of a solar still integrated in a greenhouse," *Desalination,* vol. 203, pp. 435-443, 2007.

[101] A. H. Salah, G. E. Hassan, M. Elhelw, H. Fath, and S. M. Elsherbiny, "Performance improvement of roof transparent solar still coupled with agriculture greenhouse," *Journal of Renewable Energy and Sustainable Development,* vol. 3, pp. 96-111, 2017.

[102] K. Murase, H. Tobata, M. Ishikawa, and S. Toyama, "Experimental and numerical analysis of a tube-type networked solar still for desert technology," *Desalination,* vol. 190, pp. 137-146, 2006.

[103] K. Murase, Y. Yamagishi, Y. Iwashita, and K. Sugino, "Development of a tube-type solar still equipped with heat accumulation for irrigation," *Energy,* vol. 33, pp. 1711-1718, 2008.

[104] A. Ahsan and T. Fukuhara, "Mass and heat transfer model of Tubular Solar Still," *Solar Energy,* vol. 84, pp. 1147-1156, 2010.

[105] A. Ahsan, K. M. S. Islam, T. Fukuhara, and A. H. Ghazali, "Experimental study on evaporation, condensation and production of a new Tubular Solar Still," *Desalination,* vol. 260, pp. 172-179, 2010.

[106] A. Ahsan, M. Imteaz, A. Rahman, B. Yusuf, and T. Fukuhara, "Design, fabrication and performance analysis of an improved solar still," *Desalination,* vol. 292, pp. 105-112, 2012.

[107] Z. Chen *et al.*, "Analysis of the characteristics of heat and mass transfer of a three-effect tubular solar still and experimental research," *Desalination,* vol. 330, pp. 42-48, 2013.

[108] N. Rahbar, J. A. Esfahani, and E. Fotouhi-Bafghi, "Estimation of convective heat transfer coefficient and water-productivity in a tubular solar still – CFD simulation and theoretical analysis," *Solar Energy,* vol. 113, pp. 313-323, 2015.

[109] T. Arunkumar *et al.*, "Effect of heat removal on tubular solar desalting system," *Desalination,* vol. 379, pp. 24-33, 2016.

[110] G. M. Cappelletti, "An experiment with a plastic solar still," *Desalination,* vol. 142, pp. 221-227, 2002.

[111] M. K. Phadatare and S. K. Verma, "Influence of water depth on internal heat and mass transfer in a plastic solar still," *Desalination,* vol. 217, pp. 267-275, 2007.

[112] M. K. Phadatare and S. K. Verma, "Effect of cover materials on heat and mass transfer coefficients in a plastic solar still," *Desalination and Water Treatment,* vol. 2, pp. 254-259, 2012.

[113] R. Bhardwaj, M. V. ten Kortenaar, and R. F. Mudde, "Inflatable plastic solar still with passive condenser for single family use," *Desalination,* vol. 398, pp. 151-156, 2016.

[114] B. I. Ismail, "Design and performance of a transportable hemispherical solar still," *Renewable Energy,* vol. 34, pp. 145-150, 2009.

[115] T. Arunkumar *et al.*, "An experimental study on a hemispherical solar still," *Desalination,* vol. 286, pp. 342-348, 2012.

[116] Sangeeta Suneja and G. N. Tiwari, "Optimization of number of effects for higher yield from an inverted absorber solar still using the Runge-Kutta method," *Desalination,* vol. 120, pp. 197-209, 1998.

[117] G. N. Tiwari and S. Suneja, "Performance evaluation of an inverted absorber solar still," *Energy Conversion and Management,* vol. 39, pp. 173-180, 1998.

[118] Sangeeta Suneja, G. N. Tiwari, and S. N. Rai, "Parametric study of an inverted absorber double-effect solar distillation system," *Desalination,* vol. 109, pp. 177-186, 1997.

[119] Sangeeta Suneja and G. N. Tiwari, "Effect of water depth on the performance of an inverted absorber double basin solar still," *Energy Conversion and Management,* vol. 40, pp. 1885-1897, 1999.

[120] Sangeeta Suneja and G. N. Tiwari, "Parametric study of an inverted absorber triple effect solar still," *Energy Conversion and Management,* vol. 40, pp. 1871-1884, 1999.

[121] S. A. Abdul-Wahab and Y. Y. Al-Hatmi, "Study of the Performance of the Inverted Solar Still Integrated with a Refrigeration Cycle," *Procedia Engineering,* vol. 33, pp. 424-434, 2012.

[122] A. A. El-Sebaii, "Parametric study of a vertical solar still," *Energy Conversion and Management,* vol. 39, pp. 1303-1315, 1998.

[123] M. Boukar and A. Harmim, "Development and testing of a vertical solar still," *Desalination,* vol. 158, p. 179, 2003.

[124] M. Boukar and A. Harmim, "Parametric study of a vertical solar still under desert climatic conditions," *Desalination,* vol. 168, pp. 21-28, 2004.

[125] M. Boukar and A. Harmim, "Performance evaluation of a one-sided vertical solar still tested in the Desert of Algeria," *Desalination,* vol. 183, pp. 113-126, 2005.

[126] M. Boukar and A. Harmim, "Design parameters and preliminary experimental investigation of an indirect vertical solar still," *Desalination,* vol. 203, pp. 444-454, 2007.

[127] A. K. Kaushal, M. K. Mittal, and D. Gangacharyulu, "Development and experimental study of an improved basin type vertical single distillation cell solar still," *Desalination,* vol. 398, pp. 121-132, 2016.

[128] Y. P. Yadav, "Analytical performance of a solar still integrated with a flat plate solar collector: Thermosiphone mode," *Energy Conversion and Management* vol. 31, pp. 255-263, 1991.

[129] C. Tiris, M. Tiris, Y. Erdalli, and M. Sohmen, "Experimental studies on a solar still coupled with a flat-plate collector and a single basin still," *Energy Conversion and Management,* vol. 39, pp. 853-856, 1998.

[130] G.N. Tiwari, Vimal Dimri, and A. Chel, "Parametric study of an active and passive solar distillation system: Energy and exergy analysis," *Desalination,* vol. 242, pp. 1-18, 2009.

[131] S. Kumar, G. N. Tiwari, and H. N. Singh, "Annual performance of an active solar distillation system," *Desalination,* vol. 127, pp. 79-88, 2000.

[132] k. Schwarzer, M. E. Vieira, C. Faber, and C. Muller, "Solar thermal desalination system with heat recovery," *Desalination,* vol. 137, pp. 23-29, 2001.

[133] K. Voropoulos, E. Mathioulakis, and V. Belessiotis, "Experimental investigation of a solar still coupled with solar collectors," *Desalination,* vol. 138, pp. 103-110, 2001.

[134] H. N. Singh and G. N. Tiwari, "Monthly performance of passive and active solar stills for different Indian climatic conditions," *Desalination,* vol. 168, pp. 145-150, 2004.

[135] O. O. Badran and H. A. Al-Tahaineh, "The effect of coupling a flat-plate collector on the solar still productivity," *Desalination,* vol. 183, pp. 137-142, 2005.

[136] A. A. Badran, I. A. Al-Hallaq, I. A. Eyal Salman, and M. Z. Odat, "A solar still augmented with a flat-plate collector," *Desalination,* vol. 172, pp. 227-234, 2005.

[137] V. K. Dwivedi and G. N. Tiwari, "Experimental validation of thermal model of a double slope active solar still under natural circulation mode," *Desalination,* vol. 250, pp. 49-55, 2010.

[138] R. Tripathi and G. N. Tiwari, "Effect of water depth on internal heat and mass transfer for active solar distillation," *Desalination,* vol. 173, pp. 187-200, 2005.

[139] V. Dimri, B. Sarkar, U. Singh, and G. N. Tiwari, "Effect of condensing cover material on yield of an active solar still: an experimental validation," *Desalination,* vol. 227, pp. 178-189, 2008.

[140] H. Mousa and M. Abu Arabi, "Desalination and hot water production using solar still enhanced by external solar collector," *Desalination and Water Treatment,* vol. 51, pp. 1296-1301, 2013.

[141] H. Taghvaei *et al.*, "A thorough investigation of the effects of water depth on the performance of active solar stills," *Desalination,* vol. 347, pp. 77-85, 2014.

[142] A. A. El-Sebaii, S. J. Yaghmour, F. S. Al-Hazmi, A. S. Faidah, F. M. Al-Marzouki, and A. A. Al-Ghamdi, "Active single basin solar still with a sensible storage medium," *Desalination,* vol. 249, pp. 699-706, 2009.

[143] T. Rajaseenivasan, P. Nelson Raja, and K. Srithar, "An experimental investigation on a solar still with an integrated flat plate collector," *Desalination,* vol. 347, pp. 131-137, 2014.

[144] S. Kumar and G. N. Tiwari, "Life cycle cost analysis of single slope hybrid (PV/T) active solar still," *Applied Energy,* vol. 86, pp. 1995-2004, 2009.

[145] S. Kumar and G. N. Tiwari, "Estimation of internal heat transfer coefficients of a hybrid (PV/T) active solar still," *Solar Energy,* vol. 83, pp. 1656-1667, 2009.

[146] S. Kumar, G. N. Tiwari, and M. K. Gaur, "Development of empirical relation to evaluate the heat transfer coefficients and fractional energy in basin type hybrid (PV/T) active solar still," *Desalination,* vol. 250, pp. 214-221, 2010.

[147] S. Kumar and A. Tiwari, "Design, fabrication and performance of a hybrid photovoltaic/thermal (PV/T) active solar still," *Energy Conversion and Management,* vol. 51, pp. 1219-1229, 2010.

[148] G. Singh, S. Kumar, and G. N. Tiwari, "Design, fabrication and performance evaluation of a hybrid photovoltaic thermal (PVT) double slope active solar still," *Desalination,* vol. 277, pp. 399-406, 2011.

[149] M. K. Gaur and G. N. Tiwari, "Optimization of number of collectors for integrated PV/T hybrid active solar still," *Applied Energy,* vol. 87, pp. 1763-1772, 2010.

[150] M. M. Morad, H. A. M. El-Maghawry, and K. I. Wasfy, "Improving the double slope solar still performance by using flat-plate solar collector and cooling glass cover," *Desalination,* vol. 373, pp. 1-9, 2015.

[151] M. Al-harahsheh, M. Abu-Arabi, H. Mousa, and Z. Alzghoul, "Solar desalination using solar still enhanced by external solar collector and PCM," *Applied Thermal Engineering,* vol. 128, pp. 1030-1040, 2018.

[152] S. A. Kalogirou, "Solar thermal collectors and applications," *Progress in Energy and Combustion Science,* vol. 30, pp. 231-295, 2004.

[153] H. Tanaka and Y. Nakatake, "A vertical multiple-effect diffusion-type solar still coupled with a heat-pipe solar collector," *Desalination,* vol. 160, pp. 195-205, 2004.

[154] H. Tanak, Y. Nakatake, and K. Watanabe, "Parametric study on a vertical multiple-effect diffusion-typesolar still coupled with a heat-pipe solar collector," *Desalination,* vol. 171, pp. 243-255, 2004.

[155] K. Mahkamov and J. S. Akhatov, "Experimental study of the performance of multieffect solar thermal water desalination system," *Applied Solar Energy,* vol. 44, pp. 31-34, 2008.

[156] M. I. M. Shatat and K. Mahkamov, "Determination of rational design parameters of a multi-stage solar water desalination still using transient mathematical modelling," *Renewable Energy,* vol. 35, pp. 52-61, 2010.

[157] K. Sampathkumar and P. Senthilkumar, "Utilization of solar water heater in a single basin solar still—An experimental study," *Desalination,* vol. 297, pp. 8-19, 2012.

[158] A. E. Kabeel, A. Khalil, Z. M. Omara, and M. M. Younes, "Theoretical and experimental parametric study of modified stepped solar still," *Desalination,* vol. 289, pp. 12-20, 2012.

[159] H. Panchal and P. K. Shah, "Performance analysis of double basin solar still with evacuated tubes," (in English), *Applied Solar Energy,* vol. 49, pp. 174-179, 2013.

[160] R. V. Singh, S. Kumar, M. M. Hasan, M. E. Khan, and G. N. Tiwari, "Performance of a solar still integrated with evacuated tube collector in natural mode," *Desalination,* vol. 318, pp. 25-33, 2013.

[161] S. Kumar, A. Dubey, and G. N. Tiwari, "A solar still augmented with an evacuated tube collector in forced mode," *Desalination,* vol. 347, pp. 15-24, 2014.

[162] Sanjay Kumar and S. Sinha, "Transient model and comparative study of concentrator coupled regenerative solar still in forced circulation mode," *Energy Conversion and Management,* vol. 37, pp. 629-636, 1996.

[163] Bhagwan Prasad and G. N. Tiwari, "Effect of glass cover inclination and parametric studies of concentrator-assisted solar distillation system," *Int. J. of Energy Research,* vol. 20, pp. 495-505, 1996.

[164] S. K. Singh, V. P. Bhatnagar, and G. N. Tiwari, "Design parameters for concentrator assisted solar distillation system," *Energy Conversion and Management,* vol. 37, pp. 247-252, 1996.

[165] Z. S. Abdel-Rehim and A. Lasheen, "Experimental and theoretical study of a solar desalination system located in Cairo, Egypt," *Desalination,* vol. 217, pp. 52-64, 2007.

[166] T. Arunkumar, D. Denkenberger, A. Ahsan, and R. Jayaprakash, "The augmentation of distillate yield by using concentrator coupled solar still with phase change material," *Desalination,* vol. 314, pp. 189-192, 2013.

[167] T. Arunkumar, D. Denkenberger, R. Velraj, R. Sathyamurthy, H. Tanaka, and K. Vinothkumar, "Experimental study on a parabolic concentrator assisted solar desalting system," *Energy Conversion and Management,* vol. 105, pp. 665-674, 2015.

[168] T. Arunkumar, R. Jayaprakash, A. Ahsan, D. Denkenberger, and M. S. Okundamiya, "Effect of water and air flow on concentric tubular solar water desalting system," *Applied Energy,* vol. 103, pp. 109-115, 2013.

[169] T. Arunkumar, R. Velraj, D. C. Denkenberger, R. Sathyamurthy, K. V. Kumar, and A. Ahsan, "Productivity enhancements of compound parabolic concentrator tubular solar stills," *Renewable Energy,* vol. 88, pp. 391-400, 2016.

[170] A. E. Kabeel and M. Abdelgaied, "Observational study of modified solar still coupled with oil serpentine loop from cylindrical parabolic concentrator and phase changing material under basin," *Solar Energy,* vol. 144, pp. 71-78, 2017.

[171] K. Voropoulos, E. Mathioulakis, and V. Belessiotis, "Experimental investigation of the behavior of a solar still coupled with hot water storage tank," *Desalination,* vol. 156, pp. 315-322, 2003.

[172] H. Tanaka and C. D. Park, "Distillation utilizing waste heat from a portable electric generator," *Desalination,* vol. 258, pp. 136-142, 2010.

[173] H. Tanaka and C. D. Park, "Experimental study of distiller with heat pipe utilizing waste heat from a portable electric generator," *Desalination,* vol. 302, pp. 43-49, 2012.

[174] K. S. Maheswari, K. Kalidasa Murugavel, and G. Esakkimuthu, "Thermal desalination using diesel engine exhaust waste heat — An experimental analysis," *Desalination,* vol. 358, pp. 94-100, 2015.

[175] C. D. Park, B. J. Lim, K. Y. Chung, S. S. Lee, and Y. M. Kim, "Experimental evaluation of hybrid solar still using waste heat," *Desalination,* vol. 379, pp. 1-9, 2016.

[176] S. Al-Kharabsheh and D. Y. Goswami, "Experimental study of an innovative solar water desalination system utilizing a passive vacuum technique," *Solar Energy,* vol. 75, pp. 395-401, 2003.

[177] H. Al-Hussaini and I. K. Smith, "Enhancing of solar still productivity using vacuum technology," *Energy Conversion and Management,* vol. 36, pp. 1047-1051, 1995.

[178] M. Abu-Jabal, I. Kamiya, and Y. Narasaki, "Proving test for a solar-powered desalination system in Gaza-Palestine," *Desalination,* vol. 137, pp. 1-6, 2001.

[179] M. K. Gnanadason, P. S. Kumar, G. Sivaraman, and J. E. S. Daniel, "Design and Performance Analysis of a Modified Vacuum Single Basin Solar Still," *Smart Grid and Renewable Energy,* vol. 02, pp. 388-395, 2011.

[180] Y. A. Abakr and A. F. Ismail, "Theoretical and Experimental Investigation of a Novel Multistage Evacuated Solar Still," *Journal of Solar Energy Engineering,* vol. 127, p. 381, 2005.

[181] M. I. Ahmed, M. Hrairi, and A. F. Ismail, "On the characteristics of multistage evacuated solar distillation," *Renewable Energy,* vol. 34, pp. 1471-1478, 2009.

[182] P. V. Kumar, A. K. Kaviti, Om Prakash, and K. S. Reddy, "Optimization of design and operating parameters on the year round performance of a multi-stage evacuated solar desalination system using transient mathematical analysis," *Int. J. of Energy and Environment,* vol. 3, pp. 409-434, 2012.

[183] K. S. Reddy, K. Ravi Kumar, Tadhg S. O'Donovan, and T. K. Mallick, "Performance analysis of an evacuated multi-stage solar water desalination system," *Desalination,* vol. 288, pp. 80-92, 2012.

[184] A. E. Kabeel, Z. M. Omara, and F. A. Essa, "Improving the performance of solar still by using nanofluids and providing vacuum," *Energy Conversion and Management,* vol. 86, pp. 268-274, 2014.

[185] K. S. Reddy and H. Sharon, "Environmental benefits and Economic Feasibility of Single Effect and Multi Effect Active Vertical Solar Desalination Units," in *9th International Exergy, Energy and Environment Symposium,* Split, Croatia, 2017.

[186] K. Bourouni, M. T. Chaibi, and L. Tadrist, "Water desalination by humidification and dehumidification of air: State of the art," *Desalination,* vol. 137, pp. 167-176, 2001.

[187] G. P. Narayan, M. H. Sharqawy, E. K. Summers, J. H. Lienhard, S. M. Zubair, and M. A. Antar, "The potential of solar-driven humidification–dehumidification desalination for small-scale decentralized water production," *Renewable and Sustainable Energy Reviews,* vol. 14, pp. 1187-1201, 2010.

[188] M. Zamen *et al.,* "Experimental investigation of a two-stage solar humidification–dehumidification desalination process," *Desalination,* vol. 332, pp. 1-6, 2014.

[189] J. Orfi *et al.,* "Experimental and theoretical study of a humidification-dehumidification water desalination system using solar energy," *Desalination,* vol. 168, pp. 151-159, 2004.

[190] J. J. Hermosillo, C. A. Arancibia-Bulnes, and C. A. Estrada, "Water desalination by air humidification: Mathematical model and experimental study," (in English), *Solar Energy,* vol. 86, pp. 1070-1076, 2012.

[191] A. M. A. Dayem, "New solar desalination system using humidificationo-dehumidification process," *Int. J. of Energy and Environment* vol. 4, pp. 629-640, 2013.

[192] F. Farshchi Tabrizi, M. Khosravi, and I. Shirzaei Sani, "Experimental study of a cascade solar still coupled with a humidification–dehumidification system," *Energy Conversion and Management,* vol. 115, pp. 80-88, 2016.

[193] S. W. Sharshir, G. Peng, N. Yang, M. A. Eltawil, M. K. A. Ali, and A. E. Kabeel, "A hybrid desalination system using humidification-dehumidification and solar

stills integrated with evacuated solar water heater," *Energy Conversion and Management,* vol. 124, pp. 287-296, 2016.

[194] Sandeep Parekh, M. M. Farid, J. R. Selman, and S. Al-Hallaj., "Solar desalination with a humidification-dehumidification technique — a comprehensive technical review," *Desalination,* vol. 160, pp. 167-186, 2004.

[195] J. Orfi, N. Galanis, and M. Laplante, "Air humidification–dehumidification for a water desalination system using solar energy," *Desalination,* vol. 203, pp. 471-481, 2007.

[196] A. Al-Karaghouli, D. Renne, and L. L. Kazmerski, "Solar and wind opportunities for water desalination in the Arab regions," *Renewable and Sustainable Energy Reviews,* vol. 13, pp. 2397-2407, 2009.

[197] G. Yuan and H. Zhang, "Mathematical modeling of a closed circulation solar desalination unit with humidification–dehumidification," *Desalination,* vol. 205, pp. 156-162, 2007.

[198] C. Yamalı and İ. Solmuş, "Theoretical investigation of a humidification-dehumidification desalination system configured by a double-pass flat plate solar air heater," *Desalination,* vol. 205, pp. 163-177, 2007.

[199] C. Yamalı and İ. Solmus, "A solar desalination system using humidification–dehumidification process: experimental study and comparison with the theoretical results," *Desalination,* vol. 220, pp. 538-551, 2008.

[200] S. Hou and H. Zhang, "A hybrid solar desalination process of the multi-effect humidification dehumidification and basin-type unit," *Desalination,* vol. 220, pp. 552-557, 2008.

[201] H. Marmouch, J. Orfi, and S. B. Nasrallah, "Effect of a cooling tower on a solar desalination system," *Desalination,* vol. 238, pp. 281-289, 2009.

[202] Mohammad Zamen, Seyyed Mehdi Soufari, and M. Amidpour., "Improvement of solar humidification-dehumidification desalination using multi-stage process," *Chemical Engineering Transaction,* vol. 25, pp. 1091-1096, 2011.

[203] H. Kang, W. Luo, H. Zheng, Z. Yu, and P. Cheng, "Performance of a 3-stage regenerative desalination system based on humidification-dehumidification process," *Applied Thermal Engineering,* vol. 90, pp. 182-192, 2015.

[204] H. Kang, T. Wang, and H. Zheng, "Comparative analysis of regenerative and air-extraction multi-stage humidification–dehumidification desalination system using pinch technology," *Desalination,* vol. 385, pp. 158-166, 2016.

[205] E. Mathioulakis, V. Belessiotis, and E. Delyannis, "Desalination by using alternative energy: Review and state-of-the-art," *Desalination,* vol. 203, pp. 346-365, 2007.

[206] H. Ettouney, "Design and analysis of humidification dehumidification desalination process," *Desalination,* vol. 183, pp. 341-352, 2005.

[207] T. Ming, T. Gong, R. K. de Richter, W. Liu, and A. Koonsrisuk, "Freshwater generation from a solar chimney power plant," *Energy Conversion and Management*, vol. 113, pp. 189-200, 2016.

[208] X. Zhou, B. Xiao, W. Liu, X. Guo, J. Yang, and J. Fan, "Comparison of classical solar chimney power system and combined solar chimney system for power generation and seawater desalination," *Desalination*, vol. 250, pp. 249-256, 2010.

[209] L. Zuo, Y. Zheng, Z. Li, and Y. Sha, "Solar chimneys integrated with sea water desalination," *Desalination*, vol. 276, pp. 207-213, 2011.

[210] L. Zuo, Y. Yuan, Z. Li, and Y. Zheng, "Experimental research on solar chimneys integrated with seawater desalination under practical weather condition," *Desalination*, vol. 298, pp. 22-33, 2012.

[211] N. Niroomand and M. Amidpour, "New combination of solar chimney for power generation and seawater desalination," *Desalination and Water Treatment*, vol. 51, pp. 7401-7411, 2013.

[212] P. Refalo, R. Ghirlando, and S. Abela, "The use of a solar chimney and condensers to enhance the productivity of a solar still," *Desalination and Water Treatment*, pp. 1-14, 2015.

[213] S. Rajesh and R. B. Choudary, "A Cost Effective Desalination Plant Using a Solar Chimney with Recycled Aluminum Can Collector," *Journal of Solar Energy*, vol. 2016, pp. 1-10, 2016.

[214] N. Setoodeh, R. Rahimi, and A. Ameri, "Modeling and determination of heat transfer coefficient in a basin solar still using CFD," *Desalination*, vol. 268, no. 1-3, pp. 103-110, 2011.

[215] J. P. Holman, *Heat Transfer*, tenth ed. New York: McGraw-Hill, 2010.

[216] I. W. Eames, G. G. Maidment, and A. K. Lalzad, "A theoretical and experimental investigation of a small-scale solar-powered barometric desalination system," *Applied Thermal Engineering*, vol. 27, pp. 1951-1959, 2007.

[217] H.T. El-Dessouky and H. M. Ettouney, *Fundamentals of Salt Water Desalination*, First ed. Amsterdam: Elsevier Science B.V., 2002.

[218] P. T. Tsilingiris, "The influence of binary mixture thermophysical properties in the analysis of heat and mass transfer processes in solar distillation systems," *Solar Energy*, vol. 81, pp. 1482-1491, 2007.

[219] P. T. Tsilingiris, "Modeling heat and mass transport phenomena at higher temperatures in solar distillation systems – The Chilton–Colburn analogy," *Solar Energy*, vol. 84, pp. 308-317, 2010.

[220] J. A. Duffie and W. A. Beckman, *Solar Engineering of Thermal Processes*, fourth ed. New Jersey: John Wiley & Sons, Inc., 2013.

[221] K. Mahkamov, E. Orda, B. Belgasim, and I. Makhkamova, "A novel small dynamic solar thermal desalination plant with a fluid piston converter," *Applied Energy*, vol. 156, pp. 715-726, 2015.

[222] M. I. M. Shatat, "Solar Water Desalination," MsC, School of Engineering, Durham University, Durham, 2008.

[223] POLYMAX. (2016, 15/11/2016). *Foam Strips* Available: https://www.polymax.co.uk/rubber-sheet/epdm-cr-strips/sponge-epdm-neoprene-foam-strips-sab

[224] POLYMAX. (2017, 01/03/2017). *Cyanoacrylate Cord Adhesive*. Available: https://www.polymax.co.uk/polymax-cyanoacrylate-cord-adhesive

[225] R. K. Mishra, V. Garg, and G. N. Tiwari, "Thermal modeling and development of characteristic equations of evacuated tubular collector (ETC)," *Solar Energy*, vol. 116, pp. 165-176, 2015.

[226] S. P. PLUS. (2017, 31/03/2017). *Evacuated Tube Solar Collectors*. Available: http://www.solarpanelsplus.com/evacuated-tube-collectors/

[227] B. Belgasim, "Theoretical and experimental investigation of the dynamic solar water desalination unit," PhD, School of Engineering and Environment Northumbria University Newcastle Upon Tyne, 2013.

[228] GE. (2017, 15/02/2017). *UNIK 5000 Pressure Sensor*. Available: https://www.gemeasurement.com/sensors-probes-transducers/pressure-transducers-and-transmitters/unik-5000-silicon-pressure-sensor

[229] T. DIRECT. (2017, 02/08/2017). *Single Pair Thermocouple Cables*. Available: http://www.tcdirect.co.uk/Default.aspx?level=2&department_id=260/43

[230] OMEGA. (2017 02/02/2017). *Flow Sensor*. Available: http://www.omega.co.uk/pptst/FTB2000.html#nav

[231] OMEGA. (2017, 02/02/2017). *Flow meter*. Available: http://www.omega.com/temperature/pdf/DPF700.pdf

[232] OMEGA. (2017, 01/04/2017). *Water Test Meter* Available: https://www.omega.co.uk/pptst/HHWT-SD1.html

[233] OMEGA. (2016, 12/04/2016). *Digital Pressure Gauge*. Available: http://www.omega.com/manuals/manualpdf/M4999.pdf#search=DPG2001B-15V15G%20%20/-%2015.00%20PSIG%20GAUGE

[234] CPS-Products. (2017, 11/04/2017). *Vacuum Pump*. Available: http://www.cpsproducts.com/product-details/vp2s/

[235] S. Light. (2017, 21/04/2017). *PMA2200 Single-Input Radiometer*. Available: https://solarlight.com/product/pma2200-single-input-radiometer/

[236] RS. (2017, 10/05/2017). *Digital Desk Stopwatch*. Available: http://uk.rs-online.com/web/p/products/2355059/?grossPrice=Y&cm_mmc=UK-PLA-_-google-_-PLA_UK_EN_Office_Supplies-_-Clocks_And_Timers_And_Stopwatches&mkwid=sj3Wovnaf_dc

[237] ISG. (2017). *Electrical Balance*. Available: http://www.international-scientific.com/prod/balance-high-range-16kg-x-01g

[238] N. Instruments. (2017, 02/02/2017). *CompactDAQ-9178 Chassis*. Available: http://search.ni.com/nisearch/app/main/p/bot/no/ap/global/lang/en/pg/1/q/NI-cDAQ-9178%20/?y=7&x=8

[239] N. Instrument. (2017, 13/01/2017). *Pressure Input Module NI-9222*. Available: http://www.ni.com/en-gb/support/model.ni-9222.html

[240] N. Instruments. (2017, 13/01/2017). *Temperature Input Module NI-9213*. Available: http://www.ni.com/en-gb/support/model.ni-9213.html

[241] N. Instruments. (2017, 23/02/2017). *LabVIEW Software*. Available: http://www.ni.com/getting-started/labview-basics/

Appendix A Certificate of excellent oral presentation the 6th Int. Conference on Clean and Green Energy (ICCGE), Frankfurt, Germany, 2017.

Appendix B The thermo-physical properties of the vapour-air mixture

All values of the thermo-physical properties of the vapour-air mixture in equations 3.17 to 3.29 can be estimated as proposed in [218, 219] as follows:

$$\rho_{mi} = \rho_0 + \rho_1 T_{av} + \rho_2 T_{av}^2 + \rho_3 T_{av}^3 \quad \text{(B.1)}$$

where:

$$\rho_0 = 1.299995662$$

$$\rho_1 = -6.0436625845 \times 10^{-3}$$

$$\rho_2 = 4.697926602 \times 10^{-5}$$

$$\rho_3 = -5.760867827 \times 10^{-7}$$

Then:

$$\mu_{mi} = \mu_0 + \mu_1 T_{av} + \mu_2 T_{av}^2 + \mu_3 T_{av}^3 + \mu_4 T_{av}^4 \quad \text{(B.2)}$$

where:

$$\mu_0 = 1.685731754 \times 10^{-5}$$

$$\mu_1 = 9.151853945 \times 10^{-8}$$

$$\mu_2 = -2.16276222 \times 10^{-9}$$

$$\mu_3 = 3.413922553 \times 10^{-11}$$

$$\mu_4 = -2.644372665 \times 10^{-13}$$

Furthermore:

$$k_{mi} = k_0 + k_1 T_{av} + k_2 T_{av}^2 + k_3 T_{av}^3 \quad \text{(B.3)}$$

where:

$$k_0 = 0.02416826077$$

$$k_1 = 5.526004579 \times 10^{-5}$$

$$k_2 = 4.631207189 \times 10^{-7}$$

$$k_3 = -9.489325324 \times 10^{-9}$$

Moreover:

$$\alpha_{mi} = \alpha_0 + \alpha_1 T_{av} + \alpha_2 T_{av}^2 + \alpha_3 T_{av}^3 \quad \text{(B.4)}$$

where:

$$\alpha_0 = 1.881493006 \times 10^{-5}$$

$$\alpha_1 = 8.027692454 \times 10^{-8}$$

$$\alpha_2 = 1.496456991 \times 10^{-9}$$

$$\alpha_3 = -2.112432387 \times 10^{-11}$$

And:

$$D_i = D_0 + D_1 T_{av} + D_2 T_{av}^2 \quad \text{(B.5)}$$

where:

$$D_0 = 1.820034881 \times 10^{-5}$$

$$D_1 = -1.324098731 \times 10^{-7}$$

$$D_2 = 1.978458093 \times 10^{-10}$$

Appendix C Data acquisition system

The variation of temperature during the experiment was monitored and recorded by means of the data acquisition system by National Instruments. The components of the data acquisition system are schematically presented in Figure 4.23. The system is composed of three modules, namely a NI-9222 module and two NI-9213 modules. The three modules were installed on a compact DAQ chassis, namely the NI-cDAQ-9178 USB cDAQ module.

The NI-cDAQ-9178 USB cDAQ module:

This eight-slot compact DAQ chassis has a built-in timing controller for the sampling process and data transfer between the modules and a computer [238].

The NI-9222 module:

A high-speed, 4-channel simultaneous analogue module which has channel-to-channel isolation with enhanced sampling rate and accuracy. Each channel of the four high-speed channels in this module has a maximum sampling rate of 500 kHz with an accuracy of ±0.2%. The pressure sensor was connected to one of these channels [239].

The NI-9213 module:

The NI-9213 module with sixteen channels has a maximum sampling rate of 1200 Hz along with a minimum of 75 Hz sampling for each working channel when all channels are connected to thermocouples. This module features open-thermocouple detection, and includes a built-in cold-junction compensation for high-accuracy temperature measurement. The temperature measurements accuracy of the NI-9213 module is ±0.02 ^{o}C [240].